UNIVERSITEIT VAN PRETORIA
UNIVERSITY OF PRETORIA
YUNIBESITHI YA PRETORIA

Reactions between Country Rock Xenoliths and the Magma of the Uitkomst Complex, with Implications for the Origin of the Sulphide Mineralisation

Vierah Hulley

Submitted in fulfillment of the requirements of the degree of Master of Science in the Department of Geology, University of Pretoria (Pretoria, South Africa)
2005

CONTENTS

LIST OF FIGURES

LIST OF TABLES

LIST OF APPENDICES

ABSTRACT

The layered basic to ultrabasic Uitkomst Complex is situated on the Mpumalanga escarpment, approximately 260 km due east of Pretoria and 80 km south of Lydenburg. The Uitkomst Complex concordantly intruded the sedimentary bedding planes of the lower Transvaal Supergroup and plunges at approximately 4-8^0 to the north-west. Quartzite and shale of the lower Timeball Hill Formation forms the roof of the intrusion, forming a prominent escarpment in the north-west. The intrusion consists of seven major lithological units viz. (from bottom to top): the Basal Gabbronorite, Lower Harzburgite, Chromitiferous Harzburgite, Main Harzburgite, Pyroxenite, Main Gabbronorite and Upper Gabbronorite Units. The Ni-Cu-PGE-Cr- mineralised Uitkomst Complex is the only satellite body of the Bushveld Complex presently known to carry economic magmatic sulphide ores.

The association of the country rock xenoliths with the sulphide mineralised rock units of the Uitkomst Complex is not unique and has been made in similar intrusions around the world, suggesting a genetic link between the ore forming processes and the presence of the xenoliths. The aim of this thesis is to constrain these possible links by presenting a detailed documentation of the various types of xenoliths, the textural relationship between the xenoliths and their host rocks, and the mineralogical variation within the xenoliths and their immediate igneous matrix.

For the purpose of this study, special consideration has been given to the presence of xenoliths found in the vicinity and enclosed by the MSB. In addition to this, xenoliths associated with the Basal Mineralised Zone (BMZ) as well as Main Mineralised Zone (MMZ) are also considered. A section through a selected borehole (UK119) from the MMZ was examined using petrographical and geochemical methods. The borehole consisted of a dolomite xenolith sandwiched between chromititic pyroxenite. Pyrite and chalcopyrite are associated with the areas close to the contact zones of the dolomite with the mafic rocks.

Li *et al*. (2002) found a crustal S-isotopic signature in the sulphides of the igneous rocks of the Uitkomst Complex. The present study confirms a crustal S and O isotopic signature of the igneous host rocks to the xenoliths. The spread of the $\delta^{34}S$ values from –9‰ to +2‰ is larger than would be expected for mantle-derived igneous rocks (0±1‰), indicating the contribution of crustal sulphur to the Uitkomst Complex. Of additional importance is that the xenoliths tend to have a heavier S-isotopic signature than their igneous host rocks, suggesting that the dolomites are not the source of the crustal S in the ores. Another source, perhaps within the Timeball Hill shales or the Archaean basement granites, should be envisaged. Devolatilsation of the dolomites may have played a role in the lowering of the S solubility of the magma by means of oxidation of FeO. Devolatilisation is further indicated by the significant decrease in L.O.I. at the margins of the xenoliths, and by the O and C isotopic fractionation. There is limited variation in the O and C isotopes with height in the examined xenolith (UK119). This is in accord with a model of late-stage fluid infiltration. The fluids may be responsible for the formation of pyrite, pentlandite and chalcopyrite from original magmatic pyrrhotite.

The xenoliths associated with the Uitkomst Complex, consist of dolomite, calc-silicates, quartzites and granite. Calc-silicate mineralogy is pervasive in the samples examined, with the most common mineral assemblage being calcite-pyroxene-tremolite. All prograde reactions observed indicate decarbonation of the xenoliths, especially along the edges. Distinct reaction rims consisting of hydrous minerals are found at the contacts between the xenoliths and the magma. These reaction rims indicate the remobilization of fluids towards the margins during the metamorphic reactions. Using the estimate of Irvine and Sharpe (1982) for the temperature of Bushveld magmas at between 1200 and 1300^{o}C, a pressure of 1.1 - 1.6 kbars (~3–5 km) is inferred for the metamorphism of the xenoliths.

A distinct zonation in the sulphide mineralisation is observed: Pyrite is the dominant sulphide mineral in the interior of the xenolith away from the margins. Chalcopyrite and

pentlandite are more dominant at the immediate contact between the xenolith and the host rock. Pyrrhotite is the dominant sulphide mineral in the host rock.

A possible model of late magmatic and hydrothermal processes would have given rise to the variations in the stable isotope compositions. In light of the results from this study, the following model is proposed:

1. The intruding magma interacted with the country rocks, causing a volume loss of up to 40%, and the development of prograde metamorphic mineral facies.
2. The segregating sulphide melt (from an external source) then infiltrated the xenoliths at a later stage.
3. Finally, the rocks underwent hydrothermal alteration and fluid flux as evidenced by S-isotopic disequilibria of the sulphide minerals and O and C isotopic fractionation.

1. INTRODUCTION

1.1. General

The layered basic to ultrabasic Uitkomst Complex (Gauert *et al*., 1995, 1996; De Waal and Gauert, 1997) is situated on the Mpumalanga escarpment, approximately 260 km due east of Pretoria and 80 km south of Lydenburg (Figure 1. 1). It is an elongated, tube-like body measuring *ca.* 1km in width and height and at least 12 km in length (Figure 1. 2). The Uitkomst Complex outcrops on the farms Uitkomst 541 JT and Slaaihoek 540 JT over a total distance of 9 km. Available borehole data indicate that the intrusive body extends to the north-west for at least 3 km beneath the cover of the sedimentary rocks of the Pretoria Group (Transvaal Supergroup), to the farm Little Mamre 538 JT. Due to lack of borehole data, possible further extension of the body towards the north-west is unknown.

The Uitkomst Complex concordantly intruded the sedimentary bedding planes of the lower Transvaal Supergroup and plunges at approximately 4-8^0 to the north-west. Quartzite and shale of the lower Timeball Hill Formation forms the roof of the intrusion, forming a prominent escarpment in the north-west.

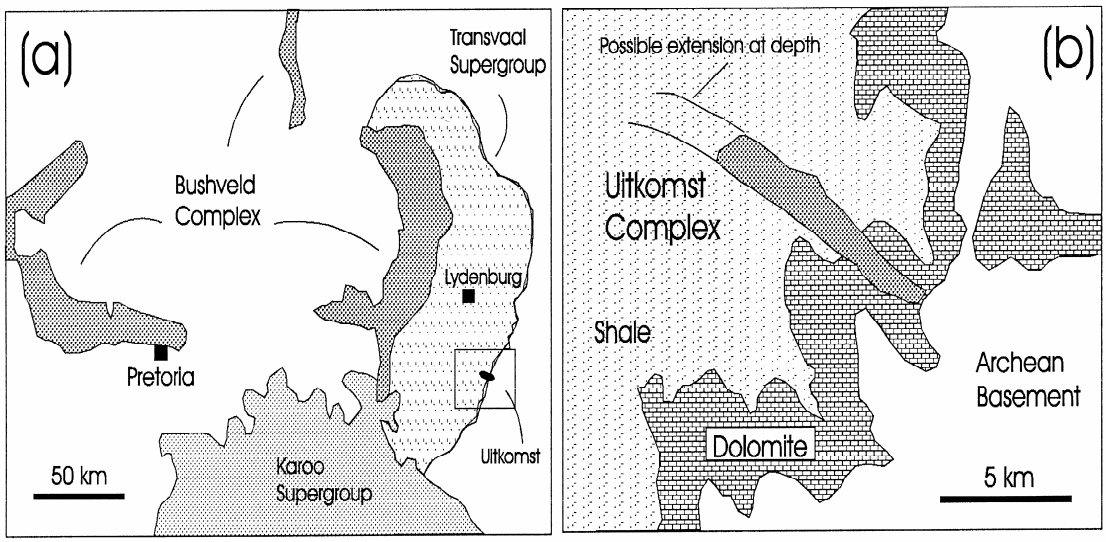

Figure 1. 1: Locality and general geology map of the Uitkomst Complex, Mpumalanga (Figure from Maier *et al.* 2004).

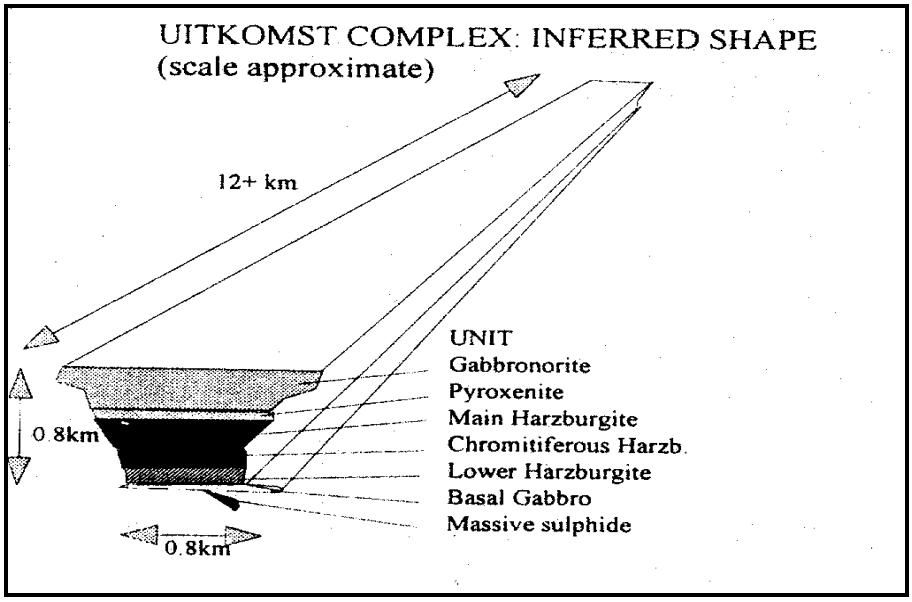

Figure 1. 2: Schematic shape of the Uitkomst Complex (Figure from Maier *et al.*, 1998).

The Uitkomst Complex has a concordant $^{207}Pb/^{206}Pb$ zircon age of 2045± 8 Ma and is one of about 20 satellite intrusions related to the Rustenburg Layered Suite of the Bushveld

Complex (De Waal *et al*., 2001). The intrusion consists of seven major lithological units viz. (from bottom to top): the Basal Gabbronorite, Lower Harzburgite, Chromitiferous Harzburgite, Main Harzburgite, Pyroxenite, Main Gabbronorite and Upper Gabbronorite Units (Figure 1. 3) (Gauert *et al*., 1995, 1996; De Waal and Gauert, 1997; Maier *et al*., 2004). According to Gauert *et al*. (1995), the Uitkomst Complex crystallised in two main stages. The bulk of the harzburgitic units crystallised under open system conditions from magma that flowed through the magma chamber i.e. the conduit stage. In contrast the upper 50 m of the Main Harzburgite Unit together with the Pyroxenite, Main Gabbronorite and Upper Gabbronorite Units crystallised under more stagnant conditions i.e. the closed system stage.

Comment [V1]: Additional unit!!!

The Ni-Cu-PGE-Cr- mineralised Uitkomst Complex is the only satellite body of the Bushveld Complex presently known to carry economic magmatic sulphide ores. However, the geochemical mechanisms that might have had a bearing on the formation of the sulphide ores associated with the Complex remain poorly understood. Two main models may be distinguished: Von Scheibler *et al.* (1995) suggest a two-stage model whereby the Complex was formed by magma progressively eroding into the country rock. Assimilation of graphitic Timeball Hill shale increased the S-solubility, and subsequent assimilation of dolomitic material caused oxidation and triggered sulphide segregation. De Waal and Gauert (1997) proposed that the bulk of the sulphides were entrained from a staging chamber at depth to be crystallised in their present setting.

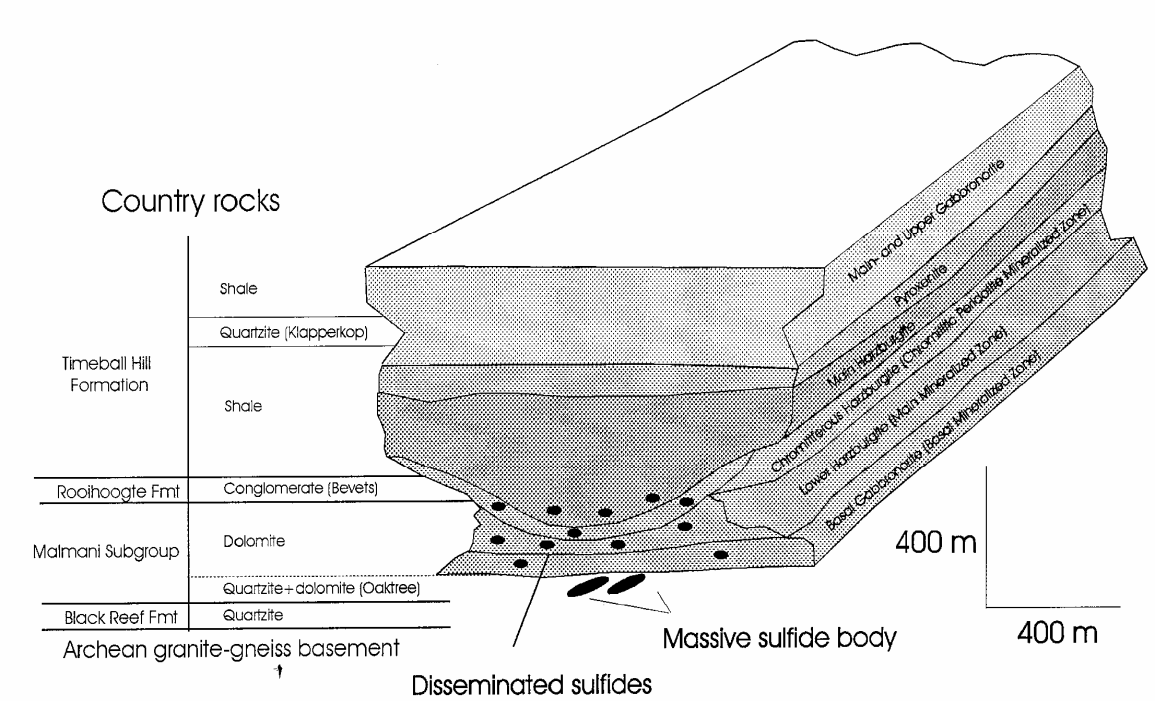

Figure 1. 3: Lithological subdivision of the Uitkomst Complex (Figure from Maier *et al.*, 2004).

1.2. Aims/Objectives of study

The presence of a large number of country rock xenoliths associated with the sulphide mineralised rock units close to the base of the Uitkomst Complex is one of the most distinctive aspects of the body. Analogous associations of xenoliths with sulphide mineralisation have been observed in the Voisey's Bay Intrusion (Li and Naldrett, 2000), the Pants Lake Intrusion (Kerr, 1999), and the Insizwa Complex (Lightfoot *et al*., 1984), suggesting a genetic link between the ore forming processes and the presence of the xenoliths.

This thesis attempts to constrain these possible links by presenting a detailed documentation of the various types of xenoliths, the textural relationship between the xenoliths and their host rocks, and the mineralogical variation within the xenoliths and their immediate igneous matrix. It is hoped that this will lead to a better understanding of how the interaction had changed the composition of the magma, and whether the interaction triggered the segregation of the sulphide melt that accumulated to form the ores.

1.3. Exploration history

In his book on the Platinum Deposits and Mines of South Africa, Wagner (1929) was the first to report on the disseminated nickel sulphides in cumulates on the farm Uitkomst 541 JT. The similarity between the sulphide mineralisation to that at Sudbury, Ontario, was highlighted in his book, and a correlation of the Uitkomst intrusion with the ultramafic rocks present in the Barberton Mountain Land was proposed.

In 1970, Dr. Louis Coetzee of Anglo American Corporation of South Africa Ltd. (AAC) recognised the potential for a magmatic ore deposit on the farm Uitkomst 541 JT in the Waterval Boven District. In the same year, the farm Uitkomst 541 JT was optioned by AAC and transferred to the Kaffrarian Metal Holdings under a joint venture agreement with the International Nickel Company of Canada Ltd. (INCO) (Woolfe, 1996). The preliminary field mapping, which located the mineralised outcrop of the lower harzburgite unit, was followed by geochemical and geophysical surveys, intended to more accurately delineate the morphology of the intrusion as well as to prospect for further intrusions and/or extensions to the known extent of the Uitkomst Complex. Drilling started in September 1972 under INCO management. This first drilling program indicated 100 Mt of ore grading 0.4% Ni and 0.2% Cu.

The results of the initial appraisal study by AAC in May 1975, based on the results of 61 boreholes, indicated a large tonnage (178.7Mt), low grade (0.32% Ni and 0.13% Cu) open pit resource of nickel and copper. Subsequently, further work included closer spaced (100m) drilling, the planning of some deeper exploratory holes to the north-west, more detailed mine planning and optimisation exercises. The development of a 107 metre adit started in December 1975, in order to obtain a bulk ore sample for pilot metallurgical test work. However, in 1976, exploration activity on the project ceased due to the deterioration of the nickel market at that time as well as the marginal nature of the project. Mineral rights to Uitkomst were purchased by AAC in 1977, and in 1980 AAC also acquired INCO's interest in the joint venture, resulting from INCO's decision to withdraw from South Africa due to political reasons.

Eastern Transvaal Consolidated Mines Ltd. (ETC) carried out some preliminary geological and geophysical work in 1975 in order to investigate the nickel potential on the farm Slaaihoek 540 JT. The mineral rights had already been purchased by ETC in 1929 to mine epithermal gold within the Timeball Hill shale at the Mamre and Slaaihoek mines. Assessment of previous data on Uitkomst by AAC in 1987 warranted a feasibility study from 1989 to 1991. The marginal nature of the results from this study discouraged the development of a mining operation.

ETC drilled their first three boreholes on Slaaihoek 540 JT in 1989. Positive results from the boreholes as well as bench scale metallurgical tests and a preliminary mining feasibility study led to a further drilling campaign guided by ground geophysics, between 1990 and 1992. The results from this drilling expedition motivated a more detailed evaluation of the Slaaihoek property.

In August 1993, Middle Witwatersrand (Western Areas) Ltd. (Midwits), a subsidiary of Anglovaal Ltd., and ETC joined partnership to form the Nico Joint Venture. The objective was to pursue the main geological and metallurgical evaluation programme that was required in order to conclude a feasibility study of the Uitkomst Complex on Slaaihoek.

The Nkomati Joint Venture, between Anglo American's Kaffrarian Metal Holdings and Nico Joint Venture, was formed in June 1995.

In 1995, bulk samples of the Main Mineralised Zone (MMZ), Basal Mineralised Zone (BMZ), and Massive Sulphide Body (MSB) were processed at a pilot plant constructed on site. The same year saw the viability of mining of the Massive Sulphide Body being investigated through a feasibility study. A mineral resource of 3Mt grading 2.04% Ni, 1.13% Cu, 0.09% Co, 1.65g/t Pt, 4.18g/t Pd, 0.16g/t Rh and 0.18g/t Au was indicated. The announcement to develop the Nkomati mine was made in March 1996. The first tonnes of massive sulphide ore were milled in December 1996.

Comment [V2]: When was MSB discovered – Look in Theart and De Nooy paper – SAJG!!!

1.4. Previous work

As mentioned in §1.3, the Uitkomst Complex was first investigated in 1929 when Wagner reported on the disseminated nickel sulphides in cumulates on the farm Uitkomst 541 JT.

The investigation by Kenyon *et al.* (1986) suggested that the layered ultramafic series of the Uitkomst Complex is coeval with the Bushveld Complex. This was based on the result obtained from a single Rb-Sr age determination on biotite. Petrochemical and microprobe analyses of chromite indicated affinities of the Uitkomst Complex with the Lower Critical Zone of the Bushveld Complex. This was the first time that a possible association of the Uitkomst Complex with the Bushveld Complex was proposed. Kenyon *et al.* (1986) also proposed a lithostratigraphical sub-division of the Uitkomst Complex. Four distinct zones were recognised, which become progressively more ultrabasic upwards. The main sulphide mineralisation was identified in the lower units, with the best mineralisation occurring in the vicinity of dolomite country rocks and associated with the most altered rocks. Due to this observation, Kenyon *et al.* (1986) suggested that a high CO_2 content of the magma, due to degassing of the country rocks, might have led to the formation of immiscible sulphide melt.

Gauert *et al.* (1995) investigated the geology of the Uitkomst Complex based largely on extensive borehole data that had become available at that stage. They proposed two magmatic stages of formation of the Complex; an open and a closed system stage. The first pulses of magma, of broadly gabbronoritic composition, intruded into a tubular opening bordered by marginal fracture zones. This magma cooled along the walls of the chamber producing the marginal gabbros. Upon widening of the opening, further magma of more primitive composition flushed through the centre of the conduit-like chamber, crystallising the ultramafic rocks. After the flow of magma through the conduit ceased, the uppermost third of the body crystallised ultramafic and mafic rocks in an essentially closed system.

The study of Strauss (1995) focussed on the mineral and whole-rock geochemistry of the Basal Gabbro Unit on the farm Slaaihoek 540 JT. This investigation confirmed that the Basal Gabbro Unit has a chilled margin, which may represent the composition of some of the

parental magma to the Uitkomst intrusion. The model of ore formation that was proposed involved supercooling and country rock assimilation. This model was based on the high Cu/(Cu + Ni) ratio of the Basal Gabbro Unit compared with that of the overlying Lower Pyroxenite Unit.

Von Scheibler *et al*. (1995) combined field mapping, borehole information and geochemical data to propose an alternative model for the origin of the Ni-Cu sulphide mineralisation in the Uitkomst Complex. It was suggested that the body formed due to magmatic erosion of the Timeball Hill shale by magma of komatiitic affinity that was originally emplaced above the Timeball Hill sulphidic and graphitic shale. The assimilation of graphitic material increased the S-solubility of the magma, while assimilation of sedimentary sulphides increased the S-content of the magma. Further erosion of country rocks led to intrusion of the magma into dolomites of the Malmani and Oaktree Formation. The decay of the CO_2 to O and CO increased the fO_2 of the magma causing local sulphide and chromite precipitation within the chamber. The more contaminated the magma became, the more sulphide was produced. The more contaminated magma also crystallised pyroxenite whereas peridotite crystallised from less contaminated magma.

Gauert *et al.* (1996) analysed 65 samples of massive and disseminated pyrrhotite, chalcopyrite and pyrite from the Basal Gabbro, Lower Harzburgite and Main Harzburgite Units of the Uitkomst Complex, together with samples of sulphide veins in the country rock, for sulphur isotope ratios. The $\delta^{34}S$ distributions for the Main Harzburgite and Basal Gabbro Units were found to be scattered with values ranging from -7.4 to +1.2 per mil, and -19.5 to +1.8 per mil, respectively. The samples from the Lower Harzburgite Unit showed a single skewed distribution of the $\delta^{34}S$ with an average $\delta^{34}S$ distribution of -4.5 ±1.8 per mil. It was concluded that the heterogeneity of the isotope signatures observed between the investigated layers resulted from differential contamination upon emplacement of the primary magma, which had a typical isotope signature of 0 per mil, with light sedimentary sulphur. The range in distribution of $\delta^{34}S$ in the Basal Gabbro Unit is explained through the rapid cooling of the magma, in contrast to the Lower Harzburgite Unit that cooled at a slower rate and thus had more time for isotopic homogenisation.

Van Zyl (1996) focussed her attention on the Main-, Chromitiferous- and Lower Harzburgite units. The investigation combined petrography, mineral chemistry and image analysis. The three units studied showed distinct types of alteration. The abundance of talc and carbonate in the mineralised zone suggests the development of a deuteric CO_2-rich environment in the lower three lithologies. The carbonate observed may be derived from assimilated dolomite, or it may have developed at a later stage due to the continued degassing of the dolomite during cooling. It was also noticed that in places where secondary alteration of the silicate minerals is the most intense, the sulphide minerals show marginal replacement by secondary silicate mineral intergrowths, thus affecting the beneficiation of the sulphide. Van Zyl (1996) also documented the presence of four platinum group minerals associated with pyrrhotite: kotulskite [Pd(Te,Bi)], merenskyite [(Pt,Pd)(Te,$Bi)_2$], stibiopalladinite [$(Pb,Cu)_5Sb_2$] and sperrylite ($PtAs_2$) were found to be associated with pyrrhotite.

Following on the geochemical studies of Gauert *et al*. (1995) and Strauss (1995), De Waal and Gauert (1997) investigated the nature of the parental magma of the Uitkomst Complex. The chemical variation between samples of the phaneritic rocks of the Basal Gabbro Unit was attributed to *in situ* fractionation of sulphide, silicates and chromite. Field, petrographic and petrochemical data derived from the Basal Gabbro Unit were used to propose a petrogenetic model in which the parental magma of the Uitkomst Complex (the “Bu” magma) is derived through a mixture of Bushveld B2 magma and a fractionated variant of Bushveld B1 magma. The authors further proposed that the Uitkomst Complex, while derived from a similar mantle source as the Bushveld magma, represented part of a magmatic system not directly related to the main Bushveld chamber (Figure 1. 4)

Gauert (1998) provided the most detailed description of the Uitkomst Complex at the time, with the aim of providing insight into the origin of the intrusion, as well as that of the associated mineralisation. He divided the Complex into 6 units (from bottom to top): the Basal Gabbro, Lower Harzburgite, Chromitiferous Harzburgite, Main Harzburgite, Pyroxenite and Gabbronorite Units. Based on analytical and field data, Gauert (1998) concluded that the Uitkomst Complex crystallised in 3 stages: 1. Integration Stage: This refers to the transition zone between the phaneritic Basal Gabbro Unit and the ultramafic cumulates of the Lower Harzburgite Unit. During the Integration Stage the Bu magma,

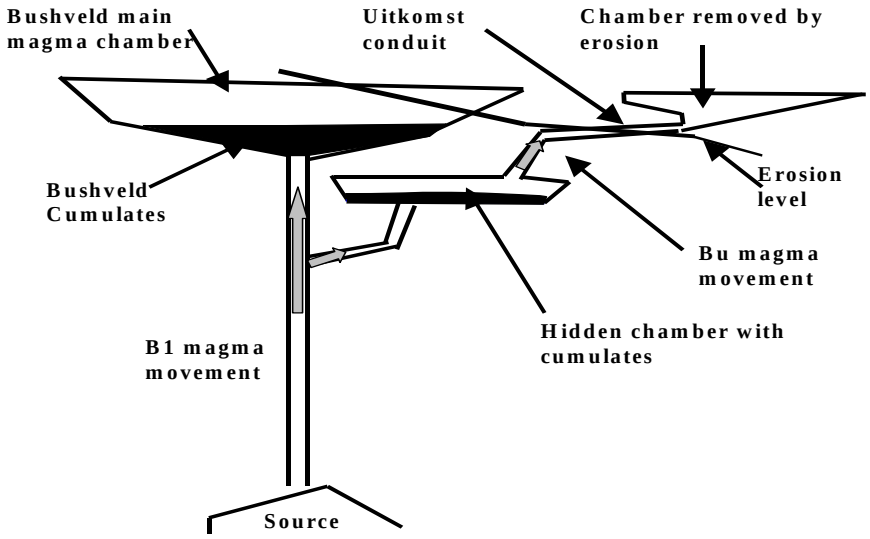

Figure 1. 4: Cartoon depicting schematically the possible connection between the Uitkomst Complex and the Bushveld Complex; the Uitkomst Complex being a conduit of a partly evolved Bushveld B1 magma (Figure from de Waal and Gauert, 1997).

which formed the Basal Gabbro Unit, was progressively flushed out of the chamber by a B1-like magma, and also hybridised with this magma. 2. Conduit Stage: This refers to crystallisation in an open system. The continuous influx of magma of constant composition gave rise to the layers of homogeneous olivine-chromite cumulates (viz. Lower Harzburgite, Chromitiferous Harzburtite and Main Harzburgite Units). 3. Closed System Stage: This was initiated after the flow of magma in the conduit ceased. As a result, the magma crystallised a sequence of progressively more differentiated rocks (harzburgite, pyroxenite, gabbronorite, diorite). Gauert (1998) also discussed the origin of the sulphide ores. He suggested that the degassing of the dolomitic xenoliths found in the Lower Harzburgite and Chromitiferous Harzburgite Units could have triggered sulphide segregation. A more recent publication by Gauert (2001) elaborates further on the likely origin of the sulphide mineralisation in the Uitkomst Complex. By means of mass balance calculations (Table 1. 1), Gauert argued that the large quantity of sulphides compared to the thickness of the Complex is best explained by separation from a larger magma pool at depth, followed by entrainment of the sulphide melt in the ascending magma and deposition in the conduit.

Table 1. 1: Mass balance of sulphides and chromite in the Uitkomst Complex (Gauert, 2001)

A) Sulphide

Rock Unit	Approximate thickness (m)	Approximate vol. % of intrusion*	Average sulphide content of rock	Sulphide content of unit (%)
Pyroxenite and Gabbronorite Units	310	43.5	0.1	0.04
Main Harzburgite (upper part)	290	35.4	0.15	0.05
Main Harzburgite (mineralised part)	40	5.3	5	0.27
Chromitiferous Harzburgite	60	8.0	5	0.4
Lower Harzburgite	50	6.7	15	1.01
Basal Gabbro	6.5	0.9	6	0.05
Massive Sulphides	2-26	0.2	≈85	0.13
Complete Intrusion	750	100	≈2	2

B) Chromite

Cr content of magma	206 ppm in average of lower and upper chilled margins
Thickness of chromitite seams	Avg: 5 m; max: 15 m
Chromite content	50%, containing 50% Cr_2O_3
Required magma column**	>8700 m at 50% extraction from magma

Where:

*: The volume calculation of the intrusion is based on the average cross section geometry of the units; and the estimated sulphide content of rock units is based on the average sulphur concentrations and macroscopic observation.

**: The magma column has been calculated assuming an average Cr content of massive chromitite layer at 171050 ppm; the average Cr content in the Uitkomst chill is 206 ppm. Enrichment factor at 50% extraction is ~1661. The ratio of the entire intrusion volume to massive chromitite volume as derived from the average cross section is 143.1. The enrichment factor divided by the volume ratio is 1661/143 = 11.62. This value multiplied by the total average thickness of the intrusion approximates the size of the magma column required for the formation of the above chromitite layer i.e. 8716 m.

The study of Hornsey (1999) concentrated on the genesis and evolution of the Nkomati Massive Sulphide Body (MSB). Hornsey (1999) argued that the massive sulphide ores are derived from the Lower Harzburgite Unit by infiltration into the floor rocks. Based on a number of observations, he concluded that the flow direction of the magma was from the north-west and that the morphology of the intrusion was influenced by a crustal stress regime of anisotropic horizontal stress conditions. His model for sulphide-ore genesis is depicted in Figure 1.5. In this model, structurally controlled influxes of aqueous S and CO_2 into the Uitkomst Complex magma chamber resulted in an increase in the S content of the magma

and the localised generation of an immiscible sulphide liquid. The finely disseminated sulphide "cloud" that was generated was then entrained within the flowing magma and coalesced. The immiscible sulphide liquid then intruded footwall sediments of the Uitkomst Complex as a discrete sill, utilising self-generated fractures.

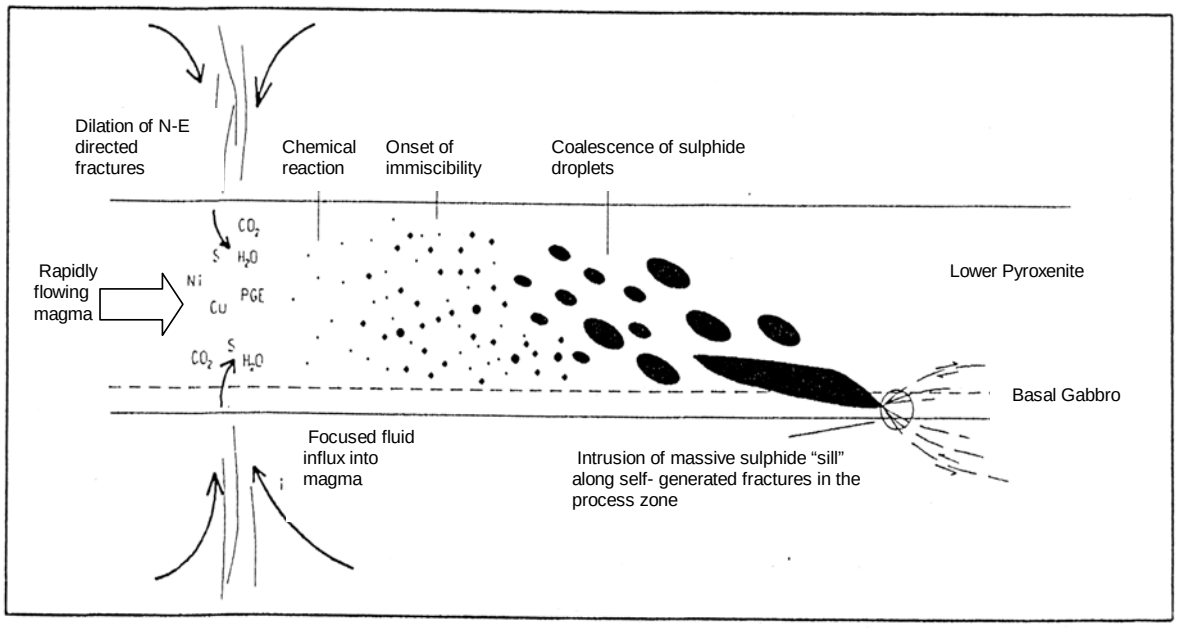

Figure 1. 5: Schematic model of the controls, generation and emplacement of the Nkomati massive sulphide mineralisation (Figure from Hornsey, 1999).

Although previous authors have suggested that the Uitkomst Complex is coeval or related to the Bushveld complex, De Waal *et al.* (2001) provided more conclusive evidence of such a relationship. The age of the Uitkomst Complex was determined to be 2045 ±8 Ma (concordant zircon SHRIMP age). Further investigations and calculations allowed De Waal *et al*. (2001) to conclude that the bulk of the cumulates of the Uitkomst Complex resulted through crystallisation of magma that has a similar composition to the high Mg andesitic B1 parental magma of the Rustenburg Layered Suite of the Bushveld Complex.

Theart and de Nooy (2001) studied the PGM in parts of the massive sulphide body. They concluded that the platinum group minerals commonly occur as composite grains or as

aggregates. The main PGM are merenskyite, michenerite, testibiopalladite, sperrylite and temagamite. The minerals are preferentially associated with pyrrhotite (60%), pentlandite (20%) and chalcopyrite (6%). In addition to this, there are also associations with host silicates (13%) and magnetite (0.1%). The majority of the PGM (69%) occur along grain boundaries between adjacent pyrrhotite or magnetite grains. The remaining percentage of PGM (31%) is completely enclosed within the host mineral grain.

Li *et al.* (2002) studied the olivines and the sulphur isotopic compositions of the various units of the Uitkomst Complex. The abrupt changes in the Ni contents of olivine between the mineralised and unmineralised units as well as within the pyroxenite unit are attributed to multiple magma flows that had varying Ni contents. Sulphur isotope ratios obtained for the sulphide ores in the harzburgite units vary between $-2.6^{0}/_{00}$ and $-7.1^{0}/_{00.}$ The negative $\delta^{34}S$ values for the ores are attributed to the addition of ^{34}S-depleted crustal sulphur, likely from the Malmani dolomite and the Timeball Hill shale. The authors suggest that addition of crustal sulphur caused sulphide saturation in the magma. Following this, the immiscible sulphide liquid droplets then got concentrated at the base of the magma.

Gomwe (2002) and Maier *et al*. (2004) investigated a complete borehole intersection through the complex and recorded variations in major and trace element chemistry (including PGE) and in Sm/Nd isotopic composition. They essentially confirmed the model of Gauert *et al*. (1995) that the complex is of Bushveld magmatic affinity and can be subdivided into a conduit and closed-system stage.

2. GENERAL GEOLOGY

2.1. General

The Uitkomst Complex intruded the late Archaean-early Proterozoic sediments of the lower Transvaal Supergroup. The Black Reef Formation forms the floor rocks of the intrusion and the Klapperkop Member of the Timeball Hill Formation forms the roof. The dominant rock types intermittent between these two mainly quartzitic horizons are the dolomite of the Malmani Subgroup and the Oaktree Formation, as well as lower shales of the Timeball Hill Formation. Table 2.1 shows the lithostratigraphy of the country rocks of the Complex. Figure 2. 1 illustrates the regional geology, emphasizing major lithological units and structural features.

Table 2. 1: **Regional lithostratigraphy of the country rocks associated with the Uitkomst Complex (after Eriksson *et al*., 1993)**

Supergroup	**Group**	**Formation or subgroup**	**Lithology**
Transvaal	Pretoria	Timeball Hill Formation	Shale, with minor ferruginous quartzite
		Rooihoogte Formation	quartzite, shale --- diamictite (Bevets Member)
	Chuniespoort	Malmani Subgroup	dolomite and minor chert layers
	Wolkberg	Black Reef Formation	quartzite conglomerate mudstone, sandstone, basalt
Pre-Transvaal		Nelshoogte Granite	Basement granite-gneiss

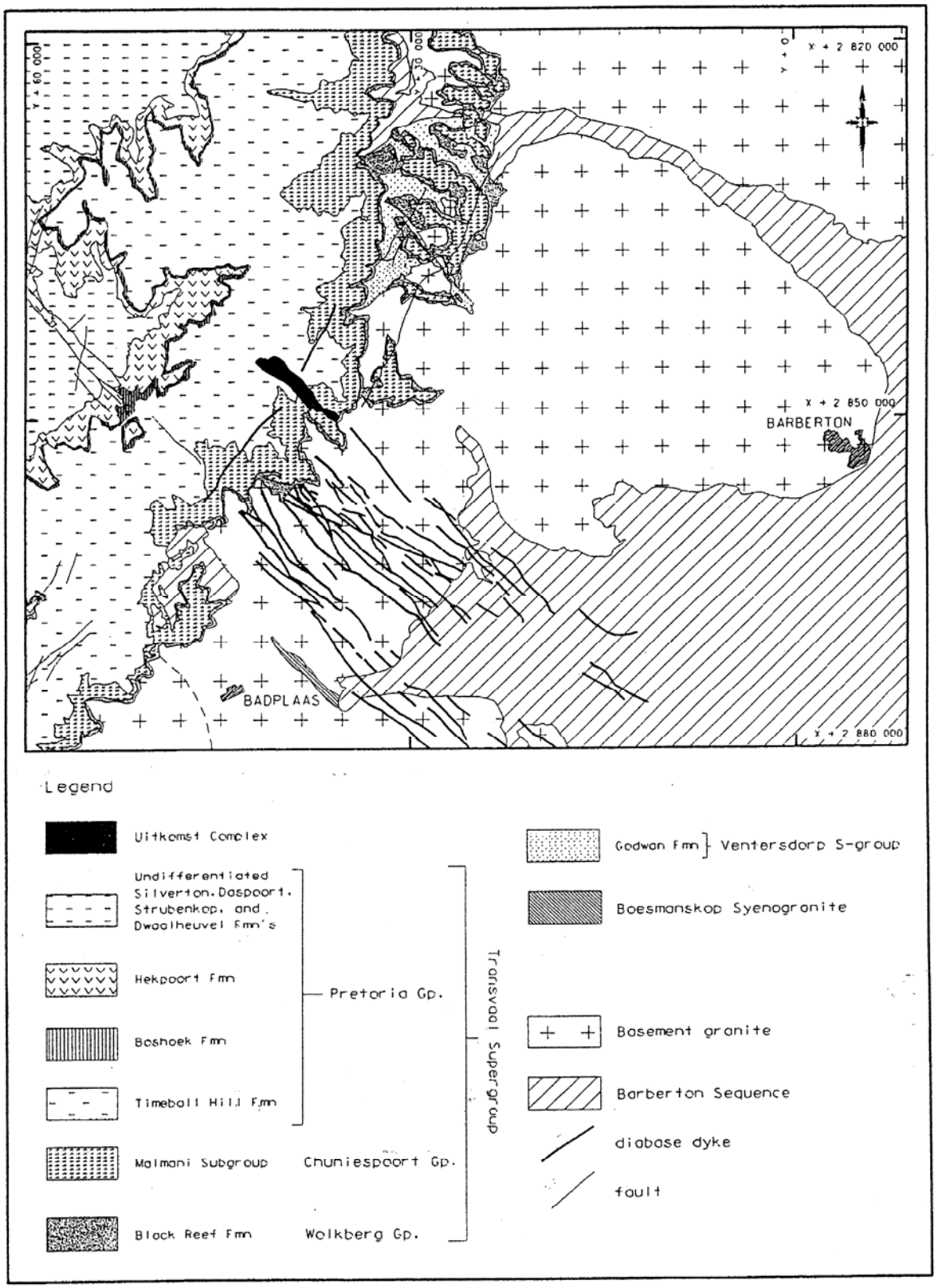

Figure 2. 1: Regional geology of the study area, illustrating the major lithological units and structural features (Figure from Hornsey, 1999).

2.2. Nelshoogte Granite

The Nelshoogte Granite gneiss forms the Archaean basement in the study area. It consists of a biotite-rich tronhjemite gneiss (Oosthuysen, 1970), belonging to the Swazian Eratherm, and is approximately 3.2-3.5 Ga in age (Anhaeusser *et al.*, 1983).

A distinct, nearly vertical planar foliation has developed in places, which generally strikes in an east-west direction (Visser *et al*, 1956). The pluton is approximately 20 km wide by 25 km in length, with the long axis oriented to the north-northeast. The gneiss displays a variation in composition from speckled grey feldspar- and quartz-rich varieties to darker, more biotite- and hornblende-rich varieties. High degrees of sericitisation and silicification occur in some parts of the pluton. The gneiss is also often cut by chlorite and quartz veins, with stringers of chalcopyrite and pyrite occurring in places. Xenoliths of quartzite and a variety of greenstone rocks are occasionally observed within the gneiss (Robb and Anhaeusser, 1983).

2.3. Transvaal Supergroup

2.3.1. General

The late Archaean to early Proterozoic Transvaal Supergroup rests nonconformably on the Nelshoogte Granite. The sediments of the Transvaal Supergroup in the Bushveld basin consist of 15 km of relatively undeformed and low grade metamorphosed mudrocks, sandstones, volcanic rocks, dolomites, and iron formations (Eriksson *et al.*, 1993; Button, 1973). The basal unit consists of clastic rocks belonging to the Black Reef Formation of the Wolkberg Group. This is overlain by chemical sediments of the Chuniespoort Group, which is only represented by chert-rich dolomites of the Oaktree and Lower Monte Christo formations (Malmani Subgroup) to the north of Badplaas. The Chuniespoort Group is overlain by the volcano-sedimentary Pretoria Group. The volcanic Rooiberg Group caps the sediments.

The Uitkomst Complex is hosted by the Black Reef Formation, the reduced Malmani Subgroup and the Rooihoogte and lower Timeball Hill formations which belong to the lower portion of the Pretoria Group (Figure 2. 2).

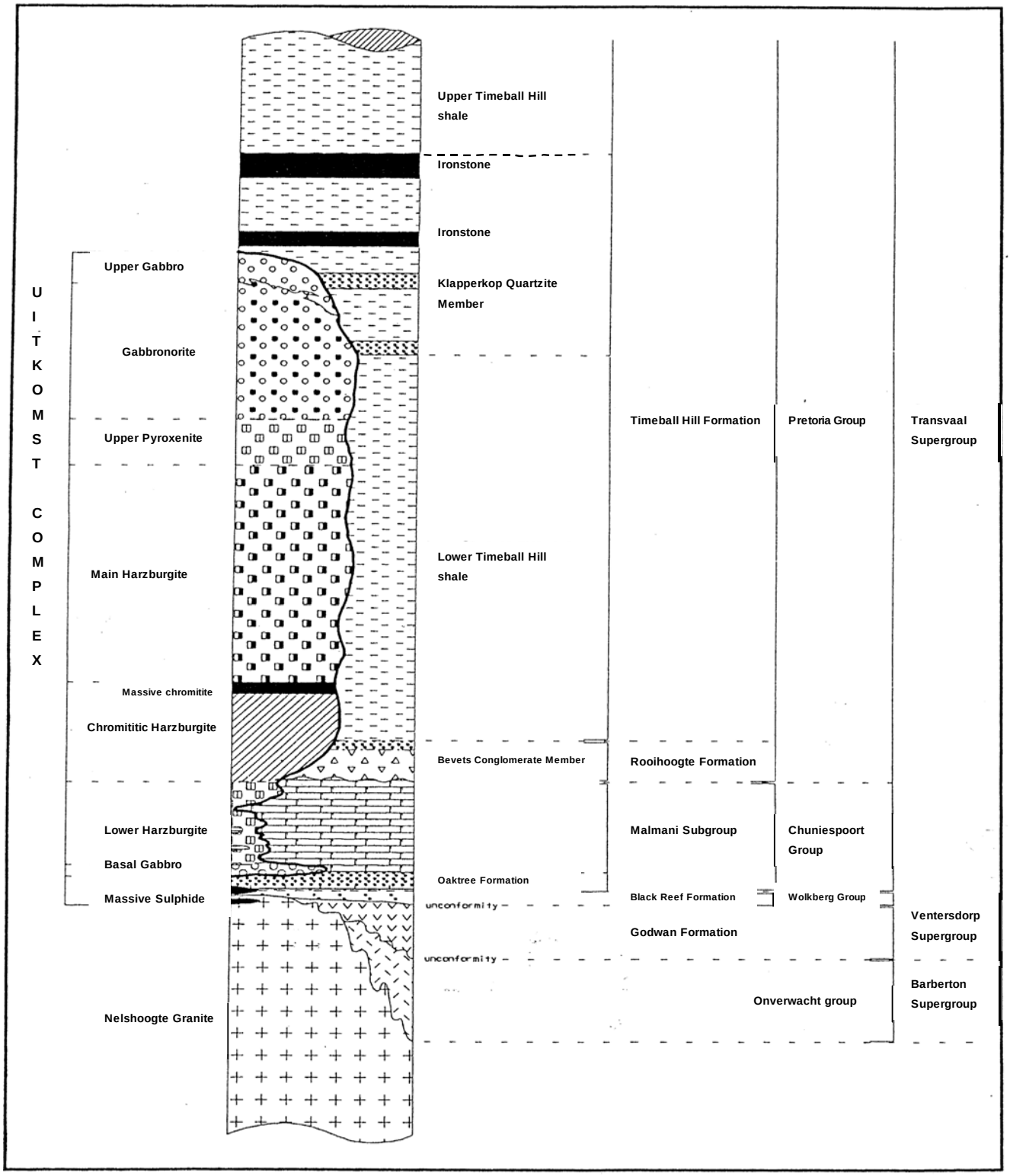

Figure 2. 2: Schematic stratigraphic column of the Nkomati Mine area (Figure from Hornsey, 1999).

2.3.2. Black Reef Formation

The Black Reef Formation forms the basal unit of the Transvaal Supergroup, nonconformably overlying the Nelshoogte Granite. The Black Reef Formation consists of a transgressive conglomerate and arenite (Figure 2. 3).

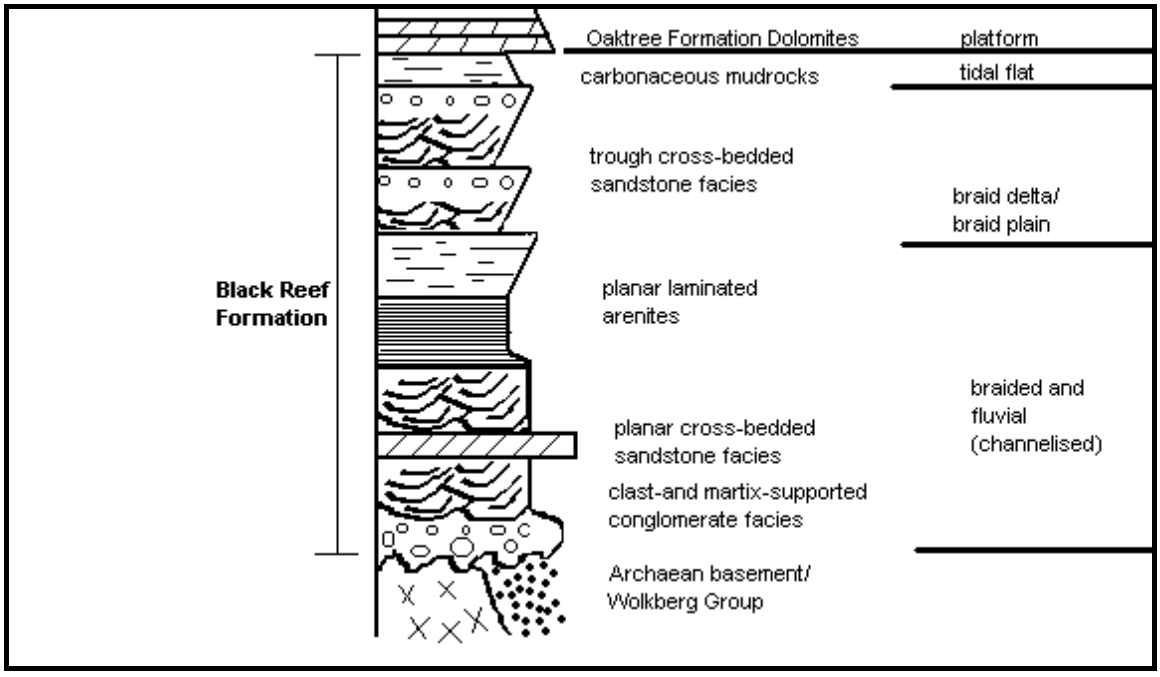

Figure 2. 3: Facies sequence and depositional environment of the Black Reef Formation in the eastern Transvaal Basin (Figure from Henry *et al.*, 1990)

It forms a continuous stratigraphic unit between Badplaas and the northwest of Potgietersrus, a distance of over 450 km (Henry *et al.*, 1990; Clendenin *et al*, 1991). The undulating basal contact of the Black Reef Formation with the underlying Nelshoogte Granite is sharp. In the study area, the Black Reef Formation is a creamy to light greenish-gray, medium-grained, locally cross-bedded quartzite. A basal conglomerate several tens of centimetres in thickness is developed in places. Clendenin *et al.* (1991) suggested that the Black Reef Formation represented an aqueous depositional environment since the quartz grains are glassy/clear. An age of 2642 ±2.3 Ma has been obtained for the time-equivalent Vryburg Formation (Walraven and Martini, 1995).

2.3.3. Chuniespoort Group

The basal Malmani Subgroup consisting of the Oaktree and Monte Christo formations is the only member of the Chuniespoort Group present at Uitkomst due to a period of uplift and erosion prior to the deposition of the Pretoria Group.

The Malmani Subgroup consists of dolomite, interbedded chert bands and mudrocks. Its lithology represents epeiric marine deposits, which were deposited over an extensive portion of the Kaapvaal craton (Eriksson *et al.*, 1993). Stromatolites of variable proportions are present throughout the unit, and characterize the carbonate-chert sequence of the Malmani Subgroup. Sedimentary structures such as ripple marks, oolites, intra-clastic breccias and cross-laminations are also common in the dolomites. An erosional unconformity with the Bevets Conglomerate Member of the Rooihoogte Formation forms the upper contact. An age of 2549.9 ±2.6 Ma has been obtained from a tuff layer within the basal Oaktree Formation (Pb-Pb single zircon method; Walraven and Martini, 1995).

The basal Oaktree Formation is an approximately 2-3 m thick well-bedded dolomite, which forms the preferred horizon for the development of a mylonitic talc schistose shear zone (components: talc, chlorite, Fe-Mg-silicates and malachite). This layer is referred to as the Basal Shear Zone and has been interpreted to be a pre-intrusive thrust zone in the country rocks that extended laterally beyond the margins of the Complex. The dolomite constituting this basal unit also has mm-scale internal laminae.

Within the Oaktree Formation, quartzite overlies the dolomite. This layer is *ca.* 2-4m thick and commonly constitutes the footwall of the Uitkomst intrusion, making it an important marker horizon. The Oaktree quartzite is a clean, slightly gritty, coarse-grained, trough crossbedded orthoquartzite. The layer has also been fractured and contains stringer mineralisation of pyrite and chalcopyrite.

A 50 cm zone containing dark green amphibole needles is present immediately below the Uitkomst Complex. This zone formed as a result of contact metamorphism, which resulted from the emplacement of the Basal Gabbro. Figure 2. 4. shows a stratigraphic column of the basal units of the Uitkomst Complex and the Transvaal Supergroup.

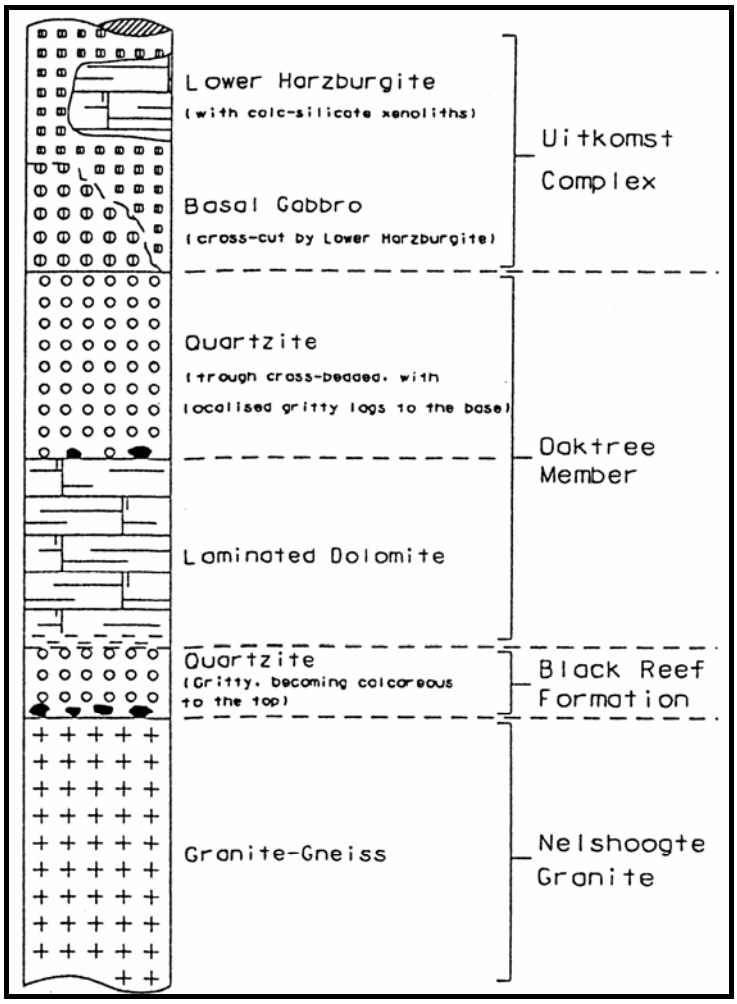

Figure 2. 4: Stratigraphic column of the basal units of the Uitkomst Complex and Transvaal Supergroup which form the host lithologies for the Nkomati Mine massive sulphide ore bodies (Figure from Hornsey, 1999).

2.3.4. Pretoria Group

The Pretoria Group unconformably overlies the chemical sedimentary rocks of the Chuniespoort Group. The Pretoria Group consists predominantly of an alternation of mudrocks and sandstones, together with less significant volcanic horizons, subordinate diamictites and conglomerates. Only rocks of the Rooihoogte and Timeball Hill Formations are preserved in the study area (Figure 2. 5). The base of the Pretoria Group is estimated to be approximately 2281 Ma (Walraven and Martini, 1995).

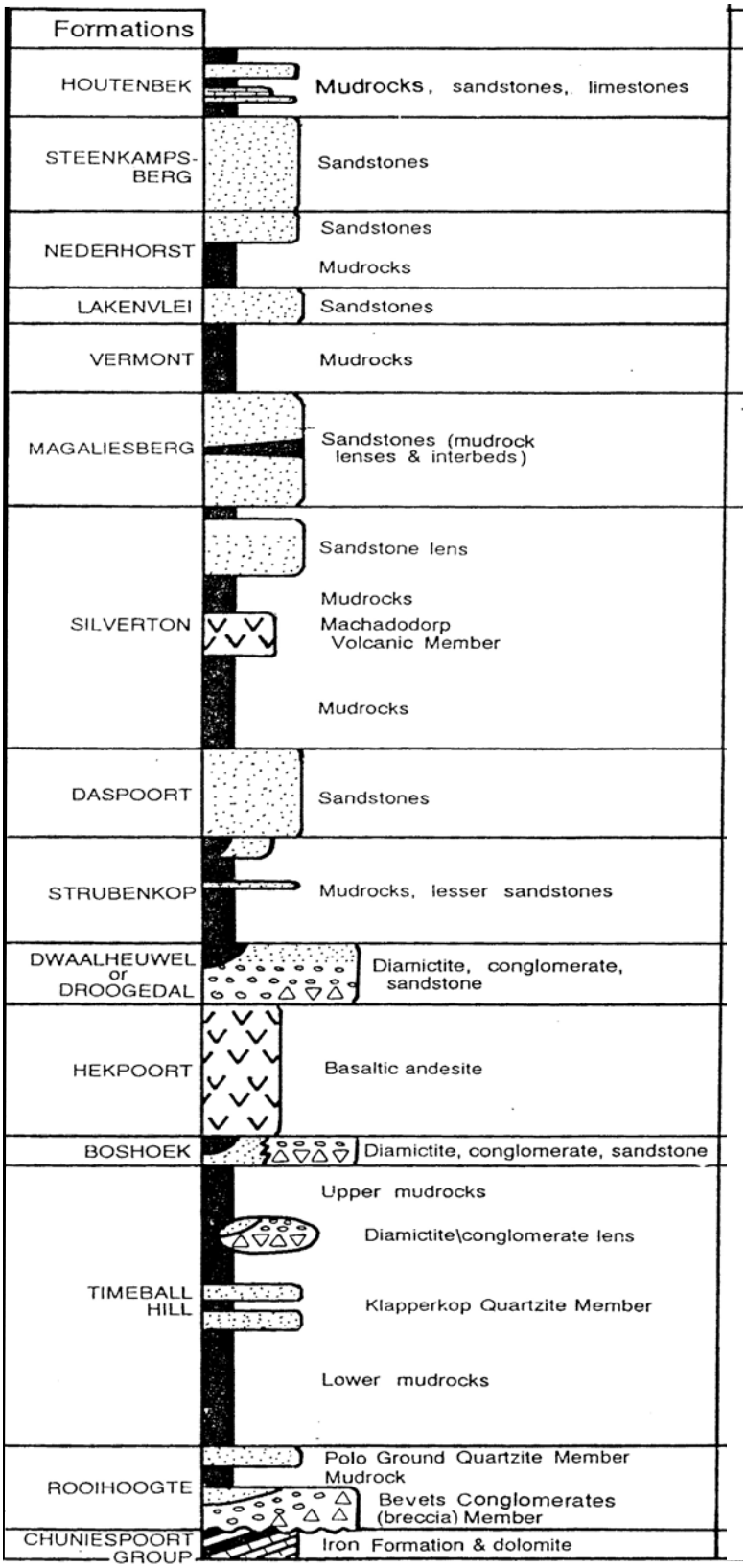

Figure 2. 5: Lithostratigraphy of the formations within the Pretoria Group found in the study area (Figure from Eriksson *et al.*, 1993).

The Rooihoogte Formation is represented by the Bevets Conglomerate Member, which has a thickness of 5-10 m in the study area (Figure 2. 5). It is a chaotic conglomerate of chert clasts set in a dark quartzitic matrix. The clasts were derived from the karst weathering and erosion of the underlying Malmani dolomite (Button, 1986). In those places where the Bevets Conglomerate is in contact with the Uitkomst Complex, it is metamorphosed into a resistant fine-grained quartzite.

The Bevets Conglomerate Member is sharply overlain by the lower shale member of the Timeball Hill Formation. The Timeball Hill Formation is the uppermost sedimentary unit present in the study area (Figure 2. 5) and hosts the upper portion of the Uitkomst Complex. Where it is in contact with the intrusion, the rocks have been metamorphosed to a corundum-andalusite hornfels, forming a 10–50 m thick aureole. The thickness of the Timeball Hill Formation in the study area is *ca*. 1200 m. Immediately above the Bevets Conglomerate Member, the unit is a pyrite-rich, thinly laminated black shale. It is composed predominantly of graphitic, laminated shale and silt with minor beds of quartzite, ferruginous quartzite and ironstone. The ironstones form discrete beds within the sequence, in which the shale becomes progressively more silty, grading through ferruginous quartzite into oolitic ironstone. The quartzitic Klapperkop Member (Figure 2. 5) forms a prominent marker horizon between the lower and upper portion of the Timeball Hill Formation. It consists of upward-coarsening sandstones possessing sedimentary structures compatible with turbidity current sedimentation (Eriksson *et al*, 1993). The base of the Klapperkop Member is highly magnetic due to finely dispersed magnetite. The quartzite forms a prominent escarpment on both sides of the Uitkomst valley since it is relatively resistant to weathering.

2.4 Uitkomst Complex

2.4.1. General

The Uitkomst Complex is a trough-shaped layered mafic-ultramafic intrusion. The intrusion forms three distinct sub-troughs: the deeper, central and upper troughs (von Scheibler *et al*., 1995). However, irregular lateral extensions may occur near the base and top of the body, forming sill-like protrusions (Figure 2. 6). The shape of the body appears to be governed by the nature of the country rock. The basal offshoot protrudes through a layer of dolomite, bounded by quartzite. The upper portion of the lower trough is bounded by conglomerate. In contrast, the central and upper troughs are hosted by shale. This is overlain by the Klapperkop Member quartzite. The exposed lateral extent of the intrusion is approximately 9 km, while it has an approximate thickness of 850 m. The Uitkomst Complex has a northwest-southeast alignment and plunges at approximately 4-8^0 to the west. Several faults are transecting the body.

Several authors (Gauert *et al.*, 1995; de Waal and Gauert, 1997; Gauert, 1998) have proposed that the Complex formed by multiple phases of magma injection. Gauert *et al.* (1995) defined six lithological units of the Uitkomst Complex. Hornsey (1999) added a seventh unit. With minor alterations, this was essentially accepted by Maier *et al.* (2004) and will also be used in the present work.

Table 2.2 presents the general petrography of the rock types constituting the various units.

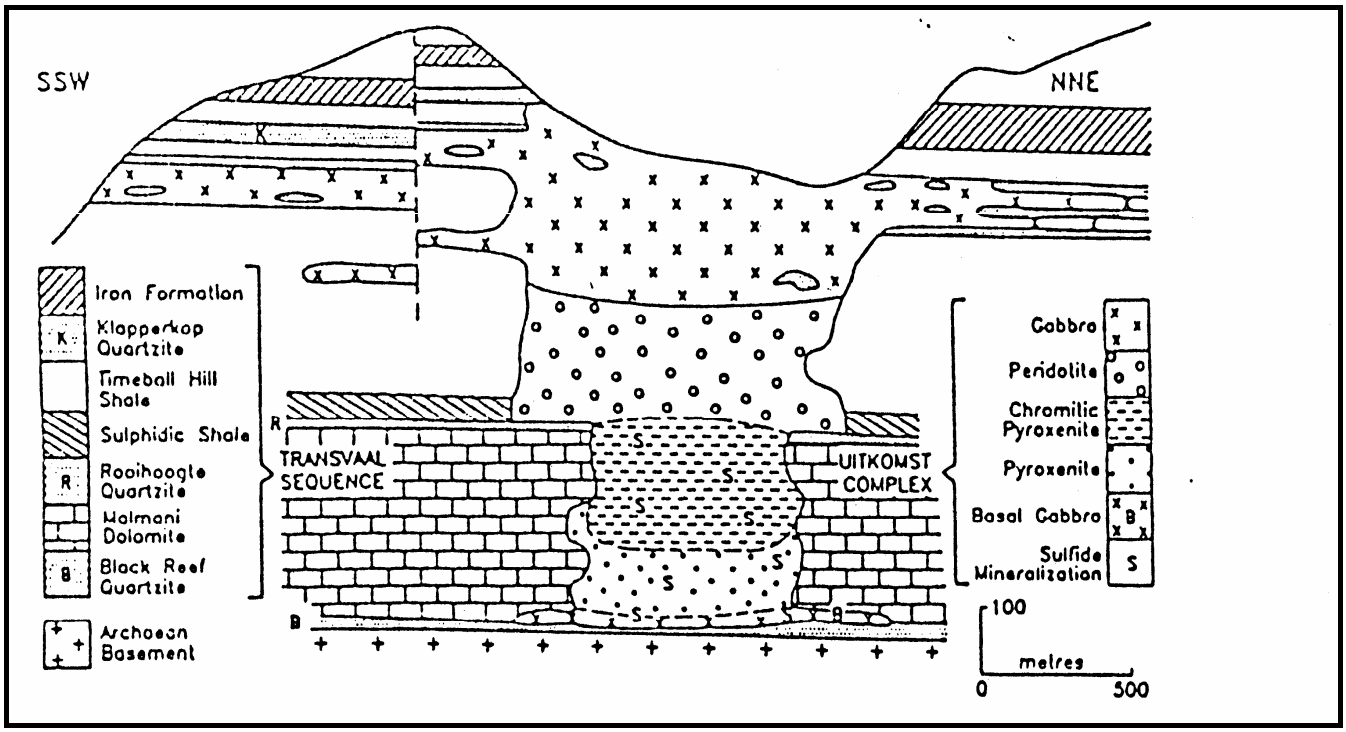

Figure 2. 6: Idealized cross section through the Uitkomst Complex (Figure from von Scheibler *et al.*, 1995).

Table 2. 2: Petrography of the main lithological units of the Uitkomst Complex (From Gauert *et al.*, 1995).

Rock type	Cumulus minerals	Intercumulus minerals	Alteration minerals	Rock unit
Chromitiferous harzburgite	olivine (Fo85-89) chromite (Mg#35-71,Cr#49-65) (poikilitic-textured orthocumulate)	orthopyroxene, clinopyroxene, amphibole, pyrrhotite (Ni0.3-0.7%), pentlandite (Co<0.05%), chalcopyrite (Co<0.05%)	serpentine, magnetite, talc, carbonate, chlorite mica, ferrit-chromite, violarite, mackinawite	Chromitiferous Harzburgite (PCR)
Harzburgite dunite	olivine (Fo86-92) (poikilitic-textured ortho- to mesocumulate)	orthopyroxene (En80-92, Cr 0-1.05%) clinopyroxene (Wo32-43, Mg#55-84, Cr 0.6-1.4%) chromite (Mg#15-72, Cr#43-65) plagioclase (An30-94, Or0-2) phlogopite pyrrhotite (Ni<0.6%) pentlandite (Co<0.5%, As<1.5%) chalcopyrite	serpentine, amphibole, talc, ferrit-chromite, magnetite, sericite, epidote, K-feldspar, chromitiferous mica, chlorite, mackinawite, violarite	Chromitiferous Harzburgite (PCR) Lower Harzburgite (LHZBG) Main Harzburgite (MHZBG) Pyroxenite (PXT)
Olivine- orthopyroxenite	olivine (Fo81-89) orthopyroxene (En80-83) (meso- to adcumulate)	chromite (Mg#13-65, Cr#43-61) phlogopite plagioclase (An30-90, Or0.05-1.8) Clinopyroxene (Wo37) pyrrhotite pentlandite	ferrit-chromite, magnetite, fuchsitic mica, chlorite, sericite, epidote, K-feldspar, amphibole, mackinawite, violarite	Main Harzburgite (MHZBG) Pyroxenite (PXT)
Orthopyroxenite	orthopyroxene (En80-83) (adcumulate)	chromite (Mg#28-57, Cr#45-60 phlogopite	magnetite	Pyroxenite (PXT)
Norite and gabbronorite	orthopyroxene (En48-80) plagioclase (An70-95) clinopyroxene (Wo36-42) (meso- to adcumulate)	phlogopite titanomagnetite pyrrhotite (Ni<0.8%, Co 0.4%, Cu<0.6%) pentlandite (Co<3.2%) chalcopyrite micropegmatite	amphibole, chlorite, sericite, epidote, K-feldspar, fuchsitic mica	Gabbronorite (GN)
Gabbro	plagioclase (An76) clinopyroxene (Wo26-41, Mg#55-57) orthopyroxene (En63-68) olivine (ortho- to mesocumulate with ophitic texture in places)	titanomagnetite ilmenite micropegmatite	magnetite, leucoxene, violarite, mackinawite saussurite, spinel, chlorite	Basal Gabbro (BGAB)

2.4.2. Basal Gabbronorite Unit (BGAB)

A strongly sheared talc-chlorite-carbonate rock defines the contact between the quartzite of the Oaktree Formation and the basal unit of the Uitkomst Complex. Overlying the sheared talc-carbonate rock is a distinct gabbronorite of up to 1.5 m that grades upwards into a phaneritic plagioclase-clinopyroxene rock. The aphinitic rock is generally interpreted to represent the chilled contact facies of the phaneritic gabbronorite. The thickness of the BGAB varies from 0.4 m in the central part of the intrusion to 15 m in the northeastern part of the intrusion. It has an average thickness of about 6 m (Gauert *et al.*, 1995).

The BGAB has sill-like offshoots extending into the sedimentary rocks (Figure 2. 6), and hence is more laterally extensive than the overlying Lower Harzburgite Unit. The offshoots are more common in the northwestern part of the intrusion. The BGAB is not always developed at the base of the Uitkomst Complex. This is particularly notable in the vicinity of the Nkomati Massive Sulphide deposit (Hornsey, 1999). The contact of the BGAB with the overlying Lower Harburgite Unit is gradational, and is often obscured by country rock xenoliths or later diabase sills (Strauss, 1995).

The BGAB is generally pervasively altered, showing intense saussuritization and uralitization. It is also well mineralised, commonly displaying finely disseminated to dense net-textured sulphides (predominantly chalcopyrite) with a high copper content. The mineralisation is mainly confined to the central part of the Complex where the Lower Harzburgite is present. The mineralised portion of the BGAB is referred to as the Basal Mineralised Zone (BMZ).

De Waal and Gauert (1997) recorded the presence of a fine-grained homogeneous gabbroic rock found between the north-eastern sidewall of the intrusion and the layered rocks of the Main Harzburgite Unit. This rock is chemically comparable to the BGAB and is referred to as the Marginal Gabbro.

2.4.3. Lower Harzburgite Unit (LHZBG)

This unit gradationally overlies the Basal Gabbronorite Unit. The Lower Harzburgite Unit has an average thickness of *ca.* 50m (max. 90m). The thickness, however, varies along strike, with an overall thickening towards the northwest (Gauert *et al.*, 1995). The LHZGB is compositionally and texturally very heterogenous. It consists mainly of poikilitic harzburgite, but locally also contains feldspar-bearing lherzolite, sulphide-rich feldspathic wehrlite and amphibolite. The main minerals of this unit include: olivine (up to 50%), orthopyroxene (up to 30%), clinopyroxene (up to 40%), chromite (up to approximately 10%), and plagioclase (up to 10%). The unit is highly altered (serpentinised, saussurised, and uralised) and contains quartzitic and dolomitic xenoliths of country rock which are flattened in the direction of the original sedimentary layering and form rafts that are oriented parallel to the igneous layering. The majority of the dolomite xenoliths are metamorphosed to calc-silicate. Hornsey (1999) observed that the margins of the xenoliths appear to have reacted with the intruding magma. Gauert *et al.* (1995) observed that in the vicinity of the xenoliths, pegmatoids tend to be developed. These pegmatoids consist of coarse-grained clinopyroxene, orthopyroxene, amphibole and plagioclase, with interstitial pyrrhotite, pentlandite, chalcopyrite and magnetite. The LHZBG hosts the bulk of the mineralisation within the Complex, including the Main Mineralised Zone (MMZ). The texture of the mineralisation ranges from net-textured to blebby sulphide pods, to massive sulphide lenses.

2.4.4. Chromitiferous Harzburgite Unit (PCR)

The PCR has a gradational contact with the underlying Lower Harzburgite Unit. The unit has an average thickness of 60 m, but the thickness ranges from 13-82 m due to erosion and thinning of the flanks of the deeper trough (Gauert, 1998). Olivine and chromite are the predominant cumulus phases, while orthopyroxene is the main intercumulus phase, poikilitically enclosing olivine and chromite. Lenses of chromitite progressively increase in abundance towards the top of the unit, becoming more massive and showing well-preserved igneous layering on a decimetre-scale (Gauert *et al.*, 1995). The top of the unit is defined by a massive chromite layer 3-14 m thick. Sulphides may constitute 1-5% of the unit. The original magmatic minerals are pervasively altered to talc, carbonate, phlogopite, chlorite and serpentine. Unlike in the underlying units, there is an almost total absence of any xenoliths in

this unit.

2.4.5. Main Harzburgite Unit (MHZBG)

The MHZBG forms the bulk of the Uitkomst Complex. It has an average thickness of 330 m and constitutes more than a third of the total thickness of the Uitkomst Complex. The MHZBG is best exposed from the northwestern part of the farm Uitkomst 541JT to the centre of Slaaihoek 540JT. The unit extends laterally for about 200m over the margin of the lower trough. The unit is composed predominantly of serpentinised harzburgite grading locally into pyroxenite and dunite (Gauert *et al.*, 1995). Olivine, chromite and orthopyroxene are the main phases. A distinct poikilitic texture is developed with the olivine and chromite forming chadacrysts within oikocrysts of orthopyroxene. The unit shows a weak metre-scale layering caused by modal and grain-size variations. However, there is a subtle facies change to the northwest, where the mineral layering becomes more prominent, and the dunitic layers more abundant. This coincides with the appearance of numerous thin chromitite layers (Hornsey, 1999).

The MHZBG is poorly mineralised in terms of sulphides. Elevated concentrations of pyrrhotite are confined to the lower 50-70 m of the unit (Hornsey, 1999).

2.4.6. Pyroxenite Unit (PXT)

The PXT has a transitional contact with the underlying MHZBG. Feldspathic pegmatites are often developed at the contact. In areas were the unit is fully developed, it has an average thickness of 60 m. Gauert *et al.* (1995) subdivided the PXT into three sub-units: a lower olivine-orthopyroxenite overlain by a homogeneous orthopyroxenite (with minor accessory chromite and sulphide), and an upper noritic and gabbronoritic zone that shows increasing amounts of plagioclase and clinopyroxene. The appearance of plagioclase as the main phase in the upper portion of the PXT indicates that the unit forms a transitional sequence between the lower ultramafic units and the overlying Main Gabbronorite Unit. The PXT is relatively unaffected by secondary alteration. The unit is sparsely mineralised with the concentration of the sulphides rarely greater than 1 modal %.

2.4.7. Main Gabbronorite (MGN) and Upper Gabbronorite Units (UGN)

Several authors (Gauert, 1998; Hornsey, 1999; etc) referred to these units as the Gabbronorite Unit (GN). Based on trace element data (Gomwe, 2002; Maier et al., 2004) the GN was found to consist of two distinct units (the MGN and the UGN). Due to their low economic importance, the MGN and UGN remain poorly studied.

The average thickness of the MGN is approximately 262 m (Theart and de Nooy, 2001). The unit is lithologically heterogeneous and ranges from a basal noritic rock (orthopyroxene-plagioclase cumulate), through gabbro, to diorite in the upper parts. The diorite is highly enriched in incompatible elements such as Zr, P, Nb, Y and LREE and represents the most differentiated rocks of the Uitkomst Complex (Gomwe, 2002).

The UGN represents the uppermost unit of the Uitkomst Complex. The contact between the MGN and the UGN is marked by a 5.5 m magmatic breccia of diorite. The UGN displays strong alteration, with the rocks consisting of saussuritized plagioclase, tremolite, chlorite and biotite. The rocks of the UGN are more primitive than the underlying diorites, indicated by a sharp reversal towards higher whole-rock MgO, Ni and Cr contents, followed by about 72 m of gabbronorite grading upward into leucograbbronorite (Maier *et al.*, 2004). The normal differentiation trend observed for this unit could indicate that the UGN represents a distinct, older, intrusive phase of the Uitkomst Complex (Maier *et al.*, 2004). This is contrary to the model presented by Gauert *et al.* (1995), where it was proposed that the UGN represents crystallization at the roof of the initial magma pulses intruding the Complex. The unit displays a well-defined aphanitic chill zone against the roof rocks which consist of shale of the lower Timeball Hill Formation (Figure 2. 20) (De Waal *et al.*, 2000).

2.4.8. Massive Sulphide Body (MSB)

According to Gauert *et al.* (1995), the sulphide mineralisation in the Uitkomst Complex occurs as:

1. finely disseminated sulphides;
2. local concentrations of coarse-grained and pegmatoidal sulphides;
3. net-textured sulphides enclosing olivine and orthopyroxene; and

4. a massive sulphide ore body

Generally, the sulphides are more abundant near xenoliths of country rock in the lower part of the Complex. The massive sulphide ore body is stratigraphically situated in the footwall lithologies of the Uitkomst Complex. Minor lenses of massive sulphide are additionally found in the BGAB and the LHZBG (Hornsey, 1999). Figure 2. 7 shows a plan view of the three lenticular bodies (lenses 1, 2, 3) of predominantly massive sulphide of the Nkomati Massive Sulphide Deposit. The maximum thickness of the ore body is about 20 m. It consists mainly of massive pyrrhotite. Smaller amounts of pentlandite, chalcopyrite, pyrite and magnetite are also found. Theart and de Nooy (2001) describe a variety of PGE-bearing minerals.

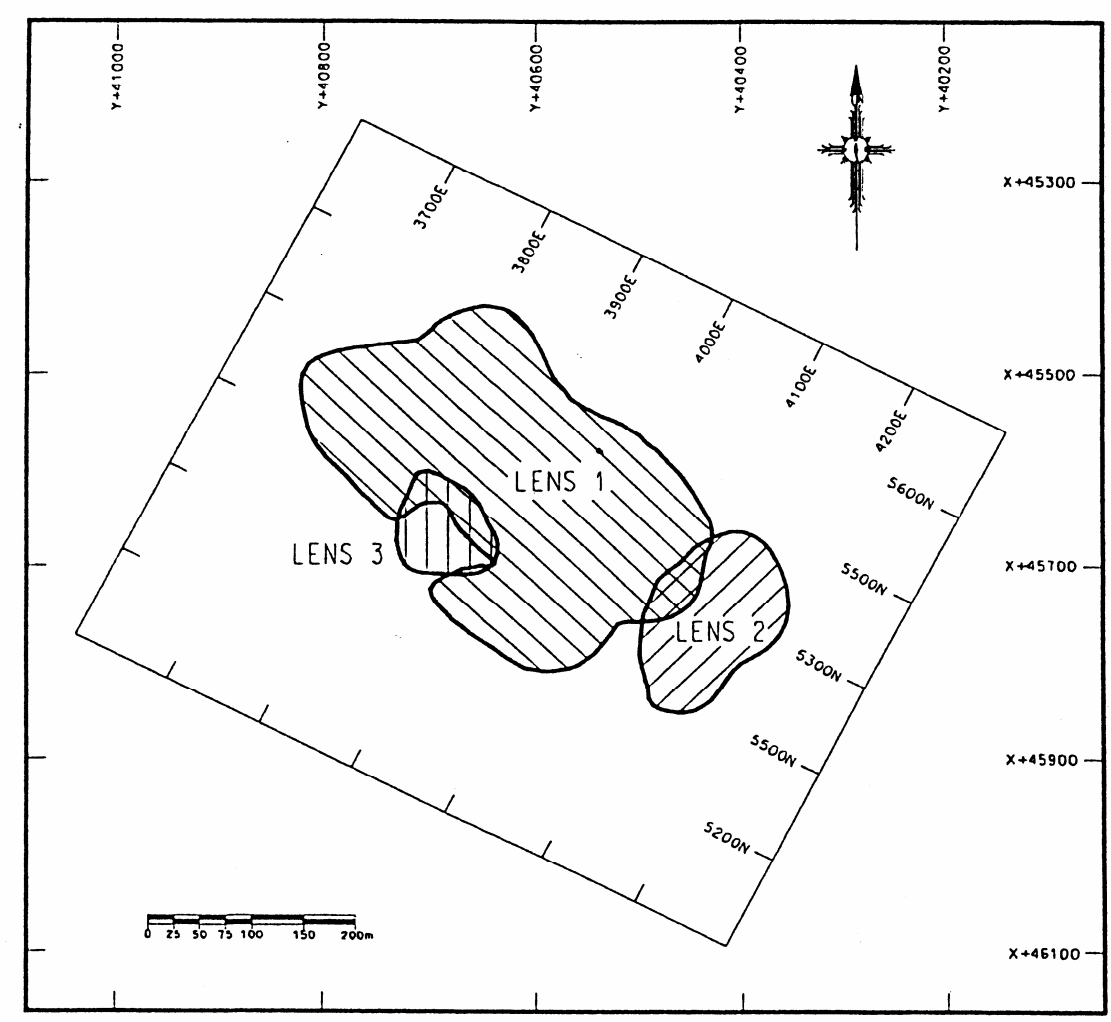

Figure 2. 7: Plan of the Nkomati massive sulphide ore bodies, illustrating their spatial extent (Figure from Hornsey, 1999).

For the purpose of this study, special consideration will be given to the presence of xenoliths found in the vicinity and enclosed by the MSB; particularly that of Lens 1. In addition to this, xenoliths associated with the Basal Mineralised Zone (BMZ) as well as Main Mineralised Zone (MMZ) are also considered.

2.5. Diabase intrusions

These intrusions consist mainly of sills and, to a lesser extent, dykes that cross-cut the Uitkomst Complex. Hornsey (1999) records three sets of dykes in the study area. The diabase sills are inferred to be of post-Bushveld age (Boer et al., 1995). These sills are fine- to medium-grained, grey-green rocks. They contain characteristic chill zones on their upper and lower boundaries, and are concordant to the host lithologies of the Uitkomst Complex. Their thickness ranges from less than 1 m to 30 m. They have a gabbroic composition with the main mineral phases being pyroxene, altered plagioclase, hornblende, biotite, and opaque minerals. Minor phases include quartz, calcite, chlorite and epidote. Minor sulphide mineralisation is present in some of these diabase sills, probably having formed as a result of contamination with material from the Complex (Kenyon *et al.*, 1986*).*

3. DISTRIBUTION AND DESCRIPTION OF XENOLITHS

3.1. General

The abundance of country rock xenoliths associated with the mineralisation in the Uitkomst Complex is not an isolated geological occurrence. The presence of country rock xenoliths associated with mineralisation has also been observed in other conduit-type intrusions, for example at the Voisey's Bay Ni-Cu deposit (Li and Naldrett, 2000). Although previous considerations have been given to the Uitkomst Complex xenoliths (for example: Gauert *et al*., 1995; von Scheibler *et al*., 1995; Gauert, 1998; etc), no detailed study has been carried out on the xenoliths and their relationship to the Uitkomst magma. This chapter provides a detailed description of the country rock xenoliths found associated with the intrusive rocks and the sulphide mineralisation. Consideration is given to the physical, textural and mineralogical relationships between the xenoliths and the magma.

3.2. Xenoliths associated with the Massive Sulphide Body (MSB)

Four dominant types of country rocks occur as xenoliths within the massive sulphide ore body of the Uitkomst Complex. These include:

- Quartzite
- Granite
- Dolomite
- Calc-silicate.

The mapped panel of Lens 1 (P29E N/SW) only contained quartzite and granite xenoliths (Appendix A). Further observations regarding the petrology and textures of the country rock xenoliths were made on borehole core (Appendix B) as well as hand specimens.

Dolomite xenoliths, possibly sourced from the Malmani Formation, were observed along other panels of Lens 1 (Figure 3. 1). The dolomite xenoliths occur as large (up to 10s of square metres), subangular, elongate inclusions within the Massive Sulphide Body (MSB). Both layered and massive dolomite xenoliths were observed. They have undulose, irregular contacts with the MSB, without apparent reaction rims. Whereas the MSB consists predominantly of pyrrhotite, elevated concentrations of pentlandite, chalcopyrite and pyrite are found near the contact with the dolomite, and forming veinlets and disseminated clusters within the dolomite. Commonly, chalcopyrite, with lesser amounts of pyrite, becomes relatively more abundant the further one moves into the dolomite. Pentlandite is more common along the contacts of the dolomite xenolith and the mafic host rock.

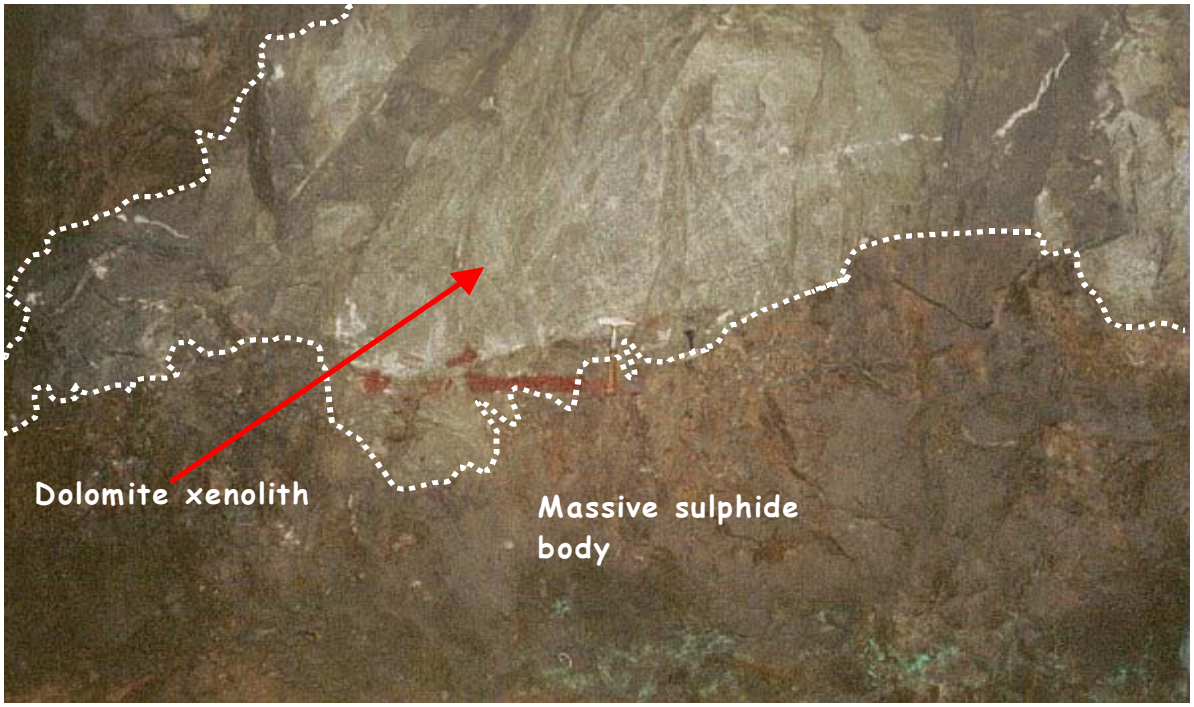

Figure 3. 1: Large dolomite xenolith (~8 m^2) found within the Massive Sulphide Body (Lens 1, P25E /SW). Geological hammer at the contact between the dolomite xenolith and the MSB is 40 cm long.

The majority of the original dolomite xenoliths have undergone alteration to form skarns (calc-silicate mineralisation). This is most apparent in the smaller xenoliths (eg Figure 3. 6).

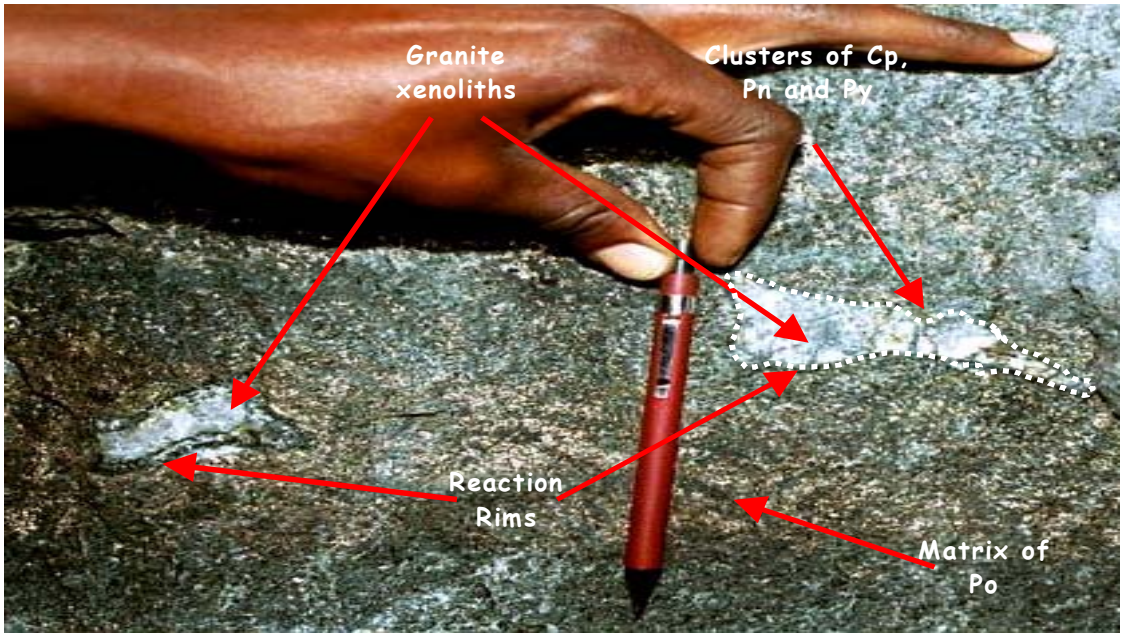

Figure 3. 2: Small granite xenoliths (~3cm long) found in the Massive Sulphide Body (P29E N/SW). Reaction rims are prominent around the edges of the xenoliths. Clusters of pentlandite (Pn), chalcopyrite (Cp) and pyrite (Py) are prominent within the xenoliths and along the edges of the xenoliths. The dominant sulphide in the matrix is pyrrhotite (Po). The pencil used for scale is 13 cm long.

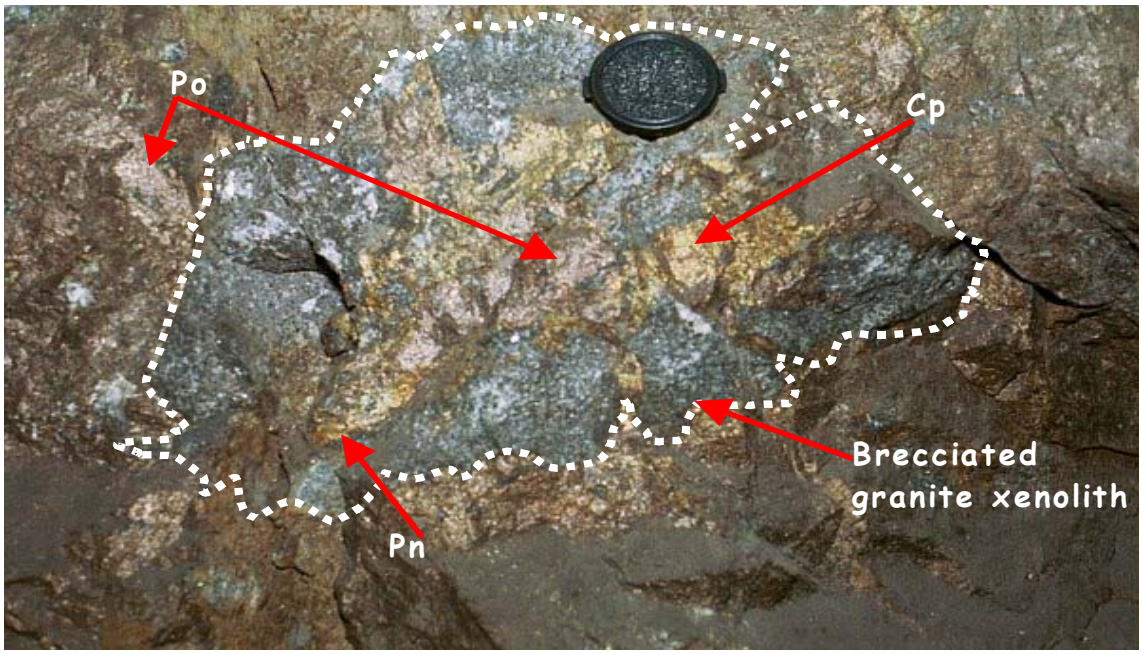

Figure 3. 3: Brecciated/fractured zone at the contact of the granite xenolith with the sulphide mineralisation (P29E N/SW). Veins of sulphide intrude the granite xenoliths. Chalcopyrite is the predominant sulphide mineral associated with the granite xenolith.

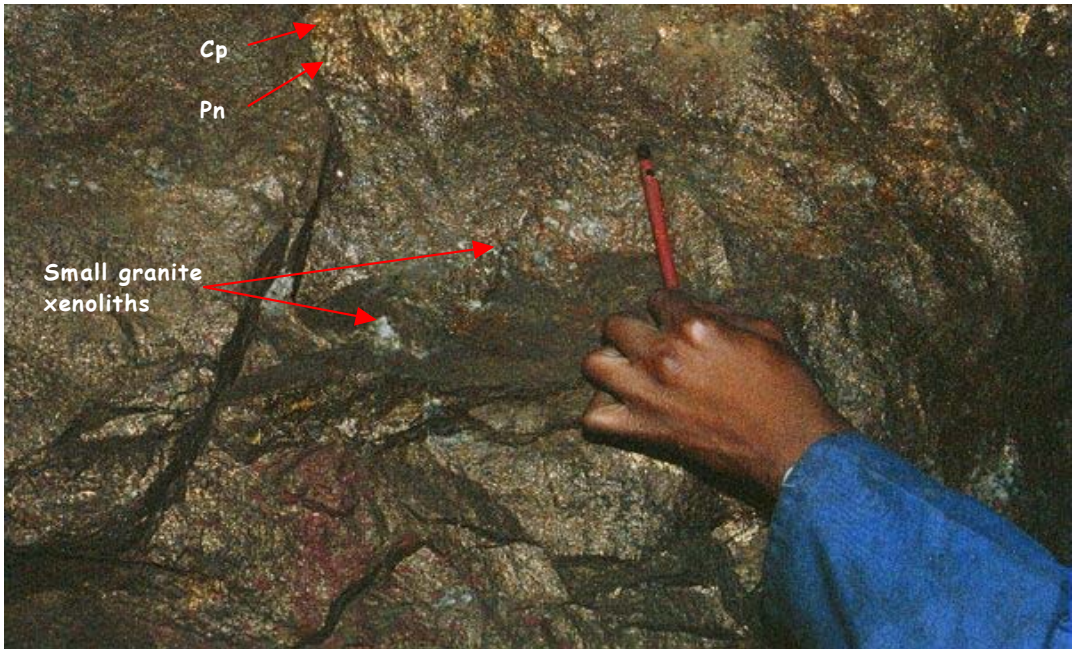

Figure 3. 4: Small (mm-scale) granite xenoliths found in the MSB (P29E N/SW). The MSB consists predominantly of pyrrhotite (Po), whereas clusters of chalcopyrite (Cp) and pentlandite (Pn), sometimes associated with pyrite, are found in the immediate vicinity of the xenoliths.

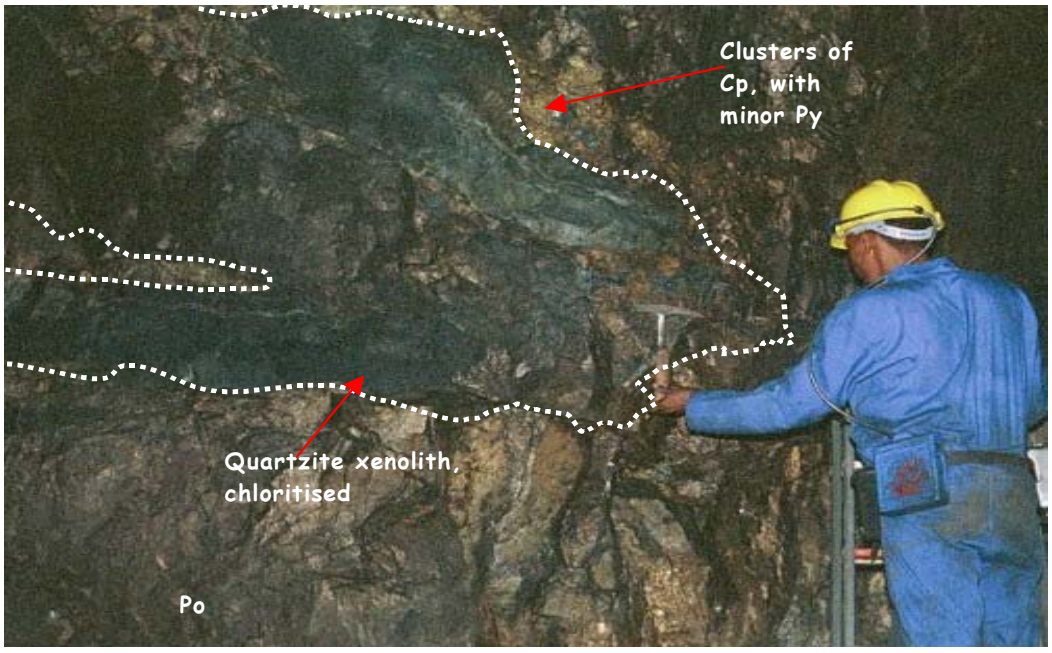

Figure 3. 5: Irregularly shaped quartzite xenolith (demarcated for clarification) found associated with the MSB (P29E N/SW) The xenolith is surrounded by clusters consisting of chalcopyrite (cp), with minor amounts of pyrite (py). The concentrations of these clusters decrease with increasing distance from the xenolith.

Quartzite and granite xenoliths (Figure 3.2 – Figure 3.5), possibly sourced from the Black Reef Formation and the Nelshoogte Granite basement respectively, form the majority of xenoliths observed within the MSB. The xenoliths range in size from about 1 mm^2 up to *ca.* 64 m^2. Granite xenoliths are the most abundant and contain very distinct, dark reaction rims along the edges. The shapes of the granite xenoliths vary but are generally angular to sub angular. Some xenoliths show elongation in an E/W direction, parallel to the base of the intrusion. Concentrations of pentlandite and chalcopyrite, and in some cases pyrite, are found around the xenoliths. Fine disseminations and veinlets of sulphides are also found in the interior of the xenoliths analogous to the dolomite xenoliths described above. Whereas pentlandite is more abundant at the contacts between the xenoliths and the mafic host rock, chalcopyrite and pyrite are the more sulphide minerals hosted in the veinlets within the xenoliths. In some cases small granite xenoliths have been completely replaced by sulphide, with only a dark amphibolitic alteration halo indicating the position of the original rock. Another common feature of the granite xenoliths found within the MSB is that they tend to break up into smaller fragments at their margins (Figure 3. 3, Appendix A).

A common feature observed within the MSB is the presence of small rafts of elongate granite xenoliths (Figure 3. 2). These xenoliths possibly represent the broken-up veins of partial melts of the pelitic country rock. Tischler *et al.* (1981) describes a similar occurrence in the Insizwa Complex.

Quartzite xenoliths found within the MSB display green chloritisation (Figure 3. 5). They show a range in size, but generally tend to be a few cm^2 in area. Most of the quartzite xenoliths have a very distinct, darkly coloured, thin (0.5 cm) reaction rim at the contact between the massive sulphides and the quartzite. Brittle fragmentation similar to that observed in the granite xenoliths is also observed in the case of the quartzite xenoliths. Localised sulphide mineralisation within the quartzite xenoliths consists of clusters comprising predominantly of chalcopyrite, pentlandite and smaller amounts of pyrite. The sulphide mineralisation occurs in veinlets or cavities caused by the partial

assimilation of the xenolith. The larger-sized quartzite xenoliths display a distinct mineral zonation, with hydrous minerals forming at the interface between the xenoliths and the magma, whereas the interior of the xenoliths tend to consist of relatively pristine quartzite.

The mineralogical and textural relationships of the sulphides in the intrusive rocks and the country rock xenoliths are discussed further in §3.3. The immediate contacts between the xenoliths and the sulphides commonly consist of a prominent pentlandite layer (Figure 3. 6) or clusters consisting of chalcopyrite and pyrite (Figure 3. 8 and Figure 3. 9). The rest of the massive sulphide stringers consist mainly of pyrrhotite. Disseminated pyrite becomes more dominant in the interior of the xenolith, away from the contact with the magma.

The contacts between the xenoliths and the sulphides are undulating. In some instances these contact zones display very prominent reaction rims consisting of a thin zone (a few mm in thickness) of darkly coloured hydrous minerals. These reaction rims are commonly associated with the quartzite and granite xenoliths and are less commonly associated with the calc-silicate xenoliths (Figure 3. 9). No reaction rims are found associated with the dolomite xenoliths.

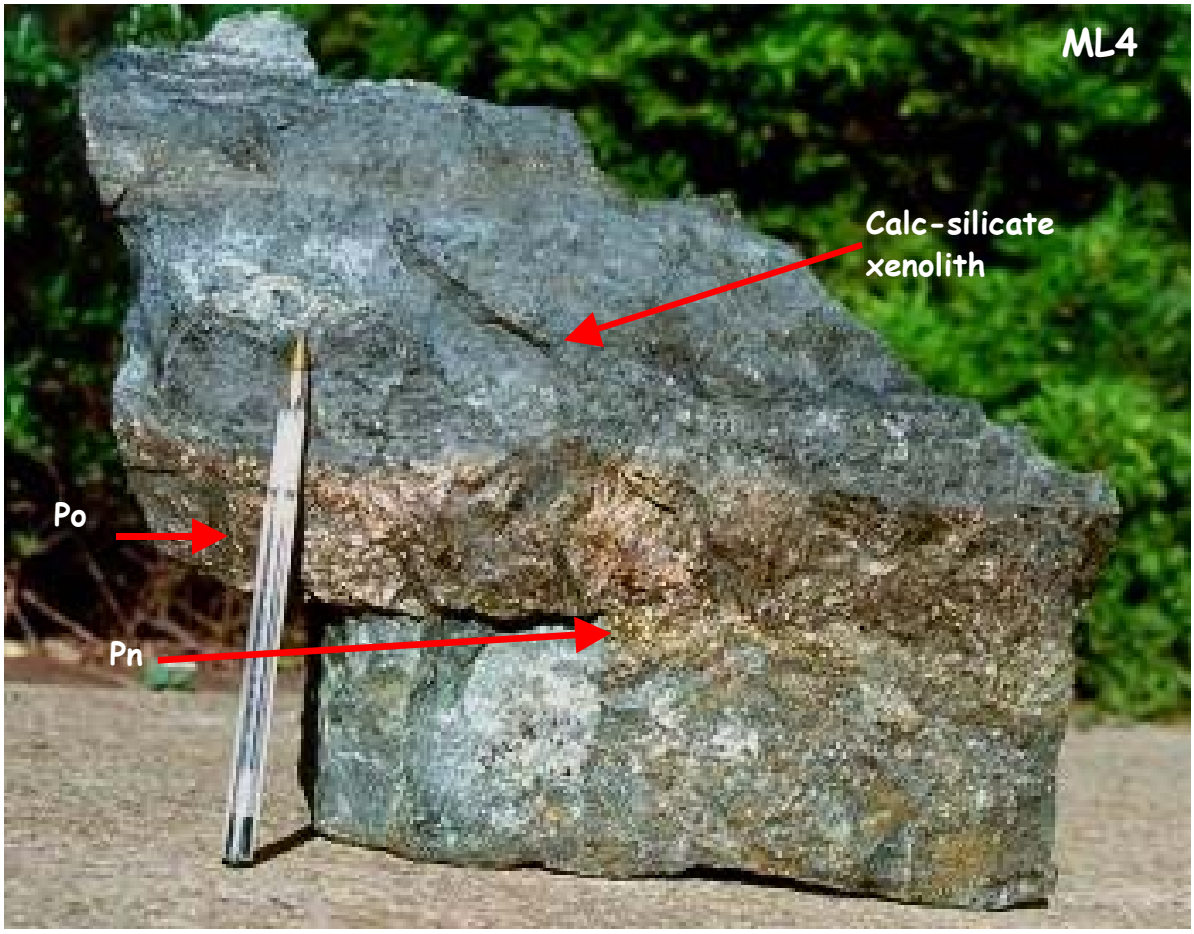

Figure 3. 6: Massive sulphide stringer consisting of pyrrhotite and a layer of pentlandite in contact with a layered calc-silicate xenolith. Sample Number ML4 taken from the upper stringer zone (Lens 2) above the MSB.

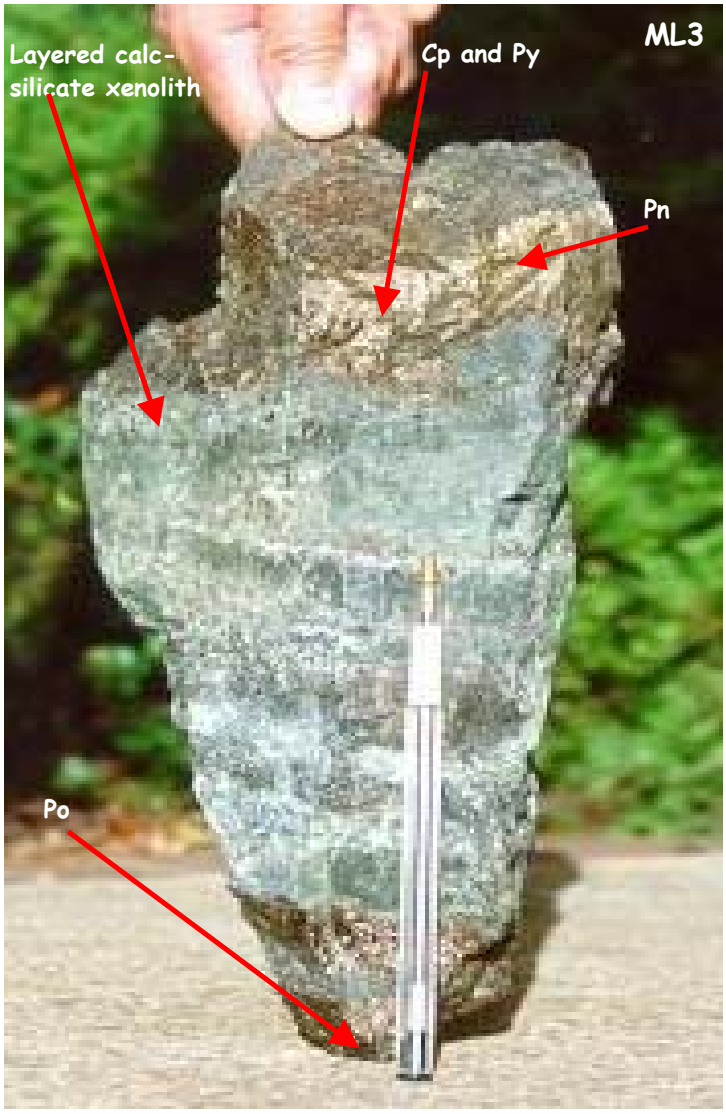

Figure 3. 7: Layered calc-silicate xenolith with massive sulphide (pyrite, pentlandite, chalcopyrite, pyrrhotite). The contacts between the sulphides and the xenolith are irregular and undulous, and are sometimes demarcated by a reaction rim. The contact zone also contains distinct "blebs" of scattered pyrite. Clusters or blebs of sulphide (predominantly pentlandite and chalcopyrite) are found within the xenolith, particularly along bedding planes. Sample Number ML3 taken from the upper stringer zone (Lens 2) above the MSB.

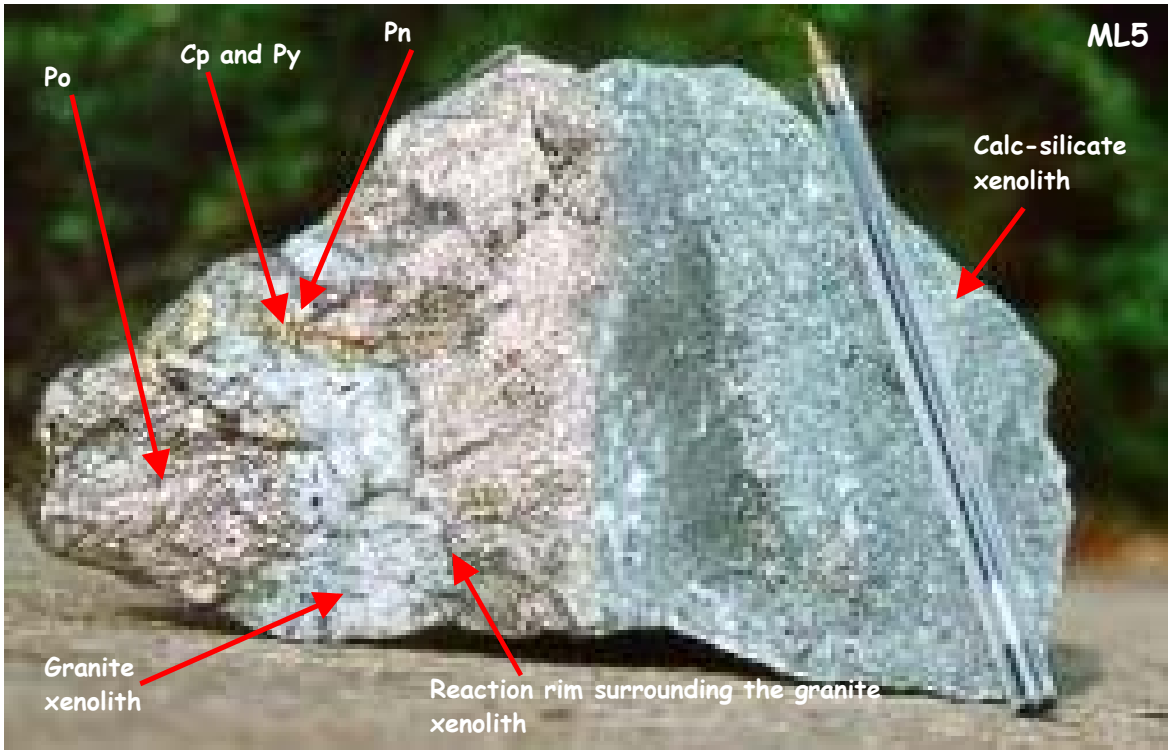

Figure 3. 8: Two xenoliths (granite and calc-silicate) separated by massive sulphide stringer consisting predominantly of pyrrhotite (Po). Clusters of pentlandite (Pn), chalcopyrite (Cp), together with pyrite (Py) are found along some contacts of the granite xenolith and in some instances infiltrating into the granite xenolith. A distinct reaction rim is present around the granite xenolith marking the wavy contact between the granite xenolith and the sulphide stringer. Disseminated sulphide grains occur within the calc-silicate xenolith. No reaction rim is present, but the contact between the calc-silicate xenolith and the sulphide stringer is very sharp.

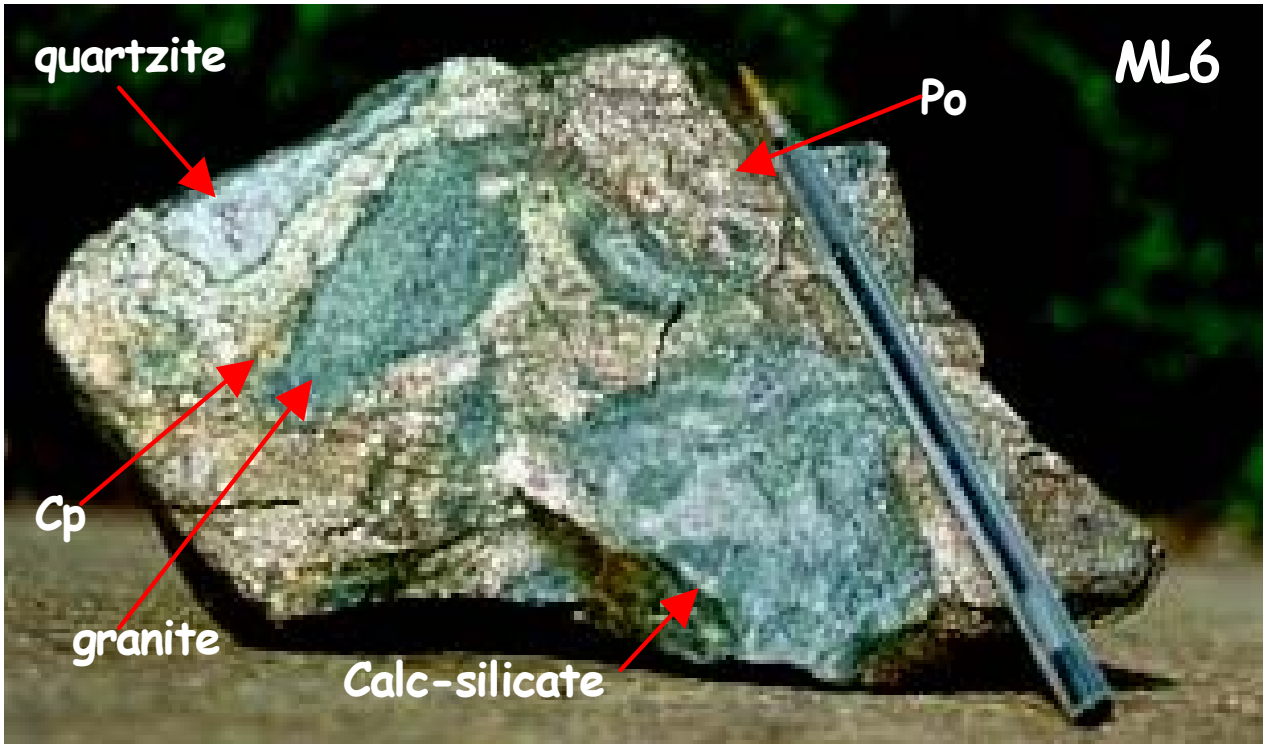

Figure 3. 9: Hand specimen (ML6) containing about 8 small xenoliths (*ca.* 3cm in width and *ca.* 6cm in length) that vary in shape (subrounded to angular) and in lithology (quartzite, granite, calc-silicates). The xenoliths are encased by massive sulphide mineralisation. Prominent reaction rims are observed on the outer edges of the granite and quartzite xenoliths, where they are in contact with the massive sulphide.

3.3. Xenoliths associated with the Basal Mineralised Zone (BMZ)

The Basal Gabbronorite unit directly overlies the quartzite member of the Oaktree Formation. The ores within the Basal Gabbronorite are referred to as the Basal Mineralised Zone (BMZ; Anonymous, 1996). This zone is exposed in the face of the Bulk Sample Drive of the Nkomati Mine, on which the following description is based. A map showing the relationships between the xenoliths and the magma is provided in Appendix A.

Two types of xenoliths are associated with the BMZ:

1. Dolomite xenoliths associated with massive sulphide stringers at the base of the unit, and
2. Calc-silicate xenoliths associated with coarse-grained gabbro.

The calc-silicate xenoliths associated with the BMZ have particularly high length – height ratios, i.e. they can be laterally very extensive (Figure 3. 10 and Figure 3. 11). The width of the elongate calc-silicate xenoliths varies from ~0.5 m - 0.25 m along the lateral extent of the xenolith (~2m – 5 m).

The sulphide mineralogy associated with the immediate exterior of the xenoliths consists primarily of chalcopyrite with some pyrite. The sulphide mineralogy in the interior is different in that it consists predominantly of clusters of disseminated pyrite. The pyrite can extend up to 0.3 m into the interior of the xenolith. Commonly, the pyrite mineralisation is concentrated along the bedding planes within the xenolith. Coarse-grained, pegmatoidal gabbro may underlie some of the calc-silicate xenoliths (Figure 3. 11), and the pegmatoidal gabbro tends to be enriched in large quartz grains (Figure 3. 12). The gabbroic rocks that are not in the immediate contact with the xenoliths are poorly mineralised or, in some cases, barren.

Significant sulphide mineralisation is associated with the wedge - shaped dolomite xenolith that occurs at the base of the unit (Figure 3. 10). The bottom of the xenolith is in direct contact with massive sulphide mineralisation. Stringers of massive sulphide

penetrate the xenolith forming finger-like structures (Figure 3. 13). The massive sulphide stringers consist predominantly of pyrrhotite. However at the immediate contact between the xenolith and the ore chalcopyrite and pyrite predominate. Disseminated sulphide mineralisation is found in the interior of the dolomite xenolith, up to 15 cm from the margins. This consists predominantly of pyrite. The pyrite mineralisation is found along the bedding planes of the dolomite (Figure 3. 15). No alteration rim is evident between the dolomite xenolith and the surrounding massive sulphides.

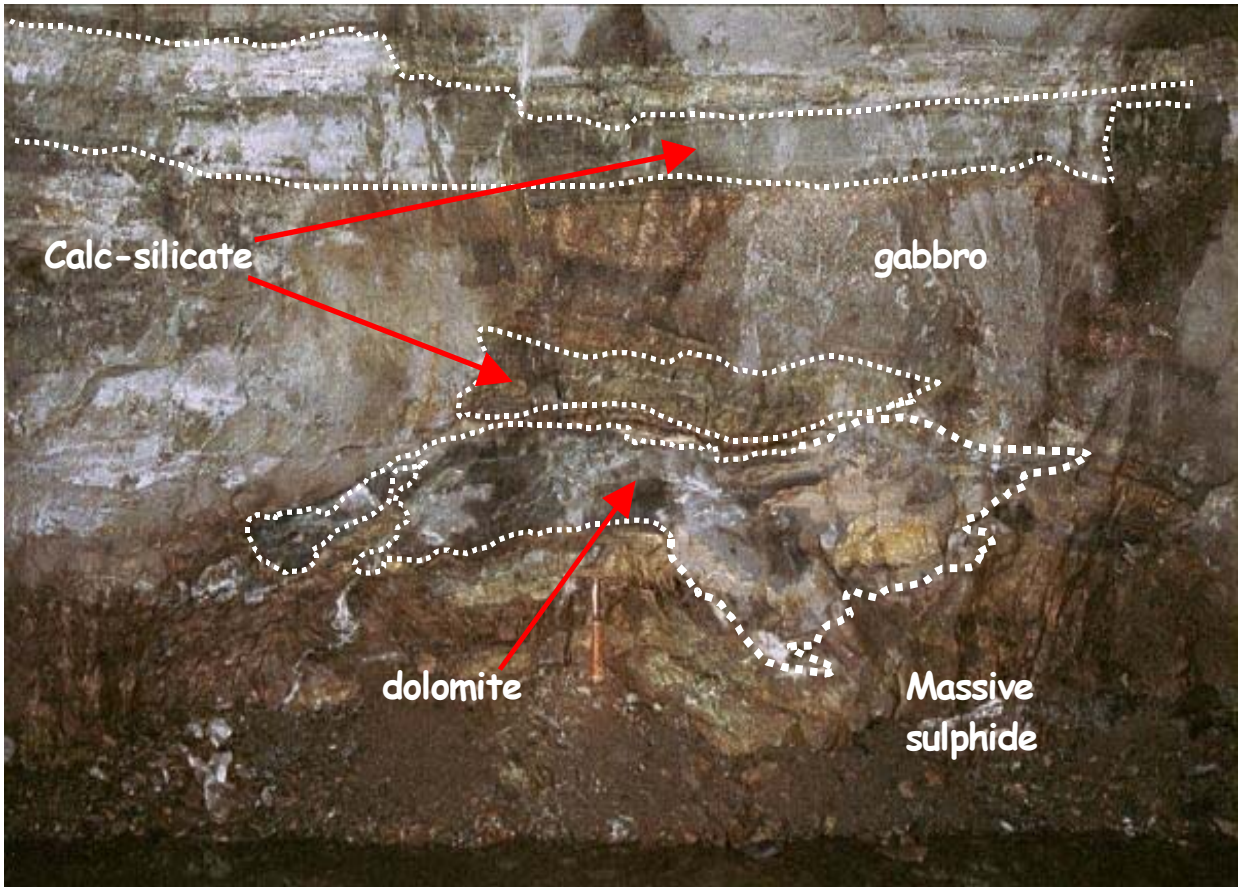

Figure 3. 10: Dolomite and calc-silicate xenoliths with variably mineralised gabbro in the Basal Mineralised Zone (BMZ) of the Uitkomst Complex. The upper calc-silicate xenolith is elongated parallel to the layering, while the lower calc-silicate xenolith is wedge-shaped, pinching out towards the margins. The dolomite xenolith also pinches out towards the margins. Bulk Sample Drive.

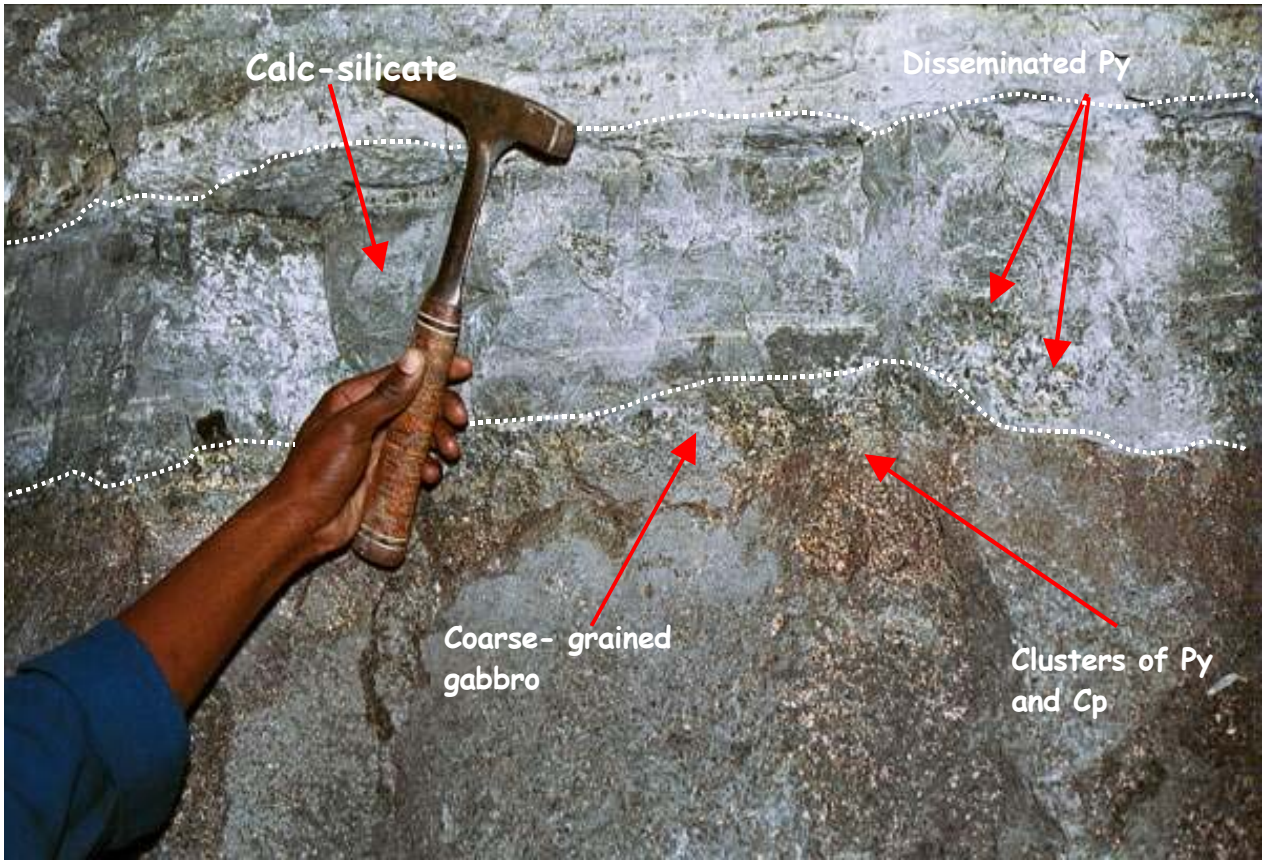

Figure 3. 11: The calc-silicate xenolith is underlain by coarse-grained gabbro, which is in turn underlain by a zone of mineralised gabbro. The disseminated mineralisation at the boundary between the coarse-grained gabbro and the calc-silicate dolomite consists predominantly of pyrite. The amount of sulphide increases with depth forming disseminated and semi-massive ores containing pyrite, chalcopyrite, pyrrhotite, and in some cases pentlandite. Bulk Sample Drive.

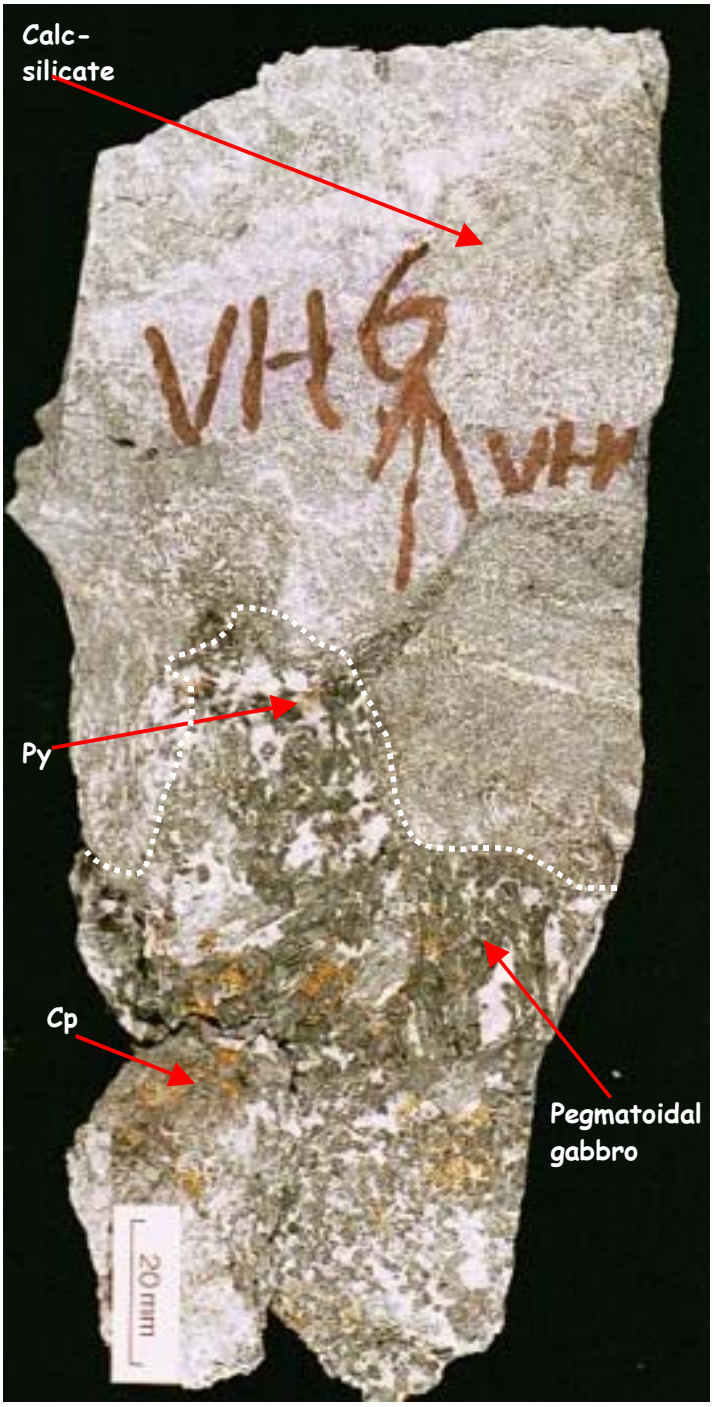

Figure 3. 12: Hand specimen from the BMZ bulk sample drive, showing the development of sulphides in the pegmatoidal gabbro close to the contact with the calc-silicate xenolith. Sample Number: VH6.

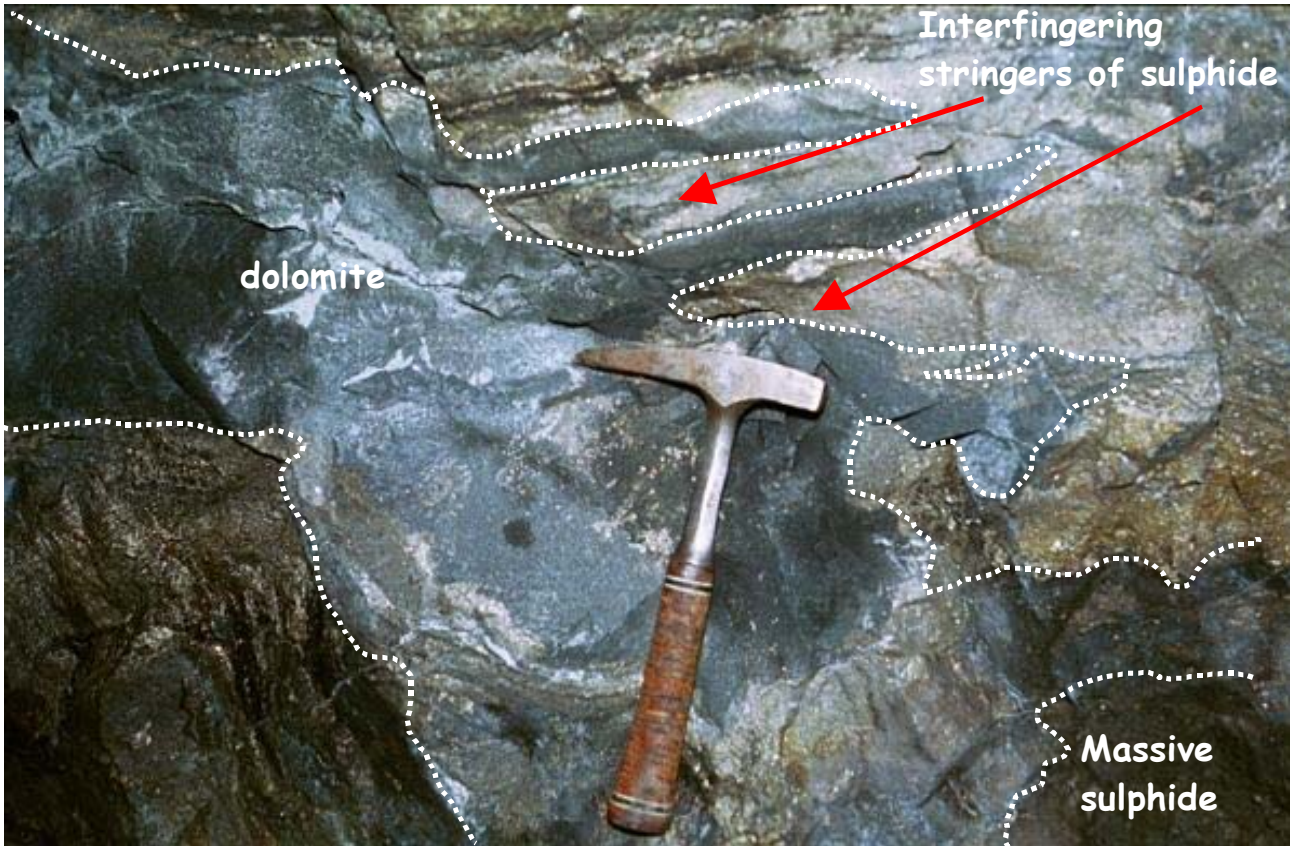

Figure 3. 13: Stringers of sulphide interlayered with dolomite xenolith in BMZ. Note disseminated sulphides within the xenolith.

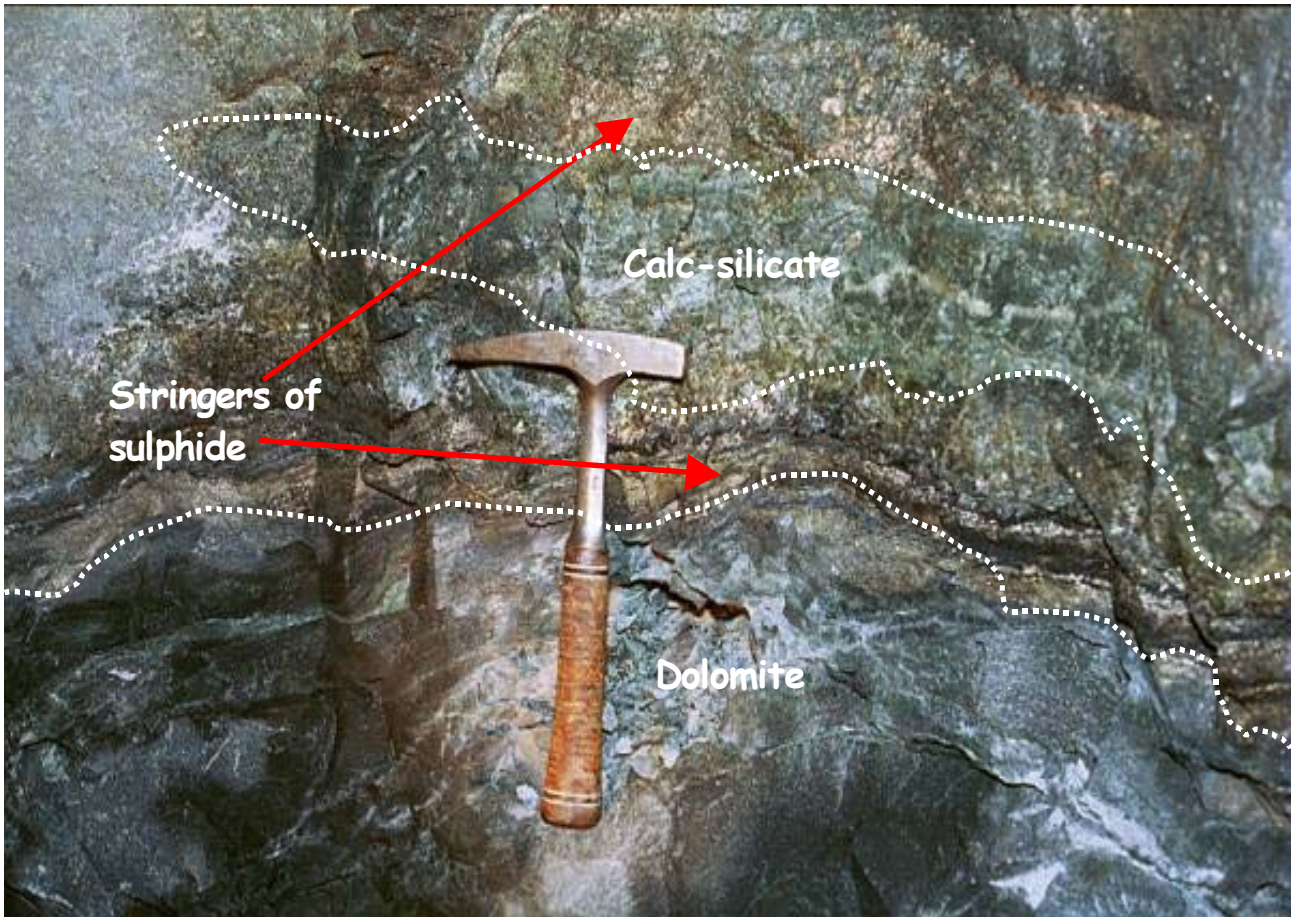

Figure 3. 14: Calc-silicate and dolomite xenoliths within a matrix of semi-massive sulphide of the BMZ. Bulk Sample Drive.

Figure 3. 15: Hand specimen showing pyrite (Py) mineralisation along the bedding planes in the dolomite xenolith. Sample Number: VH3. Bulk Sample Drive, BMZ.

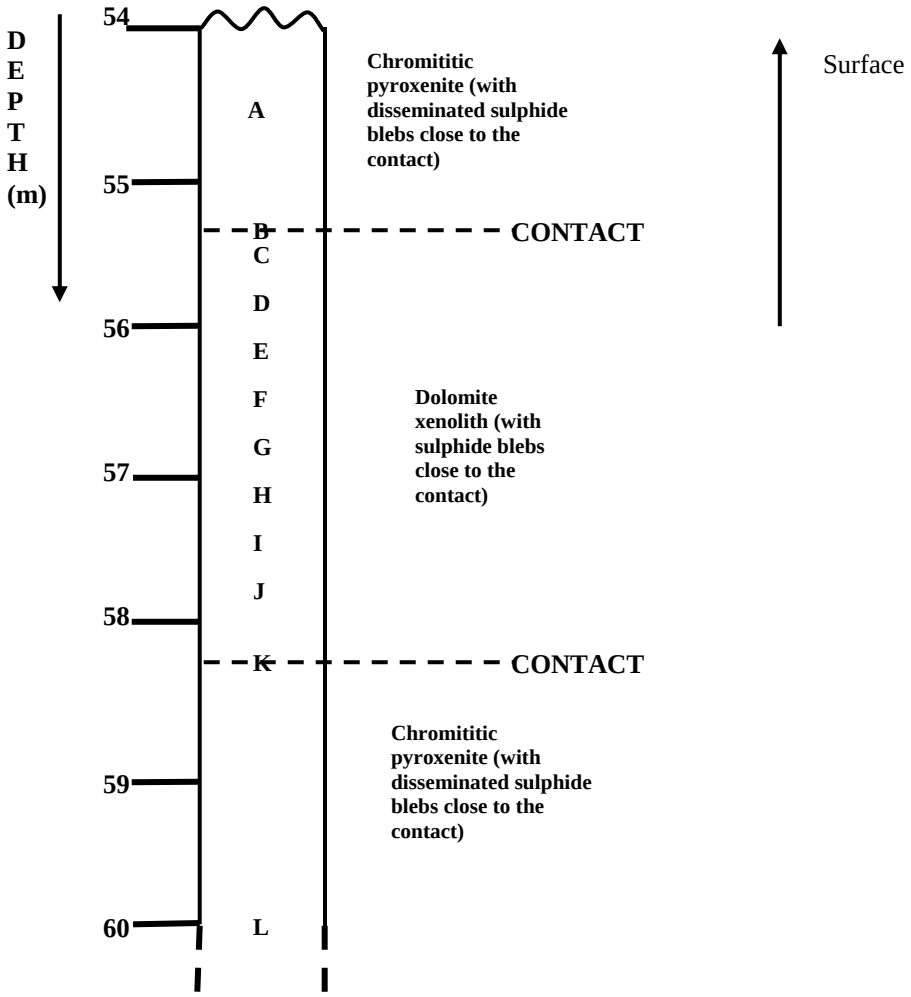

Figure 3. 16: Schematic log of borehole UK119, indicating the positions of the sections used for petrographic and chemical analyses. Also shown are the positions of the contacts between the intrusion and the dolomite xenolith. Sulpide mineralisation (pyrite and chalcopyrite) is associated with the contact zones.

3.4. Xenoliths associated with the Main Mineralised Zone (MMZ)

The mineralisation associated with the Lower Harzburgite Unit (LHZBG) is referred to as the Main Mineralised Zone (MMZ). It hosts the bulk of the sulphides within the Uitkomst Complex (Anonymous, 1996). The LHZBG unit is situated within well-bedded dolomite and chert that immediately overlies the quartzites of the Oaktree Formation. The unit is characterised by an abundance of dolomite xenoliths that have been altered to calc-silicates. Approximately one third of the stratigraphic thickness of the LHZB unit is composed of xenoliths.

At the time of this study, the Main Mineralised Zone at the Nkomati Mine could not be accessed. However, a hand specimen was available for the study (Figure 3. 19). In addition to this, study of the MMZ was based on a borehole core (UK119) (Figure 3. 16). A full photographic record of the portion of borehole UK119 used is provided in Appendix B.

Assessment of the core indicated that there is an apparent zonation in the mineralisation in the host rocks. The textural and mineralogical relationships are discussed further in §3.4. Pyrite and chalcopyrite (Figure 3. 18) are associated with the areas close to the contact zones of the dolomite with the mafic rocks whereas pyrrhotite is predominant in the intrusive rocks further away from the contact. The contact between the xenolith and the intrusive host rocks is undulose but sharp (Figure 3. 17).

Similar to the xenoliths found associated with the MSB, the xenoliths associated with the MMZ also range in size from a few square centimetres to a few square metres.

Figure 3. 17: Part of borehole core UK119, showing the undulous, sharp contact between the intrusive rocks (chromititic pyroxenite) and the dolomite xenolith.

Figure 3. 18: Part of borehole core UK119, showing disseminated pyrite (Py) and chalcopyrite (Cp) grains in the dolomite xenolith close to the contact with the intrusive rocks.

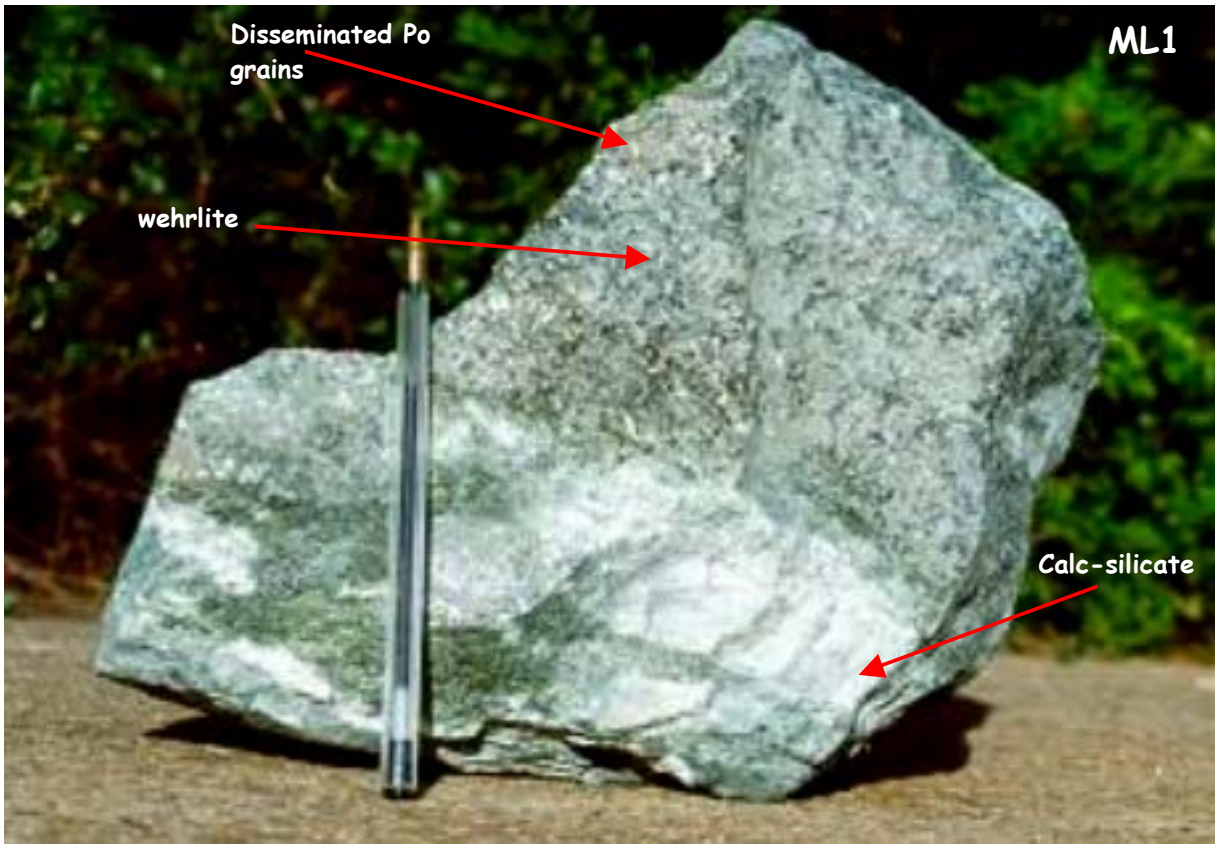

Figure 3. 19: Calc-silicate xenolith hosted by wehrlite that contains disseminated sulphide mineralisation (predominantly Po). Sample number ML1.

The MMZ contains sulphide-bearing, feldspathic wehrlite (Figure 3. 19). The interstitial sulphides associated with these rocks consist predominantly of pyrrhotite. According to Gauert (1998), the wehrlites show a sill-like distribution throughout the LHZBG, reaching widths of up to 10 m. No reaction rims are present between the calc-silicate xenolith and the wehrlite.

4. MINERAL ASSOCIATIONS

4.1. General

Thirty-four (34) polished thin sections were analysed using the following techniques:

- The optical microscope
- The scanning electron microscope (SEM), and
- The electron microprobe (EMP)

In addition to the above, mineral identification was assisted by the use of X-ray diffraction (XRD) techniques. Details about the individual techniques are provided in Appendix C. Detailed descriptions of the thin sections together with the XRD and EMP results are provided in Appendix D.

4.2. Dolomite xenoliths

Dolomite xenoliths are rare in the Uitkomst Complex, as most have been altered to calc-silicates. The studied xenolith in borehole UK119 (Figure 3.16) consists of dolomite, talc and chlorite (nimite) as the major minerals. Chlorite is commonly formed by deuteric or hydrothermal alteration of primary ferromagnesian minerals such as mica, pyroxene, amphibole, garnet and olivine (Bailey, 1988). Chlorite has a general formula of $(Mg, Al, Fe)_{12}[(Si, Al)_8O_{20}] (OH)_{16}$ (Shelley, 1974). The chlorite present in the analysed xenolith as well as in the mafic host rock is nickel-rich (nimite). A further phyllosilicate occurring in the dolomite xenolith and its ultramafic host rock in UK119 is talc, which occurs as long wispy or fan-like grains. Talc has the following formula: $Mg_6[Si_8O_{20}](OH)_4$ (Shelley, 1974). The composition of the talc in the host rock varies from the talc in the dolomite xenolith in that the former is nickel-rich (possibly willemsite) whereas the latter is more iron - rich.

The contact between the dolomite and the mafic-ultramafic rock is undulating, but sharp. The contact is defined by the presence of euhedral and subheral chromite grains in the mafic portion. The chromite crystals increase in size towards the contact with the xenolith. Further away from the contact, aggregates of chromite may be partially annealed by magnetite.

The sulphide mineralisaton in the xenolith is dominated by disseminated blebs of chalcopyrite, pentlandite and pyrite. The chalcopyrite and pentlandite tend to be more dominant closer to or at the contact between the dolomite and the host rock, while pyrite becomes the more dominant sulphide mineral further away from the contact.

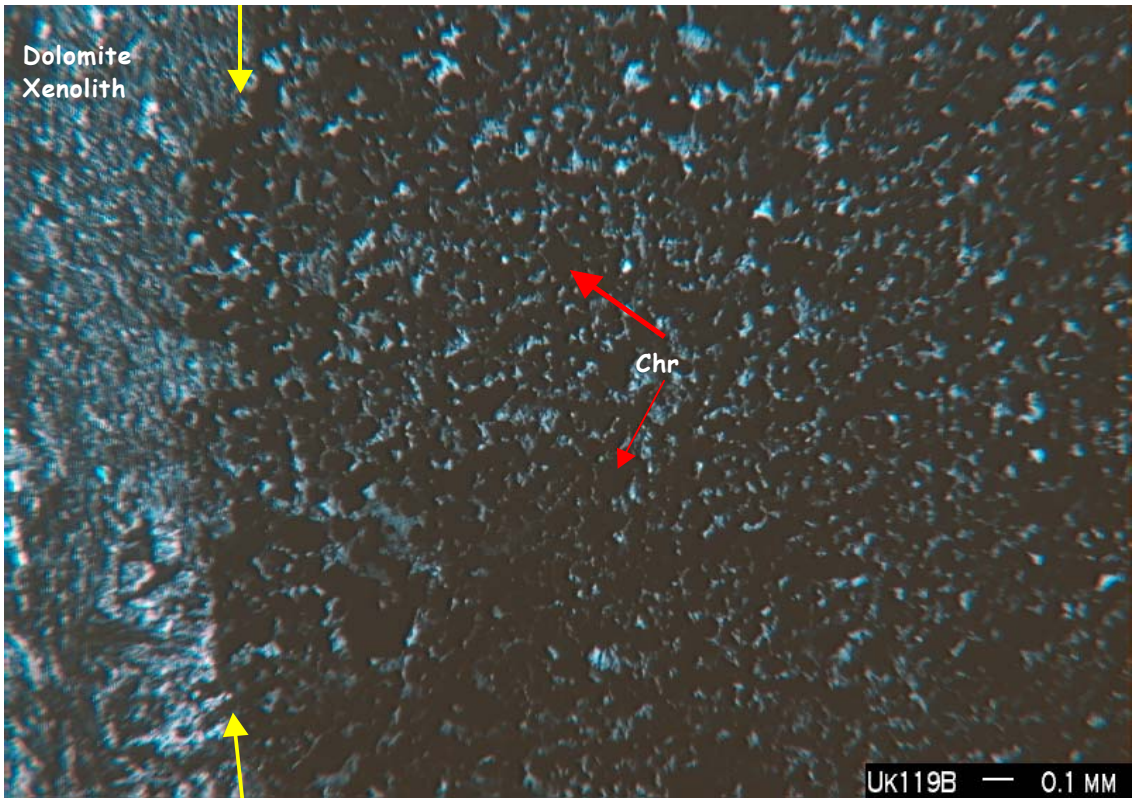

Figure 4. 1: Sharp contact between the dolomite xenolith on the left and the ultramafic rock on the right. The yellow arrows indicate the contact between the xenolith and the host rock. The ultramafic portion consists of euhedral and subhedral grains of chromite (Chr) in a matrix of Ni-rich talc and chlorite. The xenolith consists of dolomite, talc and chlorite grains. Sample Number: UK119B. Cross polarised light.

4.3. Calc-Silicate xenoliths

Bowen (1940) undertook the first comprehensive study of calc-silicates. He proposed that the progressive metamorphism of siliceous dolomite is a process of decarbonation. The following list of index minerals was suggested by considering the sequence of joints broken in moving away from the CO_2 apex in the system CaO-MgO-SiO_2-CO_2:

1. tremolite
2. forsterite
3. diopside
4. periclase
5. wollastonite
6. monticellite
7. akermanite
8. spurrite
9. merwinite
10. larnite

Skippen (1974) considered the phases in the CaO-MgO-SiO_2 plane (Figure 4. 2). A group of 8 mineral phases can be combined into 56 unique assemblages consisting of five mineral phases. The five mineral phases are described by Korzhinskii (1959), together with the associated mineral assemblages that can be used to distinguish between the stable and metastable equilibria. The stable reactions among the phases forsterite (Fo), diopside (Di), tremolite (Tr), talc (Tc), enstatite (En), quartz (Q), calcite (Cc), dolomite (Do) are listed below (Skippen, 1974):

1. $Tc = 3En + Q + H_2O$
2. $Tc + 3Cc + 2Q = 3Di + 3CO_2 + H_2O$
3. $Tr = 2Di + 3En + Q + H_2O$

4. $3Do + 4Q + H_2O = Tc + 3Cc + 3CO_2$
5. $4Tc + 5Do = 5Di + 6Fo + 10CO_2 + 4H_2O$
6. $Tr + 3Cc + 2Q = 5Di + 3CO_2 + H_2O$
7. $5Tc + 5Cc + 4Q = 3Tr + 6CO_2 + 2H_2O$
8. $Do + 2Q = Di + 2CO_2$
9. $2Tc + 3Cc = Tr + Do + CO_2 + H_2O$
10. $Tc + 2Do + 4Q = Tr + 4CO_2$
11. $8Q + 5Do + H_2O = Tr + 3Cc + 7CO_2$
12. $Tr + 3Cc = 4Di + Do + CO_2 + H_2O$
13. $5Tc + 2Do = Tr + 12\ En + 4CO_2 + 4H_2O$
14. $2Do + 5Q + 3En + H_2O = Tr + 4CO_2$
15. $2Tr + Do = 5Di + 6En + 2CO_2 + 2H2O$
16. $Di + 3Do = 5Fo + 4Cc + 2CO_2$
17. $Tc + 5Do = 4Fo + 5Cc + 5CO_2 + H_2O$
18. $Tr + 11Do = 8Fo + 13Cc + 9CO_2 + H_2O$
19. $3Tr + 5Cc = 11Di + 2Fo + 5CO_2 + 3H_2O$
20. $4Tr + 5Do = 13Di + 6Fo + 10CO_2 + 4H_2O$
21. $11Tc + 10Cc = 5Tr + 4Fo + 10CO_2 + 6H_2O$
22. $6.5Tc + 5Do = 2.5Tr + 6Fo + 10CO_2 + 4H_2O$
23. $En + Do = Fo + Cc + CO_2$
24. $13En + 2Do + H2O = Tr + 5Fo + 4CO_2$
25. $Tr + Fo = 5En + 2Di + H_2O$
26. $4En + Do = Di + 2Fo + 2CO_2$
27. $Tc + Fo = 5En + H_2O$

The calc-silicate rocks found in the Uitkomst Complex display both prograde and retrograde metamorphic assemblages similar to those observed in the Bushveld Complex (Wallmach *et al.*, 1989; Wallmach *et al.*, 1995). Prograde metamorphism involves the decarbonation, dehydration and mixed volatile equilibria to produce the mineral assemblages observed. Retrogression involves the hydration of the minerals (Figure 4. 3 to Figure 4. 12). In addition to these reactions, replacement of calc-silicate minerals by sulphides (Figure 4. 16) is also observed in the samples obtained from the Uitkomst Complex.

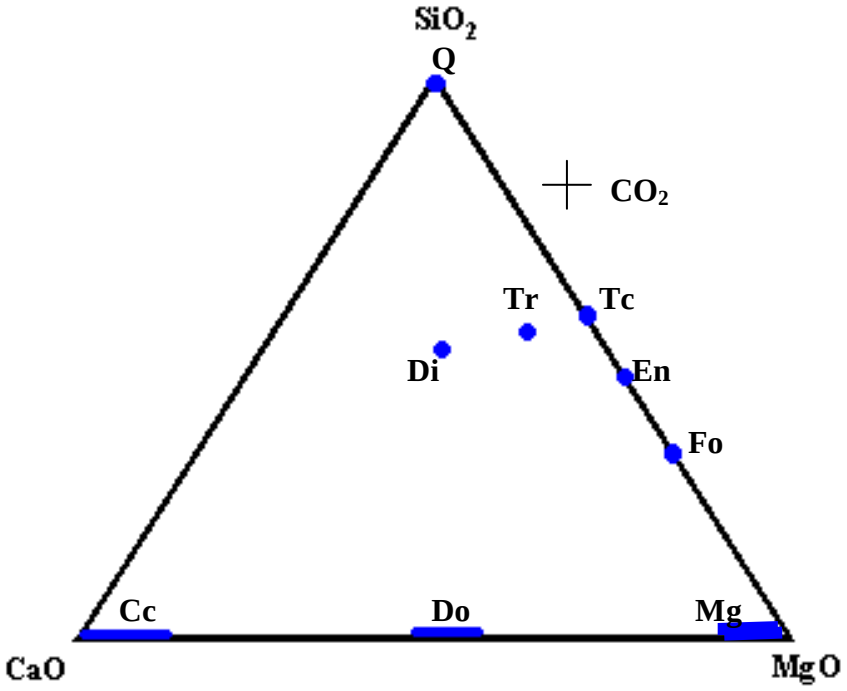

Figure 4. 2: Compositions of calcite (Cc), dolomite (Do), quartz (Q), diopside (Di), tremolite (Tr), enstatite (En), magnesite (Mg), forsterite (Fo), projected into the plane CaO-MgO-SiO_2 (after Skippen, 1974).

The precursors of the calc-silicate xenoliths are assumed to be the Malmani dolomite, Nelshoogte granite and Black Reef quartzite. This is inferred from the physical relationship between the Uitkomst Complex and the country rocks.

The mineral assemblage of pyroxene, quartz, calcite, phlogopite, talc and serpentine is common in the development of magnesian skarns (Meinert, 1992).

In the interaction between the dolomite xenoliths and the Uitkomst magma, proximal metamorphism is observed, with fluid and volatiles from the xenoliths being predominantly mobilised at the margins of the xenoliths. The most dominant mineral developed at the margins between the calc-silicate xenoliths and the ultramafic host rock is amphibole.

The most common mineral assemblage observed in the calc-silicate xenoliths enclosed in the Uitkomst magma is calcite-pyroxene-tremolite. The reaction that may have produced this assemblage is listed as number 11 in the list of Skippen (1974).

In addition to the above, several other mineral assemblages are observed (Figure 4. 3 to Figure 4. 16). The xenoliths contain combinations of the following minerals:

Diopside ($CaMgSi_2O_6$; Di), augite [$(Ca, Mg, Fe)_2(Si, Al)_2O_6$], monticellite ($CaMgSiO_4$; Mo), forsteritic olivine (Mg_2SiO_4; Fo); periclase (MgO; Pe), brucite [$Mg(OH)_2$], spinel ($MgAl_2O_4$; Sp), calcite ($CaCO_3$; Cc), tremolite [$Ca_2Mg_5Si_8O_{22}(OH)_2$; Tr], wollastonite ($CaSiO_3$; Wo), epidote [$Ca_2Fe^{3+}Al_2Si_3O_{12}(OH)$; Ep], Ba-rich phlogopite [$K_2Mg_6Si_6Al_2O_{20}(OH)_4$] and apatite [$Ca_5(PO_4)_3(Cl,F)$].

In thermally metamorphosed impure dolomite, tremolite forms early by reaction between dolomite and quartz (Deer *et al*., 1992):

$$5CaMg(CO_3)_2 + 8SiO_2 + H_2O \longrightarrow Ca_2Mg_5Si_8O_{22}(OH)_2 + 3CaCO_3 + 7CO_2$$

(1)

dolomite quartz tremolite calcite

At higher grades of metamorphism tremolite is unstable and if SiO_2 is still available after the above reaction, the tremolite reacts with calcite to form diopside:

$$Ca_2Mg_5Si_8O_{22}(OH)_2 + 3CaCO_3 + 2SiO_2 \longrightarrow 5CaMgSi_2O_6 + 3CO_2 + H_2O$$

(2)

Tremolite calcite quartz diopside

Where there is an excess of dolomite relative to quartz, the early-formed tremolite reacts with the dolomite to give forsterite and calcite:

$$Ca_2Mg_5Si_8O_{22}(OH)_2 + 11CaMg(CO_3)_2 \longrightarrow 8Mg_2SiO_4 + 13CaCO_3 + 9CO_2 + H_2O$$

Tremolite dolomite

(3)

Forsterite calcite

The mineral assemblages formed through the decarbonation reactions (1), (2) and (3) are shown in Figure 4. 3 to Figure 4. 7.

Periclase (Figure 4. 10) is a relatively high-temperature mineral that may form during metamorphism of dolomites and magnesian limestones. It is formed during the dissociation of dolomite.

$$CaMg(CO_3)_2 \longrightarrow CaCO_3 + MgO + CO_2$$

Dolomite calcite periclase

In Figure 4. 10 periclase is surrounded by a rim of brucite ($Mg(OH)_2$) that formed during the hydration of the periclase. The alteration of periclase to brucite causes distinctive cracks within associated monticellite crystals. Periclase forms after wollastonite, but at a lower temperature than monticellite. The presence of periclase might be attributed to not only the metamorphic conditions but also to a relatively high Mg content. This might have been caused by metasomatism related to the variation in the chemical potentials between the xenolith and the magma. This is discussed in a later chapter.

In most calc-silicate xenoliths, partially replaced crystals of calcite are observed. Replacement of crystals is most apparent in the contact zones between the xenoliths and the sulphide rich magma (for example, Figure 4. 9). An increase in grain size of calc-silicates towards the contact with the sulphide is observed in all the sections analysed. The contact between the sulphides and the xenolith is commonly marked by a zone of hydrous minerals, indicating the mobilisation of the volatiles towards the edges.

Poikilitic idioblasts of diopside are a common feature in most thin sections of calc-silicates (Figure 4. 10). Inclusions include smaller grains of diopside, augite, calcite and serpentine. Sphene, K-feldspar and albite occur as accessory minerals.

Epidote (Figure 4. 13) is observed in the calc-silicate xenoliths of the Basal Mineralised Zone (BMZ). The epidote grains are associated with diopside, augite and calcite. Pyrite mineralisation (Figure 4. 13 to Figure 4. 16) is also commonly associated with the epidote minerals. In Figure 4. 16, the pyrite is framboidal and appears to have injected the xenolith. Pyrite is the dominant sulphide mineral in the interior of the xenolith. Chalcopyrite and pentlandite are more dominant at the immediate contact between the xenolith and the host rock. Pyrrhotite is the dominant sulphide mineral in the host rock. The pyrite grains in the interior of the xenolith contain inclusions of calc-silicate minerals such as augite.

Grains of andradite garnet were also observed in some of the calc-silicate xenoliths. Andradite typically occurs in metamophic skarns. This involves the introduction of Fe_2O_3 ($\pm$ SiO_2) through the following reaction:

$$3CaCO_3 + Fe_2O_3 + 3SiO_2 \longrightarrow Ca_3FeSi_3O_{12} + 3CO_2$$

calcite andradite

The garnet crystals observed are idioblastic or granoblastic, and are commonly associated with vesuvianite and wollastonite.

The calc-silicate xenoliths also display retrograde metamorphic assemblages. Retrograde mineral assemblages include the presence of red vesuvianite

$[Ca_{19}(Al,Fe)_{10}(Mg,Fe)_3(Si_2O_7)_4(SiO_4)_{10}(O,OH,F)_{10}]$, especially along the margins of the calc-silicate xenoliths of the MMZ. Ito and Arem (1970, 1971), Shoji (1971, 1975), Valley and Essene (1979), Hochella *et al.* (1982) and Valley *et al.* (1985) have shown that Mg-vesuvianite can form from melilite, wollastonite, monticellite, and/or diopside under retrograde hydration of high-grade metamorphic rocks at temperatures between 400 and 600^{o}C (Shoji, 1971).

The two most common retrogressive metamorphic assemblages in the calc-silicate xenoliths of the Uitkomst Complex are:

Vesuvianite – garnet – diopside – calcite – chlorite, and

Wollastonite- K-feldspar – muscovite – apatite – calcite

In both of the above assemblages, only relics of calcite are observed. The vesuvianite grains commonly occur as inclusions in diopside. The wollastonite occurs close to the contact of the calc-silicate xenolith with the sulphides.

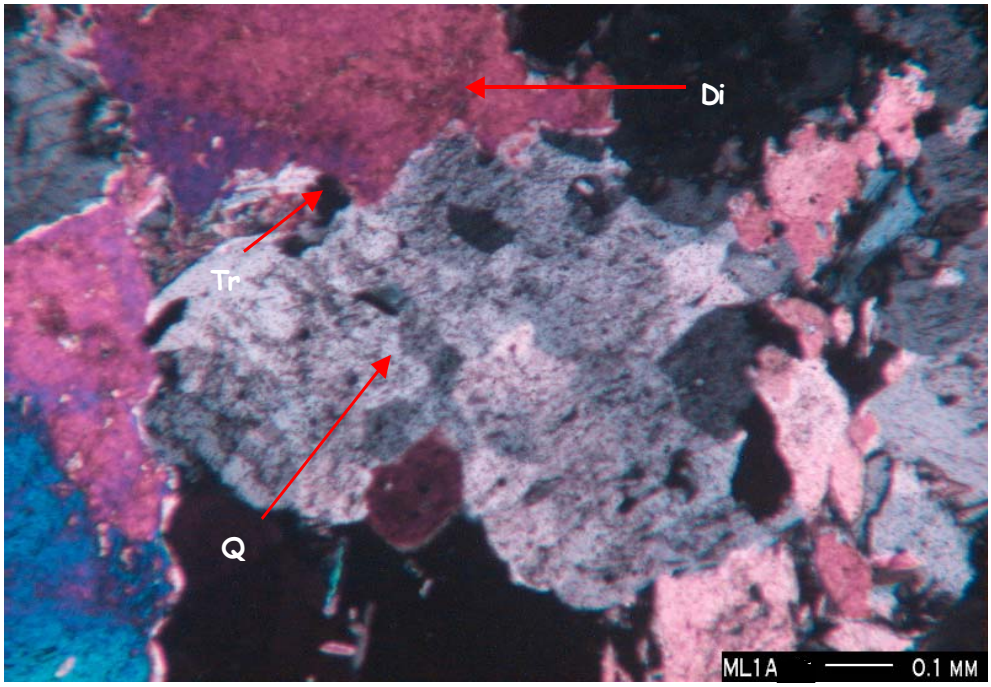

Figure 4. 3: Photomicrograph showing tremolite (Tr)-diopside (Di)-quartz (Q) assemblage. The contacts between the diopside grains and the other minerals are annealed by a corona of more aluminium-rich diopside. The quartz grain is strained as indicated by its undulous extinction. Inclusions of aluminium-rich diopside are found within the large diopside crystals. Cross polarised light. Sample Number: ML1A.

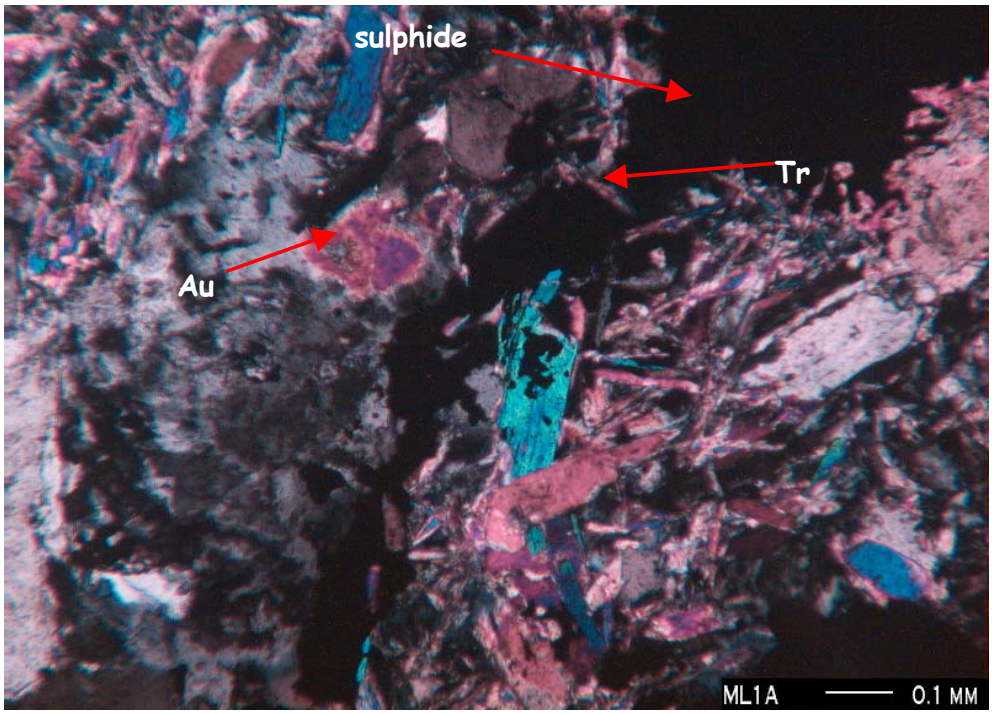

Figure 4. 4: Tremolite (Tr) laths become more dominant at the contact between the sulphide and the xenolith. Augite (Au) is also found at the contact between the sulphide and the xenolith. Cross polarised light. Sample Number: ML1A.

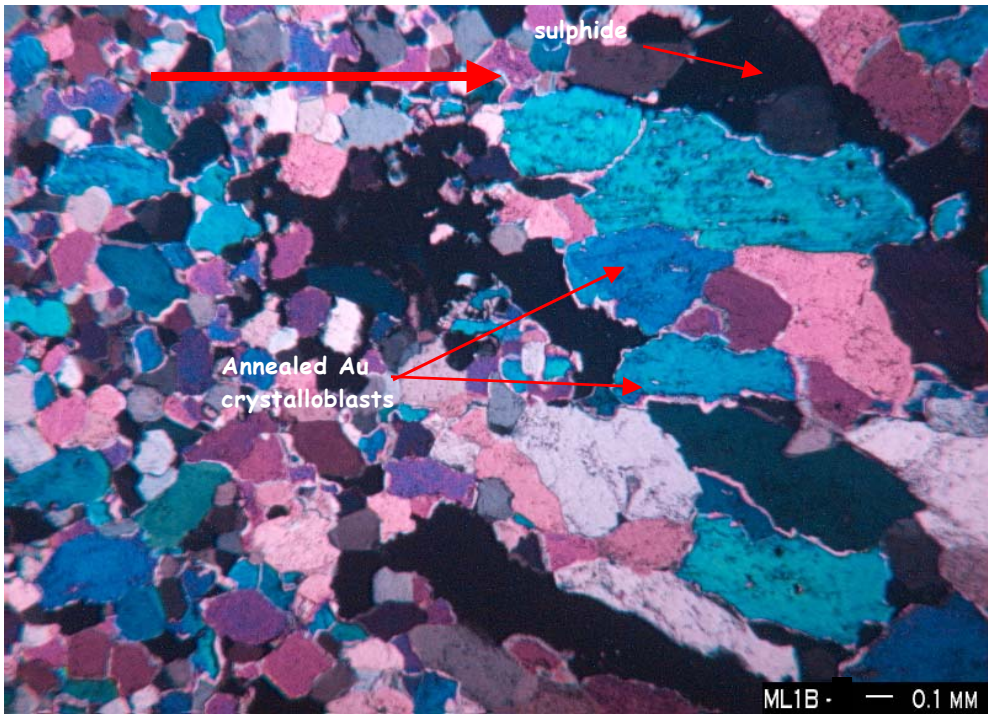

Figure 4. 5: Arrow indicates increasing size in the augite (Au) crystalloblasts with increasing proximity to the sulphide zone. Cross polarised light. Sample Number: ML1B.

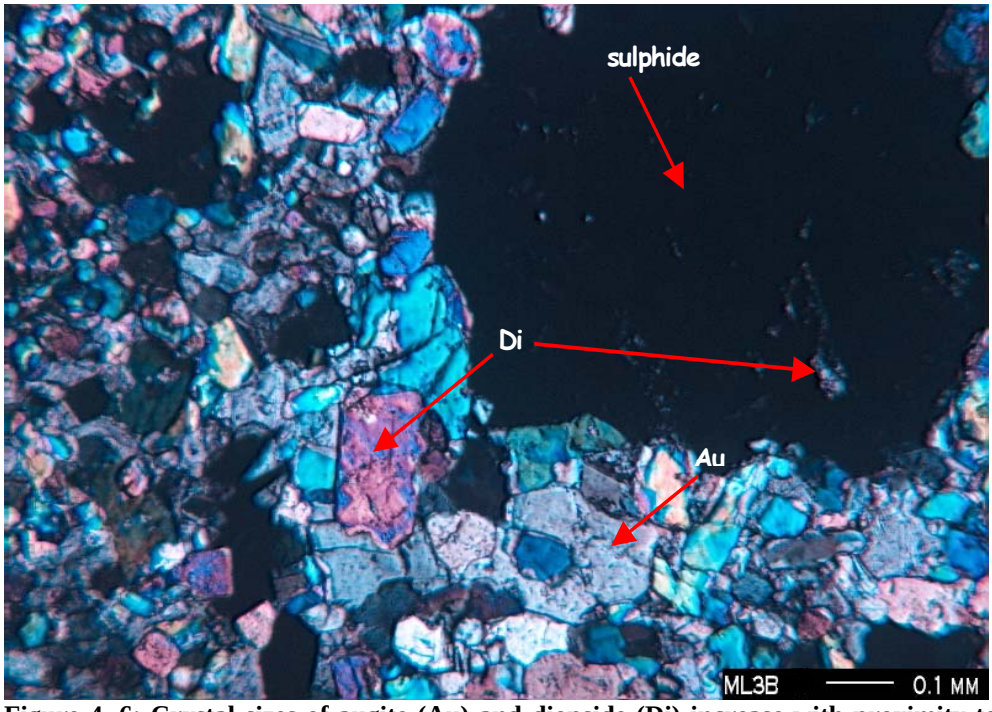

Figure 4. 6: Crystal sizes of augite (Au) and diopside (Di) increase with proximity to the sulphide. The sulphide contains inclusions of diopside. Sample Number: ML3B. Cross polarised light.

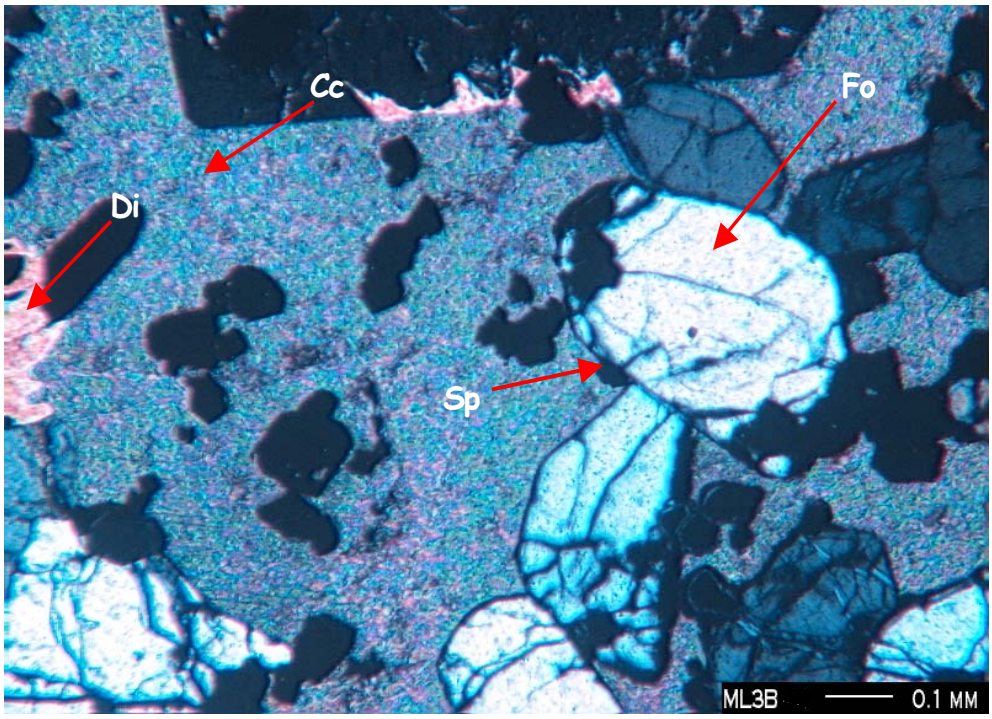

Figure 4. 7: Olivine(Fo)-calcite (Cc)-diopside (Di) crystals. Sample Number ML3B. Cross polarised light.

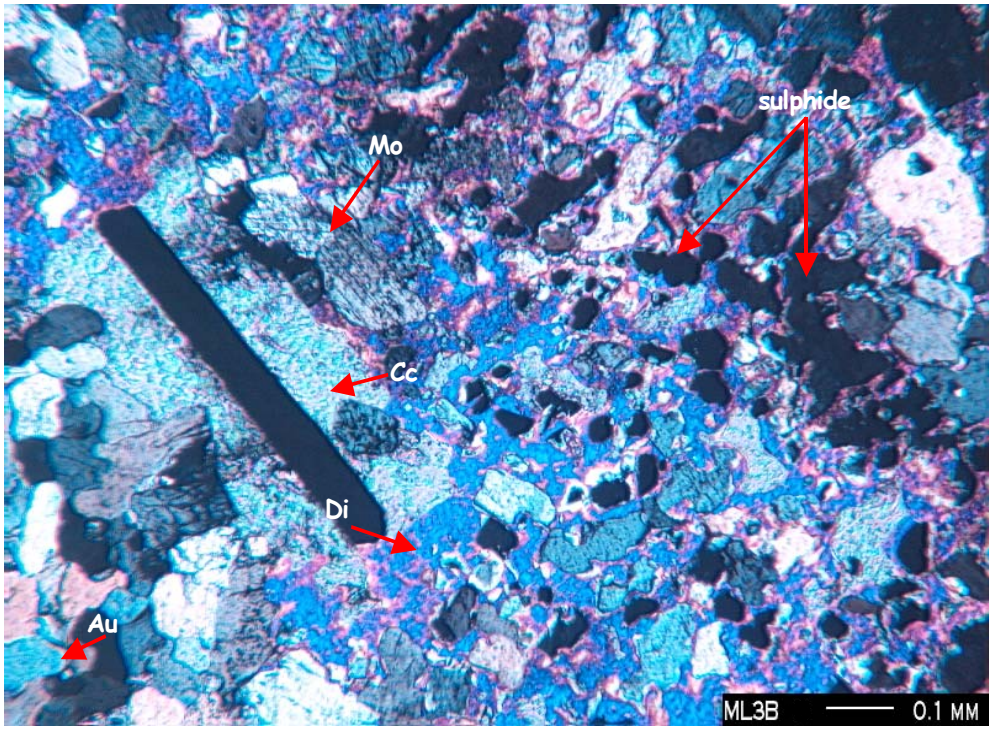

Figure 4. 8: Large diopside (Di) crystal containing inclusions of calcite (Cc) and monticellite (Mo), surrounded by inter-locking grains of augite (Au). Sample Number: ML3B. Cross polarised light.

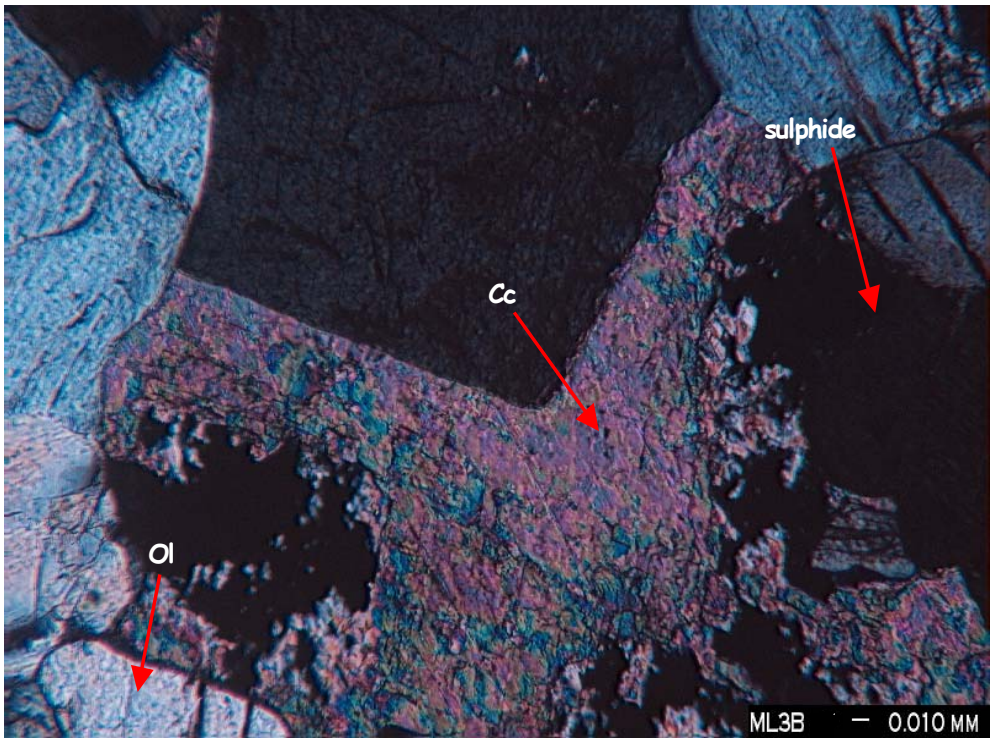

Figure 4. 9: Calcite (Cc) grain, partially replaced by sulphide. Sample Number: ML3B. Cross polarised light.

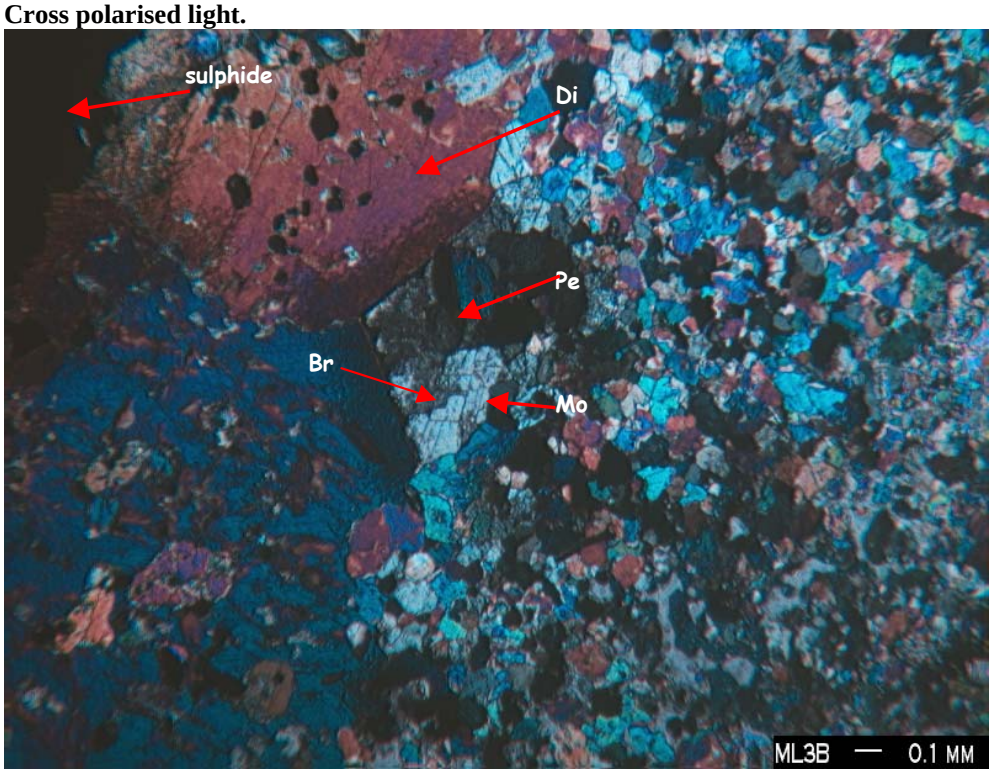

Figure 4. 10: Periclase (Pe) partially altered to brucite (Br). The periclase grain is included in a monticellite (Mo) crystal. The size of the diopside (Di) grains increases with proximity to the sulphide. Sample Number: ML3B. Cross polarised light.

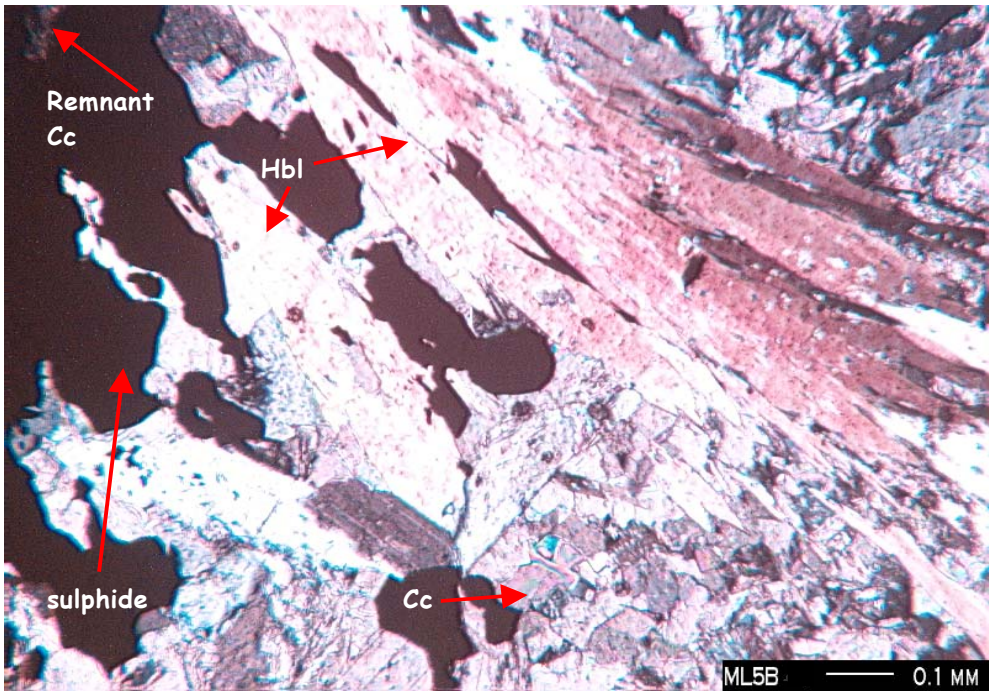

Figure 4. 11: Hornblende (Hbl) laths in the proximity of sulphide mineralisation. Remnant calcite (Cc) crystals are still visible. Sample Number: ML5B. Cross polarised light.

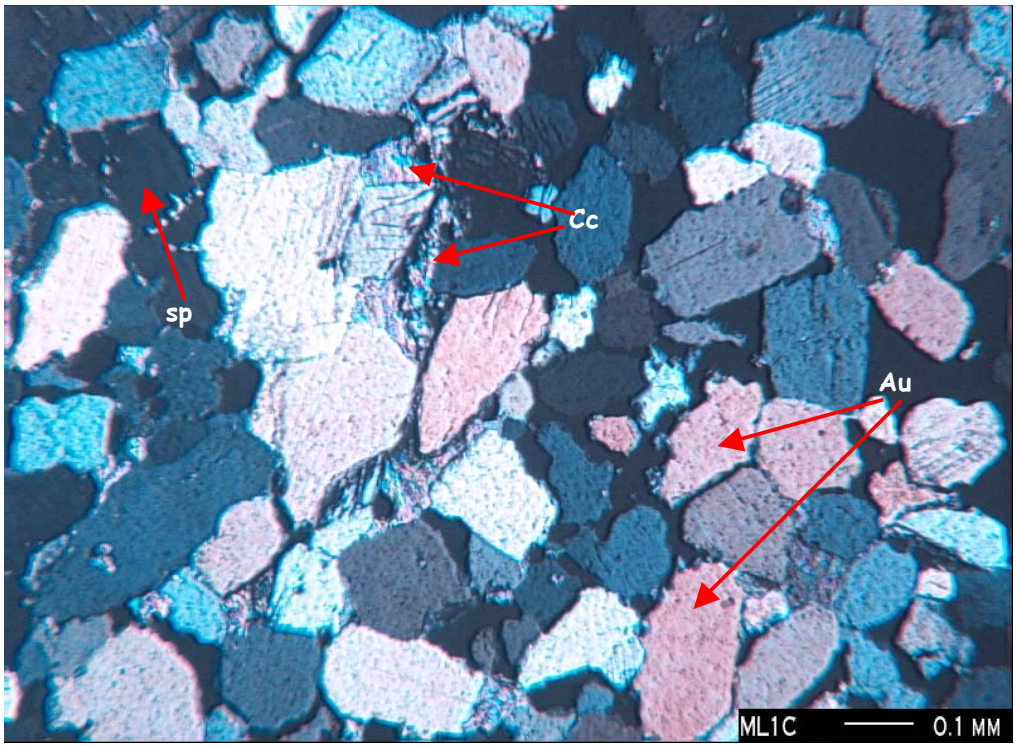

Figure 4. 12: Augite (Au) –calcite (Cc) assemblage. Spinel occurs as accessory minerals. Sample Numbert: ML1C. Cross polarised light.

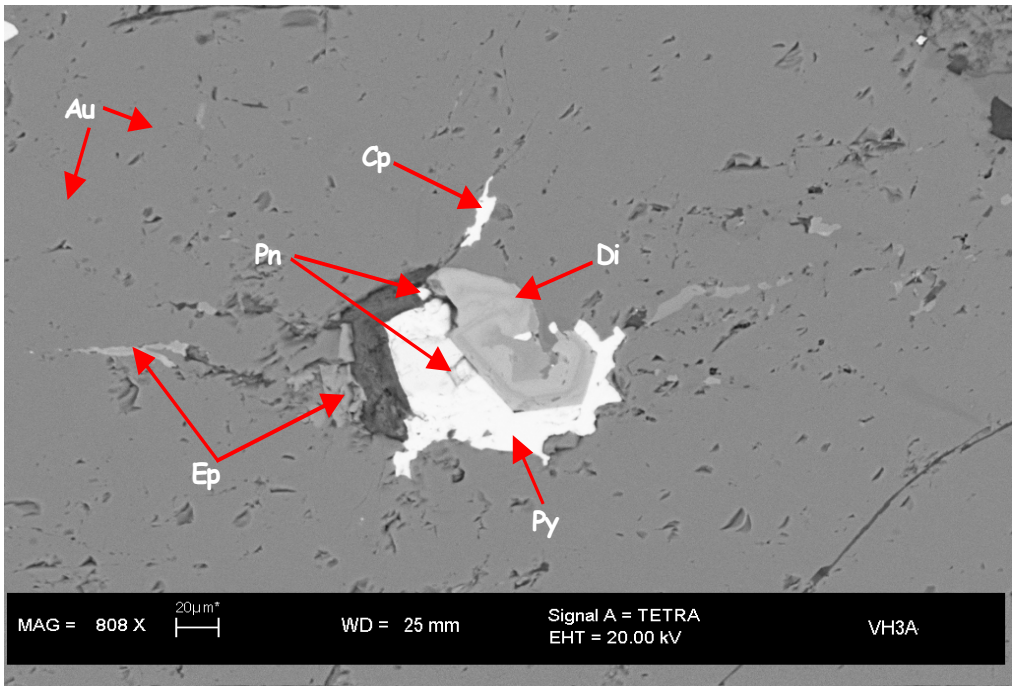

Figure 4. 13: Back-scattered scanning electron image (SEM) showing zoned diopside (Di) grain surrounded by pyrite. The diopside crystal becomes more iron-rich towards the centre. Epidote (Ep) occurs along the grain boundaries of the augite (Au). Chalcopyrite (Cp) and pentlandite (Pn) are the other sulphide minerals. Sample Number: VH3A.

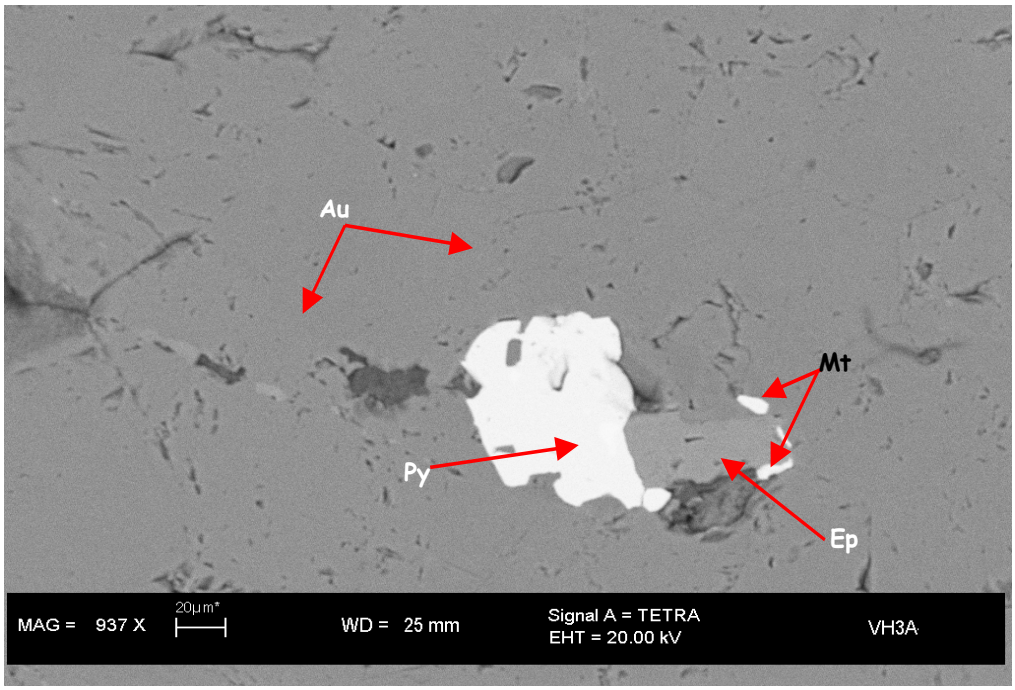

Figure 4. 14: Pyrite (Py) grain occurring at contact with epidote (Ep) crystal. Pyrite, epidote and magnetite (Mt) grains occupy the interstitial space amongst the pyroxene grains (Au). Sample Number: VH3A. Back-scattered scanning electron image.

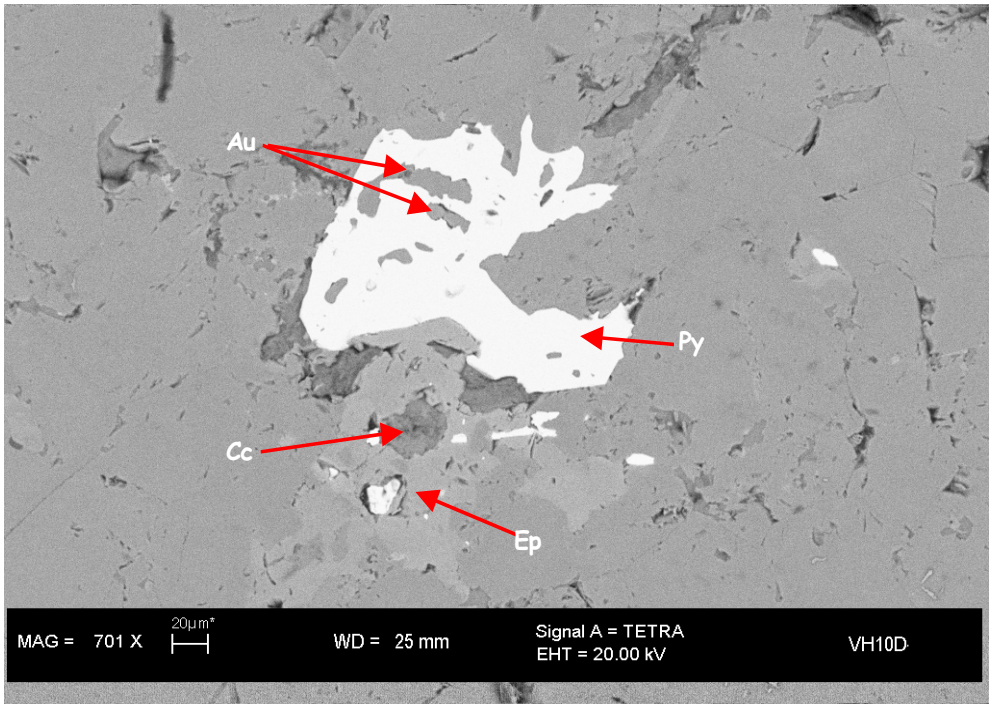

Figure 4. 15: Calcite (Cc) crystal surrounded by epidote (Ep) grains. Augite (Au) grains occur as inclusions within pyrite (Py) crystal. Sample Number: VH10D. Back-scattered scanning electron image.

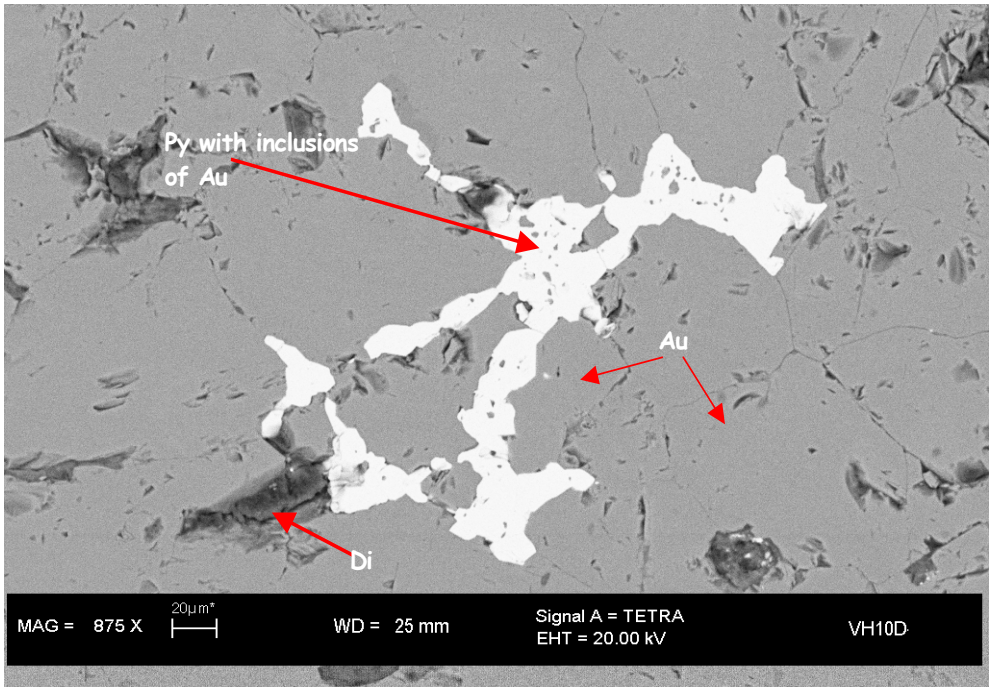

Figure 4. 16: Framboidal pyrite (Py) with inclusions of augite (Au). Also shown is a zoned grain of diopside (Di). The iron content of the diopside grain increases towards the core. Sample Number: VH10D. Back-scattered scanning electron image.

4.4. Quartzite xenoliths

The most distinct feature of the quartzite xenoliths is the prominent reaction rim that occurs at the contact between the xenoliths and the intrusive rock. The rims consist of actinolite, chlorite and some biotite associated with the quartz grains (Figure 4. 17 and Figure 4. 18). However, quartzite has little MgO, Al_2O_3 and FeO. The coronas could either have been formed through metasomatism of the quartzite by introduction of MgO, Al_2O_3 and FeO, or through the remobilisation to the margins of interstitial material in the original quartzite. The contact between the reaction rim/corona and the quartzite is sharp, favouring metasomatism as the possible cause for the generation of the rims compared to remobilisation from within the quartzite.

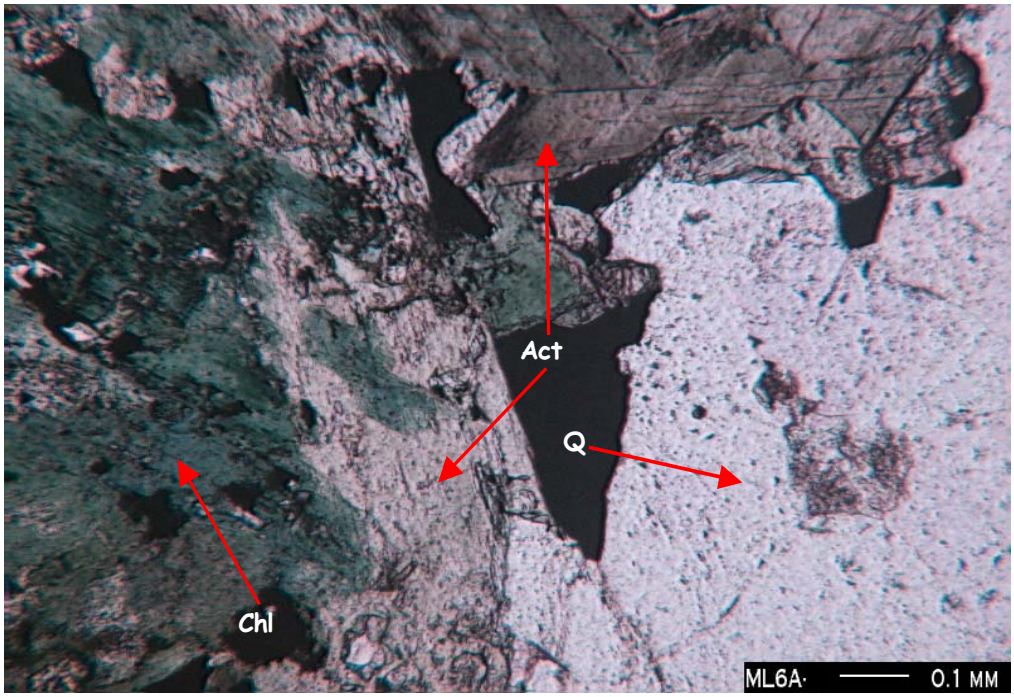

Figure 4. 17: Photomicrograph showing quartz (Q) crystals on the right of photograph in contact with sulphide mineralisation. The contact is marked by the presence of actinolite (Act) and chlorite (Chl). Sample Number: ML6A. Cross polarised light.

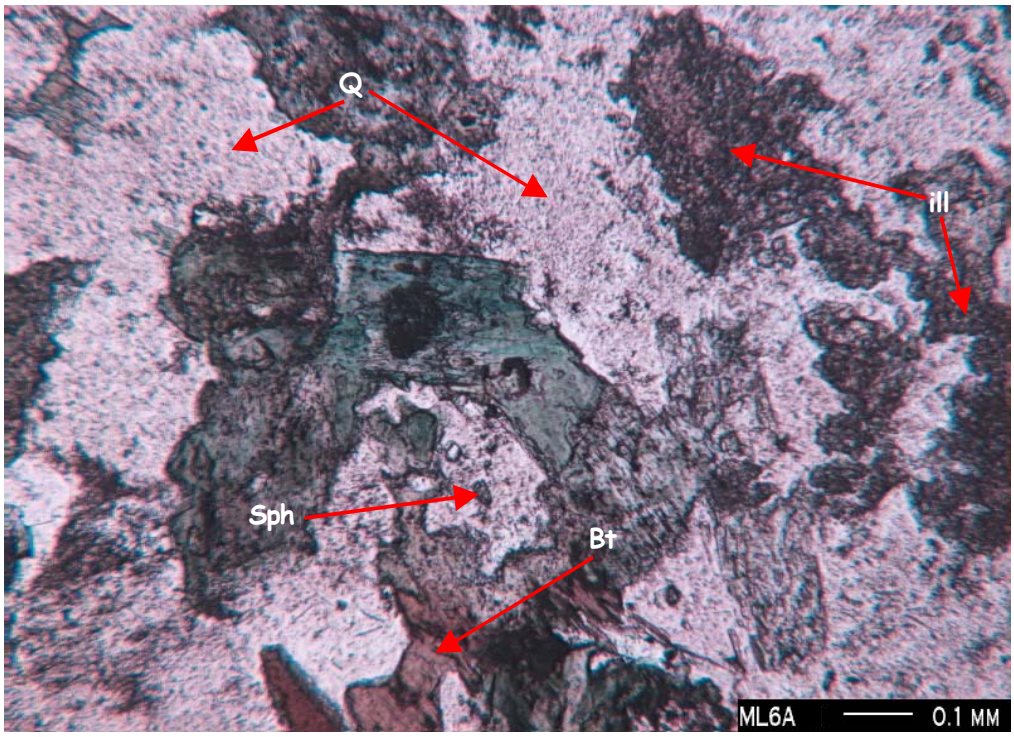

Figure 4. 18: Biotite (Bt) occurs close to the contact of the quartzite with the intrusive rock. Illite (ill) alteration is also observed. Sample Number: ML6A. Cross polarised light.

No deformation of the quartz crystals was observed. However, the grain sizes of the quartz crystals increase towards the contact with the intrusive. This indicates recrystallisation towards the edges of the xenoliths. Incipient illite formation after mica was also observed.

4.5. Granite xenoliths

The most characteristic feature of the metamorphosed granites is the occurrence of myrmekitic symplectites (Figure 4. 19). Symplectites are the result of syntactic reactions and intimate intergrowths of reacting and juxtaposing mineral phases. In Figure 4. 19 the finer-grained myrmekite surrounds the coarser grained myrmekite. This is quite common in metamorphosed granites (Augustithis, 1990). Drescher – Kaden (1948) describes generations of myrmekitization where fine quartz myrmekitic bodies might be enclosed in coarse-grained myrmekite. In the thin section studied (Figure 4. 20), chlorite and phlogopite separate the granite xenolith from the sulphides. The sulphide mineralisation developed along the margins of the granite xenolith consists predominantly of chalcopyrite and pentlandite (Figure 4. 21). Clusters of pentlandite have developed along the outer margins of the myrmekite. Chalcopyrite is developed on the outer edges of pentlandite.

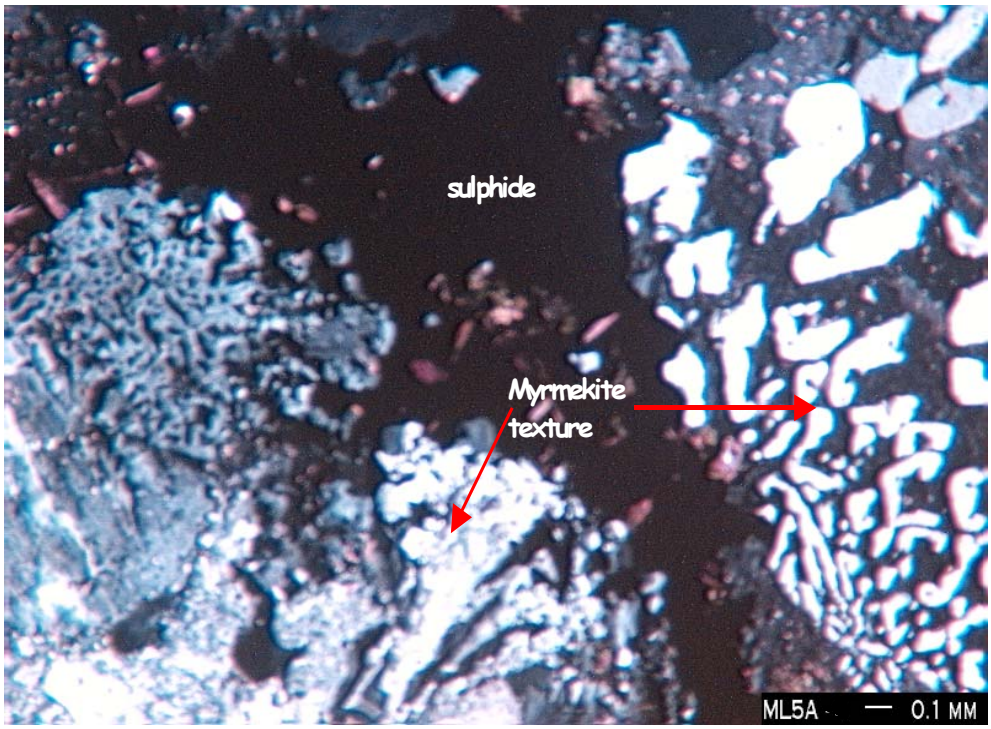

Figure 4. 19:Myrmekitic symplectites (quartz-plagioclase intergrowth) texture found in the granite xenoliths of the Uitkomst Complex. Sample Number: ML5A. Cross polarised light.

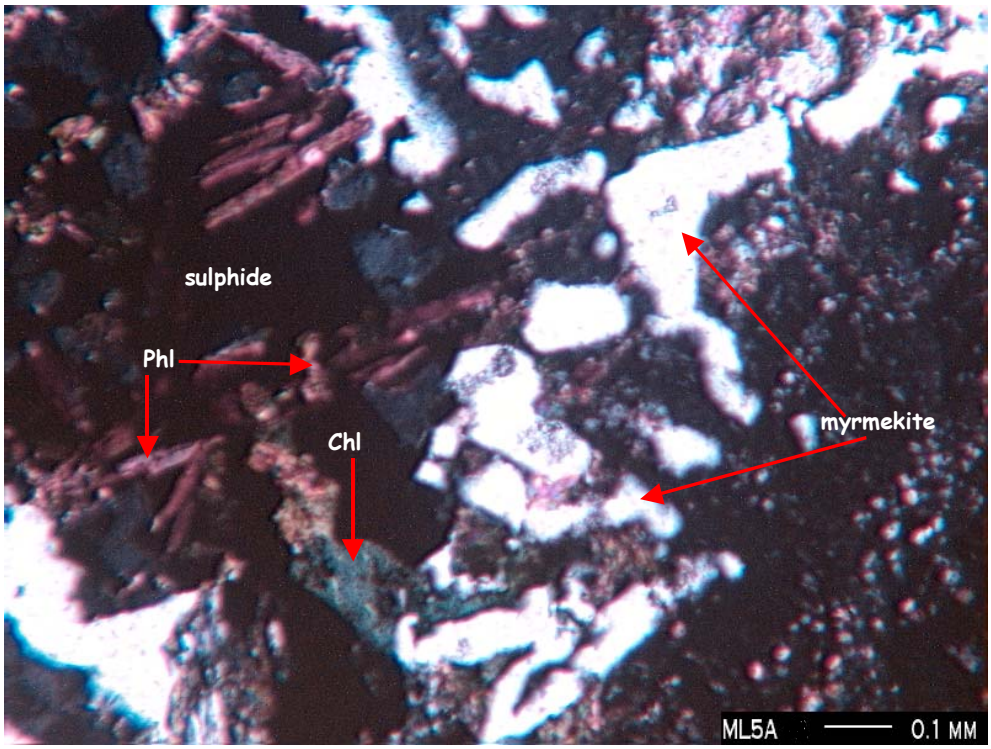

Figure 4. 20: Myrmekite separated from sulphide by chlorite (Chl) and phlogopite (Phl). Sample Number: ML5A. Cross polarised light.

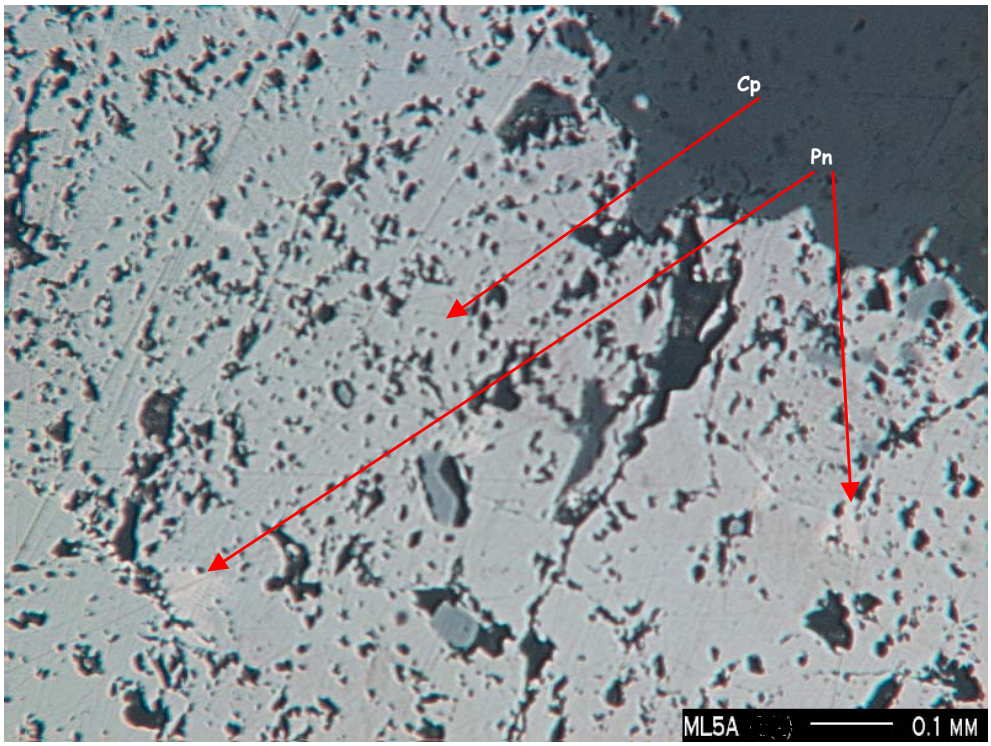

Figure 4. 21: Photomicrograph showing sulphide mineralisation associated with the granite xenolith. The immediate contacts contain abundant pentlandite (Pn). Chalcopyrite (Cp) is the predominant sulphide mineral, and forms the second zone adjacent to pentlandite. Sample Number: ML5A. Reflected light.

4.6. Constraints on the peak metamorphic P-T conditions

Wallmach *et al.* (1989) described peak metamorphic assemblages indicating temperatures in excess of 1200^{o}C in the calc-silicate xenoliths in the Marginal and Critical zones of the Bushveld Complex. In these xenoliths akermanite, merwinite, and periclase formed with increasing temperature from irreversible decarbonation reactions in which calcite was a principal reactant. Typical prograde and retrograde calc-silicate metamorphic assemblages were observed. Two groups of calc-silicates were distinguished based on field occurrence and mineral assemblages:

Group 1: Occurs in gabbronorite of the Marginal Zone and consists of melilite, monticellite, aluminium augite, diospide, forsterite, calcite, accessory spinel, kalsilite, Ba-rich phlogopite, wollastonite and apatite.

Group 2: Occurs in the Lower Critical Zone and consists of monticellite, merwinite, mellilite, and periclase mostly altered to brucite. Spinel is an accessory mineral.

The observed petrological and mineralogical features are similar to those described in the Cascade Slide xenolith in the Adirondacks (Valley and Essene, 1980) and monticellite-bearing Adirondack marbles (Tracy, 1978).

Based on the critical mineral parageneses, overburden load pressures of 0.6 – 1.6 kbars (<3-5 km) were inferred for the emplacement of the Critical Zone magma and 1.1 – 1.6 kbars (3-5 km) for the Marginal Zone magma.

Calcite, diopside and forsterite formed at the earlier stages of metamorphism (Bowen, 1940). The final stable decarbonation reaction observed in the calc-silicate xenoliths of the Uitkomst Complex is as follows:

Calcite + forsterite = monticellite + periclase + CO_2

This is similar to that observed in the Critical Zone of the Bushveld Complex (Wallmach *et al., 1995)*. Based on the estimate of Irvine and Sharpe (1982) for the temperature of Bushveld magma of between 1200 and 1300^{o}C, a pressure of 1.1 - 1.6 kbars is inferred (Figure 4. 22). This seems low, considering that the Uitkomst

Complex intruded at the base of the Transvaal Supergroup. A possible solution could be that the Uitkomst magma was more primitive and hotter than the Bushveld magma, but this is in disagreement with the findings of de Waal *et al*. (2001).

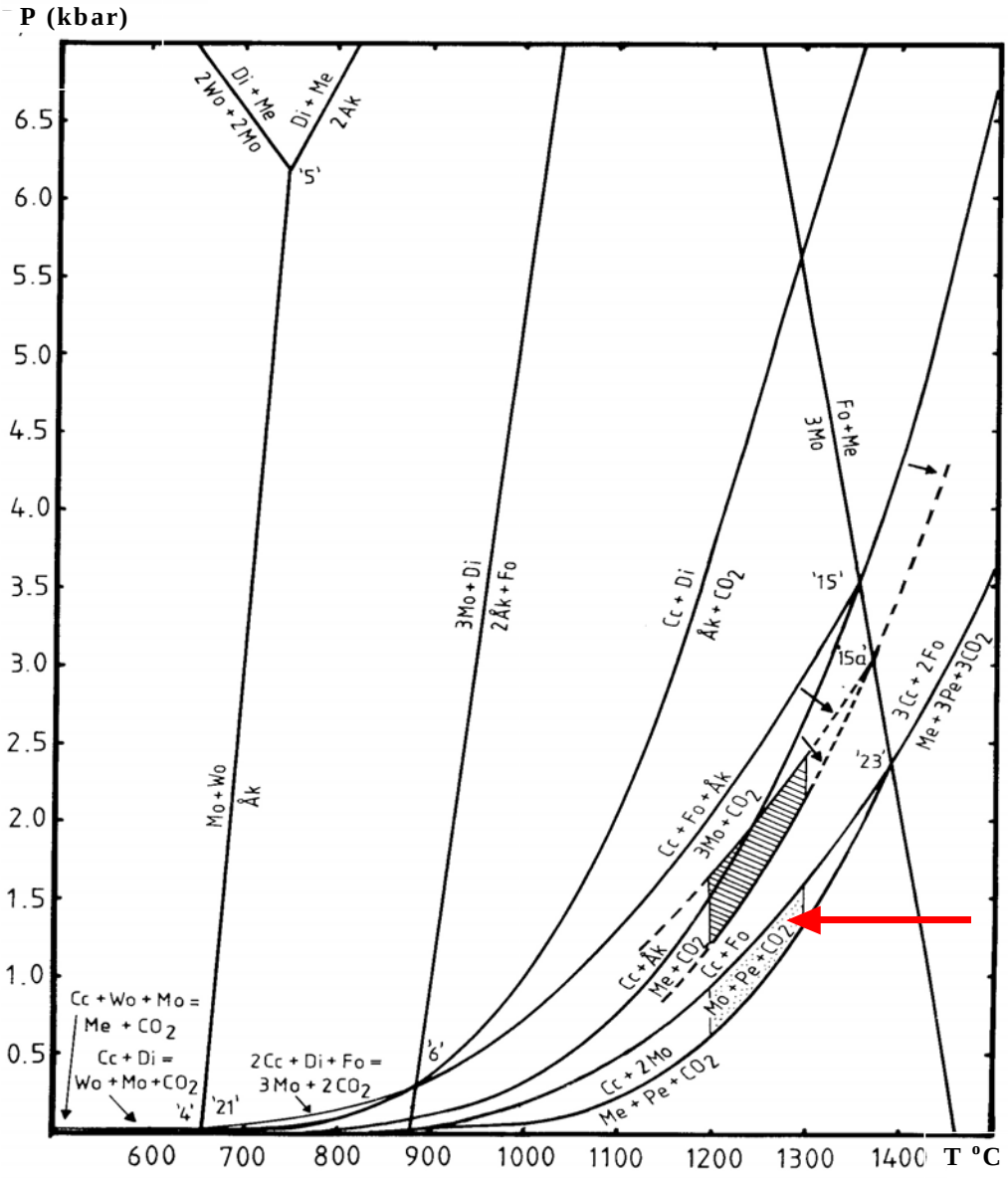

Figure 4. 22: P-T diagram showing possible mineral reactions that can occur during high-temperature metamorphism of siliceous dolomites. The hatched and the dotted areas indicate the P-T conditions under which the Marginal and Critical Zone of the Bushveld Complex magma intruded (Wallmach *et al.*, 1989). The red arrow indicates the P-T conditions under which the Uitkomst magma intruded.

5. GEOCHEMISTRY

5.1. General

Recent studies of the Uitkomst Complex (e.g. Gauert, 2000; Gomwe 2002) as well as other Ni-Cu sulphide deposits (e.g. Buchanan *et al*., 1981; Grinenko, 1985; Naldrett, *et al.*, 1995; Thériault *et al.*, 1997) indicate that contamination of the magma with various country rock materials may trigger sulphide segregation. The precise mechanism of sulphide segregation through contamination of the magma remains unclear. Some authors have suggested that the assimilation of dolomite may have been important in the triggering of sulphide segregation (de Waal, 1977; Buchanan *et al*., 1981; Harris and Chaumba, 2001). Wallmach *et al*. (1995) have shown that there is significant element flux into the magma during the reaction of dolomite with magma. It seems possible that this element flux may have caused the sulphide segregation. It is the purpose of this section to qualify and quantify this element flux, particularly by examining whether there is zonation in the xenoliths, and to thereby constrain whether contamination could have occurred and, in turn, triggered sulphide segregation.

5.2. Sample selection and analytical techniques

Thirteen samples were selected from the Main Mineralised Zone (MMZ,) and analyzed for major and trace element chemistry using the XRF method at the Council for Geoscience, Pretoria (Cloete and Truter, 2001 and Cloete, 2001). A traverse over a selected xenolith in borehole UK119 was analyzed in detail for major and trace elements in order to determine the possible interaction between the xenolith and the Uitkomst magma. The samples were further analyzed using ICP-MS at the Council for Geoscience. Sulphur and carbon dioxide concentrations were obtained by using the Leco-titration method at the Council for Geoscience. Details on the methodologies are provided in Appendix C. The XRD, electron microprobe, XRF normative and ICP-MS scan results are provided in Appendix E. The XRF data were used to calculate the CIPW normative for the samples.

5.3. Major and trace element variations with depth

The XRF results are provided in Table 5. 1 (1 and 2). Both the L.O.I. free as well as the original data are presented. The results of the Leco-titration for the carbon and sulphur concentrations are also provided in Table 5. 1. Graphical representations of compositional variation of the major and trace elements with depth are provided in Figure 5. 1.

The major and trace elements show two distinct patterns. Al, Fe, Cr, Ti, Si, As, Co, Cu, S, Ni, Ba, Zn, V show increasing concentrations near the contact of the xenolith with the intrusive, relative to the centre of the xenolith, indicating the infiltration of these elements into the xenolith from the magma. In contrast, Ca, K, Mg, Na_2O, P, C, Sr and Mn show a marked decrease in concentration within *ca.* 1 m from the contact with the dolomite to the ultramafic host rock, suggesting that these elements were lost from the xenolith to the magma.

The elevated S, Ni, Cu and Co contents are the result of the presence of disseminated sulphides in these samples (see §3.4.). The low carbon contact at the contact indicates that decarbonation occurred during the reaction with the magma. The low CaO contents (Figure 4.1f) mean that the contact indicates disintegration of the xenolith.

The following reaction:

$$5CaMg(CO_3)_2 + 8SiO_2 + H_2O \longrightarrow Ca_2Mg_5Si_8O_{22}(OH)_2 + 3CaCO_3 + 7CO_2$$

dolomite quartz tremolite calcite

explains the Si-enrichment of the xenolith in the contact zone, and simultaneous C and O loss. The variation in L.O.I. vs depth is shown in Figure 5. 1j. The L.O.I. decreases by approximately 20 wt% in the dolomite samples near the contact relative to the dolomite in the center. This further indicates devolatilisation at the contacts.

Table 5. 1: Major and trace element concentrations, recalculated to 100% L.O.I. free (1), using the recalculation (recal) factor and original XRF results (2). Carbon and sulphur concentrations were determined by Leco-titration.
1.

Sample	UK-119A	UK-119B1	UK-119B2	UK-119C	UK-119D	UK-119E	UK-119F	UK-119G	UK-119H	UK-119I	UK-119J	UK-119K	UK-119L
Rock Type	Chromitic Pyroxenite	Chromitic Pyroxenite	Dolomite	Dolomite	Dolomite	Dolomite	Dolomite	Dolomite	Dolomite	Dolomite	Dolomite	Dolomite	Chromitic Pyroxenite
Depth	*54.88*	*55.43*	*55.43*	*55.53*	*55.87*	*56.16*	*56.43*	*56.81*	*57.22*	*57.55*	*57.88*	*58.38*	*59.93*
SiO2	25.09	29.65	51.97	44.7	46.02	42.82	47.9	43.47	42.01	46.88	40.49	55.66	24.88
TiO2	0.4	0.44	0.24	0.07	0.11	0.16	0.12	0.13	0.11	0.15	0.13	0.13	0.38
Al2O3	14.06	11.15	5.57	1.46	2.22	3.99	2.7	2.51	2.32	3.46	2.75	2.58	11.31
Fe2O3(t)	23.15	20.61	6.22	4.22	3.81	4.29	3.79	4.43	4.38	4.58	11.89	10.6	25.73
MnO	0.3	0.27	0.07	0.16	0.11	0.11	0.09	0.12	0.13	0.09	0.13	0.02	0.35
MgO	17.47	19.38	30.7	33.2	33.23	33.87	33.03	33.4	33.53	32.92	29.17	28.51	12.88
CaO	0.88	0.86	2.94	15.71	13.81	14.58	11.68	15.53	17.11	11.4	12.11	0.46	3.01
Na2O	0.04	0.05	0.08	0.09	0.08	0.11	0.09	0.1	0.1	0.08	0.09	0.06	0.03
K2O	0.02	0.02	0.02	0.03	0.02	0.03	0.02	0.03	0.03	0.02	0.02	0.02	0.02
P2O3	0.03	0.02	0.02	0.03	0.02	0.03	0.02	0.03	0.03	0.02	0.02	0.02	0.02
Cr2O3	17.64	16.85	2.17	0.09	0.35	0.05	0.07	0.08	0.09	0.13	1.39	1.57	20.15
Total	**99.23**	**99.39**	**100.08**	**99.89**	**99.89**	**100.18**	**99.61**	**99.91**	**99.91**	**99.88**	**98.32**	**99.90**	**101.68**
As	16	11	<10	14	10	<10	<10	15	<10	<10	138	77	58
Ba	43	13	58	4	<5	8	<5	<5	<5	<5	7	6	51
Co	92	27	75	21	27	21	29	33	14	39	204	186	***382***
Cr		9000		486	805	337	494	503	430	645	7000	7000	
Cu	<5	34	14	29	39	6	45	69	456	98	973	1082	557
Ga	21	6	15	<5	<5	<5	<5	<5	<5	<5	<5	<5	13
Hf	<5	<5	<5	<5	<5	<5	<5	<5	<5	<5	7	24	<5
Mo	<2	<2	<2	<2	<2	<2	<2	<2	<2	<2	<2	<2	<2
Nb	<2	<2	<2	<2	<2	<2	<2	<2	<2	<2	<2	<2	<2
Ni	11000	924	942	719	527	288	581	483	310	1036	***3276***	17000	9000
Pb	<5	5	<5	<5	<5	<5	<5	<5	<5	<5	<5	<5	<5
Rb	<5	<5	<5	<5	<5	<5	<5	<5	<5	<5	<5	<5	<5
Sc	25	18	29	10	11	13	10	9	10	9	12	6	33

Sample	UK-119A	UK-119B1	UK-119B2	UK-119C	UK-119D	UK-119E	UK-119F	UK-119G	UK-119H	UK-119I	UK-119J	UK-119K	UK-119L
Sr	9	36	12	169	170	207	192	180	231	202	184	7	51
Ta	<5	5	<5	<5	<5	<5	<5	<5	5	12	48	175	88
Th	5	<5	<5	<5	<5	<5	<5	<5	<5	<5	<5	<5	5
U	<3	<3	<3	<3	<3	<3	<3	<3	<3	<3	<3	<3	3
V	551	75	520	16	28	36	33	28	23	29	39	43	700
W	<3	<3	<3	<3	<3	<3	<3	<3	<3	<3	<3	16	8
Y	<3	6	4	4	3	4	5	4	5	<3	4	<3	4
Zn	700	42	578	14	19	7	21	9	195	12	29	66	582
Zr	26	24	22	7	13	24	21	23	20	20	20	15	19
C %	0.24	0.35	1.14	5.31	4.78	5.10	4.27	5.15	5.56	4.04	3.90	0.19	1.18
S %	0.01	0.01	0.16	0.12	0.14	0.19	0.14	0.17	0.01	0.24	3.90	3.54	2.62

2.

Sample	UK-119A	UK-119B1	UK-119B2	UK-119C	UK-119D	UK-119E	UK-119F	UK-119G	UK-119H	UK-119I	UK-119J	UK-119K	UK-119L
Rock Type	Chromitic Pyroxenite	Chromitic Pyroxenite	Dolomite	Dolomite	Dolomite	Dolomite	Dolomite	Dolomite	Dolomite	Dolomite	Dolomite	Dolomite	Chromitic Pyroxenite
Depth	*54.88*	*55.43*	*55.43*	*55.53*	*55.87*	*56.16*	*56.43*	*56.81*	*57.22*	*57.55*	*57.88*	*58.38*	*59.93*
SiO2	24.32	28.66	47.23	35.20	36.89	33.73	39.53	34.27	32.64	39.10	35.26	51.46	24.20
TiO2	0.39	0.43	0.22	0.05	0.09	0.12	0.10	0.10	0.09	0.13	0.11	0.12	0.37
Al2O3	13.63	10.78	5.06	1.15	1.78	3.15	2.23	1.98	1.80	2.89	2.40	2.39	11.01
Fe2O3(t)	22.45	19.92	5.65	3.33	3.06	3.38	3.12	3.49	3.40	3.82	10.36	9.80	25.03
MnO	0.29	0.26	0.06	0.13	0.09	0.09	0.07	0.09	0.10	0.08	0.11	0.02	0.34
MgO	16.93	18.74	27.91	26.15	26.64	26.69	27.26	26.32	26.05	27.46	25.41	26.36	12.53
CaO	0.86	0.83	2.67	12.37	11.07	11.49	9.64	12.24	13.29	9.50	10.54	0.43	2.93
Na2O	0.04	0.04	0.07	0.07	0.07	0.09	0.08	0.08	0.08	0.07	0.08	0.06	0.03
K2O	0.02	0.02	0.02	0.02	0.02	0.02	0.02	0.02	0.02	0.02	0.02	0.02	0.02
P2O3	0.03	0.02	0.02	0.02	0.02	0.02	0.02	0.02	0.02	0.02	0.02	0.02	0.02
Cr2O3	17.10	16.29	1.97	0.07	0.28	0.04	0.06	0.06	0.07	0.11	1.21	1.46	19.60
L.O.I.	3.12	3.44	10.02	26.92	24.69	26.94	21.06	26.81	28.67	19.84	14.56	8.13	2.77
Recal Factor	1.03	1.03	1.1	1.27	1.25	1.27	1.21	1.27	1.29	1.2	1.15	1.08	1.03

Sample	UK-119A	UK-119B1	UK-119B2	UK-119C	UK-119D	UK-119E	UK-119F	UK-119G	UK-119H	UK-119I	UK-119J	UK-119K	UK-119L
Total	99.07	99.27	99.96	99.72	99.75	100.00	99.47	99.77	99.81	99.70	98.16	99.58	98.72
As	16	11	<10	14	10	<10	<10	15	<10	<10	138	77	58
Ba	43	13	58	4	<5	8	<5	<5	<5	<5	7	6	51
Co	92	27	75	21	27	21	29	33	14	39	204	186	***382***
Cr		***0.9%***		486	805	337	494	503	430	645	***0.7%***	***0.7%***	
Cu	<5	34	14	29	39	6	45	69	456	98	973	1082	557
Ga	21	6	15	<5	<5	<5	<5	<5	<5	<5	<5	<5	13
Hf	<5	<5	<5	<5	<5	<5	<5	<5	<5	<5	7	24	<5
Mo	<2	<2	<2	<2	<2	<2	<2	<2	<2	<2	<2	<2	<2
Nb	<2	<2	<2	<2	<2	<2	<2	<2	<2	<2	<2	<2	<2
Ni	***1.1%***	924	942	719	527	288	581	483	310	1036	***3276***	***1.7%***	***0.9%***
Pb	<5	5	<5	<5	<5	<5	<5	<5	<5	<5	<5	<5	<5
Rb	<5	<5	<5	<5	<5	<5	<5	<5	<5	<5	<5	<5	<5
Sc	25	18	29	10	11	13	10	9	10	9	12	6	33
Sr	9	36	12	169	170	207	192	180	231	202	184	7	51
Ta	<5	5	<5	<5	<5	<5	<5	<5	5	12	48	175	88
Th	5	<5	<5	<5	<5	<5	<5	<5	<5	<5	<5	<5	5
U	<3	<3	<3	<3	<3	<3	<3	<3	<3	<3	<3	<3	3
V	551	75	520	16	28	36	33	28	23	29	39	43	700
W	<3	<3	<3	<3	<3	<3	<3	<3	<3	<3	<3	16	8
Y	<3	6	4	4	3	4	5	4	5	<3	4	<3	4
Zn	700	42	578	14	19	7	21	9	195	12	29	66	582
Zr	26	24	22	7	13	24	21	23	20	20	20	15	19
C %	0.24	0.35	1.14	5.31	4.78	5.10	4.27	5.15	5.56	4.04	3.90	0.19	1.18
S %	0.007	0.015	0.160	0.115	0.139	0.194	0.144	0.174	0.012	0.237	3.902	3.537	2.618

Results of major (wt%) and trace (ppm) analysed by X-ray fluorescence spectrometry
Exceeds upper limit of calibration range

UK119

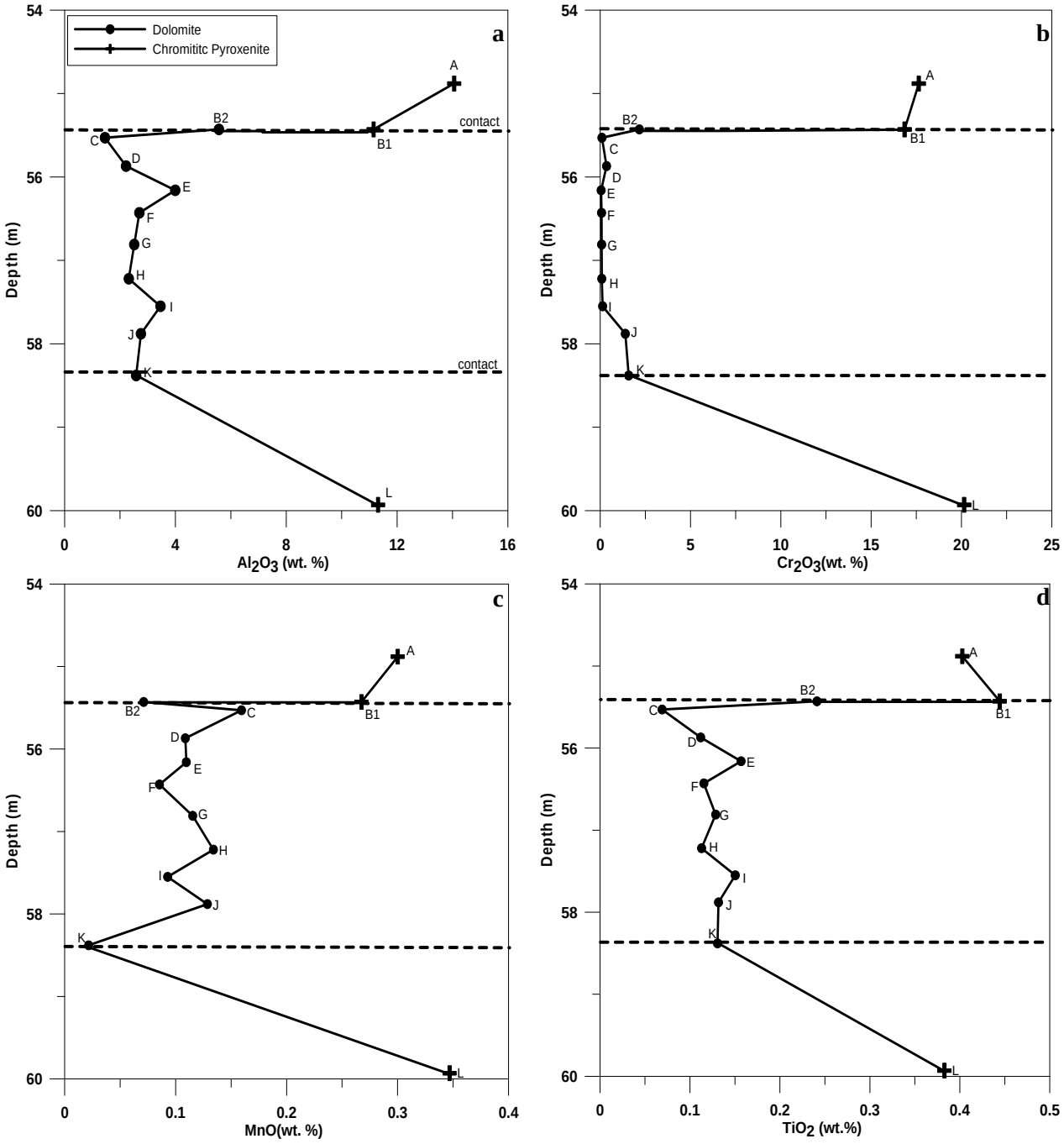
a
Dolomite
Chromititc Pyroxenite
contact
contact
Depth (m)
Al_2O_3 (wt. %)
b
Cr_2O_3(wt. %)
c
MnO(wt. %)
d
TiO_2 (wt.%)

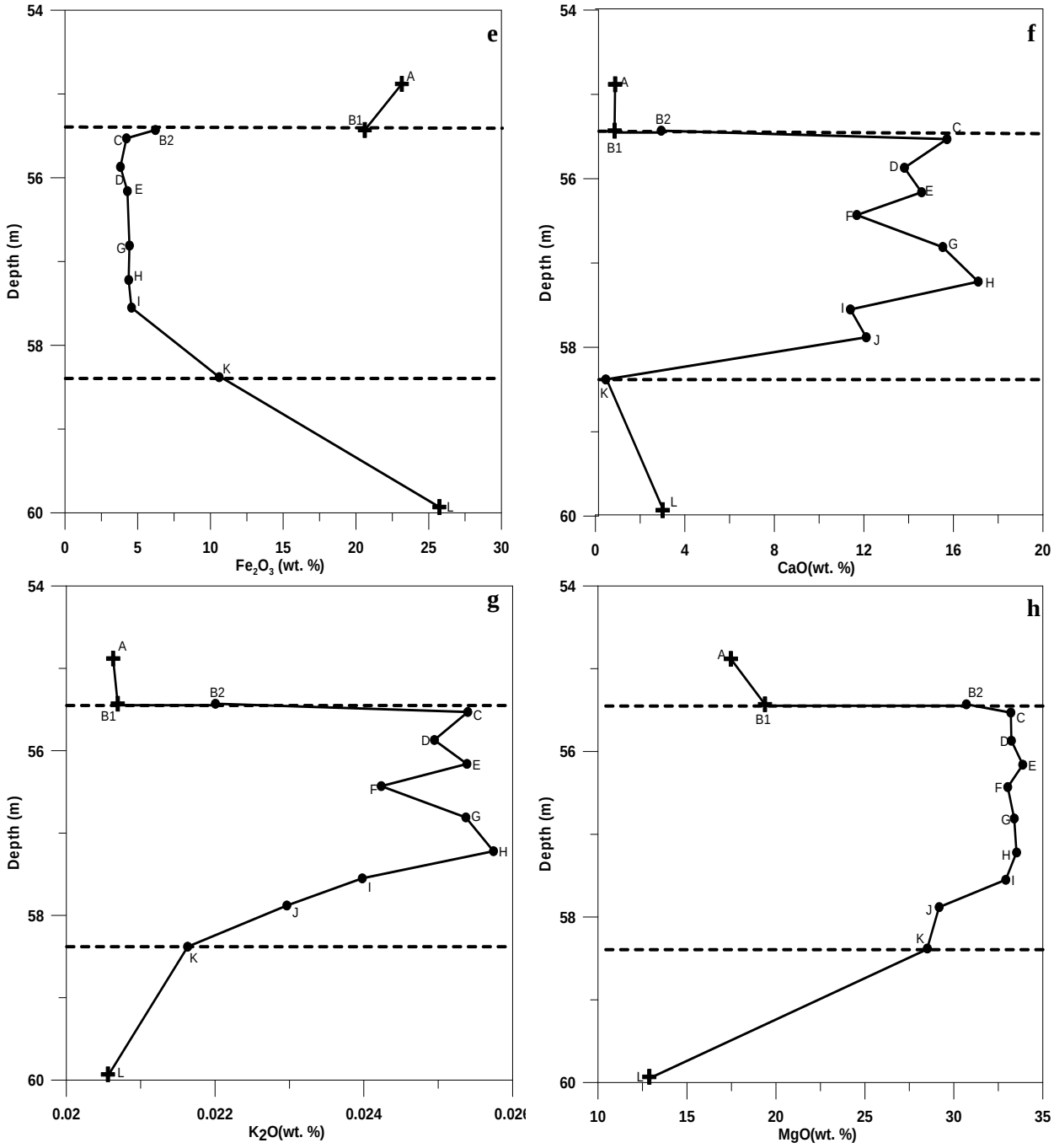
e
Depth (m)
Fe_2O_3 (wt. %)
f
CaO(wt. %)
g
K_2O(wt. %)
h
MgO(wt. %)

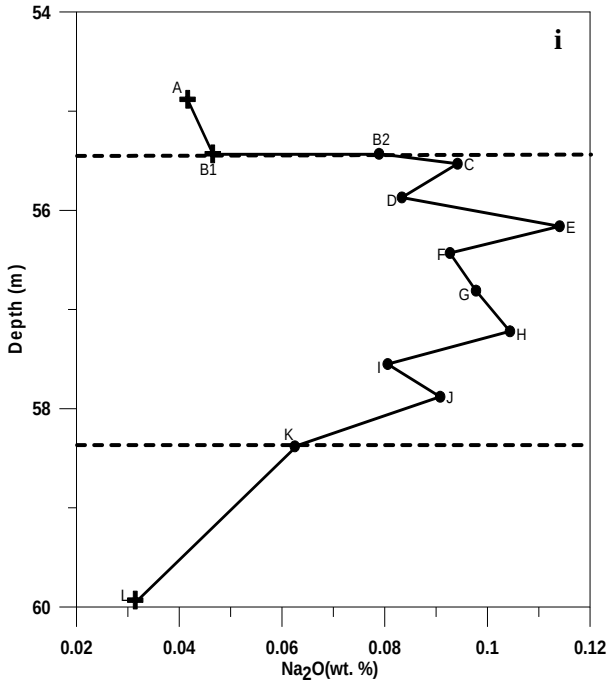
i
Depth (m)
54
56
58
60
A
B1
B2
C
D
E
F
G
H
I
J
K
L
0.02
0.04
0.06
0.08
0.1
0.12
Na2O(wt. %)

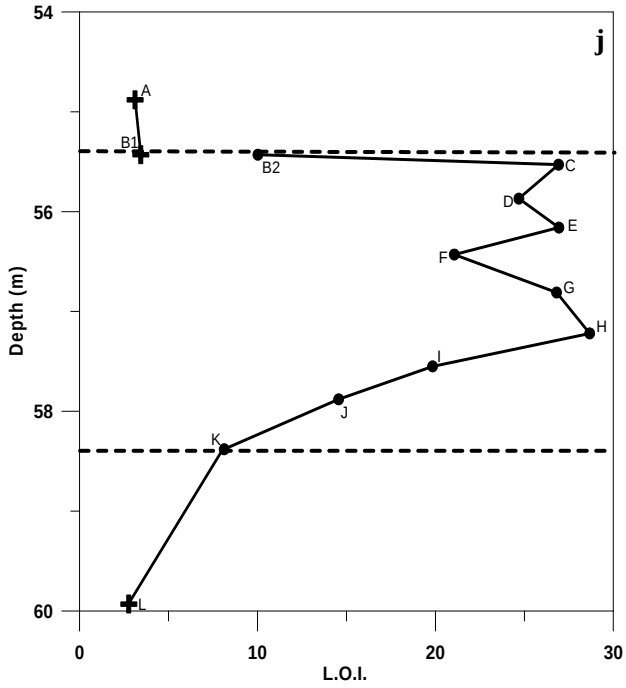
j
Depth (m)
54
56
58
60
A
B1
B2
C
D
E
F
G
H
I
J
K
L
0
10
20
30
L.O.I.

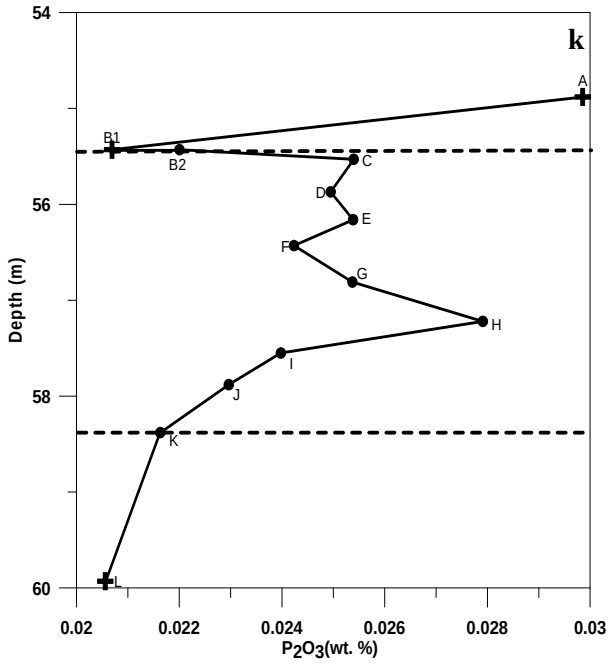
k
Depth (m)
54
56
58
60
A
B1
B2
C
D
E
F
G
H
I
J
K
L
0.02
0.022
0.024
0.026
0.028
0.03
P2O3(wt. %)

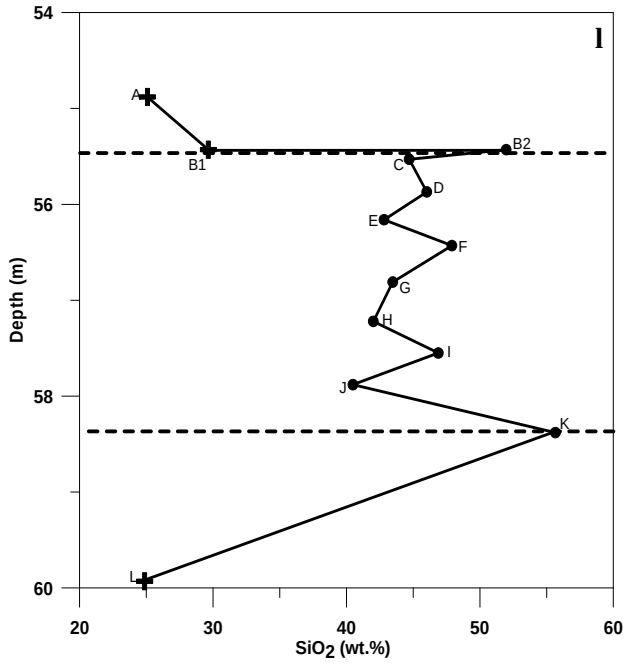
l
Depth (m)
54
56
58
60
A
B1
B2
C
D
E
F
G
H
I
J
K
L
20
30
40
50
60
SiO2 (wt.%)

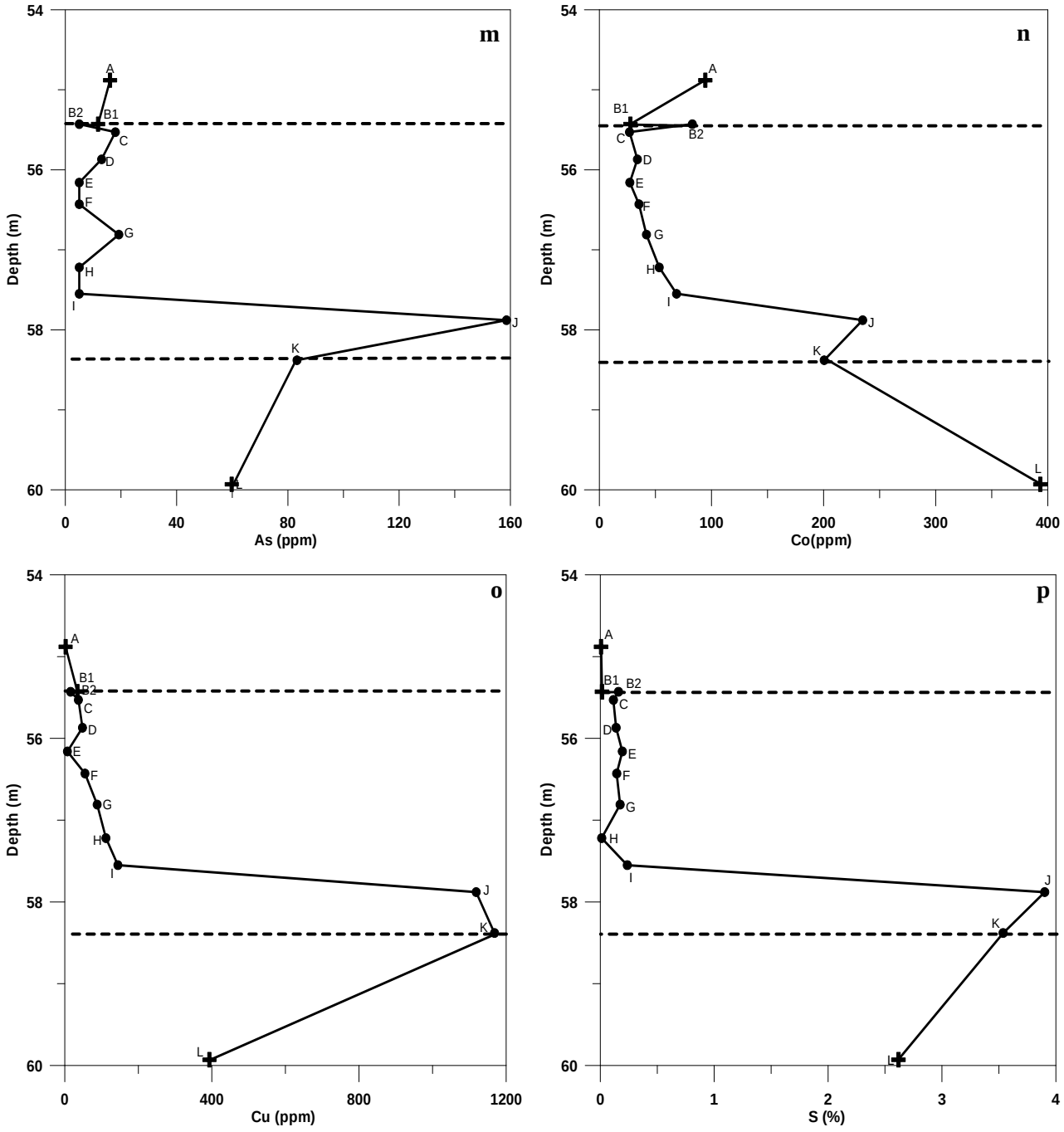
m
Depth (m)
As (ppm)
n
Co(ppm)
o
Cu (ppm)
p
S (%)

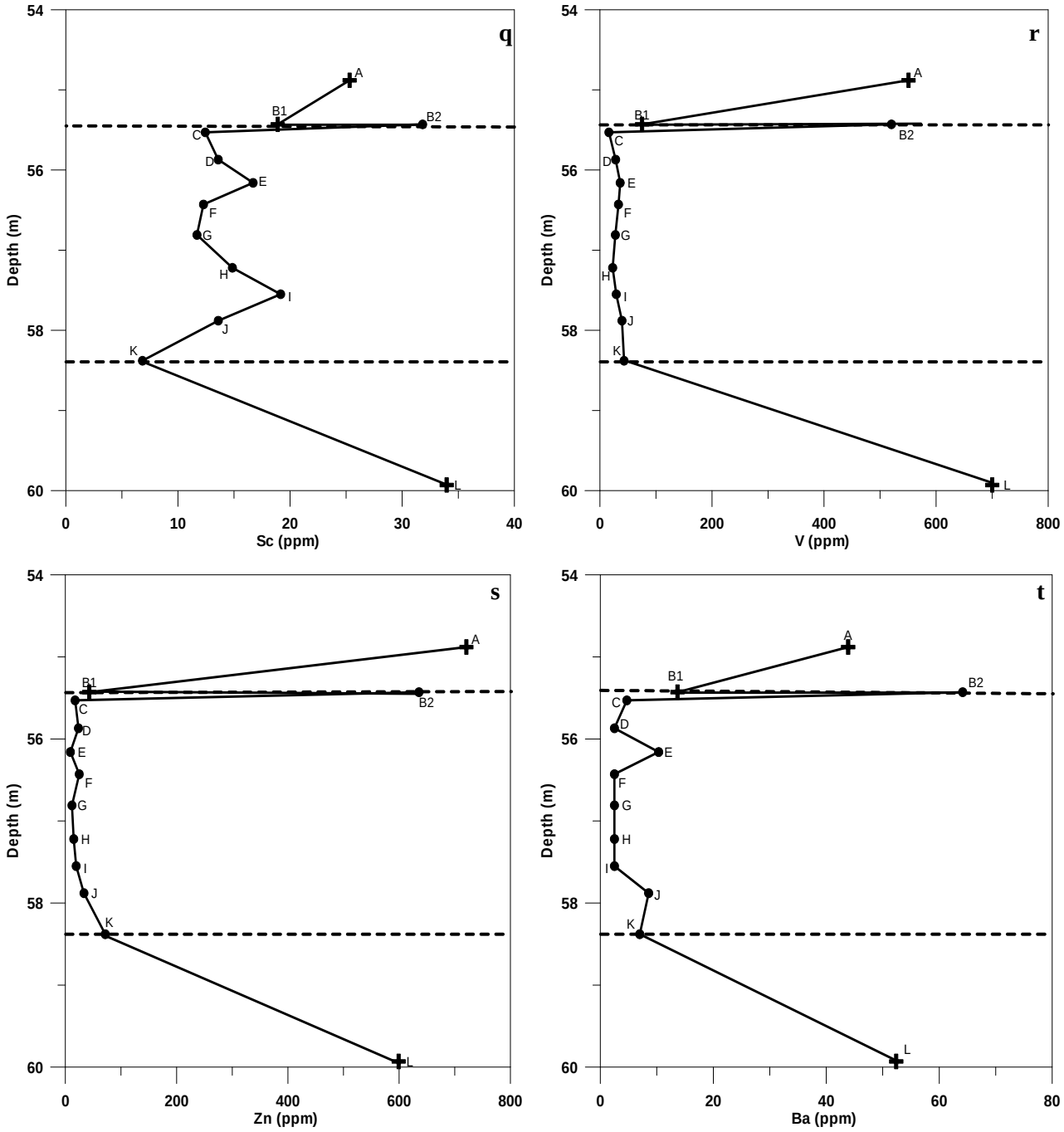
q
Depth (m)
Sc (ppm)
r
V (ppm)
s
Zn (ppm)
t
Ba (ppm)
A
B1
B2
C
D
E
F
G
H
I
J
K
L

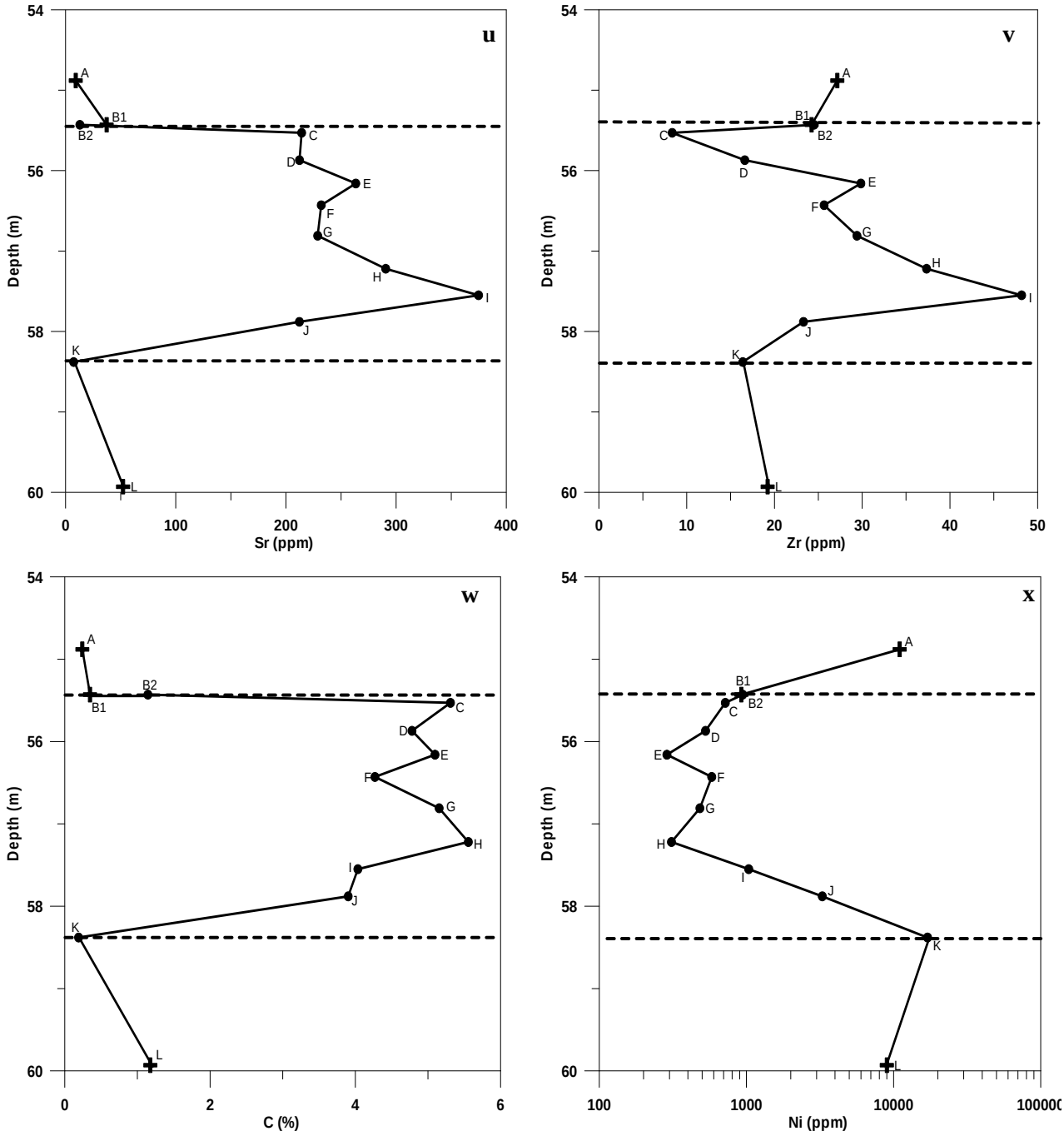

Figure 5. 1: Variations in the major and trace element chemistry with depth for borehole UK119

5.4. Stable isotope chemistry

5.4.1. Introduction

The term “isotope” is derived from the Greek, meaning equal places and refers to the same position that isotopes of the same element occupy in the periodic table of elements (Hoefs, 1973). The partitioning of isotopes between two substances or phases of the same substance with different isotope ratios is called isotope fractionation. The main phenomena producing isotope fractionation are:

1. Isotope exchange reactions, and
2. Kinetic processes, which depend primarily on differences in reaction rates of isotopic molecules.

The application of isotope studies to metamorphic rocks is useful for defining the scale of fluid migration and interaction. The stable isotope composition of a metamorphic rock is controlled by 4 factors:

1. the composition of the pre-metamorphic protolith,
2. the effects of volatilisation
3. exchange with infiltrating fluids (with variable composition and fluid/rock ratio)
4. the temperature of exchange.

Sulphur isotope studies have been applied to the Uitkomst Complex by previous authors to constrain the source of sulphur in the ore (Gauert *et al*., 1996, Li *et al*., 2002). These authors have proposed the addition of isotopically light sedimentary sulphur to the magma as a possible mechanism for the triggering of the sulphide segregation in the Uitkomst Complex. The possible addition of externally derived sulphur through the assimilation and contamination of country rock has also been proposed for the Duluth Complex (Ripley, 1981; Ripley and Al-Jasar, 1987; Arcuri *et al*., 1998) and Noril’sk (Godlevsky and Grinenko, 1963; Naldrett *et al*., 1996). The use of sulphur isotopes as a tool for determining the role of the contamination of the

magma by crustal rocks in triggering sulphide mineralisation is illustrated in Figure 5. 2. It is seen that at Noril'sk there is a good correlation between the mineralisation and the amount of crustal Sulphur.

Prograde metamorphism of sediments causes the liberation of "volatile" elements by the reaction of lower temperature minerals. Decarbonation commonly occurs in carbonate-bearing lithologies, and CO_2 is often liberated with H_2O during metamorphism of siliceous limestones and marls. Large volumes of rock (up to 40%) can be volatised with the potential for significant isotopic shift. Carbon and oxygen isotopes are used in this study, in order to support the petrological evidence in §3 and 4 for decarbonation at the margins of the xenoliths. The purpose of this section is thus to constrain the possible mechanisms that might have caused the segregation of the sulphides in the Uitkomst Complex.

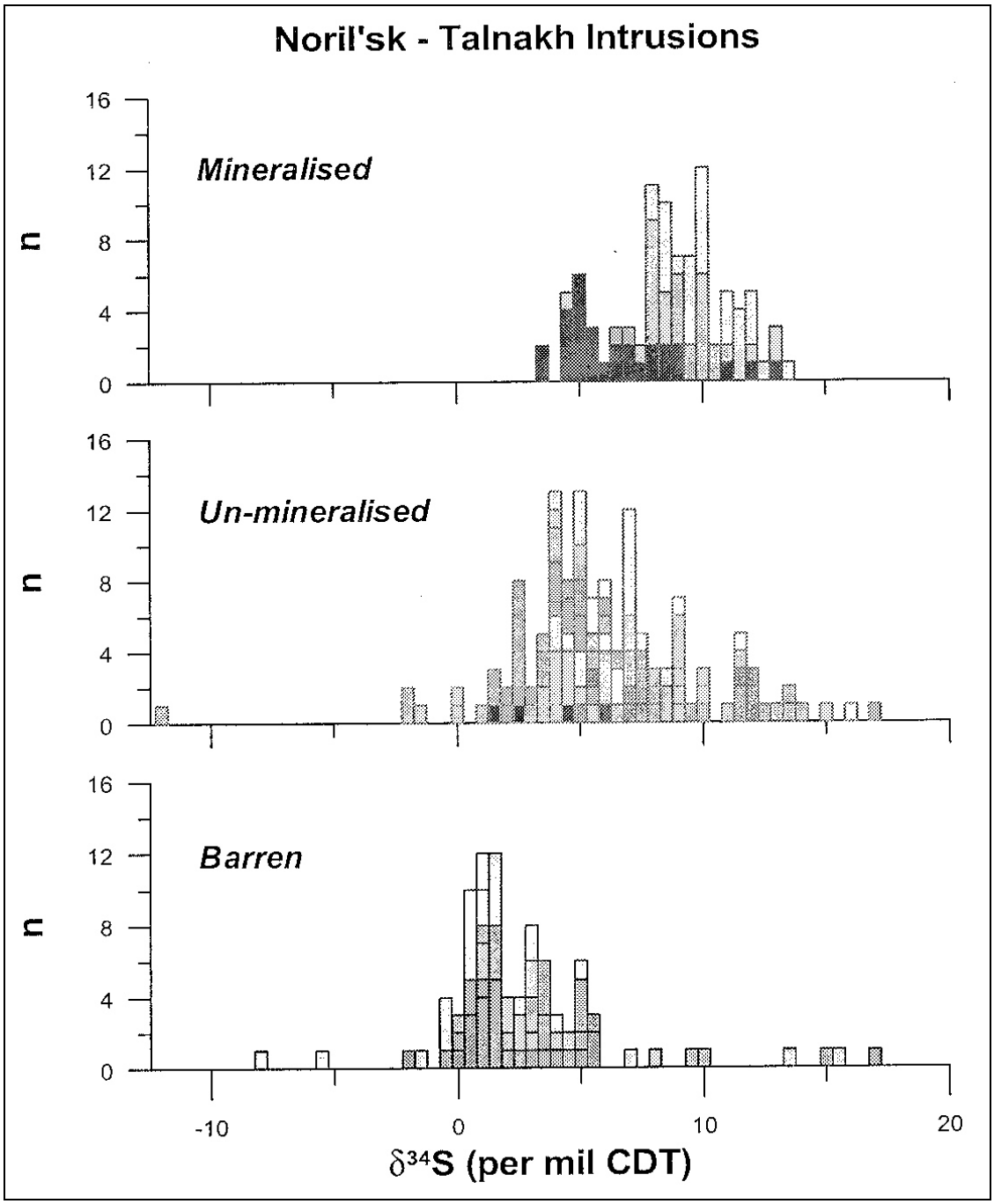

Figure 5. 2: Variation of sulphur isotope composition for barren, un-mineralised and mineralised intrusions of the Noril'sk – Talnakh area (Figure from Grinenko, 1985)

5.4.2. Sample selection

Fifteen carbonate samples (calcites and dolomites) from the xenoliths found within the Basal and Main Mineralised Zones of the Uitkomst Complex were analysed for carbon and oxygen isotopes at the Council for Geoscience.

The mineralogical composition of the samples was determined by XRD at the Council for Geoscience. Sufficient carbonate was detected in all samples. Calcite and dolomite were the only carbonate species detected petrographically, with dolomite making up between 30% and 40% of the samples from the Main Mineralised Zone (denoted UK…). Samples from the Basal Mineralised Zone (denoted VH…) contain between 4% and 17% calcite, but no dolomite.

In addition to this, seven additional samples from the Uitkomst Complex were submitted to the University of Cape Town for whole rock oxygen isotope analysis.

Forty-two sulphide samples were prepared and submitted for S isotope analysis. The S stable isotope analyses were carried out at the IAEA Environmental Isotope Laboratory of the Schonland Research Institute at the University of the Witwatersrand, Johannesburg.

The sample preparations and analytical techniques are detailed in Appendix C.

5.4.3. Carbon and oxygen isotope variations

The carbon and oxygen isotope results for the MMZ and BMZ samples are provided in Table 5. 2.

Table 5. 2: Carbon and oxygen stable isotope ratios for carbonates and oxygen isotope results in carbonates from the BMZ and MMZ. Seven samples were additionally analysed for oxygen isotopes in whole rocks.

SAMPLE	MINERAL	δ^{13}C ‰ PDB	δ^{18}O‰ PDB	δ^{18}O‰ SMOW
UK119C	**Dolomite**	-2.4	-16.5	13.8
UK119D	**Dolomite**	-2.3	-16.5	13.9
UK119E	**Dolomite**	-2.2	-16.5	13.8
UK119F	**Dolomite**	-2.1	-16.4	13.9
UK119G	**Dolomite**	-2.1	-16.4	14.0
UK119H	**Dolomite**	-2.1	-16.4	14.0
UK119I	**Dolomite**	-2.0	-16.3	14.0
UK119Jx	**Dolomite**	-2.0	-16.4	13.9
UK119L	**Dolomite**	-2.4	-16.2	14.1
VH09A	**Calcite**	-4.6	-17.9	12.4
VH09B	**Calcite**	-4.9	-17.9	12.4
VH09D	**Calcite**	-4.9	-17.8	12.5
VH09E	**Calcite**	-5.1	-17.8	12.5
VH09F	**Calcite**	-5.2	-17.8	12.5
VH11	**Calcite**	-5.1	-17.7	12.6
UK119A1				8.4
UK119A2				7.8
UK119K2				7.3
UK119L				8.9
SH176UP5				9.0
SH176UP19				6.9
SH176UP40				7.2

UK119

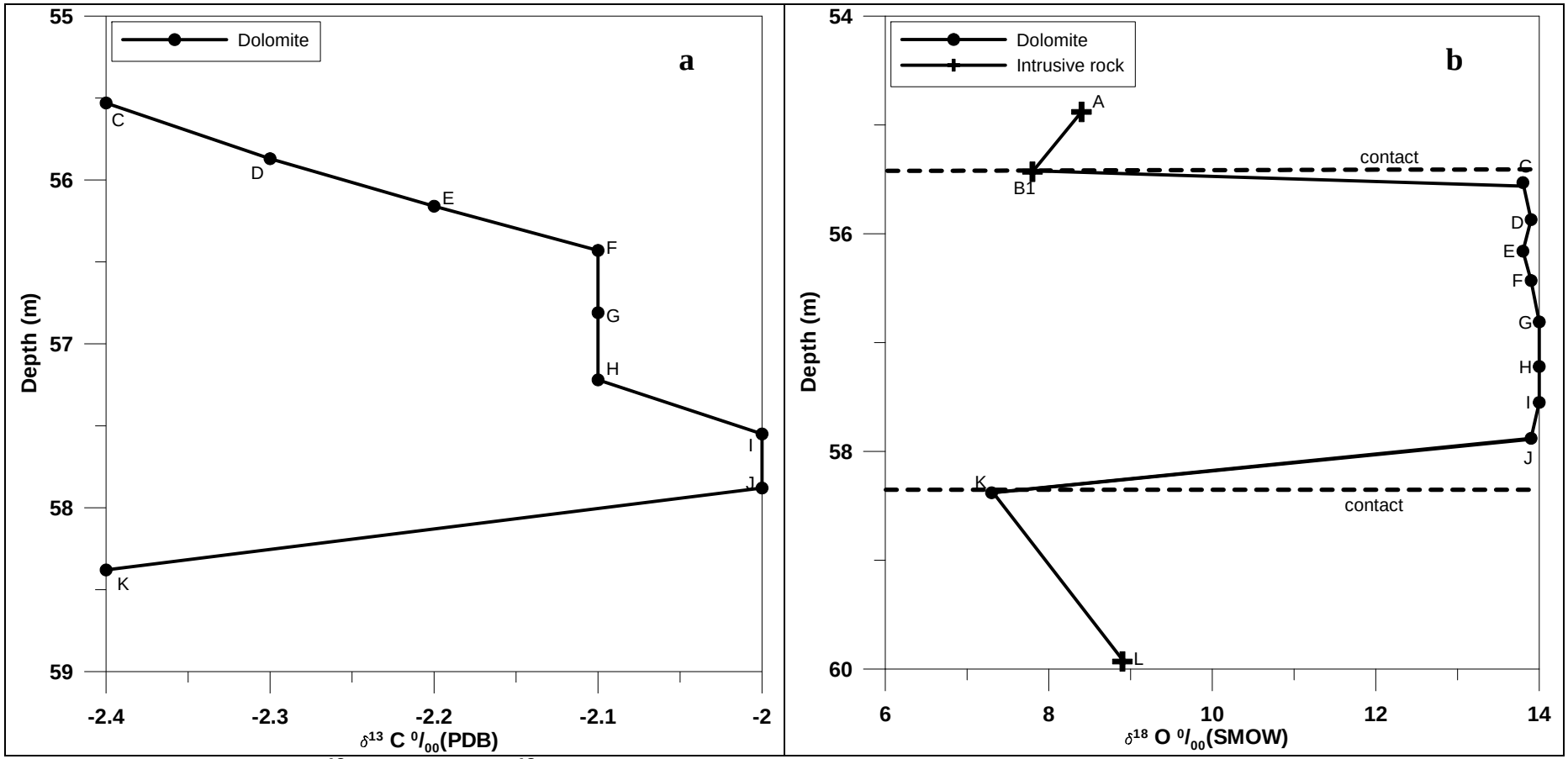

Figure 5. 3: Variations in $\delta^{13}C$ ‰ (a) and $\delta^{18}O$‰ (b) with depth in borehole UK119.

The variations in the $\delta^{18}O$ and $\delta^{13}C$ values with depth for the samples from borehole UK119 (MMZ) are plotted in Figure 5. 3. It is seen that the contact zones have lower values for both $\delta^{18}O$ and $\delta^{13}C$.

Figure 5. 4 graphically illustrates the variation in $\delta^{13}C$ with $\delta^{18}O$ for the samples. Calcites and dolomites are clearly distinguished with the calcites clustering around a $\delta^{13}C$ value of $\approx -5‰$ and a $\delta^{18}O$ value of $\approx 12‰$. The dolomites have a distinctly higher isotopic composition around $\delta^{13}C \approx -2‰$ and $\delta^{18}O \approx 14‰$. The Uitkomst Complex samples (Table 5. 2) have $\delta^{18}O$ values between 6.9 and 9.0‰. This is much lower than that observed for the xenoliths.

The general C/O isotope compositional field of Transvaal Dolomite (Beukes *et al*., 1990; Veizer *et al*., 1992; Horstmann, unpubl. data) is drawn into Figure 5. 4. Also included in the diagram are the "normal" (marine) sedimentary carbonate composition of $\delta^{13}C = 0‰$ and $\delta^{18}O = 22‰$, as well as the "carbonatite box" of Taylor *et al*. (1967). The C/O isotopes of the Uitkomst carbonates lie between these compositional fields.

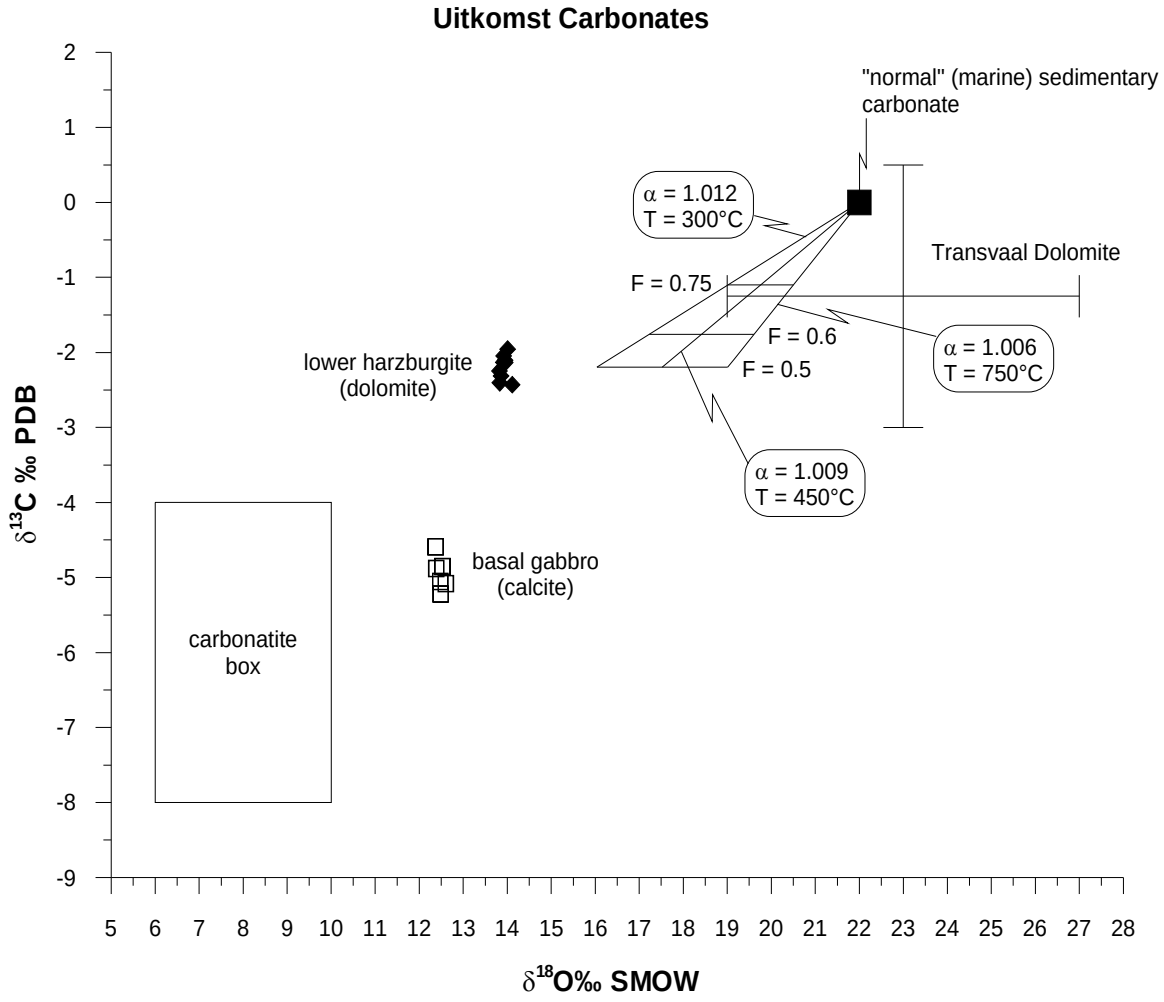

Figure 5. 4: $\delta^{18}O$ vs. $\delta^{13}C$ of Uitkomst carbonates in relation to igneous values ("carbonatite box" after Taylor *et al.*, 1967 and Keller and Hoefs, 1995) and sedimentary carbonates (Transvaal Dolomite after Beukes *et al.*, 1990; Veizer *et al.*, 1992). Normal marine sedimentary carbonate and batch volatilisation pathways after Valley (1986). Values of the mole fraction of O remaining in the rock after volatilisation (F) are also indicated, defining tie–lines between O isotopic compositions and the various fractionation factors (temperatures). Fractionation factors from Valley (1986).

The liberation of volatile elements through the reaction of lower temperature minerals during prograde metamorphism of sedimentary rocks is outlined by Valley (1986). The most common reaction is dehydration, but decarbonation occurs in carbonate–bearing lithologies. Oxygen and carbon, as well as hydrogen and sulphur show the greatest stable isotope fractionation.

Tentative pathways for the decarbonation of a sedimentary carbonate are indicated in Figure 5. 4. Three curves are shown for oxygen fractionation factors of $\alpha_{CO_2\text{–rock}}$ corresponding to metamorphic temperatures of 750°C, 450°C and 300°C, respectively. For carbon, a fractionation factor $\alpha_{CO_2\text{–rock}} = 1.0022$ was chosen (Valley, 1986). Values of the mole fraction of O remaining in the rock after volatilisation (F) are also indicated, defining tie–lines between O isotopic compositions and the various fractionation factors (temperatures).

Assuming normal calc–silicate decarbonation reactions, the devolatilisation curves in Figure 5. 4 explain the lowering of the $\delta^{13}C$ and $\delta^{18}O$ values of the Uitkomst carbonates. However, this only remains valid to a certain extent. Valley (1986) discussed that there is a "calc–silicate limit" of $F \geq 0.6$ for oxygen values. This limit is introduced by silicate minerals which will always be the dominant oxygen reservoir in the residual metamorphosed rock. Theoretically possible lower values of F (i.e. more complete devolatilisation/decarbonation reactions) are highly unlikely in nature. In this case, devolatilisation would lead to a depletion of a sedimentary carbonate rock down to $\delta^{13}C$ of about –2‰ and $\delta^{18}O$ values of 16‰ to 19‰. Most of the Uitkomst carbonates lie well below these values and cannot realistically be explained by devolatilisation/decarbonation reactions only.

Given this limitation, another process is needed to change the isotopic composition of the Uitkomst carbonates to the observed values. Coupled O–C trends with decreasing $\delta^{13}C$ and $\delta^{18}O$ values at increasing metamorphic grade were compiled by Valley (1986). These values start at normal marine compositions and decrease towards the "carbonatite box", i.e. approaching igneous values. The C and O isotope depletion in almost all cases is too big to be explained by volatilisation alone and fluid infiltration is indicated. Such fluids may be derived from surface waters (meteoric or sea water), magmatic crystallisation or sedimentary waters (Sheppard, 1986). The effectiveness of these fluids depends on the fluid availability, the magnitude of isotopic differences, the degree of permeability and on the rock type.

The dolomites were overprinted at a lower temperature compared to the calcites. Their C/O isotopic composition plots in the field of secondary alteration (by e.g. meteoric waters) as suggested by Hall and Veizer (1996). However, late–stage (post–metamorphic) fluid movement at 400–500°C cannot be excluded (Taylor and O'Neil, 1977). Several stages must probably be envisaged for the formation of the dolomites. First, a "mostly magmatic" stage occurred with $X_{CO_2} < 0.035$ and T = 480–550°C (Taylor and O'Neil, 1977), which involved fluid infiltration combined with decarbonation. These early magmatic fluids later gave way to meteoric waters at lesser temperatures, a trend that is often observed in skarns (For example So *et al*., 1983; Bowman *et al*., 1985a,b).

The ultramafic rocks of the Uitkomst Complex are pervasively altered to talc and serpentine, presumably due to late-stage hydrothermal infiltration (van Zyl, 1996; Gauert, 1998). In addition to this, evidence from this study (i.e the limited variation in the O and C isotopes with height in the xenolith) is in accord with a model of late-stage fluid infiltration (i.e. it is not the infiltration by the magma that caused the variation). Sample UK119K forms an exception, in that it has a magmatic O isotope signature, most likely due to magma infiltration. This sample also shows the most pronounced increase in SiO_2 and decrease in CaO and C.

5.4.4. Sulphur isotope results

Results of the S isotopic analyses are summarised in Table 5. 3.

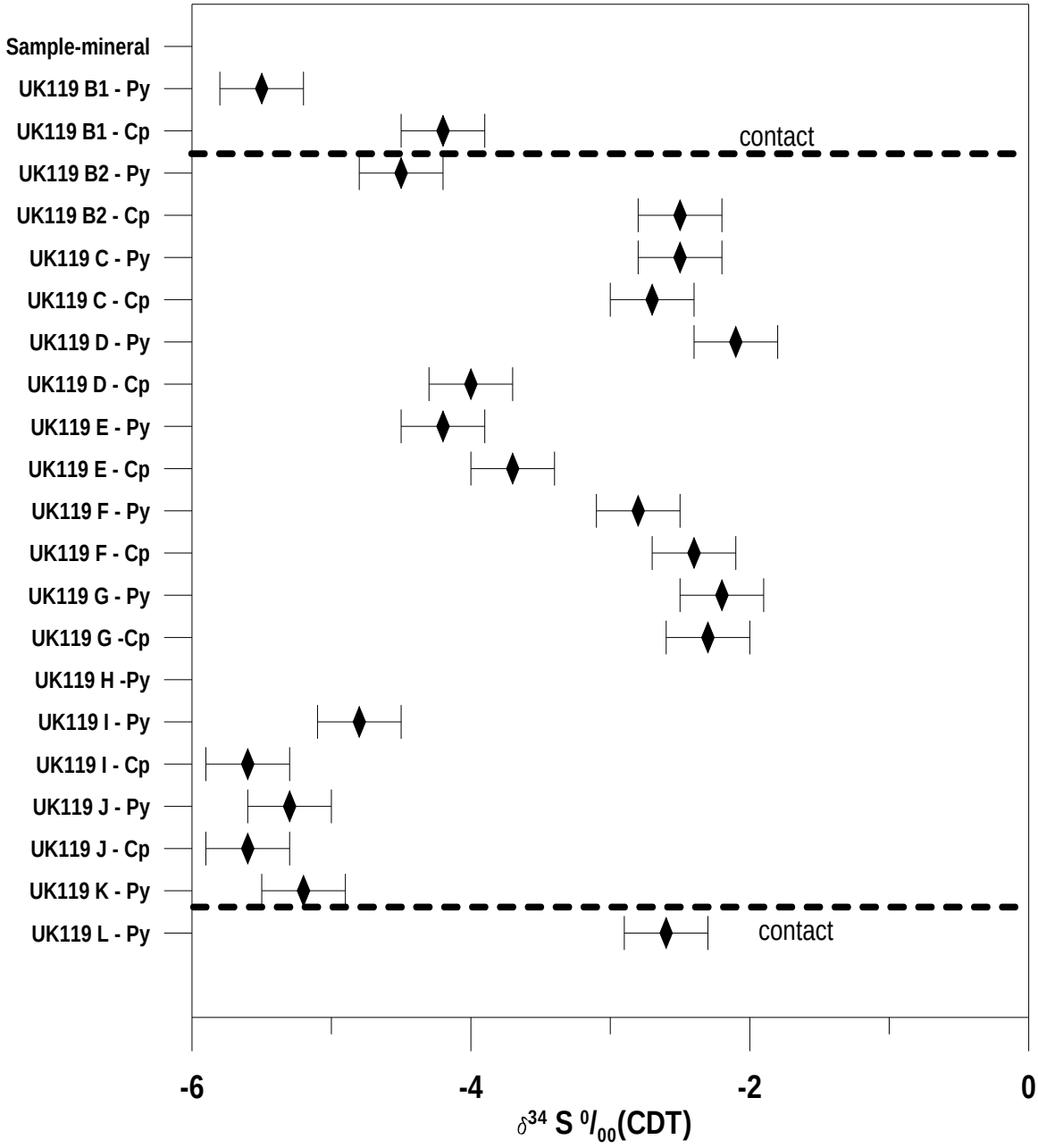

Figure 5. 5: Distribution of $\delta^{34}S$ values in the sample suite. Error bars denote analytical error of ± 0.3‰. Py = pyrite, Cp = chalcopyrite

Table 5. 3: S isotope results

SAMPLE	LITHOLOGY	UNIT	DESCRIPTION / MINERAL	$\delta^{34}S‰$ CDT
UK119 B1	Chromititic Pyroxenite	MMZ	non-mag. sulphides (pyrite)	-5.5
UK119 B1	Chromititic Pyroxenite	MMZ	M1.0 / 5° sulphides (chalcopyrite)	-4.2
UK119 B2	Dolomite	MMZ	non-mag. sulphides (pyrite)	-4.5
UK119 B2	Dolomite	MMZ	M1.5 / 5° sulphides (chalcopyrite)	-2.5
UK119 C	Dolomite	MMZ	non-mag. sulphides (pyrite)	-2.5
UK119 C	Dolomite	MMZ	M1.5 / 5° sulphides (chalcopyrite)	-2.7
UK119 D	Dolomite	MMZ	non-mag. sulphides (pyrite)	-2.1
UK119 D	Dolomite	MMZ	M1.5 / 5° sulphides (chalcopyrite)	-4.0
UK119 E	Dolomite	MMZ	non-mag. sulphides (pyrite)	-4.2
UK119 E	Dolomite	MMZ	M1.5 / 5° sulphides (chalcopyrite)	-3.7
UK119 F	Dolomite	MMZ	non-mag. sulphides (pyrite)	-2.8
UK119 F	Dolomite	MMZ	M1.5 / 5° sulphides (chalcopyrite)	-2.4
UK119 G	Dolomite	MMZ	non-mag. sulphides (pyrite)	-2.2
UK119 G	Dolomite	MMZ	M1.5 / 5° sulphides (chalcopyrite)	-2.3
UK119 H	Dolomite	MMZ	non-mag. sulphides (pyrite)	n/a
UK119 I	Dolomite	MMZ	non-mag. sulphides (pyrite)	-4.8
UK119 I	Dolomite	MMZ	M1.5 / 5° sulphides (chalcopyrite)	-5.6
UK119 J	Dolomite	MMZ	non-mag. sulphides (pyrite)	-5.3
UK119 J	Dolomite	MMZ	M1.5 / 5° sulphides (chalcopyrite)	-5.6
UK119 K	Chromititic Pyroxenite	MMZ	pyrite?	-5.2
UK119 L	Chromititic Pyroxenite	MMZ	pyrite	-2.6
VH03 A		BMZ	M1.0 / 5° sulphides (chalcopyrite)	-0.8
VH09 A		BMZ	M1.0 / 5° sulphides (chalcopyrite)	-8.0
VH09 B		BMZ	M1.0 / 5° sulphides (chalcopyrite)	-5.6
VH09 C		BMZ	sulphides	-1.7
VH09 D		BMZ	pyrite	-1.3
VH09 D		BMZ	M1.0 / 5° sulphides (chalcopyrite)	-2.4
VH09 E		BMZ	pyrite?	-2.9
VH09 E		BMZ	M1.0 / 5° sulphides (chalcopyrite)	-1.1
VH09 F		BMZ	pyrite?	-1.1
VH09 F		BMZ	M1.0 / 5° sulphides (chalcopyrite)	-2.2
VH10 A		BMZ	M1.0 / 5° sulphides (mixed)	1.7
VH10 B		BMZ	M1.0 / 5° sulphides (mixed)	0.1
VH10 D		BMZ	M0.5 / 5° sulphides (chalcopyrite)	-2.8
VH11		BMZ	non-mag. sulphides (mixture)	-1.4
VH11		BMZ	non-mag. sulphides (pyrite)	-1.2
VH11		BMZ	M1.5 / 5° sulphides (chalcopyrite)	-2.4
VH2		BMZ	pyrite	-4.6
VH2		BMZ	pyrrhotite	-5.8
VH2		BMZ	M0.5 / 5° chalcopyrite	-5.5
SHU60		MMZ	pyrrhotite	-6.1
SHU61		MMZ	pyrrhotite	-5.9

Figure 5. 5 illustrates the sulphur isotopic composition of the samples from UK119. The spread of the samples from this borehole is between –2‰ and -6‰. The other

samples taken from the basal mineralised zone (denoted VH…) show a larger spread in $\delta^{34}S$ values, with the results ranging between 2‰ and –9‰. The spread of the $\delta^{34}S$ values from –9‰ to +2‰ is larger than would be expected for mantle-derived igneous rocks (0±1‰; e.g. Ohmoto, 1986).

Ohmoto (1986) discussed the S isotopic composition of magmas generated by partial melting of the mantle and concluded that igneous rocks produced from such magmas could not have $\delta^{34}S$ values outside the range of –3‰ to +3‰. Assimilation of crustal sulphur is the most likely process that generated rocks with a wider spread of S isotopic compositions. Naldrett (1966, 1981) investigated the S isotopic composition of Ni- Cu sulphide deposits and suggested that assimilation of crustal sulphur by magmas was an important condition for the formation of such deposits.

The chemistry of ore fluids and their influence on the S isotopic composition of precipitated mineral phases is discussed by Rye and Ohmoto (1974). Rye and Ohmoto (1974) illustrated the variation of $\delta^{34}S$ of sulphate, H_2S, and sulphide minerals with the variation of the H_2S/SO_4^{2-} ratio of the hydrothermal solution. The $\delta^{34}S$ of a precipitated sulphide mineral depends on two factors:

1. the isotopic composition of the total S (ΣS) in the fluid system, and
2. the chemical partitioning of S components in the ore fluid (i.e., the H_2S/SO_4^{2-} ratio).

S isotope thermometry was applied to some of the samples in this study. S isotope thermometry requires two prerequisites:

1. very clean mineral separates, and
2. the assumption of isotopic equilibrium between the mineral pairs and the ore fluid they precipitated from.

The latter is not fulfilled in all cases. Table 5. 4 lists pyrite/ chalcopyrite pairs and one pyrite-pyrrhotite pair where the application of S isotope thermometry may be feasible. In other cases, either the fractionation between pyrite and chalcopyrite is too small, leading to unrealistically high temperatures or the fractionation turns out negative. Both observations would indicate that isotopic equilibrium was not attained. The more realistic fractionations yield temperatures in the range of hydrothermal fluids, if the S isotope thermometer equations of Ohmoto and Rye (1979) are applied. Hydrothermal activity is thus indicated by the S isotope fractionation between certain pyrite/pyrrhotite and chalcopyrite pairs from the sample suite.

Table 5. 4: S-isotope thermometry for the Uitkomst sulphide samples

Sample	Description / Mineral	$\delta^{34}S$‰ CDT	$\Delta_{py\text{-}cpy}$	$\Delta_{py\text{-}pyr}$	T [°C]
UK119 B1	non-mag. sulphides (pyrite)	-5.5			
	M1.0 / 5° sulphides (chalcopyrite)	-4.2	-1.3		
UK119 B2	non-mag. sulphides (pyrite)	-4.5			
	M1.5 / 5° sulphides (chalcopyrite)	-2.5	-2.0		
UK119 C	non-mag. sulphides (pyrite)	-2.5			
	M1.5 / 5° sulphides (chalcopyrite)	-2.7	0.2		*1303**
UK119 D	non-mag. sulphides (pyrite)	-2.1			
	M1.5 / 5° sulphides (chalcopyrite)	-4.0	2.0		232
UK119 E	non-mag. sulphides (pyrite)	-4.2			
	M1.5 / 5° sulphides (chalcopyrite)	-3.7	-0.5		
UK119 F	non-mag. sulphides (pyrite)	-2.8			
	M1.5 / 5° sulphides (chalcopyrite)	-2.4	-0.4		
UK119 G	non-mag. sulphides (pyrite)	-2.2			
	M1.5 / 5° sulphides (chalcopyrite)	-2.3	0.1		*1850**
UK119 I	non-mag. sulphides (pyrite)	-4.8			
	M1.5 / 5° sulphides (chalcopyrite)	-5.6	0.8		497
UK119 J	non-mag. sulphides (pyrite)	-5.3			
	M1.5 / 5° sulphides (chalcopyrite)	-5.6	0.3		*983**
VH09 D	pyrite	-1.3			
	M1.0 / 5° sulphides (chalcopyrite)	-2.4	1.1		392
VH09 E	pyrite?	-2.9			
	M1.0 / 5° sulphides (chalcopyrite)	-1.1	-1.8		
VH09 F	pyrite?	-1.1			
	M1.0 / 5° sulphides (chalcopyrite)	-2.2	1.1		418
VH11	non-mag. sulphides (pyrite)	-1.2			
	M1.5 / 5° sulphides (chalcopyrite)	-2.4	1.2		371
VH2	pyrite	-4.6			
	pyrrhotite	-5.8		1.1	394
	M0.5 / 5° chalcopyrite	-5.5	0.9		470

Per-mil fractionation of sulphides (Δ) approximated as $\delta^{34}S_{py} - \delta^{34}S_{cp}$ and $\delta^{34}S_{py} - \delta^{34}S_{po}$ respectively (py = pyrtite; po = pyrrhotite; cp = chalcopyrite). Temperature calculated using equations of Ohmoto and Rye (1979) with errors of about ± 40°C. * = not feasible temperature due to too small isotope fractionation with probably no isotopic equilibrium attained.

6. DISCUSSION AND CONCLUSIONS

6.1. General

Magmatic sulphide ores in magma conduit systems from around the world show evidence for crustal contamination playing an important role in ore formation (for example: Voisey's Bay (Li and Naldrett, 2000), Noril'sk (Naldrett *et al*., 1996), Pants Lake (Lightfoot *et al*., 1984) intrusions. This is expressed by the abundance of xenoliths of the country rocks within the ore and by the crustal S and O isotopic ratios in the ores and their igneous host rocks. The aim of the present study was to determine whether the Uitkomst Complex shows similar features, and if so, whether the crustal contamination could have triggered sulphide melt segregation.

6.2. Evidence for contamination of the Uitkomst magma

The use of isotopes has been a useful instrument in previous studies of the Uitkomst Complex to indicate contamination of the magma. Gomwe (2002) found a crustal Nd isotope signature in the igneous rocks, Gauert (1998) found a crustal Sr isotope signature, and Gauert *et al.* (1996) and Li *et al*. (2002) found a crustal S-isotopic signature in the sulphides of the igneous rocks. The present study has confirmed a crustal S and O isotopic signature of the igneous host rocks to the xenoliths. Of additional importance is that the xenoliths tend to have a heavier S-isotopic signature than their igneous host rocks (Figure 5.5), suggesting that the dolomites are not the source of the crustal S in the ores.

Several points from this study provide further evidence for contamination of the Uitkomst magma with country rock xenoliths. These include:

- Visual inspection of the xenoliths illustrates that the host rock has disintegrated. Some of the smaller xenoliths (few mm to few cm in size) tend

to be largely ingested by the magma, while the larger xenoliths (few m) tend to display brecciation by the intruding magma.

- The xenoliths have distinct reaction rims at the contact zones between the xenolith and the magma. In the interaction between the dolomite xenoliths and the Uitkomst magma, proximal metamorphism is observed, with fluid and volatiles from the xenoliths being predominantly mobilised at the margins of the xenoliths.

The most common mineral assemblage observed in the calc-silicate xenoliths enclosed in the Uitkomst magma is: Calcite-pyroxene-tremolite
All prograde reactions observed indicate decarbonation of the xenoliths, especially along the edges. Devolatilisation is further indicated by the significant decrease in L.O.I. at the margins of the xenoliths, and by the O and C isotopic fractionation (Figure 4.4).

6.3. The role of contamination in the formation of the sulphide mineralisation

The present study provides compelling evidence for interaction of the Uitkomst magma with dolomite xenoliths. However, the difference in the S-isotopic ratios between the xenoltih and the igneous rocks suggests that the crustal S present in the ores is not derived from the dolomites. Another source, perhaps within the Timeball Hill shales or the Archaean basement granites, should be envisaged. Devolatilsation of the dolomites may, however, have played a role in the lowering of the S solubility of the magma by means of oxidation of FeO.

6.4. Late magmatic and hydrothermal processes

The segregating sulphide melt appears to have infiltrated the xenoliths, possibly facilitated by the volume loss of the latter. This would have occurred at a relatively late stage during the solidification of the rocks.

Finally, the rocks underwent hydrothermal alteration and fluid flux as evidenced by S-isotopic disequilibria of the sulphide minerals and O and C isotopic fractionation. The hydrothermal fluids may have been responsible for the precipitation of the pyrite and chalcopyrite along bedding planes in the dolomites and calc-silicates. Hydrothermal alteration is also indicated by the fact that the ultramafic rocks of the Uitkomst Complex are pervasively altered to talc and serpentine.

6.5. Conclusions

1. The xenoliths associated with the Uitkomst Complex, consist of dolomite, calc-silicates, quartzites and granite. The xenoliths vary in size (few mm to few m square) and in shape (angular to subangular). In the BMZ the calc-silicate xenoliths occur as elongated rafts.
2. The xenoliths show evidence of decarbonation reactions that may have played a role in triggering sulphide segregation in the magma, especially along the contacts of the xenoliths with the magma.
3. The reaction rims of the xenoliths consist of hydrous minerals, indicating the remobilization of fluids towards the margins during the metamorphic reactions. However, reaction rims are also observed in the quartzite xenoliths, indicating metasomatism as a mechanism for the formation of the reaction rims.
4. Talc, chlorite, serpentine and illite alteration is pervasive in the xenoliths.
5. Using the estimate of Irvine and Sharpe (1982) for the temperature of Bushveld magmas at between 1200 and 1300^{o}C, a pressure of 1.1 - 1.6 kbars (~3–5 km) is inferred for the metamorphism of the xenoliths.
6. The spread of the $\delta^{34}S$ values from –9‰ to +2‰ is larger than would be expected for mantle-derived igneous rocks (0±1‰). This indicates the contribution of crustal sulphur to the Uitkomst Complex.
7. The dolomites have S-isotopic ratios distinct from those of the igneous host rocks. This suggests that the crustal S in the ores is derived from another source, possibly the Timeball Hill shales or the granite-gneiss basement rocks.
8. A distinct zonation in the sulphide mineralisation is observed: Pyrite is the dominant sulphide mineral in the interior of the xenolith away from the margins. Chalcopyrite and pentlandite are more dominant at the immediate contact between the xenolith and the host rock. Pyrrhotite is the dominant sulphide mineral in the host rock.

9. There is limited variation in the O and C isotopes with height in the xenolith (UK119). This is in accord with a model of late-stage fluid infiltration. The fluids may be responsible for the formation of pyrite, pentlandite and chalcopyrite from original magmatic pyrrhotite.

7. REFERENCES

Arcuri, T., Ripley, E.M. and Hauck, S.A. (1998). Sulphur and oxygen isotopic studies of the interaction between xenoliths and basaltic magma at the Babbitt and Serpentine Cu-Ni deposits, Duluth Complex, Minnesota. *Economic Geology*, *93*, 1063-1075

Anhaeusser, C.R., Robb, L.J. and Viljoen, M.J. (1983). Notes on the Provisional Geological Map of the Barberton Greenstone Belt and surrounding Granitic terrane, Eastern Transvaal and Swaziland. In: Contrbutions to the Geology of the Barberton Mountain Land, *Special Publication of the Geological Society of South Africa*, *9*, 221-223

Anonymous (1996). *Joint announcement of the exploitation of the Massive Sulphide Zone.* Business Day, 7 March.

Augustithis, S.S. (1990). *Atlas of metamorphic – metasomatic textures and procedures*. Elsevier, New York. 22219pp

Bailey, S.W. (1988). Chlorites: Structures and crystal chemistry. In: Bailey, S.W. (Editor) Hydrous Phyllosilicates (Exclusive to Micas). Mineralogical Society of America, *Reviews in Mineralogy*, *19*, 347-403

Beukes, N.J., Klein, C., Kaufman, A.J. and Hayes, J.M. (1990). Carbonate Petrography, Kerogen Distribution, and Carbon and Oxygen Isotope Variations in an Early Proterozoic Transition from Limestone to Iron-Formation Deposition, Transvaal Supergroup, South Africa. *Economic Geology*, *85*, 663-690.

Boer, R.H., Meyer, F.M., Robb, L.J., Graney, J.R., Vennemann, T.W., and Kessler, S.E. (1995), Mesothermal-Type Mineralisation in the Sabie-Pilgrim's Rest Gold Field, South Africa. *Economic Geology*, *90*, 860-876.

Bowen, N.L. (1940). Progressive metamorphism of siliceous limestone and dolomite. *Journal of Geology, 48*, 225-274

Bowman, J.R., Covert, J.J., Clark, A.H. and Mathieson, G.A. (1985b). The Cantung E zone Scheelite orebody, Tungsten, NW Territories: O, H, and C isotope studies. *Economic Geology, 80*, 1872–1985.

Bowman, J.R., O'Neil, J.R. and Essene, E.J. (1985a). Contact skarn formation at Elkhorn, Montana. II: Origin and evolution of C–H–O skarn fluids. *American Journal of Science*, *285*, 621–660.

Button, A. (1973). A regional Study of the Stratigraphy and the development of the Transvaal Basin in the eastern and north-eastern Transvaal. PhD Thesis (unpubl.). University of the Witwatersrand, Johannesburg

Button, A. (1986). The Transvaal sub-basin of the Transvaal Sequence. In: Mineral Deposits of Southern Africa. Anhaeusser, C.R. and Maske, S. (Eds.). *Geological Society of South Africa*, *1*, 811-817

Buchanan, D.L., Nolan, J., Suddaby, P., Rouse, J.E., Viljoen, M.J. and Davenport, J.W.J. (1981). The genesis of sulphide mineralization in a portion of the Potgietersrus Limb of the Bushveld Complex. *Economic Geology*, *76*, 568-579

Clendenin, C.W., Henry, G. and Charlesworth, E.G. (1991). Characteristics of and influences on the Black Reef Depositional Sequence in the eastern Transvaal. *South African Journal of Geology*, *94* (4), 321-327

Cloete, H.C.C. (2001). *MajTraXRF – A Delphi application for the major and trace element analysis by X-ray fluorescence spectrometry*. Council for Geoscience Open File Report 2001-0075

References

Cloete, H.C.C. and Truter, J. (2001). *Major and trace element analysis by X-ray fluorescence Spectrometry at the Council for Geoscience*. Council for Geoscience Open File Report 2001-0074

Deer, W.A., Howie, R.A. and Zussman, J. (1992). *An introduction to the rock-forming minerals.* Addison Wesley Longman Limited, England, 696pp

De Waal, S.A. and Gauert C.D.K. (1997). The Basal Gabbro Unit and the identity of the parental magma of the Uitkomst Complex, Badplaas, South Africa. *South African Journal of Geology, 100*, 349-362

De Waal, S.A., Maier, W.D., Armstrong, R.A. and Gauert C.D.K. (2001). The age and parental magma of the Uitkomst Complex. *Canadian Mineralogist, 39*, 557-572

Drescher-Kaden, F.K. (1948). *Die feldspar – quartz – reaktionsgefüge granite ung gneise, und ihre genetische bedeutung*. Springer, Heidelberg, 259pp

Eriksson, P.G., Sweitzer, J.K., Bosch, P.J. A., Schereiber, U.M, Van Deventer, J.L. and Hatton, C.J. (1993). The Transvaal Sequence: an overview. *Journal of African Earth Sciences, 16*, 25-51

Gauert, C.D.K., De Waal, S.A. and Wallmach, T. (1995). Geology of the ultrabasic to basic Uitkomst Complex, eastern Transvaal, South Africa: an overview. *Journal of African Earth Sciences, 21*, 553-570

Gauert, C.D.K., Jordaan, L.D., De Waal, S.A. and Wallmach, T. (1996). Isotopic constraints on the source of the sulphur for the base metal sulphides of the Uitkomst Complex, Badplaas, South Africa. *South African Journal of Geology, 99*, 41-50

Gauert, C.D.K. (1998). The petrogenesis of the Uitkomst Complex, Mpumalanga Province, South Africa. PhD Thesis (unpubl.). University of Pretoria, Pretoria

Gauert, C.D.K. (2001). Sulphide and oxide mineralisation in the Uikomst Complex, South Africa: origin in a magma conduit. *Journal of African Earth Sciences*, *32* (2), 149-161

Godlevsky, M.N. and Grinenko, L.N. (1963). Some data on the isotopic composition of sulfur in the sulfides of the Noril'sk deposit. *Geochemistry*, *1*, 335-341

Gomwe, T.E.S. (2002). A geochemical profile through the Uitkomst Complex on the farm Slaaihoek, with special reference to the platinum-group elements and Sm-Nd isotopes. MSc Thesis (unpubl.). University of Pretoria, Pretoria

Grinenko, L.I. (1985). Sources of sulphur of the nickeliferous and barren gabbro-dolerite intrusions of the northwest Siberian platform. *International Geology Review*, *21*, 595-606

Hall, S.M. and Veizer, J. (1996). Geochemistry of Precambrian carbonates VII. Belt supergroup, Montana and Idaho, USA. *Geochimica et Cosmochimica Acta, 60***,** 667–677.

Harris, C. and Chaumba, J.B. (2001). Crustal contamination and fluid-rock interactions during the formation of the Platreef,, northern limb of the Bushveld Complex, South Africa. *Journal of Petrology*, *42*, 1321-1347

Henry, G., Clendenin, C.W. and Charlesworth, E.G. (1990). Depositional Facies of the Black Reef Quartzite Formation in the eastern Transvaal. *Geocongress*, *90* (Cape Town, South Africa): Abstracts, 230-233

Hochella, M.F, Jr, Liou, J.G., Keskinen, M.J. and Kim, H.S. (1982). Synthesis and stability relations of magnesium idocrase. *Economic Geology*, *77*, 798-808

Hoefs, J. (1973). *Stable Isotope Geochemistry*. Springer-Verlag, Berlin. 201pp

Hornsey, R.A. (1999). The Genesis and Evolution of the Nkomati Mine Ni-sulphide Deposit: Mpumalanga Province, South Africa. Msc Thesis (unpubl.). University of Natal, Durban

Irvine, T.N. and Sharpe, M.R. (1982). Source-rock compositions and depth of origin of Bushveld and Stillwater magmas. *Carnergie Institute of Washington Year Book, 81*, 294-303

Ito, J. and Arem, J.E. (1970). Idocrase: synthesis, phase relations and crystal chemistry. *American Mineralogist*, *55*, 880-912

Ito, J. and Arem, J.E. (1971). Idocrase: synthesis, phase relations and crystal chemistry. *Mineralogical Society Japan Special Papers*, *1*, 63-66

Kenyon, A.K., Attridge, R.L. and Coetzee, G.L. (1986). The Uitkomst Nickel-Copper Deposit, Eastern Transvaal. In: *Mineral Deposits of Southern Africa*. Anhaeusser, C.R. and Maske, S. (Eds.). Geological Society of South Africa, Johannesburg, 1009-1019

Keller, J. and Hoefs, J. (1995). Stable isotope characteristics of recent natrocarbonatites from Oldoinyo Lengai. In: Bell, K. and Keller, J. (Editors), *Carbonatite Volcanism: Oldoinyo Lengai and the petrogenesis of natrocarbonatites.* Springer Verlag, Berlin, 113-123

Kerr, A. (1999). Mafic rocks of the Pants Lake Intrusion and related Ni-Cu-Co mineralisation in north-central Labrador: Newfoundland Department of Mines and Energy, *Geological Survey Report 99-1*

Korzhinskii, D.S. (1959. *Physiochemical basis of the analysis of the paragenesis of minerals*. Consultants Bureau, New York, 142pp

Li, C. and Naldrett, A.J. (2000). Melting reactions of gneissic inclusions with enclosing magma at Voisey's Bay, Labrador, Canada: Implications with respect to ore genesis. *Economic Geology*, *95* (4), 801-814

Li, C. Ripley, M., Maier, W.D., and Gomwe, T.E.S. (2002) Olivine and sulphur isotope

compositions of the Uitkomst sulfide-bearing intrusion, South Africa: records for multiple flows of magmas and their roles in ore formation in a magma conduit. *Chemical Geology, 188* (3-4), 149-159

Lightfoot, P.C., Naldrett, A.J., and Hawkesworth, C.J. (1984). The geology and geochemistry of the Waterfall Gorge section of the Insizwa complex, with particular reference to the origin of nickel sulfide deposits. *Economic Geology, 79*, 1857-1879

Maier, W.D., Barnes, S-J., and De Waal, S.A. (1998). Exploration for magmatic Ni-Cu- PGE sulphide deposits: a review of recent advances in the use of geochemical tools and their application to some South African ores. *South African Journal of Geology, 101* (3), 237-253

Maier, W.D., Gomwe, T., Barnes, S-J., Li, C., Theart, H. (2004). Platinum-group elements in the Uitkomst Complex, South Africa. *In press.*

Meinert, D.P. (1992). Skarns and skarn deposits. *Geoscience Canada, 19* (4), 145-162

Naldrett, A.J. (1966). The role of sulfurization in the genesis of iron–nickel sulfide deposits of the Porcupine district, Ontario. *Can. Inst. Mining Metallurgy Trans., 69,* 147–155

Naldrett, A.J. (1981). Nickel sulphide deposits: Classification, composition and genesis. *Economic Geology, 75th Anniv. Volume*, 628–685.

Naldrett, A.J., Fedorenko, V., Lightfoot, P.C., Kunilov, V., Gorbachev, N.S., Doherty, W. and Zohan, A. (1995). Ni-Cu-PGE deposits of Noril'sk region, Siberia: their formation in conduits for flood basalt volcanism. *Transactions of Institution of Mining and Metallurgy, B104*, 18-36

Ohmoto, H. (1986). Stable isotope geochemistry of ore deposits. In: Valley, J. W., Taylor, H. P., and O'Neil, J. R., *Stable Isotopes in High Temperature Geological Processes. Reviews in Mineralogy, 16*, Mineralogical Society of America, 491-559.

Oosthuysen, E.J. (1970). The Geochronology of a suite of rocks from the Granitic Terrain surrounding the Barbeton Mountain Land. PhD Thesis (unpubl.). University of the Witwatersrand, Johannesburg

Robb, L.J. and Anhaeusser, C.R. (1983). Chemical and Petrogenetic Characteristics of Archaean Tonalite-Trondhjemite Gneiss plutons in the Barbeton Mountain Land. In: Contributions to the Geology of the Barbeton Mountain Land, *Special Publication of the Geological Society of South Africa, 9,* 103-116

Rye, R. O. and Ohmoto, H. (1974). Sulfur and carbon isotopes and ore genesis: A review. *Economic Geology, 69,* 826-842

Ripley, E.M. (1981). Sulphur isotopic studies at the Dunka Road Cu-Ni deposit, Duluth Complex, Minnesota. *Economic Geology*, *76,* 610-620

Ripley E.M. and Al-Jassar, T.J. (1987). Sulphur and oxygen isotopic studies of melt-country rock interaction, Babbitt Cu-Ni deposit, Duluth Complex, Minnesota. *Economic Geology*, *82*, 87-107

Shelley, D. (1974). *Optical Mineralogy*. Christchurch, New Zealand. 321pp

Sheppard, S.M.F. (1986). Characterization and isotopic variations in natural waters. In: Valley, J. W., Taylor, H. P., and O'Neil, J. R. (Editors), *Stable Isotopes in High Temperature Geological Processes.* Reviews in Mineralogy, *16,* Mineralogical Society of America, 165–183.

Shoji, T. (1971). Vesuvianite: synthesis and occurrence in skarn. *Mineralogy Geology*, *21*, 457-460

Shoji, T. (1975). Role of temperature and CO_2 pressure in the formation of skarn and its bearing on mineralization. *Economic Geology, 70,* 739-749

Schriffies, C.M. and Rye, D.M. (1990). Stable Isotopic Systematics of the Bushveld Complex:II. Constraints on Hydrothermal Processes in Layered Intrusions. *American Journal of Science*, *290,*

209-245

Skippen, G. (1974). An experimental model for low pressure metamorphism of siliceous dolomitic marble. *American Journal of Science*, *274*, 487-509

So, C.S., Rye, D.M. and Shelton, K.L. (1983). C, H, O, and S isotope and fluid inclusion study of the Weolag tungsten–molybdenum deposit, Korea: Fluid histories of metamorphic and ore–forming events. *Economic Geology, 78,* 1551–1573.

Strauss, T.A.L. (1995) Petrology and Geochemistry of the Basal Gabbro Unit, Uitkomst Complex. Msc. Thesis (unpubl.) Rhodes University, Grahamstown

Taylor, H. P. J., Frechen, J., and Degens, E. T. (1967). Oxygen and carbon isotope studies of carbonatites from the Laacher See District, West Germany, and the Alnö District, Sweden. *Geochimica et Cosmochimica Acta*, *31***,** 407-430.

Taylor, B.E. and O'Neil, J.R. (1977). Stable isotope studies of metasomatic Ca–Fe–Al–Si skarns and associated metamorphic and igneous rocks, Osgood Mountains, Nevada. *Contributions to Mineralogy and Petrology, 63,* 1-49.

Theart, H.F.L. and de Nooy, C.D. (2001) The platinum-group minerals in two parts of the massive sulphide body of the Uitkomst Complex, Mpumulanga, South Africa. *South African Journal of Geology*, *104* (4), 287-300

Thériault, R.D., Barnes, S-J. and Sevenson, M.J. (1997) The influence of country-rock assimilation and silicate to sulphide ratios (R factor) on the genesis of the Dunka Road Cu-Ni-platinum-group element deposit, Duluth Complex, Minnesota. *Canadian Journal of Earth Sciences*, *34*, 375-389

Tischler, S.E., Cawthorn, R.G., Kingston, G.A. and Maske, S. (1981). Magmatic Cu-Ni-PGE

mineralisation at Waterfall Gorge, Insizwa, Pondoland, Transkei. *Canadian Mineralogy, 19*, 607-618

Tracy, R.J. (1978). Monticellite marble at Cascade Mountain, Adirondack Mountains, New York. *American Mineralogist, 63*, 991-999

Valley, J. W. (1986). Stable isotope geochemistry of metamorphic rocks. In: Valley, J. W., Taylor, H. P., and O'Neil, J. R. (Editors), *Stable Isotopes in High Temperature Geological Processes.* Reviews in Mineralogy, *16*, Mineralogical Society of America, 445-498.

Valley, J.W. and Essene, E.J. (1979). Vesuvianite, akermaite, monticellite and wollastonite equilibria and high $X_{H2O/CO2}$ at Cascade Slide, Mt. Marcy Quad., Adirondack Mtns. *EOS, 60,* 423

Valley, J.W. and Essene, E.J. (1980). Akermanite in the Cascade Slide xenolith and its significance for regional metamorphism in the Adirondacks. *Contributions to Mineralogy and Petrology, 74*, 143-152

Valley, J.W., Peacor, D.R., Bowman, J.R., Essene, E.J. and Allard, M.J. (1985). Crystal chemistry of Mg-vesuvianite and implications of phase equilibria in the system CaO-MgO-Al_2O_3-SiO_2-H_2O-CO_2. *Journal Metamorphic Geology, 3*, 137-153

van Eeden, O.R., Joubert, G.K., Söhnge, A.P.G., van Zyl, J.S., Rossouw, J.J., Taljaard, J.J. and Visser, D.J.L. (1956). Compiled by Visser, D.J.L. The Geology of the Barbeton Area. *Geological Survey Special Publication, 15*, 226pp

van Zyl, A.M. (1996). The sulphides of the Uitkomst Complex, Badplaas, South Africa. MSc Thesis (unpubl.). University of Pretoria, Pretoria

Veizer, J., Clayton, R.N. and Hinton, R.W. (1992). Geochemistry of Precambrian carbonates: IV. Early Paleoproterozoic (2.25 ± 0.25 Ga) seawater. *Geochimica et Cosmochimica Acta, 56*, 875-

885

Von Scheibler, W.H.T.M., Cawthorn, R.G., Kenyon, A.K. and Allen, I.V.L. (1995). Ni-Cu Sulphide Mineralization in the Uitkomst Intrusion. In: *Extended Abstracts of the Centennial Geocongess*. Geological Society of South Africa, Johannesburg, South Africa. 133-136

Wagner, P.A. (1929). *The Platinum Deposits and Mines of South Africa*. Struik. 1973 Edition, 338pp

Wallmach, T., Hatton, C. and Droop, G.T.R. (1989). Extreme facies of contact metamorphism developed in calc-silicate xenoliths in the eastern Bushveld Complex. *Canadian Mineralogist, 27*, 509-523

Wallmach, T., Hatton, C. J., de Waal, S.A. and Gibson, R.L. (1995). Retrogressive hydration of calc-silicate xenoliths in the eastern Bushveld Complex: evidence for late magmatic fluid movement. *Journal of African Earth Science, 21*, 633-646

Walraven, F. and Martini, J. (1995). Zircon Pb-avaporation age determinations of the Oak Tree Formation, Chuniespoort Group, Transvaal Sequence: Implications for Transvaal-Griqualand West Basin correlations. *South African Journal of Geology, 98* (1), 58-67

Woolfe, J.A.S. (1996). The Nkomati Joint Venture- A nickel mine in the making. *Geobulletin, 39* (1), 5-7

8. ACKNOWLEDGEMENTS

The completion of this study is an amalgamation of the patience and motivation of several people to whom the author is eternally indebted.

First and foremost, I would like to thank Professor Wolfgang Maier for his patience and his valuable contribution to the study. The author would also like to extend her gratitude to the personnel of the Council for Geoscience for assistance with the analytical techniques. In particular the author would like to thank Dr. B. Eglington, Ms. Danel van Tonder, Ms. Odette Smith, Mrs. Anabe Walliser and Dr. Buhmann. Special mention must go to Dr. U Horstmann, whose assistance on the analyses, interpretation and writing of the section on stable isotopes remains the reason that the section was put together. Assistance from Dr. T. Wallmach on the section on metamorphic mineral assemblages was invaluable to the compiling and structuring of the dissertation. The mapping exercise would not have been completed without the help of the personnel of Nkomati Mine.

Finally my thanks to my friends and family who motivated and encouraged me through it all – even at those moments when I was ready to through in the towel – thank you for believing in me.

APPENDIX A

MAPS

A1: P29E N/SW (Lens 1)

A2: Bulk Sample Drive (BMZ)

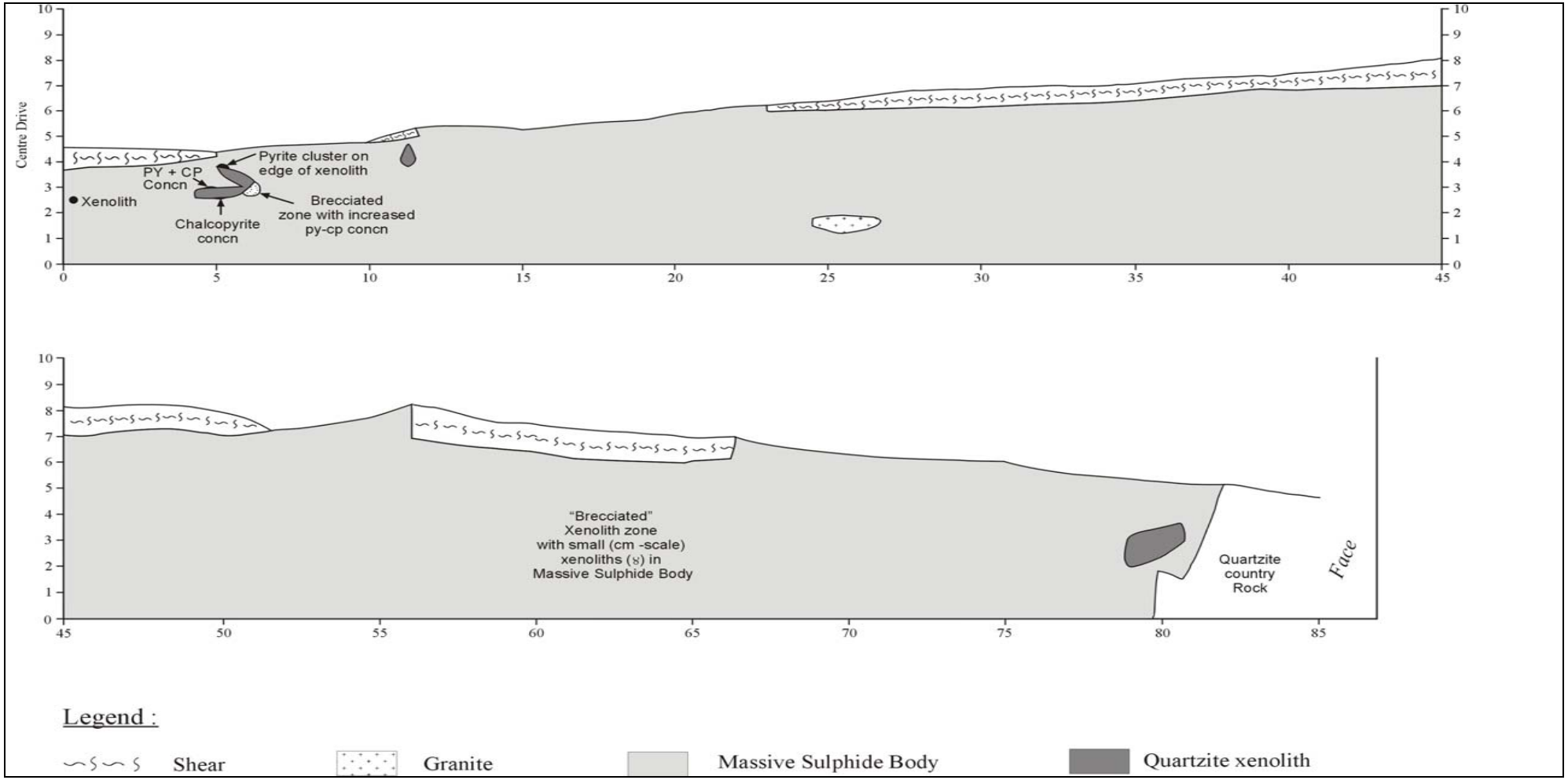

Figure A 1: Map showing the relationships between the xenoliths and the MSB (P29E N/SW, Nkomati Mine)

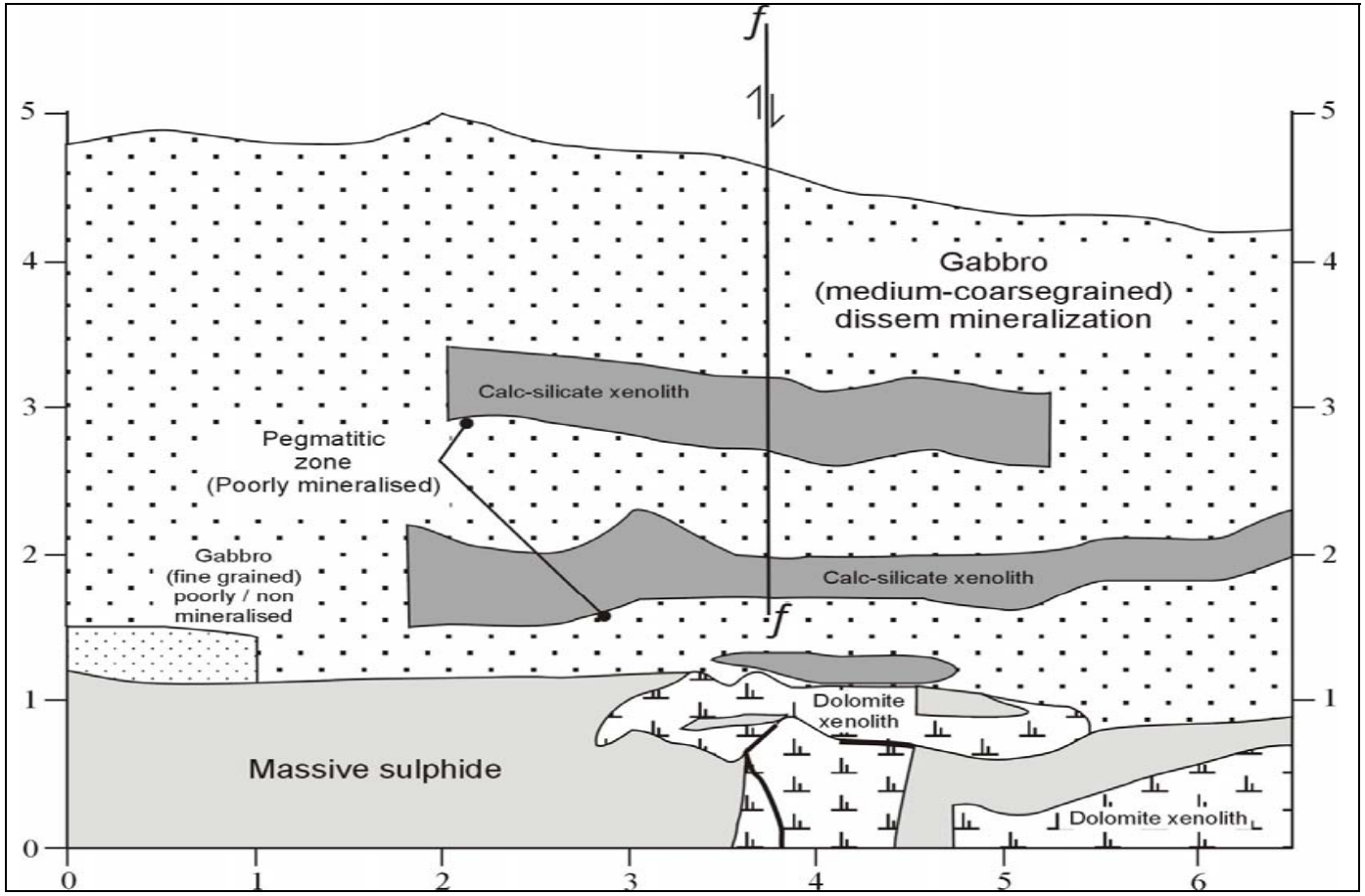

Figure A 2: Map showing the relationships between the xenoliths and the BMZ (Bulk Sample Drive, Nkomati Mine)

APPENDIX B

BOREHOLE LOGS

PHOTOS OF UK19


UK119A
UK119A
55
UK119B
55.43
55 UK119B
UK119C
55.53
UK119C
55.80
UK 119D
UK119D
56
UK119E
UK119


UK 119
UK119E
56.55
UK119F
UK119F
56.93
UK119G
56.93
UK119G
UK119 H
57


UK119H
UK119I
57.55
UK119J
57.88
58.28
160
UK119L

Borehole Log: SHU60								
Depth (m)	**Rock Type**	**Structure**	**Alteration**	**Sulphides present**	**Total % Sulphide**	**Texture of mineralisation**	**Stratigraphy**	**Comments**
0-0.6	quartzite	homogenous	chloritisation	Po, Py	2	disseminated along veins	Transvaal Supergroup	
0.61-3.88	Massive sulphide	quartzite inclusions		Po, Cp	85	massive sulphide	MSB	numberous xenoliths ranging
3.89-5.34	granite	cross-cutting veins		Py	<0.1	disseminated along upper contact	Basement Granite	small xenoliths totally altered . Py and cp more prominent closer to the xenoltihs.
5.35-6.50	Massive sulphide	granite inclusions		Po, Cp, Py		massive stringer	MSB	
6.51-7.60	granite	sulphide inclus	chloritisation			net-textured, dissemniated	Basement Granite	
7.61-14.56	Massive sulphide	granite inclusions		Po, Cp, Py	95	Massive stringer	MSB	large number of granite xenoliths. Prominent reaction rims around xenoliths.
14.57-15.3	granite	homogenous					Basement Granite	Massive sulphide interfingers with the granite. Wavy bottom contact with the massive sulphide.
15.36-15.4	Massive sulphide	small granite inclusions		Po, Pn, Cp, Py	70	Massive stringer	MSB	
15.48-21.4	granite	homogenous			<1		Basement Granite	small veins of sulphide close to the upper contact.

Borehole Log: SHU61

Borehole Log: SHU63

Depth (m)	Rock Type	Structure	Alteration	Sulphides present	Total % Sulphide	Texture of mineralisation	Stratigraphy	Comments
0.00-3.40	granite	homogenous		Py	1		Basement granite	Minor sulphide mineralisation along veins. Bottom contact is wavy
3.41-3.90	Massive sulphide	mottled, inclusions of granite xenoliths		Po, Cp, Pn, Py	100	massive sulphide	MSB	predominate around the granite xenolith contacts. The contacts between the xenoliths and the massive sulphide are
3.91-4.14	granite	homogenous					Basement granite	
4.15-4.53	Massive sulphide	mottled, inclusions of granite xenoliths		Po, Cp, Py	90	massive sulphide	MSB	laqrge number of granite xenoliths ranging in size
4.54-4.71	granite	homogenous	talc	Py	1		Basement granite	Minor sulphide mineralisation along veins.
4.72-4.95	Massive sulphide			Po, Cp	100	massive sulphide	MSB	
4.96-5.12	granite	homogenous	talc-chlorite				Basement granite	
5.13-5.3	Massive sulphide	mottled, inclusions of granite xenoliths		Po, Cp, Py	100	massive sulphide	MSB	Smaller granite xenoliths are totally alteredred/replaced by hydrous minerals
5.31-16.20	granite	gneissic layering	high pressure metamorphism				Basement granite	Sulphide mineralisation from the contact between the granite and the massive sulphide layer interfinger

APPENDIX C

METHODS OF INVESTIGATION

Methods of investigation

In order to provide a complete and detailed description of the xenoliths hosted by the Uitkomst Complex, a number of geological techniques were utilised. Below is a summary of the methods applied:

C1. Optical microscopy (transmitted and reflected light)

Thirty three polished thin sections were analysed through transmitted and reflected light using a Zeiss optical microscope.

C2. XRD (X-Ray Diffraction)

Major mineral analysis was carried out at in the laboratory of the Council for Geoscience using a Siemens D 500 X-ray goniometer equipped with Cu tube, variable slit and secondary graphite monochromator. A fine-grained powder (± 10 μm) of each sample is pressed in an aluminium frame against a rough filter paper. The sample is then is scanned from 2 to 65° 2Θ CuKα at a speed of 0,02° 2Θ step size/1 sec with generator settings of 35 KV and 25 mA.

C3. EMP (Electron Microprobe)

The major element compositions of some of the mineral phases were determined on a Jeol Superprobe 733 electron microprobe at the Council for Geoscience. The analyses were performed using an accelerated voltage of 15 kV, a beam current of 40 nA and an analysing spot of 2 to 3 microns. The counting time at the peak position was 10 seconds and 5 seconds at two symmetrical background positions. Separate calibrations were used for carbonates, sulphides, amphiboles and pyroxenes. A full calibration procedure is performed for each calibration if the instrument has been inactive for a period in excess of two days or if a filament has been changed.

C4. ICP-MS (Inductively Coupled Plasma- Mass Spectrometer)

INSTRUMENTATION

System:	Perkin Elmer SCIEX ELAN ® 6000 ICP-MS.
Detector:	ETP ® model AF 210 electron multiplier.
Nebulizer:	Standard cross-flow nebulizer.
Spray chamber:	Scott-type Ryton ® double-pass spray chamber.
Pump:	Standard three channel peristaltic pump.
Pump tubing:	Tygon ® tubing.
Autosampler:	Perkin Elmer AS 91 autosampler.
Tray:	Type F autosampler tray.
Cones:	Nickel sampler & skimmer cones.
Computer:	Dell computer.
Argon supply:	Taylor-Wharton ® XL 45 liquid argon mini-tanks.

OPERATING CONDITIONS

RF power:	1.150 kW.
Plasma gas flow rate:	15 l/min.
Nebulizer gas flow rate:	+/- 0.82 l/min.
Method:	Quantitative.
Scan mode:	Peak hopping.
Autolens:	On.
Detector mode:	Dual.
Dwell time:	50 ms.
Sweeps/reading:	10.
Readings/replicate:	3.
Replicates:	3.
Sample uptake rate:	+/- 0.75 ml/min.
Sample flush:	20 sec.
Read delay:	12 sec.
Wash time:	100 sec.

Wash solution:	5 % HNO_3 & 5 % HCl.
Internal standard:	20 ppb Indium.
Tuning solutions:	Perkin Elmer standard solutions.

C5. LECO

Infrared absorption spectrometry:

Simultaneous determination of carbon and sulphur in geological materials

Outline

The sample is combusted in free moisture oxygen atmosphere at a high temperature. Evolved gases CO_2 and SO_2 pass through the infrared (IR) detector cells where the absorbed IR energy at the precise wavelengths is measured, and compared with the IR energy for the pure oxygen environment which permits the maximum energy to reach the detector. Since the absorbed IR energy is directly related to the content of CO_2 or SO_2 respectively, the built-in microprocessor converts all output data from the detector and calculates the Carbon / CO_2 and Sulphur / SO_3 contents in the sample according to the preselected mode. The instrument used is the LECO CS 244 Carbon / Sulphur Analyser.

Procedure

1. Sample is weighed into a disposable ceramic crucible, and is covered by 1 scoop of carbon/sulphur free iron chips and 1 scoop of carbon/sulphur free tungsten metal chips. These metals act as accelerators in the induction furnace and secure complete sample melting.
2. Crucible with the sample is placed on the pedestal of the induction furnace and is automatically pushed into the quartz combustion tube.
3. After initial 30 second O_2 flushing of the whole system, the melting / burning process begins.
4. Evolved gases are carried through the sulphur IR cell first, and after removal of SO_2 at the sulphur trap, remaining CO_2 enters the carbon IR cell for detection and measurement.

5. After completion of combustion and measurement of SO_2 - CO_2 levels in the sample, the pedestal is lowered and the burned crucible is discharged into a fire-proof bin.
6. Results of both measurements are printed either in Carbon Sulphur element mode, or as CO_2 / SO_3 content mode, as desired.
7. An analysis of a blank sample should be performed, using an empty crucible, desired accelerator + blank standard LECO 501-673.
8. The standard for calibration of the instrument should be carefully selected to match the matrix of the sample as close as possible. For samples with a carbon content of up to 1%, calibration with steel standard rings is sufficient, but for samples with high CO_2 or C contents (coal & limestone), calibration with matching standards is essential. The same applies to sulphur calibration where steel rings or cast iron can be used, from 0.005 to 2,5 % of Sulphur only.

Interferences

Free and crystalline water interferes partially if water is not driven-off during the initial stage of the heating/burning process. This applies only to sulphur analysis since H_2SO_4 formation can take place, producing lower results. In carbon measurement the formation of H_2CO_3 does not represent a similar danger because of the high instability of H_2CO_3 at high temperatures. Sample mass of materials containing more than 5% of sulphur and 7% of carbon should not exceed 0.150 g, otherwise cell contamination can occur.

Range

S - 0.001	5% (at sample mass of max. 0.5 g)
S - 5%	40% (at sample mass of max. 0.15 g)
C - 0.01	7% (at sample mass of max. 1 g)
C - 7%	60% (at sample mass of max. 0.15 g)

Precision

CV%	S 3 (low level)
	S 8 (high level)
	C 2 (low level)

C 5 (high level)

Accuracy

Sulphur:	<0.1%	± 0.0005 or ± 0.5% sulphur present
	>0.1%	± 0.001 or ± 2% sulphur present
Carbon:	<0.1%	± 0.0004 or ± 0.5% carbon present
	>0.1%	± 0.001 or ± 1% carbon present

Standards and certified reference materials used

Type	**Code**	**Origin**
Steel (blank)	501-637	LECO USA
Cast Iron	501-024	LECO USA
Steel ring	501-501	LECO USA
Steel ring	501-504	LECO USA
Steel ring	501-505	LECO USA
Steel ring	501-506	LECO USA
Steel ring	501-510	LECO USA
Granite	NIM G	SABS
Lujavrite	NIM L	SABS
Dunite	NIM D	SABS
Cu concentrate	CCU 1	CANMET
Devonian Ohio shale	SDO 1	USGS
Green River shale	SGR 1	USGS
Soil	SO 2	CANMET
Soil	SO 3	CANMET
Dolomitic Limestone	88 a	NIST
Dolomitic Limestone	88 b	NIST
River sediment	NBS 1645	NIST

C6. Sulphur isotopes: preparation and analytical procedure

1. **Crushing:**

Larger hand samples were crushed using the Jawcrusher at the Council for Geoscience. Smaller samples were manually crushed using a metallic mortar. The jawcrusher and mortar were cleaned after each sample using the iron brush, followed by alcohol and pressurised air.

2. **Sieving:**

75µm, 250µm, 400µm and 500µm sieves were used together with a receiver pan and lid. The sieves were cleaned after each sample using a brush and pressurised air. The different fractions were put into different sample containers and labelled correctly.

3. **Mineral Separation**

Hand Magnet

A hand magnet was passed over each sample and the pyrrhotite and magnetite separated from the rest of the sample.

Frantz Magnetic Separator

Pyrite and chalcopyrite were separated using the Frantz Magnetic Separator, based on their magnetic properties. The instrument can be tilted sideways and forward. A combination of these angles can be helpful in separating the minerals more accurately. The more magnetic minerals fall into the front cup and the less magnetic minerals into the back cup.

Heavy Liquids

Tetrabromoethane (TBE) was used to further separate the minerals based on varying densities. Separation is performed in a glass funnel. Grains with a lower RD than the heavy liquid, eg quartz, will float on top and the heaviest grains like pyrite etc will fall to the bottom of the separation funnel. The tap at the bottom can be let open to allow only the heavy grains through and they are caught in the filter paper in the open funnel. Another funnel with filter paper is used to catch the rest of the grains.

4. Handpicking:

The samples were cleaned using acetone and handpicked using a syringe and tweezers to separate the suphides from any gangue material. The sulphides were put into vials and are labelled.

5. S isotope analysis

A modern, rapid analytical facility was recently established at the IAEA Environmental Isotope Group of the Schonland Research Institute at the University of the Witwatersrand, Johannesburg. This laboratory is equipped with a state of the art mass–spectrometer including peripheral instruments for sample preparation.

The equipment used at Schonland for S (and C/N) isotope analysis consists of a GEO 20-20 mass–spectrometer connected to an ANCA–GSL (automated nitrogen and carbon analysis for gases, solids and liquids) sample preparation system. The principle followed is the coupling of an elemental analyser (ANCA–GSL) to a continuous flow IRMS (isotope ratio mass–spectrometer, GEO 20-20) and is depicted in Fig. 1. Isotope ratios are determined by recording and integrating the peak areas of the mass (M/Z) 66 and mass (M/Z) 64 beams. This is in contrast to a conventional dual inlet system, where peak–height detection is used to evaluate the ratio of the heavier to the lighter isotope of a given element.

The S isotopic composition of the samples was determined using this new method as outlined below. Samples were analysed in duplicate and international standards were used for calibration. The latter reproduced to about ±0.5‰ relative to their accepted values. S isotope data are given in the conventional δ–notation relative to CDT (Cañyon Diablo Troilite) according to:

$$\delta^{34}S(‰) = \left[\frac{(^{34}S/^{32}S)_{sample}}{(^{34}S/^{32}S)_{standard}} - 1 \right] \times 1000$$

Methodology of $\delta^{34}S$ analysis by EA–GC–CF–IRMS

Samples were weighed into tin capsules where vanadium pentoxide (VnO_5) was added to aid combustion. Samples were then loaded into a carousel on the ANCA–GSL. They were then dropped into a furnace held at 1020°C where they were combusted in the presence of oxygen. The combusted gases were swept in a helium stream over a combustion and reduction catalyst to purify the gas to sulphur dioxide. Water was removed by a Nafion™ membrane and magnesium perchlorate chemical trap. SO_2 gas was separated from N_2 and CO_2 by a gas chromatograph. The resultant chromatographic peak of SO_2 entered the ion source of the GEO 20-20 CF–IRMS where it was ionised and accelerated. ^{32}S and ^{34}S were separated in a magnetic field then simultaneously measured on a Faraday cup universal collector array. Sample time was about ten minutes per sample.

C7. C/O Isotope Analytical Procedure

All samples were reacted following a technique modified after McCrea 1950. Depending on their carbonate content, determined by XRD, between 10 mg and 11 mg of each sample and 2 ml of 100% H_3PO_4, prepared after the method of Coplen *et al*. (1983), were enclosed separately in a reaction vessel. The vessels were thoroughly evacuated and thereafter both sample and acid were thermally equilibrated in a water bath for about 1 hour and subsequently reacted. Equilibration / reaction temperatures were 25°C for calcite and 50°C for dolomite. The samples were digested overnight for about 17-21 hours.

The liberated CO_2 was pumped kryostatically through cold traps using dry-ice and liquid nitrogen in order to remove water and other condensable gases. The yield was measured and found in all cases to be about 100% which indicated a complete reaction of the sample material as far as can be judged from the given mineralogical identification of carbonate species. The CO_2 gas was finally collected in reusable sample bottles and / or break–seal tubes.

Isotope analyses were performed using a Finnigan MAT-251 gas-source mass-spectrometer with a sequential, multiport sample inlet system. Sample isotope ratios

were measured against a working gas, taken from a commercial CO_2 bottle, which was calibrated and controlled against internal laboratory standards included in each batch of samples. The internal standards had been calibrated against NBS19 as international reference sample.

Isotopic compositions are given relative to VPDB for carbon and oxygen in terms of the δ notation:

$\delta\ (‰) = (R_{sample}/R_{std} - 1) * 1000$

where R is $^{13}C/^{12}C$ or $^{18}O/^{16}O$ for sample and standard. Oxygen isotopic compositions are also noted relative to SMOW (Vienna-SMOW) according to:

$\delta_{SMOW} = 1.03086\ \delta_{PDB} + 30.86$

(Friedman and O'Neil, 1977). Corrections were made for the analytical fractionation of oxygen between phosphoric acid and carbon dioxide, using the fractionation factors:

$\alpha_{CO_2\text{-calcite}}$ = 1.01025 at 25°C (corrected from Sharma and Clayton, 1965 in Friedman and O'Neil, 1977), and $\alpha_{CO_2\text{-dolomite}}$ = 1.01065 (Rosenbaum and Sheppard, 1986).

Calibration and Analytical Error

The calibration of the working gas was done by analysing international reference materials using NBS19, which is defined as reference Vienna–PDB by:

$\delta^{13}C_{NBS19}/VPDB$ = 1.95‰ and

$\delta^{18}O_{NBS19}/VPDB$ = –2.20‰

(Hut, 1987).

A calibration curve was calculated for C and O respectively and has been used to correct the mass–spectrometric analytical results. Repeated analysis of internal standards (MHS1, MDS1 and MD4) yielded values in an interval of ±0.1‰ (1σ) for both $\delta^{13}C$ and $\delta^{18}O$ values.

APPENDIX D

POLISHED THIN SECTION DESCRIPTIONS

Sample Number: UK119A
Description:
Euhedral chromite grains increase in size towards the contact with the dolomite xenolith. Talc and chlorite alteration is pervasive interstitially and the original mineralogy has been obliterated. Magnetite is found as accessory minerals in the cracks between the chlorite and talc. Euhedral pyrite grains are present. Pyrite consits of about 1% of the section and occurs interstitially.
Rock Type: Chromititc pyroxenite

Sample Number: UK119B
Description:
A distinct band consisting of aligned talc grains are present at the contact between the mafic portion and the xenolith. Augen-shaped zones consisting predominantly of talc and chlorite are present in the mafic portion.

Sample Number: UK119C
Description:
Buck-shot/net-textured pyrite grains (~1%) are associated with the chlorite grains. Euhedral grains of pyrite are also present. Dolomite is the predominant.

Sample Number: UK119D
Description:
A few grains of framboidal as well as euhedral crystals of pyrite are present interstitially amongst the dolomite crystals. Chlorite mineralisation is still fairly pervasive, with magnetite grains occurring as secondary minerals.

Sample Number: UK119E
Description:
The section consists predominantly of dolomite and chlorite grains. Fewer framboidal grains of pyrite (<1%) are present interstitially.

Sample Number: UK119F
Description:
The section consists predominantly of dolomite and chlorite grains. Fewer framboidal grains of pyrite (<1%) are present interstitially.

Sample Number: UK119G
Description:
The section consists predominantly of dolomite and chlorite grains. Fewer framboidal grains of pyrite (<1%) are present interstitially.

Sample Number: UK119H
Description:
The section consists predominantly of dolomite and chlorite grains. Fewer framboidal grains of pyrite (<1%) are present interstitially.

Sample Number: UK119I
Description:
The section consists predominantly of dolomite and chlorite grains. Disseminated grains of pyrite and some grains of pyrhotite are present.

Sample Number: UK119J
Description:
The section consists predominantly of dolomite and chlorite grains. Disseminated grains of pyrite are present.

Sample Number: UK119K
Description:
The way boundary is marked by the appearance of chromite. The density of the chromite grains increases away from the boundary. The xenolith portion contains dolomite and hydrous phases (talc and chlorite).

Sample Number: UK119L
Description:
Section samples the mafic host rock. The original mafic minerals have bee obliterated by secondary minerals (dolomite, talc and chlorite). Chromite is ubiquitous. Sphene occurs as the accessory phase.

Sample Number: ML1A
Description:
This section contains sulphide and augite crystals in the bottom left corner, surrounded by lath-shaped crystals of tremolite and feathery chlorite grains. The augite grains are approximately 8 mm in length and are partially replaced by the tremolite and chlorite crystals. The majority of augite crystals are zoned and contain inclusions of smaller pyroxene crystals. Also present are quartz grains that have coronas and are surrounded by the hydrous mineral phases. The pyroxene increases in size, from approximately 2.5 mm to 8 mm, towards the contact with the sulphides. The sulphide portion consists predominantly of pyrite minerals.

Sample Number: ML1B
Description:
The pyroxenes close to the disseminated sulphide grains appear strained. The edges of the pyroxenes are ragged and the grains contain inclusions of remnant dolomite and opaque mineral phases. The pyroxene crystals also contain exsolution lamellae. Remnant dolomite occurs associated with the pyroxenes. The section away from the sulphides contains a mosaic of pyroxene and spinel.

Sample Number: ML1C
Description:
Subhedral augite crystals are found together with remnant calcite crystals. The calcite crystals also occur as inclusions within the poikolitic augite grains. Subhedral quartz grains are found in the upper portion of the section. A zone of altered minerals separates the section. Disseminated pyrite grains are found within the section.

Sample Number: ML3A
Description:
The xenolith portion of the section is predominantly augite which increases in size, to approximately 7 mm, closer to the contact. In some areas the anhedral augite crystals are associated with calcite crystals. Spinel occurs as the accessory phase. Calcite crystals also occur as inclusions within the augite crystals. The augite is zoned. "Cracked" monticellite grains are also present. They contain isotropic periclase close to their centers. The periclase appears to be partially altered to brucite. The contct between the xenolith and the sulphide is marked by hydrous phases. The sulphide zones contain remnant quartz crystals surrounded by subhedral augite crystals. Sphene occurs as inclusions within the pyroxenes. The augite crystals are zoned. Quartz – rich myrmekitic symplectites textures have also formed.

Sample Number: ML3B
Description:
Various mineral phases occur in this section: olivine, augite, diopside, monticellite, calcite, phlogopite. Spinel occurs as the accessory phase. The grain size of the minerals increases towards the sulphide stringer.

Sample Number: ML4A
Description:
The xenolith portion of the section consists of garnet crystals set in a matrix of magnetite and chlorite. At the contact, remnant crystals of calcite and dolomite are found. Skeletal grains of garnet are also found in the sulphide portion. Under reflected light the sulphide portion consists predominantly of pyrrhotite, with smaller amounts of chalcopyrite.

Sample Number: ML5A
Description:
Symplectic textures are pervasively developed. A zone of chlorite crystals has developed between the symplectites and the sulphide mineralisation. The sulphide minerals consist of a network of pyrrhotite grains. The immediate contact consist mostly of chalcopyrite and pentlandite clusters.

Sample Number: ML5B
Description:
Large hornblende and calcite crystals of approximately 5-6 mm separate the sulphide stringer from the xenolith. The hornblende crystals radiate into the xenolith portion. Partially reacted hornblende and calcite crystals are still present within the sulphide

stringer. Further away from the contact the hornblende and calcite crystals appear more sheared and are replaced by talc and chlorite.

Sample Number: ML6A
Description:
This section consists of symplectic/myrmekitic and sieve-type textures. Disseminated sulphide grains (mostly pyrite) are surrounded by amphiboles. The quartzite xenolith contains a reaction rim at the contact with the sulphide stringer. The rim consists of amphiboles. Quartz grains surround some of the amphiboles. The sulphide stringer also contains partially reacted amphibole grains. Sphene and biotite occur as accessory minerals. The biotite grains are associated with actinolite crystals. Chlorite and illite are also present. The sulphide stringer consists predominantly of pyrrhotite.

Sample Number: ML6B
Description:
This thin section is similar to ML6A in the display of symplectic/myrmekitic textures in the xenolith. The contact between the sulphide stringer and the xenolith contains a zone containing chlorite associated with hornblende.

Sample Number: VH3A
Description:
The augite crystals in this section display a distinct granular texture. Remnant calcite occurs interstitially between the euhedral augite grains. The crystals grow larger towards the contact with the sulphides. Remnant calcite grains are visible within the sulphide stringer portion. Under reflected light the sulphides consist of chalcopyrite at the contact between the xenolith and the sulphide. Pyrhotite becomes the dominant sulphide mineral away from the immediate contact.

Sample Number: VH3B
Description:
This section contains large crystals of plagioclase and epidote displaying poiolitic textures. The enclosed crystals within these grains are hornblende laths. Additionally, the hornblende crystals appear to overprint the larger crystals.

Sample Number: VH9A
Description:
This section contains “globular”/altered calcite crystals between sulphide grains. Spinel occurs as the accessory mineral. The sulphide forms a net texture and consists predominantly of pyrite along the contacts and massive sulphide consisting of pyrhotite away from the immediate contact..

Sample Number: VH9B
Description:
This section is divided into 2 parts:

1. A portion that consists of a sulphide vein, and

2. A portion that contains very sparely disseminated sulphide minerals.

In the poorly mineralized portion, the calcite shows clear indication of reaction, with only skeletal/remnant calcite grains being visible. Chlorite is also present. Spinel occurs as the accessory mineral. Framboidal pyrite occurs as the predominant sulphide mineral. At the contacts, there is an increase in the size of the calcite grains. Pyrrhotite becomes the dominant mineral within the vein.

Sample Number: VH9C
Description:
This section contains aggregates of augite and hornblende. Garnet crystals are also present. Quartz and calcite occurs interstitially. Disseminated pyrite and chalcopyrite are present.

Sample Number: VH9D
Description:
This is a fairly homogenous section consisting of calcite and fan-shaped crystals of chlorite. Spinel (Magnetite) is the accessory phase.

Sample Number: VH10A
Description:
This section contains sutured crystals of amphibole, K-feldspar and some plagioclase. Chlorite is also present. Disseminated grains of chalcopyrite are also present.

Sample Number: VH10B
Description:
This section contains large amphibole crystals sutured together. Minor minerals include plagioclase, K-felspar and chlorite. Remnant grains of calcite are also visible. Chalcopyrite occurs dispersed within the section.

Sample Number: VH10C
Description:
This section contains platy amphibole crystals and anhedral, poikolitic crystals of diopside. Remnant grains of reacted calcite are found interstitially, together with K-feldspar, plagioclase and chlorite. Disseminated grains of chalcopyrite associated with pyrrhotite are present.

Sample Number: VH10D
Description:
This is a granular textured section containing a zone of larger crystals (calcite, pyroxene, amphibole) sandwiched between a zone of smaller crystals consisting predominantly of granular-textured amphibole. Magnetite occurs as the accessory phase.

Sample Number: VH11
Description:

The sulphide stringers in this section contain chloritised calcite grains. Magnetite occurs as the accessory phase. The sulphide stringers consist predominantly of pyrite and chalcopyrite.

APPENDIX E

ANALYTICAL RESULTS

Table E1: XRD Results

		Sulphides					Oxides				Carbonate		Silicates																						
Sample No	**Rock Type**	**Pyrite**	**Pyrrhotite**	**Pentlandite**	**Vallerite**	**Chalcopyrite**	**Magnesio-I**	**Spinel**	**Magnetite**	**Clinoclase**	**Dolomite**	**Calcite**	**Quartz**	**Albite**	**Microcline**	**Augite**	**Diopside**	**Andradite**	**Monticellite**	**Annite**	**Phlogopite**	**Muscovite**	**K-Paragasite**	**Magnesio-I**	**Actinolite**	**Tremolite**	**Willemsite**	**Talc**	**Serpentine**	**Nimite**	**Clinochore**	**Sepiolite/S**	**Illite/Smect**	**Zincochron**
ML1A-s	**Pyroxenite**	9											1			51										10					30			
ML1A-x	**calc-silicate**			1								5	1			79															15			
UK119A	**Chromitic Pyroxenite**							29																			24			47				
UK119B	**Chromitic Pyroxenite**																										33			53				14
UK119B	**Dolomite**																											14		86				
UK119C	**Dolomite**										34																	56		11				
UK119D	**Dolomite**										31																	47		22				
UK119E	**Dolomite**										42																	31		27				
UK119F	**Dolomite**										30																	38		32				
UK119G	**Dolomite**										31																	48		20				
UK119H	**Dolomite**										39																	46		15				
UK119I	**Dolomite**										13																	56		30				
UK119J-	**Dolomite**	3									23																	55		19				
UK119J-	**Dolomite**										24																	62		14				
UK119K	**Dolomite**							28			1	1															34			37				
UK119K	**Dolomite**											1															54			44				
UK119L	**Chromitic Pyroxenite**							39			9		6														12			34				

Table E2: XRD Results (BMZ)

Sample no.	Rock Type	Pyrite	Pyrrhotite	Chalcopyrite	Quartz	Spinel (magnetite ?)	Plagioclase	K-feldpar	Pyroxene	Amphibole	Chlorite	Talc	Calcite	Epidote Miner	Garnet
VH3A	**calc-silicate**	-	-	1	-	7	-	-	58	-	31	-	3	-	-
VH3B	**calc-silicate**	-	-	-	-	-	35	-	-	59	-	-	-	6	-
VH9A	**calc-silicate**	15	4	-	-	14	-	-	-	-	56	3	8	-	-
VH9B	**calc-silicate**	13	-	1	1	6	-	-	-	-	66	-	13	-	-
VH9C	**calc-silicate**	4	-	2	2	-	-	-	41	3	1	-	2	-	45
VH9D	**calc-silicate**	-	-	-	-	2	-	-	-	-	81	-	17	-	-
VH10A	**calc-silicate**	-	-	8	-	-	2	6	-	83	1	-	-	-	-
VH10B	**calc-silicate**	-	-	20	-	-	1	5	-	73	1	-	-	-	-
VH10C	**calc-silicate**	-	8	24	-	-	2	3	13	48	2	-	-	-	-
VH11	**calc-silicate**	55	-	2	-	5	-	-	-	-	31	-	7	-	-
VH10D	**calc-silicate**			-	-		6	trace	-	93	-	-	1		-
VH9E	**calc-silicate**			-	-		-	-	12	17	11	53	7		-
VH9F	**calc-silicate**			1	3		-	-	43	11	4	18	4		16

Table E3: XRD Results (MSB)

		Sulphides					Oxides				Carbonates		Silicates																						
Sample No	**Rock Type**	**Pyrite**	**Pyrrhotite**	**Pentlandite**	**Vallerite**	**Chalcopyrite**	**Magnesio-ferrite**	**Spinel**	**Magnetite**	**Clinoclase**	**Dolomite**	**Calcite**	**Quartz**	**Albite**	**Microcline**	**Augite**	**Diopside**	**Andradite**	**Monticellite**	**Annite**	**Phlogopite**	**Muscovite**	**K-Paragsite**	**Magnesio-hornblende**	**Actinolite**	**Tremolite**	**Willemsite**	**Talc**	**Serpentine**	**Nimite**	**Clinochore**	**Sepiolite/Stilpnomelane**	**Illite/Smectite Interstrat**	**Zincochromite**
ML1C	**calc-silicate**											1	49		5	42																	3	
ML3A-s	**granite**	1	79	7									2		7							4												
ML3A-x	**calc-silicate**		2													94			1			3												
ML3B-m	**calc-silicate**		6									12				40					33								9					
ML3B-x	**calc-silicate**											4	1				92				3													
ML4A-s	**calc-silicate**	3	34	3			56			3			1																					
ML4A-x	**calc-silicate**				2		43											38											7		10			
ML5A-s	**calc-silicate**		34	3		31	20						5	5	2																			
ML5A-x	**calc-silicate**					20							31	19	11						7											5		
ML5B-m	**calc-silicate**	2	28	3		51	5			6																				5				
ML5B-x	**calc-silicate**											42												5			26			26				
ML6A-m	**calc-silicate**										18			12	14										29					10			17	
ML6A-x	**calc-silicate**												99		1																			
ML6B-s	**calc-silicate**		64	5					3				4	5	9							3		5						2			
ML6B-x	**calc-silicate**					12							8	6	6					18			49										

Table E4: Electron Microprobe Results

SAMPLE	NUMBER	SIO2	TIO2	AL2O3	CR2O3	FE2O3	FEO	MNO	MGO	CAO	TOTAL	OXYG	SI	TI	AL	CR	FE3	FE2	MN	MG	CA	NA	K	SUM	CA1	MG1	FE1	CAN	MGN	CRN	LD76
ML1A1	1	52.97	0.14	0.72	0.00	0.00	3.68	0.30	15.63	24.34	97.78	6	1.985	0.004	0.032	0.000	0.000	0.115	0.010	0.873	0.977	0.000	0.000	3.995	49.72	44.41	5.87	52.82	88.33	0.00	0.0
ML1A1	2	53.02	0.25	0.38	0.00	0.00	4.62	0.35	15.10	24.02	97.74	6	1.995	0.007	0.017	0.000	0.000	0.145	0.011	0.847	0.968	0.000	0.000	3.990	49.40	43.19	7.42	53.35	85.35	0.00	0.0
ML1A1	3	31.32	0.00	16.75	0.00	0.00	0.94	0.12	33.50	0.39	83.02	2	0.437	0.000	0.275	0.000	0.000	0.011	0.001	0.696	0.006	0.000	0.000	1.426	49.40	43.19	7.42	53.35	85.35	0.00	0.0
ML1A1	4	53.31	0.11	0.46	0.00	0.00	3.50	0.23	15.97	24.41	97.99	6	1.991	0.003	0.020	0.000	0.000	0.109	0.007	0.889	0.977	0.000	0.000	3.996	49.46	45.01	5.54	52.36	89.05	0.00	0.0
ML1A1	5	33.56	0.00	13.73	0.00	0.00	1.13	0.00	35.41	0.00	83.83	2	0.463	0.000	0.223	0.000	0.000	0.013	0.000	0.727	0.000	0.000	0.000	1.426	49.46	45.01	5.54	52.36	89.05	0.00	0.0
ML1A1	6	33.65	0.00	13.09	0.00	0.00	1.14	0.00	35.49	0.00	83.37	2	0.466	0.000	0.214	0.000	0.000	0.013	0.000	0.733	0.000	0.000	0.000	1.427	49.46	45.01	5.54	52.36	89.05	0.00	0.0
ML1A1	7	52.21	0.17	1.20	0.00	0.00	3.54	0.30	15.75	24.23	97.40	6	1.965	0.005	0.053	0.000	0.000	0.111	0.010	0.883	0.977	0.000	0.000	4.004	49.55	44.80	5.65	52.52	88.80	0.00	0.0
ML1A1	8	33.94	0.00	12.81	0.00	0.00	1.20	0.00	35.74	0.00	83.69	2	0.469	0.000	0.209	0.000	0.000	0.014	0.000	0.736	0.000	0.000	0.000	1.427	49.55	44.80	5.65	52.52	88.80	0.00	0.0
ML1A1	9	42.14	0.00	0.86	0.00	0.00	4.30	0.18	37.36	0.08	84.92	2	0.580	0.000	0.014	0.000	0.000	0.049	0.002	0.766	0.001	0.000	0.000	1.413	49.55	44.80	5.65	52.52	88.80	0.00	0.0
ML1A1	10	35.28	0.00	11.81	0.00	0.00	1.38	0.09	35.36	1.06	84.98	2	0.482	0.000	0.190	0.000	0.000	0.016	0.001	0.719	0.016	0.000	0.000	1.423	49.55	44.80	5.65	52.52	88.80	0.00	0.0
ML1A2	1	32.62	0.00	14.55	0.00	0.00	1.13	0.00	35.18	0.12	83.60	2	0.452	0.000	0.237	0.000	0.000	0.013	0.000	0.726	0.002	0.000	0.000	1.430	49.55	44.80	5.65	52.52	88.80	0.00	0.0
ML1A2	2	54.12	0.00	0.00	0.00	0.00	0.10	0.00	18.80	25.12	98.14	6	1.989	0.000	0.000	0.000	0.000	0.003	0.000	1.030	0.989	0.000	0.000	4.011	48.92	50.93	0.15	49.00	99.70	0.00	712.9
ML1A2	3	54.38	0.00	0.00	0.00	0.00	0.00	0.00	18.52	25.45	98.35	6	1.994	0.000	0.000	0.000	0.000	0.000	0.000	1.012	1.000	0.000	0.000	4.006	49.70	50.30	0.00	49.70		0.00	515.3
ML1A2	4	54.50	0.00	0.00	0.00	0.00	0.15	0.00	18.38	25.13	98.16	6	2.001	0.000	0.000	0.000	0.000	0.005	0.000	1.006	0.988	0.000	0.000	3.999	49.46	50.31	0.23	49.57	99.54	0.00	568.4
ML1A2	5	53.94	0.00	0.15	0.00	0.00	0.66	0.00	18.71	24.53	97.99	6	1.987	0.000	0.007	0.000	0.000	0.020	0.000	1.027	0.968	0.000	0.000	4.010	48.03	50.96	1.01	48.52	98.06	0.00	786.6
ML1A2	6	53.03	0.06	1.45	0.00	0.00	1.68	0.00	17.43	25.06	98.71	6	1.953	0.002	0.063	0.000	0.000	0.052	0.000	0.956	0.989	0.000	0.000	4.014	49.51	47.90	2.59	50.83	94.87	0.00	0.0
ML1A2	7	51.11	0.00	2.00	0.00	0.00	2.81	0.16	16.34	24.73	97.15	6	1.928	0.000	0.089	0.000	0.000	0.089	0.005	0.918	0.999	0.000	0.000	4.028	49.81	45.77	4.42	52.11	91.20	0.00	0.0
ML1A2	8	50.92	0.00	2.79	0.00	0.00	3.74	0.00	16.01	24.79	98.25	6	1.906	0.000	0.123	0.000	0.000	0.117	0.000	0.893	0.994	0.000	0.000	4.033	49.60	44.56	5.84	52.68	88.41	0.00	0.0
ML1A2	9	54.37	0.00	0.00	0.00	0.00	0.14	0.00	18.56	25.22	98.29	6	1.995	0.000	0.000	0.000	0.000	0.004	0.000	1.015	0.991	0.000	0.000	4.005	49.31	50.47	0.21	49.42	99.58	0.00	618.0
ML1A2	10	53.95	0.06	0.53	0.00	0.00	0.48	0.00	18.20	25.52	98.74	6	1.976	0.002	0.023	0.000	0.000	0.015	0.000	0.994	1.002	0.000	0.000	4.011	49.84	49.43	0.73	50.20	98.54	0.00	0.0
ML1A5	1	53.80	0.00	0.00	0.00	0.00	0.10	0.00	18.57	24.74	97.21	6	1.994	0.000	0.000	0.000	0.000	0.003	0.000	1.026	0.983	0.000	0.000	4.006	48.85	51.00	0.15	48.92	99.70	0.00	726.0
ML1A5	2	51.01	0.00	2.38	0.00	0.00	2.56	0.00	16.63	24.69	97.27	6	1.918	0.000	0.105	0.000	0.000	0.080	0.000	0.932	0.995	0.000	0.000	4.030	49.56	46.43	4.01	51.63	92.05	0.00	0.0
ML1A5	3	53.33	0.00	0.10	0.00	0.00	0.36	0.12	18.66	24.98	97.55	6	1.977	0.000	0.004	0.000	0.000	0.011	0.004	1.031	0.992	0.000	0.000	4.020	48.78	50.68	0.55	49.04	98.93	0.00	704.1
ML1A5	4	49.42	0.00	3.52	0.00	0.00	3.41	0.00	15.57	24.30	96.22	6	1.887	0.000	0.158	0.000	0.000	0.109	0.000	0.886	0.994	0.000	0.000	4.034	49.98	44.54	5.47	52.88	89.05	0.00	0.0
ML1A5	5	30.58	0.00	17.09	0.00	0.00	1.33	0.00	34.41	0.05	83.46	2	0.425	0.000	0.280	0.000	0.000	0.015	0.000	0.713	0.001	0.000	0.000	1.435	49.98	44.54	5.47	52.88	89.05	0.00	0.0
ML1A5	6	53.92	0.00	0.00	0.00	0.00	0.14	0.00	18.32	24.90	97.28	6	1.998	0.000	0.000	0.000	0.000	0.004	0.000	1.012	0.989	0.000	0.000	4.002	49.32	50.47	0.22	49.42	99.57	0.00	616.3
ML1A5	7	46.59	0.05	5.64	0.00	0.00	4.21	0.00	14.87	24.09	95.45	6	1.807	0.001	0.258	0.000	0.000	0.137	0.000	0.859	1.001	0.000	0.000	4.063	50.13	43.04	6.84	53.81	86.29	0.00	0.0
ML1A5	8	49.73	0.08	3.62	0.00	0.00	3.82	0.00	15.46	24.37	97.08	6	1.885	0.002	0.162	0.000	0.000	0.121	0.000	0.873	0.990	0.000	0.000	4.032	49.88	44.01	6.10	53.13	87.82	0.00	0.0
ML1A5	9	46.98	0.06	5.52	0.00	0.00	4.77	0.00	14.38	24.30	96.01	6	1.815	0.002	0.251	0.000	0.000	0.154	0.000	0.828	1.006	0.000	0.000	4.057	50.60	41.65	7.75	54.85	84.31	0.00	0.0
ML1A5	10	53.49	0.00	0.06	0.00	0.00	0.17	0.00	18.67	25.13	97.52	6	1.981	0.000	0.003	0.000	0.000	0.005	0.000	1.031	0.997	0.000	0.000	4.017	49.05	50.69	0.26	49.18	99.49	0.00	676.5
ML1A3	1	48.93	0.00	4.39	0.00	0.00	4.30	0.00	15.07	24.82	97.51	6	1.855	0.000	0.196	0.000	0.000	0.136	0.000	0.851	1.008	0.000	0.000	4.047	50.51	42.66	6.83	54.22	86.20	0.00	0.0
ML1A3	2	50.19	0.00	3.61	0.00	0.00	3.89	0.00	15.70	24.80	98.19	6	1.882	0.000	0.160	0.000	0.000	0.122	0.000	0.877	0.997	0.000	0.000	4.038	49.93	43.96	6.11	53.18	87.79	0.00	0.0
ML1A3	3	47.95	0.09	5.11	0.00	0.00	4.88	0.00	14.59	24.67	97.29	6	1.829	0.003	0.230	0.000	0.000	0.156	0.000	0.829	1.008	0.000	0.000	4.054	50.58	41.61	7.81	54.87	84.20	0.00	0.0
ML1A3	4	53.28	0.00	0.00	0.00	0.00	0.29	0.00	18.20	25.40	97.17	6	1.984	0.000	0.000	0.000	0.000	0.009	0.000	1.010	1.013	0.000	0.000	4.016	49.86	49.69	0.44	50.08	99.11	0.00	0.0
ML1A3	5	47.38	0.10	5.97	0.00	0.00	5.29	0.00	13.96	24.64	97.34	6	1.810	0.003	0.269	0.000	0.000	0.169	0.000	0.795	1.008	0.000	0.000	4.053	51.14	40.30	8.57	55.93	82.46	0.00	0.0

Table E5: XRF Trace Element Results

Sample	As	Ba	Co	Cr	Cu	Ga	Mo	Nb	Ni	Pb	Rb	Sc	Sr	Ta	Th	U	V	W	Y	Zn	Zr	Hf	Y/Nb	Nb+Y	Na2O+K2O	FeOT/MgO
UK-119A	15.606	42.590	91.715		-5.000	20.733	-2.000	-2.000	***1.1%***	-5.000	-5.000	24.573	8.929	-5.000	5.209	-3.000	550.784	-3.000	-3.000	699.909	26.378	-5.000	-0.093	-4.524	-4.989	45.858
UK-119B1	11.420	13.257	26.916	***0.9%***	33.688	5.884	-2.000	-2.000	923.639	5.439	-5.000	18.352	36.117	5.430	-5.000	-3.000	75.309	-3.000	5.867	41.864	23.529	-5.000	0.001	929.585	929.078	13.458
UK-119B2	-10.000	58.319	75.366		14.444	15.182	-2.000	-2.000	941.896	-5.000	-5.000	28.927	11.761	-5.000	-5.000	-3.000	520.256	-3.000	3.994	577.917	22.283	-5.000	0.001	937.575	936.896	37.683
UK-119C	14.165	3.691	21.171	486.320	29.231	-5.000	-2.000	-2.000	718.660	-5.000	-5.000	9.794	168.683	-5.000	-5.000	-3.000	16.096	-3.000	3.732	13.828	6.571	-5.000	0.000	713.660	713.660	10.586
UK-119D	10.438	-5.000	27.162	805.257	38.583	-5.000	-2.000	-2.000	527.356	-5.000	-5.000	10.875	169.821	-5.000	-5.000	-3.000	28.141	-3.000	3.293	18.825	13.295	-5.000	0.000	522.356	522.356	13.581
UK-119E	-10.000	8.131	21.386	336.729	5.740	-5.000	-2.000	-2.000	288.189	-5.000	-5.000	13.150	207.383	-5.000	-5.000	-3.000	36.239	-3.000	3.664	7.132	23.505	-5.000	0.000	283.189	283.189	10.693
UK-119F	-10.000	-5.000	29.212	494.380	45.474	-5.000	-2.000	-2.000	580.866	-5.000	-5.000	10.146	191.767	-5.000	-5.000	-3.000	33.144	-3.000	4.817	20.644	21.206	-5.000	0.001	576.640	575.866	14.606
UK-119G	15.137	-5.000	33.094	503.234	69.434	-5.000	-2.000	-2.000	482.692	-5.000	-5.000	9.209	180.134	-5.000	-5.000	-3.000	27.653	-3.000	4.005	9.351	23.150	-5.000	0.000	477.692	477.692	16.547
UK-119H	-10.000	-5.000	13.561	429.574	455.652	-5.000	-2.000	-2.000	309.552	-5.000	-5.000	10.206	231.395	5.418	-5.000	-3.000	22.799	-3.000	5.407	195.309	20.409	-5.000	0.000	304.552	304.552	6.780
UK-119I	-10.000	-5.000	38.664	645.114	97.976	-5.000	-2.000	-2.000	1036.091	-5.000	-5.000	9.158	202.336	12.196	-5.000	-3.000	29.224	-3.000	-3.000	12.393	19.955	-5.000	0.001	1031.764	1031.091	19.332
UK-119J	137.911	7.434	204.216	***0.7%***	972.507	-5.000	-2.000	-2.000	***3275.915***	-5.000	-5.000	11.824	184.495	48.033	-5.000	-3.000	39.459	-3.000	4.241	29.108	20.270	6.618	0.000	3270.915	3270.915	102.108
UK-119K	77.104	6.457	185.675	***0.7%***	1081.663	-5.000	-2.000	-2.000	***1.7%***	-5.000	-5.000	6.332	6.765	174.730	-5.000	-3.000	43.139	16.173	-3.000	66.408	15.176	23.909	-0.111	-4.432	-4.983	92.837
UK-119L	58.070	50.855	***381.807***		557.097	12.674	-2.000	-2.000	***0.9%***	-5.000	-5.000	32.976	50.663	87.886	5.276	3.369	700.031	8.213	4.128	581.735	18.662	-5.000	-0.076	-4.613	-4.991	190.904
VH-10A	-10.000	101.895	18.617	255.278	1215.081	-5.000	-2.000	5.888	157.630	201.667	-5.000	33.497	213.012	18.724	-5.000	-3.000	139.428	-3.000	25.877	200.074	128.585	-5.000	0.015	364.573	359.296	9.308
VH-10B	-10.000	74.474	9.213	515.117	574.776	8.892	-2.000	3.588	73.733	12.493	-5.000	21.854	347.464	9.348	-5.000	-3.000	95.889	-3.000	30.656	62.048	132.069	5.294	0.220	105.230	86.226	4.607
VH-10C	-10.000	45.491	24.555	274.596	1330.574	9.466	-2.000	6.889	342.450	7.611	-5.000	28.350	691.687	21.478	6.791	-3.000	107.444	-3.000	34.261	98.103	220.871	6.301	0.012	354.338	350.061	12.278
VH-10D	-10.000	70.693	41.884	258.189	1857.130	-5.000	-2.000	5.611	724.672	10.669	-5.000	45.064	101.013	37.922	7.165	-3.000	173.533	-3.000	33.342	107.334	247.077	5.426	0.017	748.039	735.340	20.942
VH-11	142.125	-5.000	***0.1%***	117.988	***0.9%***	-5.000	2.506	-2.000	***2804.966***	28.257	6.918	-3.000	20.530	182.709	26.873	14.870	22.995	6.204	-3.000	-3.000	6.299	5.789	0.006	2849.012	2833.223	0.000
VH-3A	-10.000	22.276	18.504	209.446	235.680	10.225	-2.000	3.455	180.273	70.566	-5.000	15.348	30.454	5.303	8.029	-3.000	51.898	-3.000	29.476	24.031	166.770	-5.000	0.000	250.839	250.839	9.252
VH-3B	-10.000	30.477	6.847	383.302	266.754	12.107	-2.000	6.902	162.152	23.672	-5.000	15.930	698.324	-5.000	5.096	-3.000	54.910	-3.000	18.348	61.954	147.113	-5.000	0.057	196.349	185.824	3.424
VH-9A	-10.000	-5.000	9.481	53.329	371.990	-5.000	-2.000	-2.000	99.855	6.067	-5.000	9.781	80.582	-5.000	-5.000	-3.000	14.538	-3.000	6.426	33.193	36.887	-5.000	0.000	105.922	105.922	4.740
VH-9B	12.296	-5.000	14.322	47.925	297.009	-5.000	-2.000	-2.000	388.600	8.415	-5.000	11.814	77.329	6.244	6.258	3.631	14.273	-3.000	6.184	24.934	27.099	-5.000	0.000	397.014	397.014	7.161
VH-9C	103.742	-5.000	***605.796***	89.188	2064.698	-5.000	-2.000	-2.000	5362.432	20.139	5.835	4.286	28.830	76.400	18.257	13.037	9.528	7.539	-3.000	16.537	-5.000	-5.000	0.000	5382.571	5382.571	302.898
VH-9D	107.207	-5.000	***949.866***	170.740	***4932.244***	1.012	-2.000	-2.000	***1%***	23.925	6.506	-3.000	17.601	177.920	23.044	12.791	9.665	16.498	-3.000	21.919	-5.000	8.243	0.000	23.935	23.935	474.933
VH-9E	17.706	-5.000	87.174	15.182	2415.264	-5.000	-2.000	-2.000	1849.284	13.448	-5.000	8.710	11.752	57.290	-5.000	-3.000	-5.000	-3.000	-3.000	17.309	-5.000	-5.000	0.000	1863.293	1862.731	43.587
VH-9F	18.263	-5.000	52.036	8.854	***2728.774***	-5.000	-2.000	-2.000	1620.734	13.330	-5.000	9.537	-5.000	64.114	5.263	-3.000	-5.000	-3.000	-3.000	14.048	-5.000	-5.000	0.000	1634.299	1634.064	26.018

XRF Normative Results

Sample	Qz	Co	Z	Or	Pl	PlAb	PlAn	Lc	Ne	Kp	Hl	Th	Ac	Ns	Ks	Wo	Di	DiWo	DiEn	DiFs	Hy	HyEn	HyFs	Ol	OlFo	OlFa
UK-119A	0.000	16.903	0.004	0.076	5.700	0.465	5.235	0.000	0.000	0.000	0.000	0.000	0.000	0.000	0.000	0.000	0.000	0.000	0.000	0.000	45.984	45.984	0.000	10.527	10.527	0.000
UK-119B1	0.000	12.624	0.004	0.074	5.623	0.507	5.115	0.000	0.000	0.000	0.000	0.000	0.000	0.000	0.000	0.000	0.000	0.000	0.000	0.000	58.840	58.840	0.000	4.623	4.623	0.000
UK-119B2	0.000	0.106	0.003	0.062	14.612	0.679	13.933	0.000	0.000	0.000	0.000	0.000	0.000	0.000	0.000	0.000	0.000	0.000	0.000	0.000	79.195	79.195	0.000	1.537	1.537	0.000
UK-119C	0.000	0.000	0.001	0.000	3.260	0.000	3.260	0.056	0.471	0.000	0.000	0.000	0.000	0.000	0.000	0.000	34.996	17.498	17.498	0.000	0.000	0.000	0.000	50.638	50.638	0.000
UK-119D	0.000	0.000	0.002	0.000	5.239	0.000	5.239	0.055	0.417	0.000	0.000	0.000	0.000	0.000	0.000	0.000	40.705	20.353	20.353	0.000	0.000	0.000	0.000	48.634	48.634	0.000
UK-119E	0.000	0.000	0.003	0.000	9.520	0.000	9.520	0.055	0.565	0.000	0.000	0.000	0.000	0.000	0.000	0.000	20.977	10.489	10.489	0.000	0.000	0.000	0.000	56.652	56.652	0.000
UK-119F	0.000	0.000	0.003	0.067	7.203	0.774	6.429	0.000	0.000	0.000	0.000	0.000	0.000	0.000	0.000	0.000	37.968	18.984	18.984	0.000	10.933	10.933	0.000	41.151	41.151	0.000
UK-119G	0.000	0.000	0.003	0.000	5.907	0.000	5.907	0.055	0.487	0.000	0.000	0.000	0.000	0.000	0.000	0.000	27.337	13.668	13.668	0.000	0.000	0.000	0.000	53.745	53.745	0.000
UK-119H	0.000	0.000	0.003	0.000	5.375	0.000	5.375	0.056	0.520	0.000	0.000	0.000	0.000	0.000	0.000	0.000	19.677	9.838	9.838	0.000	0.000	0.000	0.000	56.774	56.774	0.000
UK-119I	0.000	0.000	0.003	0.066	9.082	0.672	8.410	0.000	0.000	0.000	0.000	0.000	0.000	0.000	0.000	0.000	35.300	17.650	17.650	0.000	8.757	8.757	0.000	43.531	43.531	0.000
UK-119J	0.000	0.000	0.003	0.000	6.949	0.000	6.949	0.053	0.480	0.000	0.000	0.000	0.000	0.000	0.000	0.000	35.507	17.754	17.754	0.000	0.000	0.000	0.000	46.010	46.010	0.000
UK-119K	10.728	1.767	0.002	0.063	2.748	0.551	2.197	0.000	0.000	0.000	0.000	0.000	0.000	0.000	0.000	0.000	0.000	0.000	0.000	0.000	77.317	77.317	0.000	0.000	0.000	0.000
UK-119L	0.000	8.467	0.003	0.081	20.306	0.378	19.928	0.000	0.000	0.000	0.000	0.000	0.000	0.000	0.000	0.000	0.000	0.000	0.000	0.000	42.754	42.754	0.000	3.635	3.635	0.000
VH-10A	10.725	0.000	0.016	1.051	20.985	5.277	15.708	0.000	0.000	0.000	0.000	0.000	0.000	0.000	0.000	0.000	57.353	28.676	28.676	0.000	0.397	0.397	0.000	0.000	0.000	0.000
VH-10B	7.013	0.000	0.016	0.684	35.195	19.004	16.191	0.000	0.000	0.000	0.000	0.000	0.000	0.000	0.000	1.549	48.798	24.399	24.399	0.000	0.000	0.000	0.000	0.000	0.000	0.000
VH-10C	8.452	0.000	0.028	0.350	26.934	4.278	22.656	0.000	0.000	0.000	0.000	0.000	0.000	0.000	0.000	0.000	46.385	23.192	23.192	0.000	6.492	6.492	0.000	0.000	0.000	0.000
VH-10D	14.639	0.000	0.031	0.804	21.968	12.699	9.269	0.000	0.000	0.000	0.000	0.000	0.000	0.000	0.000	0.000	42.145	21.073	21.073	0.000	7.851	7.851	0.000	0.000	0.000	0.000
VH-11	12.655	0.000	0.001	0.588	23.506	15.790	7.716	0.000	0.000	0.000	0.000	0.000	0.000	0.000	0.000	0.000	44.496	22.248	22.248	0.000	6.555	6.555	0.000	0.000	0.000	0.000
VH-3A	0.000	0.000	0.021	0.000	23.348	0.000	23.348	0.048	0.345	0.000	0.000	0.000	0.000	0.000	0.000	0.000	50.335	25.168	25.168	0.000	0.000	0.000	0.000	9.989	9.989	0.000
VH-3B	6.665	0.000	0.018	0.061	32.957	10.525	22.432	0.000	0.000	0.000	0.000	0.000	0.000	0.000	0.000	5.204	48.504	24.252	24.252	0.000	0.000	0.000	0.000	0.000	0.000	0.000
VH-9A	0.000	0.000	0.006	0.000	4.106	0.000	4.106	0.000	0.647	0.048	0.000	0.000	0.000	0.000	0.000	0.000	0.000	0.000	0.000	0.000	0.000	0.000	0.000	39.825	39.825	0.000
VH-9B	0.000	0.000	0.004	0.000	3.843	0.000	3.843	0.000	0.548	0.045	0.000	0.000	0.000	0.000	0.000	0.000	0.000	0.000	0.000	0.000	0.000	0.000	0.000	42.258	42.258	0.000
VH-9C	0.000	0.000	0.000	0.000	5.389	0.000	5.389	0.062	0.371	0.000	0.000	0.000	0.000	0.000	0.000	0.000	6.376	3.188	3.188	0.000	0.000	0.000	0.000	34.015	34.015	0.000
VH-9D	0.000	0.000	0.000	0.000	8.117	0.000	8.117	0.065	0.226	0.000	0.000	0.000	0.000	0.000	0.000	0.000	7.327	3.663	3.663	0.000	0.000	0.000	0.000	31.602	31.602	0.000
VH-9E	0.000	0.000	0.000	0.061	2.369	0.562	1.807	0.000	0.000	0.000	0.000	0.000	0.000	0.000	0.000	0.000	70.481	35.240	35.240	0.000	16.924	16.924	0.000	0.500	0.500	0.000
VH-9F	0.000	0.000	0.000	0.060	1.334	0.235	1.098	0.000	0.145	0.000	0.000	0.000	0.000	0.000	0.000	0.000	90.874	45.437	45.437	0.000	0.000	0.000	0.000	0.570	0.570	0.000

Sample	Cs	Mt	Cm	Il	Hm	Sp	Pf	Ru	Ap	Fl	Py	Cc	Bi	Ho	HoAct	HoEd	HoRi	Spnl	SALIC	FEMIC	TOTAL	ANPL	FAOL	ENHY	WQz	WCo
UK-119A	0.000	0.000	0.004	0.584	20.086	0.000	0.000	0.057	0.078	0.000	0.000	0.000	0.000	0.000	0.000	0.000	0.000	0.000	22.684	77.319	100.002	91.836	0.000	100.000	0.000	15.274
UK-119B1	0.000	0.000	0.003	0.728	17.445	0.000	0.000	0.012	0.026	0.000	0.000	0.000	0.000	0.000	0.000	0.000	0.000	0.000	18.324	81.678	100.002	90.976	0.000	100.000	0.000	11.532
UK-119B2	0.000	0.000	0.000	0.295	4.153	0.000	0.000	0.013	0.022	0.000	0.000	0.000	0.000	0.000	0.000	0.000	0.000	0.000	14.784	85.216	100.000	95.354	0.000	100.000	0.000	0.104
UK-119C	7.584	0.455	0.000	0.089	2.427	0.000	0.000	0.000	0.025	0.000	0.000	0.000	0.000	0.000	0.000	0.000	0.000	0.000	3.787	96.213	100.000	100.000	0.000	0.000	0.000	0.000
UK-119D	2.249	0.194	0.000	0.145	2.337	0.000	0.000	0.000	0.024	0.000	0.000	0.000	0.000	0.000	0.000	0.000	0.000	0.000	5.712	94.288	100.000	100.000	0.000	0.000	0.000	0.000
UK-119E	9.240	0.032	0.000	0.201	2.730	0.000	0.000	0.000	0.024	0.000	0.000	0.000	0.000	0.000	0.000	0.000	0.000	0.000	10.143	89.857	100.000	100.000	0.000	0.000	0.000	0.000
UK-119F	0.000	0.149	0.000	0.150	2.354	0.000	0.000	0.000	0.024	0.000	0.000	0.000	0.000	0.000	0.000	0.000	0.000	0.000	7.272	92.728	100.000	89.255	0.000	100.000	0.000	0.000
UK-119G	9.361	0.164	0.000	0.166	2.750	0.000	0.000	0.000	0.025	0.000	0.000	0.000	0.000	0.000	0.000	0.000	0.000	0.000	6.454	93.546	100.000	100.000	0.000	0.000	0.000	0.000
UK-119H	14.517	0.178	0.000	0.145	2.701	0.000	0.000	0.000	0.054	0.000	0.000	0.000	0.000	0.000	0.000	0.000	0.000	0.000	5.954	94.046	100.000	100.000	0.000	0.000	0.000	0.000
UK-119I	0.000	0.239	0.000	0.195	2.805	0.000	0.000	0.000	0.023	0.000	0.000	0.000	0.000	0.000	0.000	0.000	0.000	0.000	9.151	90.849	100.000	92.598	0.000	100.000	0.000	0.000

Table E6: ICP-MS Results

Sample	Li	Be	B	Na	Mg	Al	Si	P	K	Ca	Sc	Ti	V	Cr	Mn	Fe	Co	Ni
UK 119 A	33393	697	0	40899	68867865	14802880	0	23229	0	2896095	3145	101559	0	9448553	273957	30562922	10705	420694
UK 119 B1	19479	549	0	32809	68663682	12547292	0	5301	1557	3336895	5678	205015	0	6273705	231450	22730735	10003	358841
UK 119 B2	19185	109	0	83672	160381655	18816765	20845	9282	37523	13729512	8737	263148	0	2034459	337469	26253107	21939	688975
UK 119 C	3561	8	0	42425	130589755	3843404	0	1340	2516	57672285	2993	76269	0	289254	724896	15944970	19229	665438
UK 119 D	6105	41	0	50524	137669338	6358601	26993	1034	18962	55967771	4899	154955	0	483378	498775	14718577	22690	434380
UK 119 E	8036	44	0	42286	144071977	11796087	330046	2756	104167	57051740	5694	237687	0	0	539612	17528297	21115	216200
UK 119 F	6430	68	175	54322	149137910	9542112	882087	3142	48190	52575490	5704	150345	0	338289	456883	16720959	31190	523900
UK 119 G	4983	48	1732	44992	150371012	7873750	112721	1327	6482	59445306	4512	118381	0	313068	567836	16646830	28308	518875
UK 119 H	4758	50	173	77026	163370885	7466320	26697	20602	21007	71894449	4336	80188	0	268996	645004	18443197	10949	225734
UK 119 I	7995	28	0	60713	157354860	11126643	0	9315	33001	42349077	4514	171987	0	417243	473716	19108181	41442	1129930
UK 119 J	6725	55	0	41875	116878474	6801559	0	11699	0	41984823	3478	120130	0	1031525	526974	43064951	209296	3351664
UK 119 K	9112	24	0	99771	146959687	7022292	0	2032	19001	1772361	4474	142533	0	1571313	65789	43965935	175975	12002641
UK 119 L	19652	125	0	14332	38894795	11013305	0	15717	0	13783074	5258	72326	0	5537230	374454	34957423	242819	6634048
VH 3 A	4624	1290	0	70582	58027973	29867887	0	0	60727	117092035	3461	1032756	0	0	1667972	34358283	16129	158504
VH 3 B	3828	643	0	9693930	39752722	37023809	0	72591	160315	96150096	3934	1064649	0	0	2279948	45294217	12368	156308
VH 9 A	463	19	0	34635	67843851	4159360	0	6190	0	133146266	425	152701	0	0	765872	70842820	2461	81013
VH 9 B	425	42	0	17420	79745611	3741973	0	8547	0	129041191	488	250964	0	0	774643	74164253	18101	395199
VH 9 C	525	36	0	30295	52652066	4214911	0	2099	0	30281898	515	82075	0	0	316220	238949979	623426	3834969
VH 9 D	551	103	0	9895	47568929	6039414	0	0	0	16724993	228	50245	0	0	264391	271445091	819531	7857647
VH 9 E	1008	425	0	43161	93311684	1879908	0	0	0	83252740	0	38755	0	0	455313	65925361	101189	1817562
VH 9 F	431	614	0	43105	81321267	1504693	0	0	0	116024897	0	42945	0	0	521178	48652670	51728	1745078
VH 10 A	7181	653	0	7274106	44480050	21525909	0	91087	938054	84925478	11109	2234852	0	0	2430070	52630997	18009	123889
VH 10 B	6755	470	0	13611342	39426306	32623053	0	131875	622141	84542156	8321	1643346	0	404693	1742178	42253221	12902	69961
VH 10 C	7385	779	0	2120913	46002408	30397544	0	52097	435719	82136560	10256	1974792	0	0	2099242	72813695	25925	411282
VH 10 D	3168	557	0	12264970	43873670	19379722	0	238744	504684	63306097	18925	2695320	27747	0	2035998	67122723	39922	877583
VH 11	410	55	0	7449	37930931	3212452	0	0	0	28847750	657	243478	0	0	285882	240592311	1499578	2212980
Sample	Cu	Zn	Ga	Ge	As	Se	Br	Rb	Sr	Y	Zr	Nb	Mo	Ru	Rh	Pd	Ag	Cd
UK 119 A	10394	79980	3065	0	0	0	0	304	8037	1196	13395	224	231	38	23	105	129	62
UK 119 B1	22401	77613	2250	0	0	0	0	364	9605	1354	14075	517	0	12	18	84	129	0
UK 119 B2	24495	22440	2239	0	0	0	0	533	34460	1956	14846	490	169	14	11	280	297	0
UK 119 C	24658	13157	93	0	0	0	0	230	154141	2538	3923	160	0	0	12	133	127	0
UK 119 D	30158	18257	538	0	0	0	0	316	161459	2363	8074	308	0	0	11	99	302	28
UK 119 E	6725	8804	1567	0	0	0	0	1087	207701	2806	12119	451	0	0	8	103	188	72
UK 119 F	41361	24329	1050	0	0	0	0	566	188712	2837	12948	329	0	0	15	134	244	114
UK 119 G	73453	10774	718	0	0	0	0	342	175967	3030	13153	244	0	0	12	147	432	108
UK 119 H	458989	188523	802	0	0	0	0	319	222733	3576	12332	141	0	0	16	107	269	115
UK 119 I	87599	11732	1681	0	0	0	0	479	195506	1960	14246	587	452	30	19	146	319	16
UK 119 J	946584	13249	858	0	74166	5709	0	246	161427	2582	11666	273	822	82	92	272	692	101
UK 119 K	1267946	22996	674	0	17760	14227	0	381	5956	567	7640	392	460	136	212	868	1035	190
UK 119 L	423270	46076	790	0	0	5573	0	243	46536	1201	9417	368	275	135	115	587	330	116
VH 3 A	222526	23802	7181	0	0	0	0	978	27201	19857	115420	2140	682	0	6	501	554	0
VH 3 B	290153	61292	10233	0	0	0	0	411	733852	13007	92979	5173	746	4	32	436	494	273
VH 9 A	351898	26152	591	0	0	0	0	211	75574	4501	29787	175	0	0	8	144	253	141
VH 9 B	268898	22355	655	0	0	0	0	255	74740	5266	22300	135	0	0	7	128	290	131
VH 9 C	1648152	6648	1467	0	22242	44326	0	655	22992	2370	2048	119	66	13	94	813	1295	181

VH 9 D	4076881	32156	2172	0	26194	62311	0	272	16144	1747	1521	113	245	66	155	835	2349	317
VH 9 E	2372704	26367	31	0	0	8635	0	80	10934	1178	1665	85	70	15	48	210	1201	287
VH 9 F	2883538	23837	16	0	0	6303	0	127	5330	1153	1936	80	0	17	53	197	1555	358
VH 10 A	1148063	173827	6172	0	0	0	0	2444	210482	16067	76141	4259	463	0	28	359	869	1262
VH 10 B	641518	68031	8986	0	0	0	0	824	381289	22403	85774	2342	726	3	22	367	485	847
VH 10 C	1509191	96751	13018	0	0	0	0	863	724802	23442	138066	5168	584	18	52	662	1348	723
VH 10 D	2278934	110900	5254	0	0	892	0	838	102316	21909	133393	4004	505	10	48	746	2038	879
VH 11	7528974	29222	1459	0	61317	53915	0	259	15453	1515	4751	211	838	37	261	701	3567	440
Sample	**Sn**	**Sb**	**Te**	**I**	**Cs**	**Ba**	**La**	**Ce**	**Pr**	**Nd**	**Sm**	**Eu**	**Gd**	**Tb**	**Dy**	**Ho**	**Er**	**Tm**
UK 119 A	2013	4018	0	3	356	7855	814	2018	338	1315	288	74	239	31	174	31	98	16
UK 119 B1	8616	6335	5	9	472	7853	1607	4255	702	2473	437	91	307	35	190	35	121	22
UK 119 B2	2189	34198	64	16	584	5700	1802	4864	816	2845	500	109	432	45	238	48	146	25
UK 119 C	2042	90139	81	4	182	5424	963	2627	491	1859	417	492	458	65	389	69	197	29
UK 119 D	2231	2628	56	20	195	5780	1141	2861	541	1925	415	518	387	51	325	61	185	29
UK 119 E	2167	1776	21	19	402	7797	1080	2934	548	1913	400	491	387	52	341	73	209	33
UK 119 F	2063	6092	51	18	289	6513	1130	2985	559	2028	417	423	385	54	358	69	213	33
UK 119 G	1971	18171	97	18	238	5712	870	2499	505	1837	449	372	462	66	450	83	249	39
UK 119 H	2778	1938	16	43	261	6963	1731	4613	834	3031	673	549	644	90	573	106	319	50
UK 119 I	5954	2564	164	29	313	6913	829	1940	362	1258	264	500	253	39	269	52	180	31
UK 119 J	2116	5159	457	3	202	5245	1132	2977	534	1882	404	297	393	53	320	60	189	28
UK 119 K	3028	4850	979	10	380	4893	914	2363	385	1331	205	41	144	13	63	13	38	7
UK 119 L	7929	1761	186	0	237	5964	732	1965	345	1266	252	68	201	25	144	27	86	13
VH 3 A	9893	2907	119	3	265	10410	12129	34067	4989	16132	3011	856	2760	397	2424	421	1264	191
VH 3 B	4780	2414	94	11	75	15669	15171	35629	4609	13401	2138	622	2247	267	1557	283	863	136
VH 9 A	2608	1548	72	16	281	11450	3139	6865	1173	3325	610	145	685	90	572	107	319	49
VH 9 B	2615	4209	178	2	367	12321	3155	6913	1217	3890	742	156	806	109	678	127	365	56
VH 9 C	3165	5255	9828	2	951	6087	1138	2529	398	1253	239	37	284	37	244	46	145	24
VH 9 D	2887	5539	11605	3	892	5035	651	1620	246	793	135	18	177	25	165	30	100	18
VH 9 E	3386	1217	2231	24	205	4958	1597	3090	463	1304	215	45	188	24	140	25	68	10
VH 9 F	2744	2872	2111	5	55	4687	2613	5360	739	2137	336	97	316	33	162	26	66	8
VH 10 A	5283	2007	315	14	138	51805	11212	26460	4126	14178	2825	620	2738	358	2151	373	1080	160
VH 10 B	5024	2977	29	7	208	50817	16437	37130	5536	18932	3863	1073	3730	468	2791	478	1401	209
VH 10 C	7190	1459	141	10	110	13698	28813	59074	8443	26724	4190	1475	3962	504	2990	525	1527	232
VH 10 D	7062	1027	1090	15	92	20579	16089	37518	5681	20399	4297	824	3946	499	3140	543	1582	227
VH 11	3993	9381	18483	0	717	4734	623	1535	278	1036	200	28	206	30	193	32	99	18
Sample	**Yb**	**Lu**	**Hf**	**Ta**	**W**	**Re**	**Os**	**Ir**	**Pt**	**Au**	**Hg**	**Tl**	**Pb**	**Bi**	**Th**	**U**		
UK 119 A	114	16	262	13	38	3	1	23	0	0	0	9	1205	20	1919	366		
UK 119 B1	160	27	305	249	58	2	1	18	0	0	0	8	2071	93	2579	355		
UK 119 B2	199	32	285	18	62	3	0	11	0	0	0	16	4813	346	2042	336		
UK 119 C	238	33	95	9	16	3	0	6	0	0	0	11	1130	412	393	153		
UK 119 D	229	31	212	15	46	2	1	6	0	0	0	10	956	40	724	195		
UK 119 E	249	37	275	20	22	3	0	5	0	0	0	7	818	20	985	225		
UK 119 F	259	37	282	18	32	3	1	8	0	0	0	6	996	21	959	242		
UK 119 G	297	44	300	12	17	4	0	8	0	0	0	6	1436	44	1340	277		
UK 119 H	384	52	330	18	26	3	0	7	0	0	0	5	1661	9	1153	332		
UK 119 I	230	35	389	541	117	4	0	11	0	0	0	9	1276	26	1878	478		

UK 119 J	233	30	248	12	52	8	0	25	0	0	0	24	918	252	1792	355		
UK 119 K	64	10	181	818	70	19	1	29	254	0	0	57	1409	580	1997	186		
UK 119 L	117	16	189	638	114	10	0	41	339	0	0	23	4087	583	1441	279		
VH 3 A	1410	184	2062	382	502	3	0	7	0	0	0	18	73738	783	10823	0		
VH 3 B	1026	129	2037	307	579	4	1	6	0	0	0	11	30044	186	13072	0		
VH 9 A	354	49	395	92	29	4	1	5	0	0	0	3	2893	31	117	155		
VH 9 B	389	55	454	47	46	3	1	7	0	0	0	4	7514	215	221	247		
VH 9 C	178	25	66	11	28	22	0	27	1219	9	0	29	6629	6917	401	180		
VH 9 D	143	23	43	7	87	25	1	37	1427	6	0	67	6936	9022	908	340		
VH 9 E	81	11	35	13	73	6	0	6	102	4	0	23	10809	1453	2045	272		
VH 9 F	60	8	44	13	98	7	0	6	58	8	0	30	9865	1190	2408	416		
VH 10 A	1157	149	1680	286	704	3	0	10	0	0	0	14	199994	250	11000	0		
VH 10 B	1556	191	1959	137	557	4	0	8	0	0	0	19	11124	119	6427	0		
VH 10 C	1708	224	2902	439	581	4	1	10	0	0	0	18	8530	228	16477	0		
VH 10 D	1600	198	2780	323	424	4	0	8	0	0	0	30	8108	539	12201	0		
VH 11	127	21	253	126	199	54	0	87	2003	100	0	35	14802	17731	990	260		

UK-119J	2.294	1.077	0.000	0.180	7.423	0.000	0.000	0.000	0.024	0.000	0.000	0.000	0.000	0.000	0.000	0.000	0.000	0.000	7.485	92.515	100.000	100.000	0.000	0.000	0.000	0.000
UK-119K	0.000	0.000	0.000	0.017	7.256	0.000	0.000	0.081	0.022	0.000	0.000	0.000	0.000	0.000	0.000	0.000	0.000	0.000	15.307	84.693	100.000	79.945	0.000	100.000	12.027	1.681
UK-119L	0.000	0.018	0.004	0.714	23.993	0.000	0.000	0.000	0.029	0.000	0.000	0.000	0.000	0.000	0.000	0.000	0.000	0.000	28.857	71.146	100.003	98.140	0.000	100.000	0.000	7.372
VH-10A	0.000	0.000	0.000	0.687	7.669	0.863	0.000	0.000	0.254	0.000	0.000	0.000	0.000	0.000	0.000	0.000	0.000	0.000	32.777	67.223	100.000	74.854	0.000	100.000	11.272	0.000
VH-10B	0.000	0.000	0.000	0.437	5.357	0.606	0.000	0.000	0.345	0.000	0.000	0.000	0.000	0.000	0.000	0.000	0.000	0.000	42.908	57.092	100.000	46.003	0.000	0.000	7.508	0.000
VH-10C	0.000	0.000	0.000	0.603	10.068	0.566	0.000	0.000	0.122	0.000	0.000	0.000	0.000	0.000	0.000	0.000	0.000	0.000	35.764	64.236	100.000	84.118	0.000	100.000	8.838	0.000
VH-10D	0.000	0.000	0.000	0.724	10.146	1.074	0.000	0.000	0.617	0.000	0.000	0.000	0.000	0.000	0.000	0.000	0.000	0.000	37.442	62.558	100.000	42.194	0.000	100.000	15.276	0.000
VH-11	0.000	0.000	0.000	1.265	10.066	0.233	0.000	0.000	0.636	0.000	0.000	0.000	0.000	0.000	0.000	0.000	0.000	0.000	36.750	63.250	100.000	32.827	0.000	100.000	13.240	0.000
VH-3A	10.495	0.000	0.000	0.479	4.858	0.000	0.061	0.000	0.021	0.000	0.000	0.000	0.000	0.000	0.000	0.000	0.000	0.000	23.761	76.239	100.000	100.000	0.000	0.000	0.000	0.000
VH-3B	0.000	0.088	0.000	0.518	5.799	0.000	0.000	0.000	0.185	0.000	0.000	0.000	0.000	0.000	0.000	0.000	0.000	0.000	39.701	60.299	100.000	68.063	0.000	0.000	7.082	0.000
VH-9A	54.973	0.275	0.000	0.109	13.993	0.000	0.000	0.000	0.028	0.000	0.000	0.000	0.000	0.000	0.000	0.000	0.000	0.000	4.807	109.204	114.011	100.000	0.000	0.000	0.000	0.000
VH-9B	49.242	0.264	0.000	0.172	13.449	0.000	0.000	0.000	0.027	0.000	0.000	0.000	0.000	0.000	0.000	0.000	0.000	0.000	4.441	105.411	109.852	100.000	0.000	0.000	0.000	0.000
VH-9C	9.636	2.037	0.000	0.078	42.008	0.000	0.000	0.000	0.027	0.000	0.000	0.000	0.000	0.000	0.000	0.000	0.000	0.000	5.823	94.177	100.000	100.000	0.000	0.000	0.000	0.000
VH-9D	1.950	0.035	0.000	0.056	50.593	0.000	0.000	0.000	0.029	0.000	0.000	0.000	0.000	0.000	0.000	0.000	0.000	0.000	8.408	91.592	100.000	100.000	0.000	0.000	0.000	0.000
VH-9E	0.000	0.661	0.000	0.029	8.954	0.000	0.000	0.000	0.022	0.000	0.000	0.000	0.000	0.000	0.000	0.000	0.000	0.000	2.430	97.570	100.000	76.279	0.000	100.000	0.000	0.000
VH-9F	0.000	0.642	0.000	0.014	6.339	0.000	0.000	0.000	0.021	0.000	0.000	0.000	0.000	0.000	0.000	0.000	0.000	0.000	1.539	98.461	100.000	82.363	0.000	0.000	0.000	0.000

Sample	WZ	WOr	WPl	WPlAb	WPlAn	WLc	WNe	WKp	WHl	WTh	WAc	WNs	WKs	WWo	WDi	WDiWo	WDiEn	WDiFs	WHy	WHyEn	WHyFs	WOl	WOlFo	WOlFa	WCs	WMt
UK-119A	0.007	0.075	5.596	0.433	5.163	0.000	0.000	0.000	0.000	0.000	0.000	0.000	0.000	0.000	0.000	0.000	0.000	0.000	40.915	40.915	0.000	8.751	8.751	0.000	0.000	0.000
UK-119B1	0.006	0.074	5.577	0.477	5.100	0.000	0.000	0.000	0.000	0.000	0.000	0.000	0.000	0.000	0.000	0.000	0.000	0.000	52.926	52.926	0.000	3.885	3.885	0.000	0.000	0.000
UK-119B2	0.005	0.066	15.522	0.682	14.841	0.000	0.000	0.000	0.000	0.000	0.000	0.000	0.000	0.000	0.000	0.000	0.000	0.000	76.099	76.099	0.000	1.380	1.380	0.000	0.000	0.000
UK-119C	0.002	0.000	3.523	0.000	3.523	0.059	0.433	0.000	0.000	0.000	0.000	0.000	0.000	0.000	36.797	19.738	17.059	0.000	0.000	0.000	0.000	46.125	46.125	0.000	8.456	0.682
UK-119D	0.003	0.000	5.668	0.000	5.668	0.058	0.384	0.000	0.000	0.000	0.000	0.000	0.000	0.000	42.855	22.988	19.868	0.000	0.000	0.000	0.000	44.358	44.358	0.000	2.511	0.291
UK-119E	0.006	0.000	10.345	0.000	10.345	0.059	0.523	0.000	0.000	0.000	0.000	0.000	0.000	0.000	22.180	11.898	10.283	0.000	0.000	0.000	0.000	51.894	51.894	0.000	10.361	0.048
UK-119F	0.005	0.072	7.735	0.788	6.947	0.000	0.000	0.000	0.000	0.000	0.000	0.000	0.000	0.000	39.922	21.415	18.508	0.000	10.659	10.659	0.000	37.485	37.485	0.000	0.000	0.223
UK-119G	0.006	0.000	6.395	0.000	6.395	0.059	0.449	0.000	0.000	0.000	0.000	0.000	0.000	0.000	28.796	15.446	13.350	0.000	0.000	0.000	0.000	49.046	49.046	0.000	10.457	0.246
UK-119H	0.005	0.000	5.827	0.000	5.827	0.060	0.479	0.000	0.000	0.000	0.000	0.000	0.000	0.000	20.756	11.134	9.622	0.000	0.000	0.000	0.000	51.883	51.883	0.000	16.239	0.268
UK-119I	0.005	0.071	9.755	0.684	9.072	0.000	0.000	0.000	0.000	0.000	0.000	0.000	0.000	0.000	37.051	19.874	17.177	0.000	8.522	8.522	0.000	39.582	39.582	0.000	0.000	0.358
UK-119J	0.005	0.000	7.274	0.000	7.274	0.055	0.428	0.000	0.000	0.000	0.000	0.000	0.000	0.000	36.165	19.399	16.766	0.000	0.000	0.000	0.000	40.597	40.597	0.000	2.478	1.563
UK-119K	0.003	0.065	2.820	0.539	2.281	0.000	0.000	0.000	0.000	0.000	0.000	0.000	0.000	0.000	0.000	0.000	0.000	0.000	72.422	72.422	0.000	0.000	0.000	0.000	0.000	0.000
UK-119L	0.005	0.077	19.276	0.338	18.938	0.000	0.000	0.000	0.000	0.000	0.000	0.000	0.000	0.000	0.000	0.000	0.000	0.000	36.655	36.655	0.000	2.912	2.912	0.000	0.000	0.023
VH-10A	0.026	1.024	20.130	4.841	15.289	0.000	0.000	0.000	0.000	0.000	0.000	0.000	0.000	0.000	54.316	29.135	25.181	0.000	0.349	0.349	0.000	0.000	0.000	0.000	0.000	0.000
VH-10B	0.027	0.678	33.812	17.759	16.053	0.000	0.000	0.000	0.000	0.000	0.000	0.000	0.000	1.603	47.075	25.251	21.824	0.000	0.000	0.000	0.000	0.000	0.000	0.000	0.000	0.000
VH-10C	0.045	0.339	25.842	3.904	21.938	0.000	0.000	0.000	0.000	0.000	0.000	0.000	0.000	0.000	43.703	23.443	20.260	0.000	5.672	5.672	0.000	0.000	0.000	0.000	0.000	0.000
VH-10D	0.050	0.777	20.523	11.566	8.957	0.000	0.000	0.000	0.000	0.000	0.000	0.000	0.000	0.000	39.627	21.256	18.371	0.000	6.844	6.844	0.000	0.000	0.000	0.000	0.000	0.000
VH-11	0.002	0.570	21.896	14.419	7.476	0.000	0.000	0.000	0.000	0.000	0.000	0.000	0.000	0.000	41.949	22.501	19.447	0.000	5.730	5.730	0.000	0.000	0.000	0.000	0.000	0.000
VH-3A	0.034	0.000	23.425	0.000	23.425	0.047	0.294	0.000	0.000	0.000	0.000	0.000	0.000	0.000	49.138	26.358	22.780	0.000	0.000	0.000	0.000	8.448	8.448	0.000	10.865	0.000
VH-3B	0.030	0.060	31.836	9.762	22.073	0.000	0.000	0.000	0.000	0.000	0.000	0.000	0.000	5.346	46.441	24.911	21.530	0.000	0.000	0.000	0.000	0.000	0.000	0.000	0.000	0.121
VH-9A	0.009	0.000	3.550	0.000	3.550	0.000	0.476	0.039	0.000	0.000	0.000	0.000	0.000	0.000	0.000	0.000	0.000	0.000	0.000	0.000	0.000	29.027	29.027	0.000	49.050	0.330
VH-9B	0.006	0.000	3.471	0.000	3.471	0.000	0.421	0.039	0.000	0.000	0.000	0.000	0.000	0.000	0.000	0.000	0.000	0.000	0.000	0.000	0.000	32.172	32.172	0.000	45.891	0.331
VH-9C	0.001	0.000	4.734	0.000	4.734	0.053	0.278	0.000	0.000	0.000	0.000	0.000	0.000	0.000	5.450	2.924	2.527	0.000	0.000	0.000	0.000	25.189	25.189	0.000	8.735	2.482
VH-9D	0.001	0.000	6.943	0.000	6.943	0.054	0.164	0.000	0.000	0.000	0.000	0.000	0.000	0.000	6.098	3.271	2.827	0.000	0.000	0.000	0.000	22.785	22.785	0.000	1.721	0.041
VH-9E	0.001	0.061	2.325	0.527	1.798	0.000	0.000	0.000	0.000	0.000	0.000	0.000	0.000	0.000	68.241	36.605	31.636	0.000	15.193	15.193	0.000	0.419	0.419	0.000	0.000	0.912
VH-9F	0.001	0.060	1.314	0.221	1.094	0.000	0.123	0.000	0.000	0.000	0.000	0.000	0.000	0.000	88.037	47.224	40.814	0.000	0.000	0.000	0.000	0.478	0.478	0.000	0.000	0.887

Sample	WCm	WIl	WHm	WSp	WPf	WRu	WAp	WFl	WPy	WCc	WBi	WHo	WHoAct	WHoEd	WHoRi	WSpnl	WANPL	WFAOL	WENHY	WSALIC	WFEMIC	WTOTAL	QzAbOrTQZ	QzAbOrTAB	QzAbOrTOR	QzAbOrWTQZ
UK-119A	0.005	0.785	28.426	0.000	0.000	0.081	0.085	0.000	0.000	0.000	0.000	0.000	0.000	0.000	0.000	0.000	92.269	0.000	100.000	20.952	79.048	100.000	0.000	85.985	14.015	0.000
UK-119B1	0.004	0.989	24.960	0.000	0.000	0.017	0.029	0.000	0.000	0.000	0.000	0.000	0.000	0.000	0.000	0.000	91.450	0.000	100.000	17.189	82.811	100.000	0.000	87.236	12.764	0.000
UK-119B2	0.000	0.429	6.348	0.000	0.000	0.021	0.026	0.000	0.000	0.000	0.000	0.000	0.000	0.000	0.000	0.000	95.609	0.000	100.000	15.697	84.303	100.000	0.000	91.596	8.404	0.000
UK-119C	0.000	0.131	3.763	0.000	0.000	0.000	0.029	0.000	0.000	0.000	0.000	0.000	0.000	0.000	0.000	0.000	100.000	0.000	0.000	4.016	95.984	100.000	0.000	0.000	0.000	0.000
UK-119D	0.000	0.214	3.629	0.000	0.000	0.000	0.029	0.000	0.000	0.000	0.000	0.000	0.000	0.000	0.000	0.000	100.000	0.000	0.000	6.114	93.886	100.000	0.000	0.000	0.000	0.000
UK-119E	0.000	0.298	4.258	0.000	0.000	0.000	0.029	0.000	0.000	0.000	0.000	0.000	0.000	0.000	0.000	0.000	100.000	0.000	0.000	10.932	89.068	100.000	0.000	0.000	0.000	0.000
UK-119F	0.000	0.220	3.650	0.000	0.000	0.000	0.028	0.000	0.000	0.000	0.000	0.000	0.000	0.000	0.000	0.000	89.810	0.000	100.000	7.813	92.187	100.000	0.000	92.081	7.919	0.000
UK-119G	0.000	0.245	4.272	0.000	0.000	0.000	0.029	0.000	0.000	0.000	0.000	0.000	0.000	0.000	0.000	0.000	100.000	0.000	0.000	6.909	93.091	100.000	0.000	0.000	0.000	0.000
UK-119H	0.000	0.215	4.202	0.000	0.000	0.000	0.065	0.000	0.000	0.000	0.000	0.000	0.000	0.000	0.000	0.000	100.000	0.000	0.000	6.372	93.628	100.000	0.000	0.000	0.000	0.000
UK-119I	0.000	0.286	4.342	0.000	0.000	0.000	0.028	0.000	0.000	0.000	0.000	0.000	0.000	0.000	0.000	0.000	92.993	0.000	100.000	9.831	90.169	100.000	0.000	91.083	8.917	0.000
UK-119J	0.000	0.257	11.151	0.000	0.000	0.000	0.027	0.000	0.000	0.000	0.000	0.000	0.000	0.000	0.000	0.000	100.000	0.000	0.000	7.761	92.239	100.000	0.000	0.000	0.000	0.000
UK-119K	0.000	0.023	10.811	0.000	0.000	0.121	0.026	0.000	0.000	0.000	0.000	0.000	0.000	0.000	0.000	0.000	80.877	0.000	100.000	16.597	83.403	100.000	94.587	4.860	0.553	95.214
UK-119L	0.006	0.925	32.719	0.000	0.000	0.000	0.030	0.000	0.000	0.000	0.000	0.000	0.000	0.000	0.000	0.000	98.245	0.000	100.000	26.730	73.270	100.000	0.000	82.288	17.712	0.000
VH-10A	0.000	0.911	10.712	0.987	0.000	0.000	0.274	0.000	0.000	0.000	0.000	0.000	0.000	0.000	0.000	0.000	75.952	0.000	100.000	32.452	67.548	100.000	62.892	30.944	6.164	65.778
VH-10B	0.000	0.590	7.622	0.706	0.000	0.000	0.379	0.000	0.000	0.000	0.000	0.000	0.000	0.000	0.000	0.000	47.476	0.000	0.000	42.025	57.975	100.000	26.265	71.175	2.560	28.938
VH-10C	0.000	0.797	13.989	0.644	0.000	0.000	0.131	0.000	0.000	0.000	0.000	0.000	0.000	0.000	0.000	0.000	84.892	0.000	100.000	35.064	64.936	100.000	64.619	32.705	2.676	67.562
VH-10D	0.000	0.955	14.069	1.219	0.000	0.000	0.661	0.000	0.000	0.000	0.000	0.000	0.000	0.000	0.000	0.000	43.643	0.000	100.000	36.626	63.374	100.000	52.019	45.125	2.856	55.309
VH-11	0.000	1.672	13.995	0.265	0.000	0.000	0.683	0.000	0.000	0.000	0.000	0.000	0.000	0.000	0.000	0.000	34.145	0.000	100.000	35.708	64.292	100.000	43.588	54.386	2.026	46.901
VH-3A	0.000	0.656	6.994	0.000	0.075	0.000	0.024	0.000	0.000	0.000	0.000	0.000	0.000	0.000	0.000	0.000	100.000	0.000	0.000	23.800	76.200	100.000	0.000	0.000	0.000	0.000
VH-3B	0.000	0.695	8.188	0.000	0.000	0.000	0.202	0.000	0.000	0.000	0.000	0.000	0.000	0.000	0.000	0.000	69.336	0.000	0.000	39.008	60.992	100.000	38.636	61.013	0.351	41.897
VH-9A	0.000	0.129	17.363	0.000	0.000	0.000	0.027	0.000	0.000	0.000	0.000	0.000	0.000	0.000	0.000	0.000	100.000	0.000	0.000	4.074	95.926	100.000	0.000	0.000	0.000	0.000
VH-9B	0.000	0.212	17.430	0.000	0.000	0.000	0.027	0.000	0.000	0.000	0.000	0.000	0.000	0.000	0.000	0.000	100.000	0.000	0.000	3.937	96.063	100.000	0.000	0.000	0.000	0.000
VH-9C	0.000	0.093	52.958	0.000	0.000	0.000	0.027	0.000	0.000	0.000	0.000	0.000	0.000	0.000	0.000	0.000	100.000	0.000	0.000	5.066	94.934	100.000	0.000	0.000	0.000	0.000

VH-9D	0.000	0.066	62.099	0.000	0.000	0.000	0.027	0.000	0.000	0.000	0.000	0.000	0.000	0.000	0.000	0.000	100.000	0.000	0.000	7.162	92.838	100.000	0.000	0.000	0.000	0.000
VH-9E	0.000	0.039	12.785	0.000	0.000	0.000	0.024	0.000	0.000	0.000	0.000	0.000	0.000	0.000	0.000	0.000	77.333	0.000	100.000	2.386	97.614	100.000	0.000	90.233	9.767	0.000
VH-9F	0.000	0.019	9.057	0.000	0.000	0.000	0.023	0.000	0.000	0.000	0.000	0.000	0.000	0.000	0.000	0.000	83.206	0.000	0.000	1.498	98.502	100.000	0.000	0.000	0.000	0.000

Sample	QzAbOrWTAB	QzAbOrWTOB	QzNeKpTQZ	QzNeKpTNE	QzNeKpTKP	QzNeKpWTQZ	QzNeKpWTNE	QzNeKpWTKP	OrAbAnTAN	OrAbAnTOR	OrAbAnTAB	OrAbAnWTAN	OrAbAnWTAB	OrAbAnWTOR	WAFMA	WAFMF	WAFMM	AFMA	AFMF	AFMM	WAgpaitic	Agpaitic	WFeMgRat	FeMgRat	WAlkRat	AlkRat
UK-119A	85.251	14.749	75.000	21.496	3.504	45.436	46.183	8.381	90.630	1.313	8.057	91.051	7.629	1.320	0.135	54.324	45.541	0.135	25.040	74.825	0.530	0.567	60.930	40.443	80.147	85.985
UK-119B1	86.557	13.443	75.000	21.809	3.191	45.470	46.891	7.639	89.790	1.303	8.907	90.251	8.438	1.310	0.150	48.818	51.032	0.141	21.129	78.730	0.730	0.787	55.569	35.258	81.808	87.236
UK-119B2	91.125	8.875	75.000	22.899	2.101	45.592	49.365	5.043	94.949	0.425	4.627	95.202	4.372	0.426	0.247	15.376	84.377	0.173	4.855	94.972	2.295	2.544	19.214	9.384	87.762	91.596
UK-119C	0.000	0.000	51.957	44.128	3.915	3.302	88.005	8.693	100.000	0.000	0.000	100.000	0.000	0.000	0.288	10.241	89.471	0.194	3.105	96.701	10.431	11.580	13.322	6.275	88.119	91.852
UK-119D	0.000	0.000	52.145	43.564	4.290	3.618	86.857	9.524	100.000	0.000	0.000	100.000	0.000	0.000	0.261	9.329	90.410	0.174	2.808	97.018	6.149	6.790	12.064	5.639	86.981	91.034
UK-119E	0.000	0.000	51.649	45.052	3.299	2.784	89.888	7.328	100.000	0.000	0.000	100.000	0.000	0.000	0.335	10.200	89.465	0.227	3.092	96.680	4.502	5.042	13.127	6.175	89.986	93.177
UK-119F	91.635	8.365	75.000	23.020	1.980	45.605	49.642	4.753	88.438	0.916	10.646	88.982	10.096	0.922	0.287	9.321	90.392	0.192	2.806	97.001	5.518	6.136	11.990	5.601	88.441	92.081
UK-119G	0.000	0.000	51.892	44.324	3.784	3.192	88.405	8.402	100.000	0.000	0.000	100.000	0.000	0.000	0.295	10.637	89.068	0.200	3.235	96.565	6.244	6.946	13.671	6.452	88.516	92.135
UK-119H	0.000	0.000	51.808	44.575	3.617	3.051	88.916	8.032	100.000	0.000	0.000	100.000	0.000	0.000	0.312	10.483	89.205	0.212	3.185	96.604	7.186	8.012	13.539	6.385	89.023	92.496
UK-119I	90.587	9.413	75.000	22.771	2.229	45.577	49.074	5.349	91.932	0.719	7.349	92.321	6.956	0.723	0.249	11.093	88.658	0.169	3.385	96.446	3.806	4.204	14.154	6.699	87.048	91.083
UK-119J	0.000	0.000	51.849	44.452	3.699	3.121	88.665	8.214	100.000	0.000	0.000	100.000	0.000	0.000	0.256	26.771	72.973	0.198	9.313	90.488	5.274	5.874	32.364	17.242	88.774	92.319
UK-119K	4.270	0.516	98.906	0.983	0.112	97.394	2.313	0.293	78.160	2.233	19.607	79.050	18.691	2.259	0.192	25.018	74.790	0.145	8.567	91.288	4.050	4.435	30.149	15.818	85.246	89.776
UK-119L	81.402	18.598	75.000	20.572	4.428	45.334	44.098	10.568	97.749	0.399	1.852	97.853	1.748	0.399	0.116	64.180	35.704	0.128	33.480	66.392	0.532	0.555	70.161	50.590	75.351	82.288
VH-10A	28.249	5.973	91.983	6.685	1.332	81.302	15.303	3.394	71.284	4.770	23.946	72.276	22.885	4.839	3.612	46.710	49.678	3.330	20.177	76.493	15.948	16.765	55.807	35.488	76.761	83.389
VH-10B	68.448	2.614	82.702	16.697	0.601	61.434	37.080	1.485	45.127	1.905	52.968	46.543	51.491	1.966	12.411	38.455	49.134	11.686	15.900	72.414	33.001	37.811	51.169	31.340	94.816	96.528
VH-10C	29.846	2.592	92.385	7.039	0.576	82.358	16.168	1.473	83.039	1.283	15.679	83.793	14.912	1.295	2.206	53.522	44.273	2.275	24.750	72.975	8.314	9.267	61.522	41.050	88.940	92.436
VH-10D	41.878	2.814	89.385	9.983	0.632	75.715	22.686	1.599	40.704	3.530	55.766	42.051	54.301	3.648	6.171	52.135	41.694	6.465	24.290	69.244	37.405	42.142	62.363	41.917	91.224	94.047
VH-11	51.079	2.020	87.283	12.261	0.457	71.181	27.671	1.148	32.026	2.441	65.533	33.279	64.184	2.538	7.349	51.394	41.258	7.772	23.884	68.344	44.973	51.485	62.279	41.830	94.642	96.409
VH-3A	0.000	0.000	52.251	43.248	4.501	3.795	86.214	9.991	100.000	0.000	0.000	100.000	0.000	0.000	0.365	30.918	68.717	0.292	11.175	88.533	1.218	1.341	37.734	20.886	86.343	90.573
VH-3B	57.750	0.353	86.010	13.910	0.080	68.515	31.285	0.200	67.939	0.183	31.878	69.206	30.607	0.187	6.746	43.143	50.111	6.570	18.176	75.254	16.332	19.091	53.714	33.580	99.133	99.428
VH-9A	0.000	0.000	50.000	46.570	3.430	0.000	92.422	7.578	100.000	0.000	0.000	100.000	0.000	0.000	0.355	48.589	51.056	0.343	21.000	78.657	11.034	12.356	55.316	35.023	89.935	93.141
VH-9B	0.000	0.000	50.000	46.192	3.808	0.000	91.593	8.407	100.000	0.000	0.000	100.000	0.000	0.000	0.300	46.154	53.546	0.282	19.418	80.300	10.227	11.395	52.855	32.802	88.867	92.384
VH-9C	0.000	0.000	52.630	42.110	5.260	4.433	83.900	11.668	100.000	0.000	0.000	100.000	0.000	0.000	0.111	76.018	23.871	0.151	47.113	52.735	5.572	6.068	80.428	64.144	84.046	88.897
VH-9D	0.000	0.000	54.065	37.806	8.129	6.837	75.167	17.996	100.000	0.000	0.000	100.000	0.000	0.000	0.068	79.701	20.232	0.095	52.448	47.457	2.621	2.736	83.556	68.867	75.369	82.303
VH-9E	89.695	10.305	75.000	22.558	2.442	45.554	48.590	5.856	74.370	2.503	23.127	75.371	22.091	2.538	0.233	38.704	61.063	0.200	15.067	84.733	13.381	14.699	45.103	26.346	85.874	90.233
VH-9F	0.000	0.000	67.742	28.645	3.613	31.481	60.082	8.437	78.809	4.315	16.876	79.579	16.062	4.359	0.248	34.219	65.533	0.202	12.751	87.046	18.051	19.643	40.453	22.827	83.915	88.800

Sample	OxidationRat	WOxidationRa	WrightsAlkInd	TotalAlkalis	DiffInd	WDiffInd	WatsonM	R1	R2	ChemicalIndex	RoserKorschD	RoserKorschD	RoserKorschD	RoserKorschD	PeraluminousIn	DebonLefortA	DebonLefortB
UK-119A	0.000	0.000	1.007	0.050	0.541	0.507	0.415	1030.532	1199.245	89.282	-9.309	-30.232	-16.989	18.155	8.330	235.313	706.053
UK-119B1	0.000	0.000	1.010	0.055	0.582	0.551	0.444	1380.049	1229.850	87.109	-15.751	-31.846	-15.514	31.910	6.757	180.148	719.605
UK-119B2	0.000	0.000	1.021	0.082	0.741	0.748	2.136	2969.613	1769.851	50.369	-42.298	-38.400	21.581	156.528	1.015	1.453	765.785
UK-119C	0.000	0.000	1.013	0.084	0.526	0.492	51.378	2229.993	2643.449	4.825	-37.534	-31.903	126.840	670.710	0.051	-421.361	690.924
UK-119D	0.000	0.000	1.012	0.077	0.472	0.442	28.778	2351.137	2541.217	8.071	-38.968	-32.922	84.080	442.740	0.088	-362.350	700.268
UK-119E	0.000	0.000	1.014	0.100	0.620	0.581	18.333	2123.743	2614.666	13.008	-37.750	-32.729	43.960	248.382	0.150	-351.034	705.907
UK-119F	0.000	0.000	1.015	0.087	0.840	0.860	19.227	2521.440	2427.670	11.198	-40.454	-34.223	67.590	360.914	0.126	-302.839	716.517
UK-119G	0.000	0.000	1.012	0.087	0.543	0.508	30.326	2161.433	2654.375	8.131	-37.333	-32.125	71.087	389.846	0.089	-400.308	698.066
UK-119H	0.000	0.000	1.012	0.091	0.576	0.539	37.558	2054.284	2749.679	6.895	-36.421	-31.337	78.193	424.842	0.074	-441.542	689.846
UK-119I	0.000	0.000	1.013	0.077	0.738	0.755	14.937	2478.337	2435.781	14.232	-39.965	-34.636	48.454	277.651	0.166	-284.714	730.489
UK-119J	0.000	0.000	1.014	0.089	0.534	0.483	21.858	2054.528	2435.651	11.051	-31.553	-33.499	19.092	278.678	0.124	-331.710	761.461
UK-119K	0.000	0.000	1.049	0.068	11.341	12.632	0.733	3154.565	1400.566	72.923	-39.666	-38.905	25.054	295.155	2.693	29.438	778.148
UK-119L	0.000	0.000	1.006	0.041	0.459	0.416	1.586	961.420	1150.696	67.155	-1.035	-25.151	-25.459	8.425	2.045	110.296	628.991
VH-10A	0.000	0.000	1.063	0.737	17.053	17.137	9.829	2928.664	2491.001	17.135	-2.974	-11.542	-9.230	33.042	0.204	-510.622	394.859
VH-10B	0.000	0.000	1.186	2.189	26.701	25.945	7.037	2606.024	2369.224	22.084	-0.705	-7.314	-4.660	18.455	0.280	-471.102	316.817
VH-10C	0.000	0.000	1.043	0.513	13.080	13.081	7.171	2694.139	2372.239	23.106	-0.011	-13.507	-14.356	19.353	0.297	-406.918	437.454
VH-10D	0.000	0.000	1.177	1.483	28.142	27.619	8.718	2679.273	1961.242	18.499	-3.559	-13.232	-15.288	33.134	0.221	-387.528	435.444
VH-11	0.000	0.000	1.216	1.442	29.032	28.230	9.079	2051.968	1590.329	17.789	-4.442	-11.617	-14.744	32.860	0.215	-323.546	351.204
VH-3A	0.000	0.000	1.004	0.073	0.393	0.342	12.404	2737.986	3437.452	16.289	-5.077	-12.837	-3.181	39.495	0.194	-696.420	432.504
VH-3B	0.000	0.000	1.083	1.153	17.251	16.904	7.509	2802.189	2647.142	21.420	1.905	-7.837	-7.874	15.261	0.273	-518.661	319.718
VH-9A	0.000	0.000	1.007	0.099	0.695	0.515	206.130	626.353	3741.271	2.432	-1.036	-14.415	-70.355	215.375	0.025	-980.162	545.183
VH-9B	0.000	0.000	1.006	0.090	0.593	0.460	173.561	845.300	3662.466	2.509	-4.468	-17.082	-63.090	262.841	0.026	-926.138	590.617
VH-9C	0.000	0.000	1.015	0.063	0.433	0.331	39.905	-111.866	1448.826	11.110	12.132	-30.796	-314.828	-66.281	0.125	-220.629	929.386
VH-9D	0.000	0.000	1.014	0.041	0.290	0.218	15.855	-387.279	1021.434	25.734	16.539	-32.210	-263.714	-94.044	0.347	-82.694	965.977
VH-9E	0.000	0.000	1.008	0.071	0.623	0.588	94.792	2787.406	2821.768	2.292	-15.730	-23.482	-41.233	569.577	0.023	-615.621	625.384
VH-9F	0.000	0.000	1.005	0.062	0.440	0.403	181.785	3008.631	3255.995	1.174	-12.205	-17.935	-2.049	817.417	0.012	-802.530	527.328